New Insights into Metallocene Electrochemistry and their Potential Use for Catalysis

Synthesis, Properties and Redox Behaviour

Dissertation

Zur Erlangung des Grades

„Doktor der Naturwissenschaften“

im Promotionsfach Chemie

am Fachbereich Chemie, Pharmazie, Geographie

und Geowissenschaften

der Johannes Gutenberg-Universität Mainz

Sven Daniel Waniek

geboren am 25. Mai 1990 in Mainz

Mainz, Juli 2022

Die vorliegende Arbeit wurde unter der Betreuung von [redacted] in der Zeit von Februar 2017 bis Juli 2022 am Institut für Anorganische Chemie und Analytische Chemie sowie dessen Nachfolger, dem Department Chemie der Johannes Gutenberg-Universität Mainz angefertigt.

Mainz, 21. Juli 2022

Dekanin: Prof. Dr. Tanja Schirmeister

1. Berichterstatter: [redacted]

2. Berichterstatter: [redacted]

Tag der mündlichen Prüfung: 29.09.2022

Ich, Sven Daniel Waniek, (ehemalige Matrikelnummer [redacted]), versichere, dass ich diese Promotionsarbeit selbstständig verfasst und keine anderen als die angegebenen schriftlichen und elektronischen Quellen genutzt habe. Alle Ausführungen, die anderen Schriften wörtlich oder sinngemäß entnommen wurden, habe ich kenntlich gemacht.

Datum: _____ Unterschrift:

Für meine Familie

Kurzzusammenfassung

Metallocene sind metallorganische Verbindungen, die elektrochemisch aktiv und deren Zusammensetzungsmöglichkeiten vielfältig sind. Ihre Elektrochemie ist geprägt von ihrer überwiegenden Redoxstabilität und -reversibilität. Ferrocen und Cobaltocenium sind stabile Vertreter dieser Stoffklasse, die reversibel oxidiert bzw. reduziert werden können. Aufgrund ihrer genau definierten elektrochemischen Potentiale und ihrer Redoxstabilität können sie als Bestandteile in den verschiedensten Reaktionen verwendet werden.

In dieser Arbeit werden verschiedene Ferrocen- und Cobaltoceniumderivate hinsichtlich ihrer Elektrochemie und den daraus folgenden Eigenschaften untersucht. Dazu werden verschiedene Komplexe entwickelt und analysiert, in denen Metallocene die unterschiedlichsten Eigenschaften aufweisen und die verschiedenste Chemie ermöglicht. Die Metallocene werden als Mediator, Teile von Carbenkomplexen und als stickstoffverbrückte Komplexe untersucht.

Ein vergleichbares Set von Ferrocenderivaten wird hinsichtlich ihrer Tauglichkeit als Redoxmediator analysiert. In dieser Position nimmt das Metallocen nicht als Katalysator an der Reaktion teil, sondern leitet vielmehr Elektronen von/zu den Elektroden zum/vom Substrat und soll somit Überpotentiale und daraus resultierende Nebenreaktionen vermeiden. Hierfür muss es redoxstabil sein und einen schnellen Elektronentransfer gewährleisten. Die Erfüllung der Anforderungen werden durch UV/Vis-, Infrarot (IR)- sowie ^{1}H Kernspinresonanz (NMR)-spektroskopische Untersuchungen überprüft.

Die Einführung substituierter, redoxaktiver Ferrocene in Diaminocarbenkomplexe soll die Eigenschaften der Komplexe mittels Redoxchemie variabel machen. Der Komplex Chlorido(isocyanoferrocen)gold(I) wird als Präkursor für die Synthese von Carbenkomplexen hergestellt. Durch nucleophile Angriffe von sekundären Aminen am Präkursor lassen sich zwei redoxaktive, acyclische und ferocenylsubstituierte Diaminocarbengold(I)-komplexe synthetisieren. Die Carbenkomplexe zeigen in der Festkörperstruktur die Bildung von aurophilen Wechselwirkungen sowie Wasserstoffbrückenbindungen zu Chlor und Eisen auf. Cyclovoltammetrie (CV), Square Wave Voltammetrie (SWV), UV/Vis- sowie Elektronenspin-resonanz (EPR)-Spektroskopie wurden verwendet um die Redoxchemie und die darauf folgenden Prozesse zu verstehen. Dabei wurde sowohl die temporäre *in situ* Bildung von Ferrocenium als auch der Elektronentransfer von Gold(I) zu Eisen(III) nachgewiesen.

Zwei stickstoffverbrückte Cobaltoceniumkomplexe, *N*,*N*-Dicobaltoceniumamin und *N*,*N*-Dicobaltoceniumamid werden hinsichtlich ihrer elektrochemischen Eigenschaften untersucht. Neben der Optimierung der Synthese erfolgte insbesondere eine Betrachtung der Säure-Base-Chemie in Abhängigkeit der Redoxpotentiale, da das Amin und das Amid im Säure-Base-Gleichgewicht zueinander stehen. Durch die zentrale Protonenquelle (Aminbrücke) und durch die Eignung der beiden Komplexe, je Metallocen ein Elektron aufnehmen zu können, besitzen diese Verbindungen zentrale Eigenschaften für die elektrochemische Darstellung von Wasserstoff. Die

Reduktion von *N*,*N*-Dicobaltoceniumamin zu *N*,*N*-Dicobaltoceniumamid führt zur Freisetzung von Wasserstoffgas, während die Oxidation von *N*,*N*-Dicobaltoceniumamid zur Bildung eines Aminyl Radikals führt, dass ein Wasserstoffatom aus Acetontiril aufnimmt. Damit ist das Paar aus Amin und Amid in der Lage Wasserstoffentwicklung durchzuführen (hydrogen evolving reaction; HER), wobei die Reaktion am Stickstoff erfolgt.

Abstract

Metallocenes are organometallic compounds that are electrochemically active with a variety of composition options. Their electrochemistry is characterized by its redox stability and reversibility. Ferrocene and cobaltocenium are stable representatives of this class which can be reversibly oxidized or reduced. Due to their well defined potentials and their redox stability, they can be used as parts in different reactions.

In this work, different ferrocene and cobaltocenium derivatives are investigated in regard to their electrochemistry and the resulting properties. Therefore, several complexes are developed and analyzed in which metallocenes show the most different properties and allow various chemistry. The metallocenes take the role of redox mediator, part of carbene complexes and nitrogen bridged complexes.

A comparable set of ferrocene derivatives is analyzed regarding its suitability for redox mediation. In this position, the metallocene does not participate in the reaction as a catalyst. It shall conduct electrons from/towards the electrodes towards/from the substrate and thus avoid overpotentials and side reactions resulting therefrom. For this reason, it must be redox stable and ensure rapid electron transfer. The fulfillment of this requirements are verified by UV/Vis, infrared (IR) and ^{1}H nuclear magnetic resonance (NMR) spectroscopic measurements.

The introduction of substituted, redoxactive ferrocenyl moieties into diaminocarbene complexes should make the properties of the complexes variable electrochemically. The complex chlorido(isocyanoferrocene)gold(I) is synthesized as a precursor for carbene complexes. By nucleophilic attack of secondary amines on the precursor, two redox active, acyclic and ferrocenyl substituted diamino carbene gold(I) complexes are synthesized. The solid-state structures of the carbene complexes shows the formation of aurophilic interactions and hydrogen bonds towards chlorine and iron. Cyclic voltammetry (CV), square wave voltammetry (SWV), UV/Vis and electron paramagnetic resonance (EPR) spectroscopy were used to understand the redox chemistry and the subsequent processes. Both, the temporary *in situ* formation of ferrocenium and the electron transfer from gold(I) to iron(III) were detected.

Two nitrogen-bridged cobaltocenium complexes, *N*,*N*-dicobaltoceniumamine and *N*,*N*-dicobaltoceniumamide will be analyzed regarding their electronic properties. In addition to the optimization of the synthesis, the acid-base chemistry was examined as a function of the redox potential, since the amine and the amide are within an acid-base equilibrium. Due to the central proton source (amine bridge) and the suitability of the two complexes to be able to accept one electron per metallocene, these compounds have central properties for the electrochemical production of hydrogen. Reduction of *N*,*N*-dicobaltoceniumamine to *N*,*N*-dicobaltoceniumamide results in the evolution, of hydrogen gas while the oxidation of *N*,*N*-dicobaltoceniumamide results in the formation of an aminyl radical that accepts a hydrogen atom from acetonitrile. Thus, the

amine-amide pair is able to perform hydrogen evolution reaction (HER), where the reaction occurs at the nitrogen.

Contents

Abbreviations

AAC	acyclic amino carbene
Ad	adamantyl
ADC	acyclic diamino carbene
AFcC	acyclic ferrocenylsubstituted carbene
$BAr^F{}_4^-$	tetrakis[3,5-bis(trifluoromethyl)phenyl]borate
BDE	bond dissociation enthalpy
BDFE	bond dissociation free energy
^{n}BuLi	*n*-butyllithium
^{t}BuLi	*tert*-butyllithium
CAAC	cyclic alkyl amino carbene
Cc	Cobaltocenyl
Cc^+	cobaltoceniumyl
CcH	cobaltocene
CcH^+	cobaltocenium
$CH_3{}^t$Bu	methyl-*tert*-butyl
cod	cyclooctatetraene
Cp	cyclopentadienyl
Cp*	1,2,3,4,5-pentamethylcyclopentadienyl
CPET	concerted proton-electron transfer
CV	Cyclic Voltammetry
DBU	diazabicycloundecen
DFT	density functional theory
Dipp	2,6-diisopropylphenyl
DMF	dimethylformamide
DMSO	dimethyl sulfoxide
dppc	diphenylphosphino
e^-	electron
E^0	standard redox potential
EPR	electron paramagnetic resonance
ES	excited state
ET	electron transfer
Et	ethyl
Fc	ferrocenyl
Fc^+	ferroceniumyl
Fc*	nonamethylferrocenyl
FcH	ferrocene
FcH^+	ferrocenium
GS	ground state

HER	hydrogen evolution reaction
^{i}Bu	isobutyl
IR	infrared
IVCT	intervalence charge transfer
k	rate constant
L_n	$ligand_{amount}$
LMCT	ligand to metal charge transfer
Me	methyl
+M effect	positive mesomeric effect
Mes	mesityl
MIC	mesoionic carbene
MP	microperoxidase
NHC	*N*-heterocyclic carbene
NIR	near infrared
NMR	nuclear magnetic resonance
OER	oxygen evolution reaction
P_3^BFe	tris(*ortho*-diisopropylphosphinophenyl)-borane
PBN	*N*-tertiary-butyl-nitrone
PCET	proton-coupled electron transfer
Ph	phenyl
pK_a	acid dissociation constant
py	pyridine
R	organic substituent
RCM	ring closure metathesis
RSC	redox switchable catalysis
SET	single electron transfer
SHE	standard hydrogen electrode
SWV	square wave voltammetry
TAPP	*meso*-tetrakis(2-aminophenyl)porhpine
TCD	thermal conductivity detection
TEMPO	2,2,6,6-Tetramethylpiperidinyloxyl
TEP	*Tolman* electronic parameter
TFA	trifluoroacetic acid
THF	tetrahydrofuran
TMAP	*meso*-tetrakis (*N*,*N*,*N*)-trimethylanilinium-4-yl)porphine chloride
TMPyP	*meso*-tetrakis(*N*-methyl-pyridinium-4-yl)porphine chloride
TOF	turn over frequency
TON	turn over number
tpfc-F8	5,10,15-tris(pentafluorophenyl)corrole
TPP	*meso*-tetraphenylporphine

TPPS	tetrakis-(*p*-sulfonatophenyl)porphyrin
TPyP	*meso*-tetrapyrid-4yl4porphine
tpfc	tris(pentafluorphenyl)corrole
TPPS	tetrakis-(*p*-sulfonatophenyl)porphyrin
trz	1,2,3-triazole
UV/Vis	ultraviolet/visible range
vs.	versus
XRD	X-ray diffraction

1 Introduction

1.1 Electron Transfer

One of the fundamental chemical reactions is the redox reaction which is based on an electron transfer (ET) from one center to another center. While redox reactions are known since the beginning of modern chemistry, the principles of electron transfer stayed unclear until the 1940s.[1–5] First experiments regarding the electron self-exchange became possible with the development of nuclear chemistry.[4,5] The availability of radionuclides enabled labeling of metal centers as well as ligands. Besides, new analytical methods were able to characterize the kinetics of fast chemical reactions such as electron transfer cross reactions (**Equation 1**).

$$Fe^{2+} + {}^{*}Fe^{3+} \rightleftharpoons Fe^{3+} + {}^{*}Fe^{2+} \qquad \textbf{Equation 1}$$

Self-exchange electron transfers have several advantages compared to ET between different substrates: Firstly, the products are identical to the reactants which makes the reaction unaffected towards changes of the thermodynamic stability of the reactants and products. Secondly, the electron transfer occurs without bond breaking or formation. In 1956 *Marcus* described redox reactions as fluctuations of coordinates on a potential energy surface without breaking a chemical bond.

1.1.1 *Marcus* Theory

Marcus discovered, that self-exchange reactions between metal ions with nearly no electronic communication (diabatic system) can occur only via thermal excitation, optical charge transfer or quantum tunneling (**Figure 1**).[6]

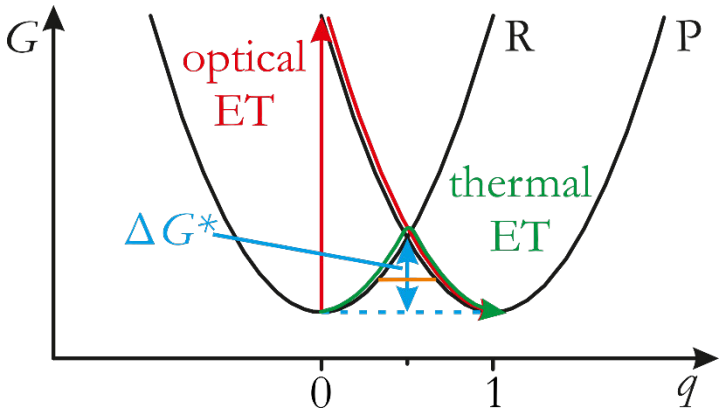

Figure 1: Plot of the diabatic free energy G of the reactants (R) and the products (P) vs. the reaction coordinate q. Additionally, optical ET (red), thermal ET (green) and quantum tunneling (orange) are displayed as well as the activation energy ΔG^* (blue).

Two rules can be applied for a diabatic ET: To perform thermal ET, the reactants have to approach each other on the potential surface but during the thermal or optical electron transfer, the coordinates of the atoms do not change relatively to the electron. Therefore the Franck-Condon principle is satisfied.[7–9] That means, that the thermal and the optical electron transfer have to be significantly faster than the motion of the atoms. Besides, ET can only occur under energy conservation.[10] This is the reason for the ET being possible only on the saddle point of the energy surface. The activation energy has to be absorbed by the system prior to the electron transfer. This can occur by optical excitation or by thermal vibration to higher vibrational modes. The standard free energy ΔG^0 equals zero in self-exchange reactions which makes the optical excitation energy identical with the reorganisation energy. The reorganisation energy λ considers solvational (λ_o) and vibrational (λ_i) components (**Equation 2**).

$$\lambda = \lambda_o + \lambda_i \qquad \textbf{Equation 2}$$

The rate constant k_{ET} for thermal ET depends on the energy barrier ΔG^* and the reorganization energy λ (**Equation 3**).[10,11] The A term depends on the nature of the ET, for example whether it is bimolecular or intramolecular.

$$k_{\mathrm{ET}} = A \exp\left(\frac{-\Delta G^*}{k_{\mathrm{B}} T}\right) \qquad \textbf{Equation 3}$$

The energy barrier ΔG^* itself is related to the change of the standard free energy ΔG^0 and the reorganization energy λ (**Equation 4**).[6,11] Since the standard free energy ΔG^0 is zero in self-exchange reactions, the energy barrier ΔG^* simplifies (**Equation 5**).[11]

$$\Delta G^* = \frac{\lambda}{4}\left(1 + \frac{\Delta G^0}{\lambda}\right)^2$$ **Equation 4**

$$\Delta G^* = \frac{\lambda}{4}$$ **Equation 5**

That is why the correlation between the rate constant of the electron transfer k_{ET} and the change of the standard free energy ΔG^0 can be formulated as followed (**Equation 6**).

$$k_{ET} = A \exp\left(\frac{-\lambda\left(1 + \frac{\Delta G^0}{\lambda}\right)^2}{k_B T}\right)$$ **Equation 6**

ET between two different states can occur in three possible cases (**Figure 2**a). In the *Marcus* normal region ($0 < -\Delta G^0 < \lambda$) the rate constant k_{ET} rises up (**Figure 2**a) black P, **Figure 2**b) left half). For the maximum rate $-\Delta G^0$ equals λ (**Figure 2**a) red P, **Figure 2**b) maximum). Since there is no energy barrier, the ET occurs directly at contact of the redox centers and is therefore only diffusion limited. The *Marcus* inverted region is reached when $-\Delta G$ exceeds λ (**Figure 2**a) blue P). Therefore, the reaction rate decreases again while becoming a more exergonic reaction (**Figure 2**b) right half).

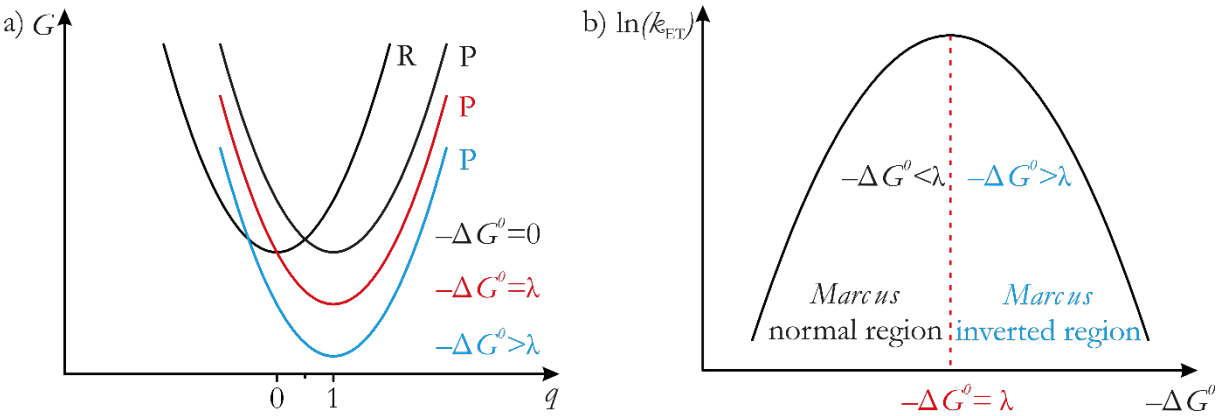

Figure 2: a) Plot of the free energy G vs. the reaction coordinate q for reactants (R) and products (P) for different values of $-\Delta G^0$. b) Plot of $\ln(k_{ET})$ vs. $-\Delta G^0$.

1.1.2 *Marcus-Hush* Theory

Hush expanded the *Marcus* theory by adiabatic systems.[12] Adiabatic systems show electronic communication between the redox centers enabled by a bridging ligand. Specifically, the communication has to exceed the thermal energy k_BT to become an adiabatic system. In the adiabatic system the diabatic free energy surfaces are coupling to adiabatic free energy surfaces where the ground state (GS) and the excited state (ES) are separated from each other (**Figure 3**). This separation is formulated by the electron coupling matrix element H_{AB}.[13] While the adiabatic ground state has a double minimum, the exited state has a single minimum. Both states are separated by an energy gap of 2 H_{AB}. The electronic coupling results in a decrease of the energy barrier which is depending on H_{AB} and two more stabilized minima, while the energy of the excited state increases depending on H_{AB} (**Equation 7**).

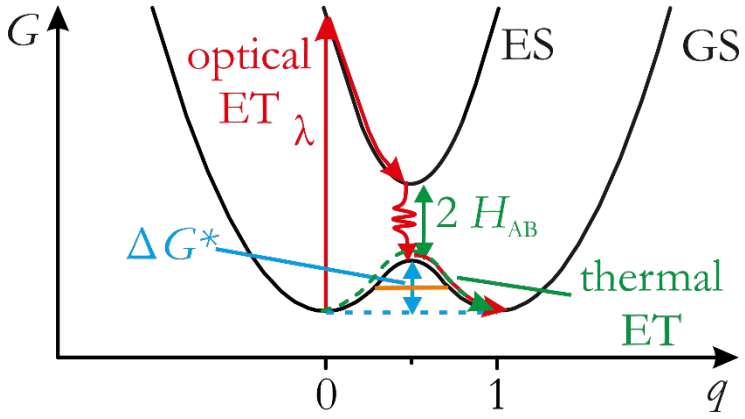

Figure 3: Plot of the adiabatic free energy curves of the ground state (GS) and the excited state (ES) vs. the reaction coordinate *q*. Additionally, optical ET (red), thermal ET (green) and quantum tunneling (orange) are displayed as well as the activation energy ΔG^* (blue).

$$\Delta G^* = \frac{(\lambda - 2H_{AB})^2}{4\lambda} \qquad \textbf{Equation 7}$$

1.1.3 *Robin-Day* classification

Depending on the electronic coupling of the redox centers, three classes of mixed-valence systems can be defined.[14,15] In the *Robin-Day* Class I no electronical communication ($H_{AB} = 0$) exists between both redox centers. Therefore, optical or thermal ET between the redox centers is not possible (**Figure 4**).[14]

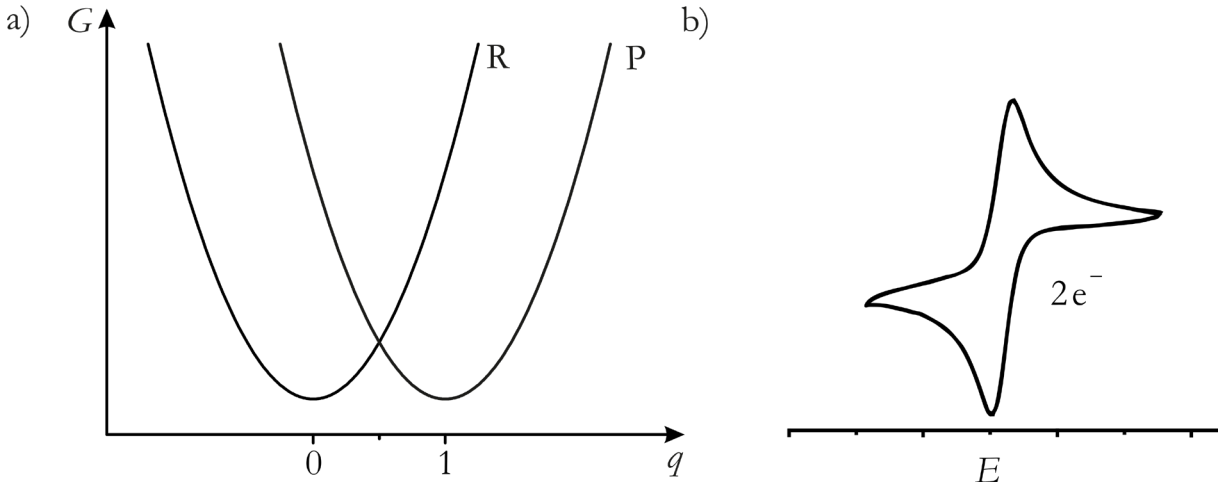

Figure 4: a) Plot of the degenerated free energy surfaces of *Robin-Day* Class I ($H_{AB} = 0$). b) Cyclic voltammogram of *Robin-Day* Class I: Due to inexistent electronic coupling the redox event takes place at the same potential leading to a two electron ET.

If the electronic coupling is smaller than the reorganisation energy λ ($0 < 2\,H_{AB} < \lambda$), it is called a *Robin-Day* Class II system. These interactions are observable by intervalence charge transfer (IVCT) bands in the electronic absorption spectrum or by shifted (lower or higher) redox potentials compared to independent redox centers (**Figure 5**).

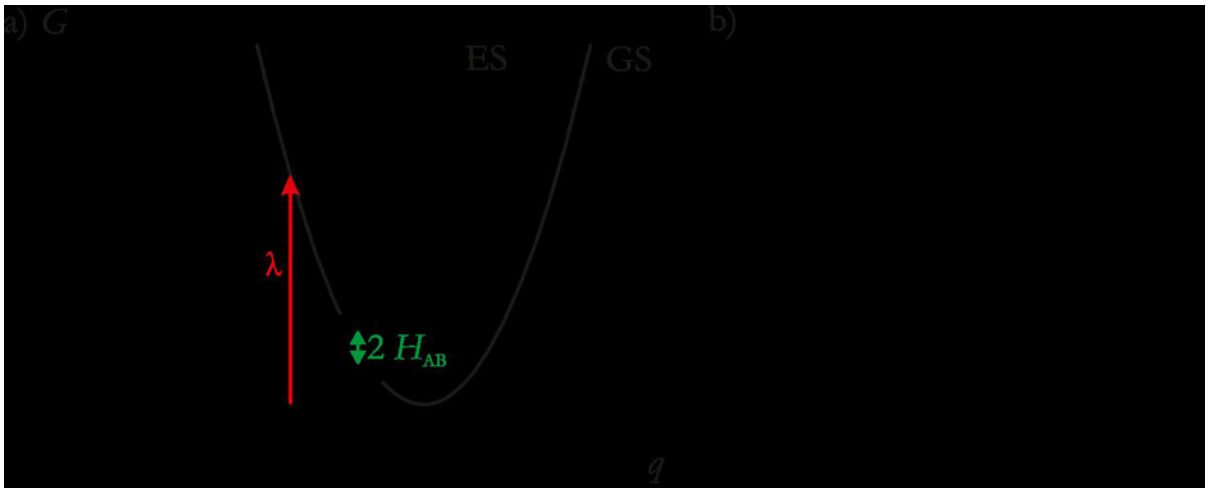

Figure 5: a) Plot of the degenerated free energy surfaces of *Robin-Day* Class II ($0 < 2\,H_{AB} < \lambda$). b) Cyclic voltammogram of *Robin-Day* Class II: Separated redox potentials due to electronic coupling of both redox centers.

H_{AB} can be calculated via shape analysis of the IVCT band by using the absorption maximum $\tilde{\nu}_{max}$, the extinction coefficient ε_{max} of the absorption maximum, the full width at half maximum (fwhm) of the band $\Delta\tilde{\nu}_{max}$ and the distance between both redox centers r_{AB} (**Equation 8**).[14]

$$H_{AB} = 0.0206\frac{\sqrt{\varepsilon_{max}\Delta\tilde{\nu}_{max}\tilde{\nu}_{max}}}{r_{AB}} \qquad \textbf{Equation 8}$$

Robin-Day Class III redox centers have no individual properties since they depend on each other (2 $H_{AB} > \lambda$). Optical excitation does not initiate electron transfer between both redox centers. Instead, the excitation to an electronically excited state with a charge resonance band occurs. Due to the large coupling, the separate minima change into one single well. This can be described as a fully delocalization of the electrons over the system (**Figure 6**).

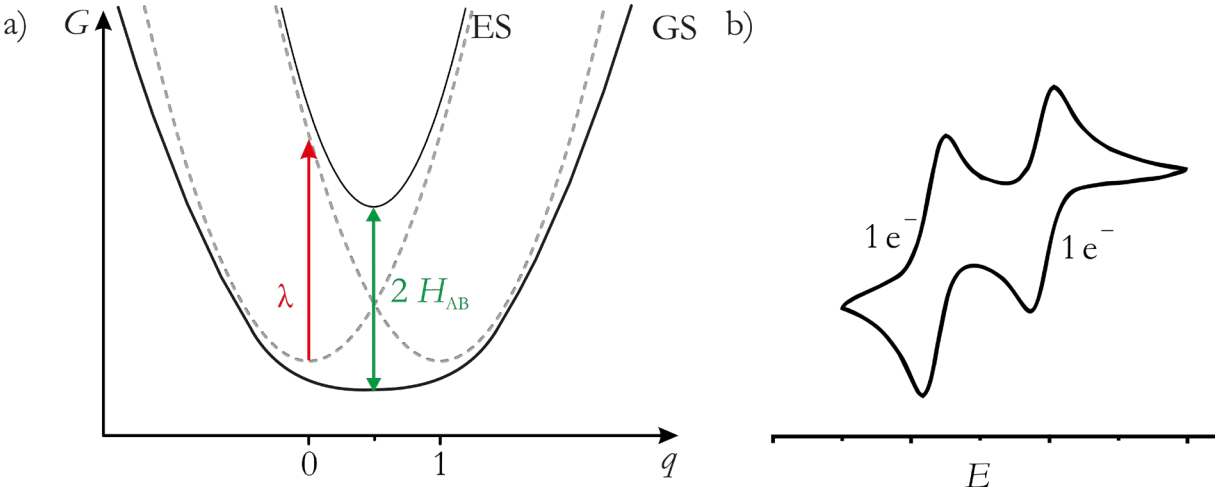

Figure 6: a) Plot of the degenerated free energy surfaces of *Robin-Day* Class III (2 $H_{AB} > \lambda$). b) Cyclic voltammogram of *Robin-Day* Class III: Completely separated redox potential due to the high electronic communication of the two redox centers.

For strongly coupled systems, half the energy of the maximum of the absorption band is defined as H_{AB} (**Equation 9**).[14]

$$H_{AB} = \frac{\tilde{\nu}_{max}}{2} \qquad \textbf{Equation 9}$$

1.1.4 Proton-coupled electron transfer (PCET)

Next to sole electron transfers, there are also proton associated electron transfers. The proton coupled electron transfer (PCET) include multiple electrons and multiple protons transfer and covers a big part of redox reactions. An example is the reduction of dioxygen O_2 to water which requires four electrons and four protons. It was found that $[Fe^{III}(H_2O)_5(OH)]^{2+}$ is less reactive in the oxidation toward $[Ru^{II}(NH_3)_6]^{2+}$ than $[Fe^{III}(H_2O)_6]^{3+}$ by a factor of 6 comparing the reaction rates. Toward $[Ru^{II}(NH_3)_5(H_2O)]^{2+}$ the reactivity is opposite with the same factor of 6 (**Figure 7**). The kinetic isotope difference for $[Ru^{II}(NH_3)_5(H_2O)]^{2+}$ in H_2O and D_2O was determined as $k(H_2O)/k(D_2O)$ ~36. Due to this accelerated reaction rate with H_2O in the inner coordination sphere, a proton transfer from $[Ru^{II}(NH_3)_5(H_2O)]^{2+}$ to $[Fe^{III}(H_2O)_5(OH)]^{2+}$ attending the electron transfer was postulated.

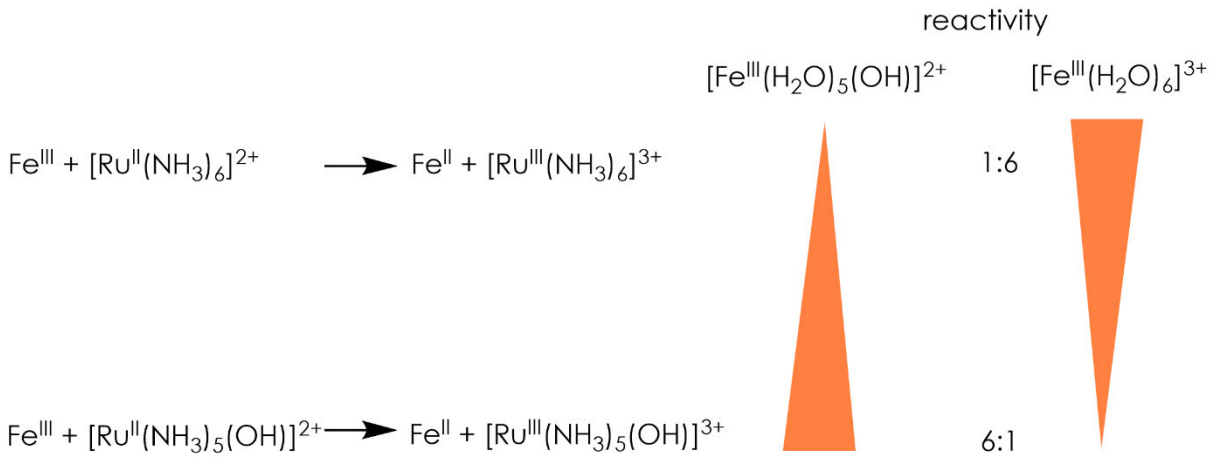

Figure 7: Different oxidation reactivity of Fe(III) compounds toward Ru(III) complexes even though exhibiting a similar driving force.[16]

Actually, the proton associated electron transfer is an omnipresent event in reactions of substrates with acidic protons. This is due to an electron loss leading to increased acidity. While $[Fe^{III}(H_2O)_6]^{3+}$ has a pK_a value of 2.2, the reduced species has a pK_a value of 9.5.[16] Originally, the PCET only referred to reactions where one proton and one electron were transferred in a single and concerted step. Since also reactions containing multiple proton and electron transfers are now called PCET, another term was established for the special case in which only one proton and one electron are transferred. This is the concerted proton-electron transfer (CPET)(**Scheme 1**).[17] It is to be mentioned, that the difference between concerted and stepwise reaction depends mainly on the temporal resolution of the analysis method. A slow method on the one hand is not able to resolve different processes in a fast reaction and therefore classify it as a concerted reaction. A fast method on the other hand may resolve different processes and classify the same reaction as stepwise reaction.

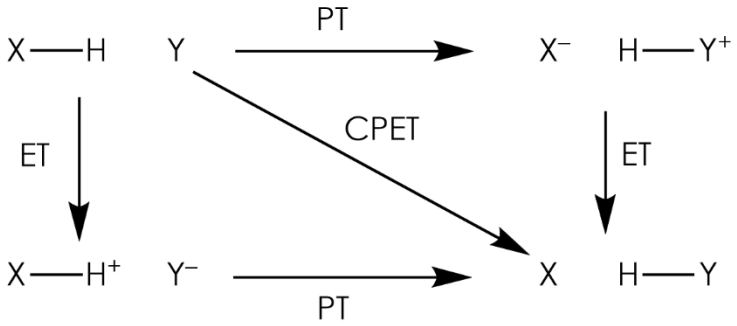

Scheme 1: Stepwise processes versus the CPET pathway from the educt (X-H; left top corner) to the product (Y-H; right bottom corner).

The thermochemistry of a CPET can be explained by a square scheme diagram and five parameters which are all free energies (**Scheme 2**).[17] While the horizontal reactions relates to the acidity of the oxidized and reduced species in the form of the pK_a value, the vertical reactions can be described by the redox potential of the protonated and deprotonated substrate $E°$. Determining the pK_a value can be done by acid base titration applying the *Henderson-Hasselbalch* equation.[18] For

the redox potential this can be done electrochemically by using the $E_{1/2}$ obtained via cyclic voltammetry (CV) as the value for the thermodynamic potential of $E°$.[19]

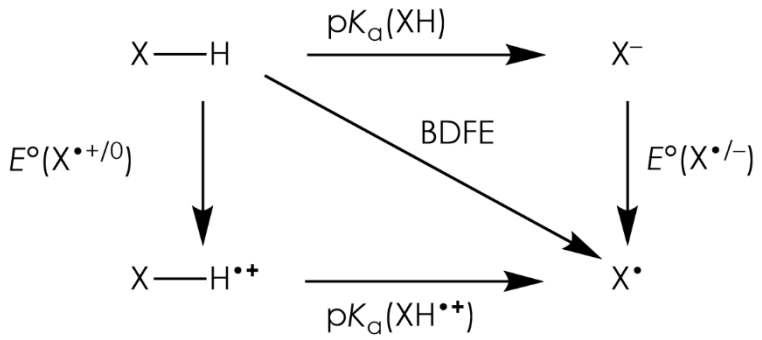

Scheme 2: Thermodynamical square scheme for a PCET reagent.

Using the pK_a values and the E^0 values the corresponding parameters can be calculated (**Equation 10**, **Equation 11**).

$$\Delta G°_{PT} = -RT\ln(K_a) = 2.303RT(\mathrm{p}K_a) = -\left(1.37 \text{ kcal mol}^{-1}\right)\mathrm{p}K_a \qquad \textbf{Equation 10}$$

$$\Delta G°_{ET} = -FE° = -\left(23.06 \text{ kcal mol}^{-1} \text{ V}^{-1}\right)E° \qquad \textbf{Equation 11}$$

Since this theory about PT, ET and CPET uses free energies, it is necessary to use bond dissociation free energies BDFEs to analyze the reaction instead of bond dissociation enthalpies (BDEs). It was also shown that the CPET reactivity correlates with the BDFE and not the BDE in transition metal complexes due to them affording big entropic contributions to the reaction.[20–22] The diagonal reaction in the square scheme diagram (**Scheme 2**) refers to the BDFE. It can be calculated using the pK_a value and the redox potential adding a solvent-dependent thermodynamic constant C_G (**Equation 12**).[23] For a given solvent, C_G is equivalent to the standard reduction potential of the H^+/H^- pair in this solvent.

$$\mathrm{BDFE_{sol}(X–H)} = 1.37\ \mathrm{p}K_a + 23.06\ E° + C_{\mathrm{G,sol}} \qquad \textbf{Equation 12}$$

One reagent that can perform CPET is cobaltocene. It can be used as CPET reagents to increase the efficiency of catalysts for example in the conversion of nitrogen to ammonia. This reaction is a crucial part for life and is also done on a massive scale industrially. Due to the thermodynamic stability of the N≡N triple bond, catalysts and much energy is required to break this bond. $P_3^BFe^+$ (P_3^B = tris(*ortho*-diisopropylphosphinophenyl)-borane) is a catalyst which can perform the conversion in the presence of the strong reductant KC_8 and *Brookhart's* acid $[H(OET_2)_2][BAr^F{}_4]$ at –78 °C. The efficiency and the turnover number of this catalyst can be improved with the use of the weaker reductant decamethylcobaltocene ($CoCp^*_2$) and an acid like diphenylammonium

triflate.[24] The decamethylcobaltocene gets protonated at the Cp* ring forming a reactive PCET reagent. This is due to the weak C-H bond that is formed with a BDFE of less than 29 kcal mol^{-1}.[25]

The CPET is a competitive reaction for the hydrogen evolution reaction (HER) which is the preferred reaction pathway (ΔG_{HER} = –20 to –60 kcal mol^{-1}).[26] Cobaltocene was tested in regard of its ability to redox mediate the electrocatalytic reductive protonation of N_2 and CO_2. It was shown that a protonation at the Cp ring was necessary to generate the CPET reagent. This also changed the σ and the π donor ability into a π acceptor ability due to the formation of the diene ligand. Consequently, the reduction potential also shifts anodically increasing the electron transfer rate and therefore prefer the HER.[25,27] Cyclic voltammetry and density functional theory (DFT) calculation show that the HER is no bimolecular reaction but rather a reduction followed by a subsequent protonation, releasing hydrogen gas (H_2) and cobaltocenium (**Scheme 3**).

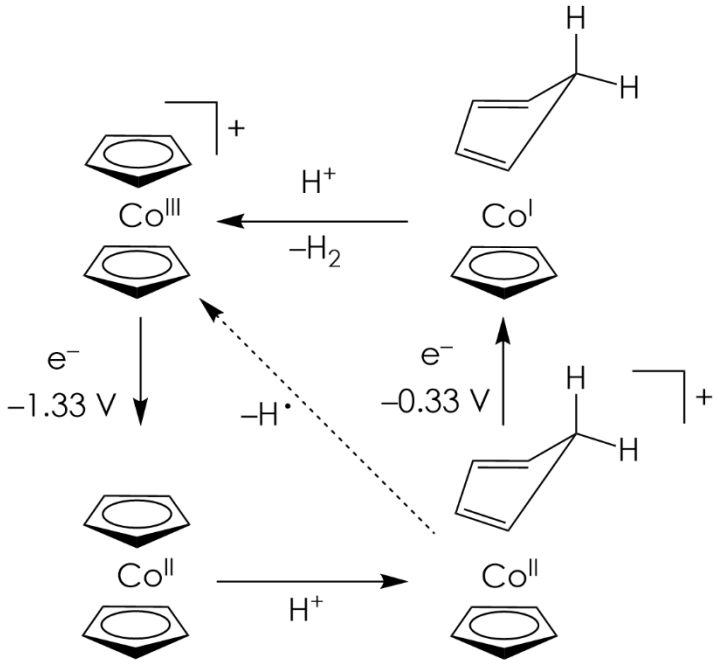

Scheme 3: Electrocatalytic pathway of cobaltocenium. The protonated [(Cp)Co(η^4-C_5H_6)] gets reduced at a potential of $E°$ = –0.33 V vs. FcH/FcH^+, followed by a protonation and hydrogen release. The CPET pathway (diagonal arrow) is not observed.

This is due to a big reorganization of the cobaltocene to form the η^4 coordinated (see **Chapter 1.2**) intermediate as well as to reform the aromatic structure. A combination of a Brønsted acid with a redox mediator lead to the CPET regeant $[(Cp)Co(Cp^{NH})]^+$ (**Scheme 4**) which enables a controlled reductive CPET by an increased protonation. In contrast to cobaltocene, in the anilinium substituted derivative, the protonation takes place at the nitrogen and therefore does not afford a high reorganization comparable to cobaltocene.

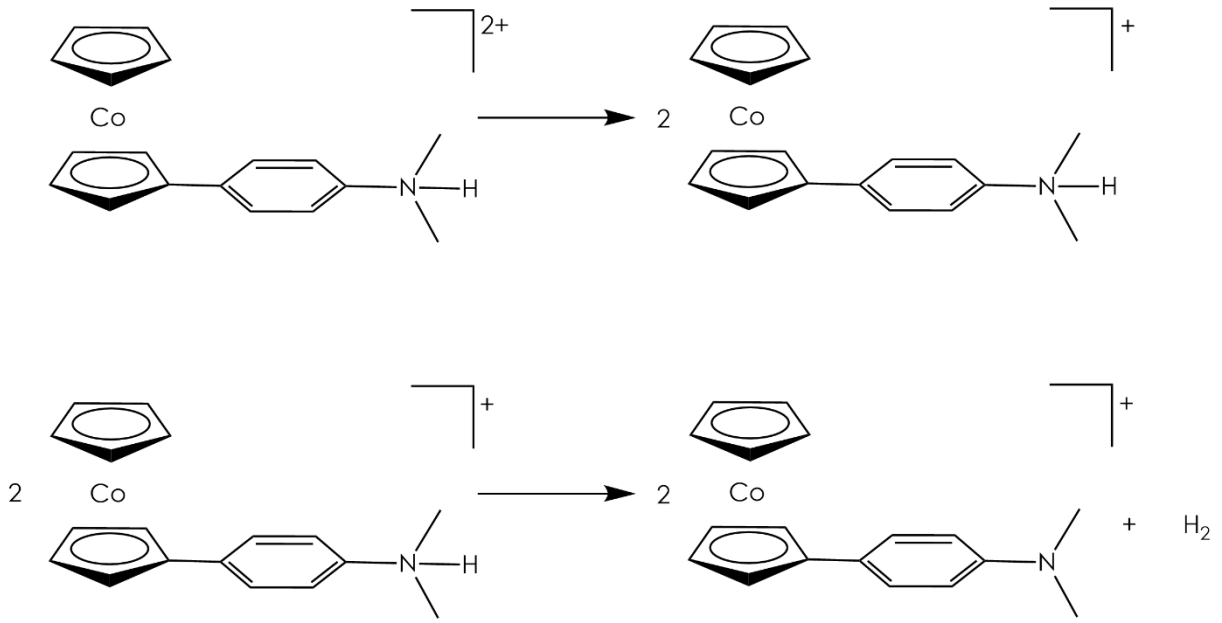

Scheme 4: Proposed mechanism of bimolecular HER.

The BDFE of $[(Cp)Co(Cp^{NH})]^{+}$ (**Scheme 5**) shows interesting behavior. While the BDFE of $[(Cp)Co(Cp^{NH})]^{2+}$ with 79 kcal mol^{-1} correlates well with the thermochemical equivalent, the reduction of the Co^{III} to Co^{II} decreases the BDFE to 39 kcal mol^{-1}.[26] This is a strong weakening of the BDFE compared to previous studies where the change of oxidations state only resulted in the lowering of the X–H bond strenght by 10 to 15 kcal mol^{-1}.[28,29]

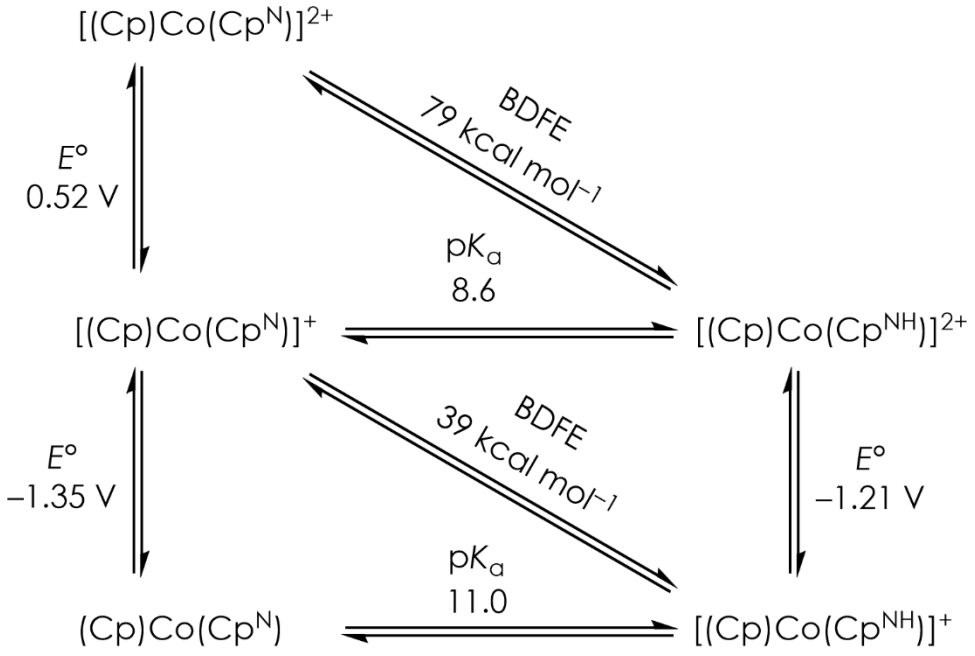

Scheme 5: Thermochemical properties of $[(Cp)Co(Cp^{NH})]^{+}$ and $[(Cp)Co(Cp^{N})]^{+}$.

Further electron transfer and proton transfer is unfeasible for $[(Cp)Co(Cp^{NH})]^{+}$, so it reacts in a bimolecular reaction forming $[(Cp)Co(Cp^{N})]^{+}$ and hydrogen gas (See **Chapter 1.5.4**) (**Scheme 4**).

Since a bimolecular reaction depends on the concentration of a substrate, decreasing it is supposed to inhibit the hydrogen formation.

1.2 Metallocenes

In 1951, ferrocene was discovered by *Kealy/Pauson*[30,31] and *Tebboth/Tremaine*[32] independently of each other. This marked the beginning of a new chapter in the field of organometallic chemistry – the metallocenes were discovered. Today more than 80% of metal organic complexes are bi cyclopentadienyl (Cp) complexes.[33] Metallocenes typically consist of two Cp anions and one metal center in between.[34] There are two possible conformations for this "sandwich-like" metallocenes. Due to the rotation of the Cp rings, there can be a staggered and an eclipsed rotamer (**Figure 8**).

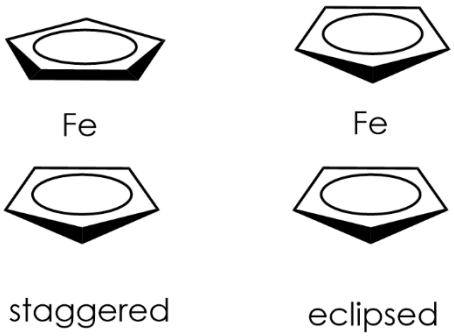

Figure 8: The two different rotamers of ferrocene.

In 1973, *E. O Fischer* and *G. Wilkinson* won the Nobel Prize in Chemistry "for their pioneering work, performed independently, on the chemistry of the organometallic, so-called "sandwich compounds".[35] They revealed the structure of ferrocene and determined the five carbon atoms of each Cp ligand to contribute equally to the bonding.[36,37] Some years later, that was proven by X-ray diffraction (XRD) of ferrocene.[34] That is why the need for a new nomenclature in organometallic chemistry was forced, in order to describe this different types of bonding. Therefore, the use of *hapticity* and the greek letter η was created by the proposal of *Cotton*.[38] The new nomenclature describes the equal bonding of all atoms of the Cp ligand to the metal center as *pentahapto* (η^5) bonding. This is the most common bonding type for Cp containing metallocenes. A η^3 coordination would be a coordination between metal atom and three of the Cp carbon atoms. Despite, there are also some other examples like uranocene, which is surrounded by two cyclooctatetraene rings with a *octahapto* (η^8) bonding.[39,40]

With the two Cp anions, each containing six valence electrons and the Fe^{2+}-ion with a d^6 electron configuration, ferrocene fulfills the 18-electron rule.[41–43] Therefore, it is a quite stable metal organic complex. At a potential of E^0 = 0.4 V vs. SHE[44,45], ferrocene (FcH) is reversibly oxidized to the ferrocenium ion (FcH^+). The oxidation is a reversible process, so following re-reduction leads to the neutral complex (**Figure 9**). The redox reaction involves a reliable single electron transfer.

Reduction of ferrocene comes with the effect of bond weakening which is bigger than the increase of charge at the metal center. That results in an increasing Fe(III)-Cp distance. The increased distance occurs at the z axis and lowers the energy of the d_{z^2} orbital, which leads to an inversion of the e_{2g} and a_{1g} orbitals (**Figure 9**).[46] Both components are stable in different nonaqueous solvents and their redox potential just slightly changes in different solvents. Therefore, the ferrocene/ferrocenium couple is frequently employed as an internal redox standard to report redox potentials in nonaqueous solvents.[47,48]

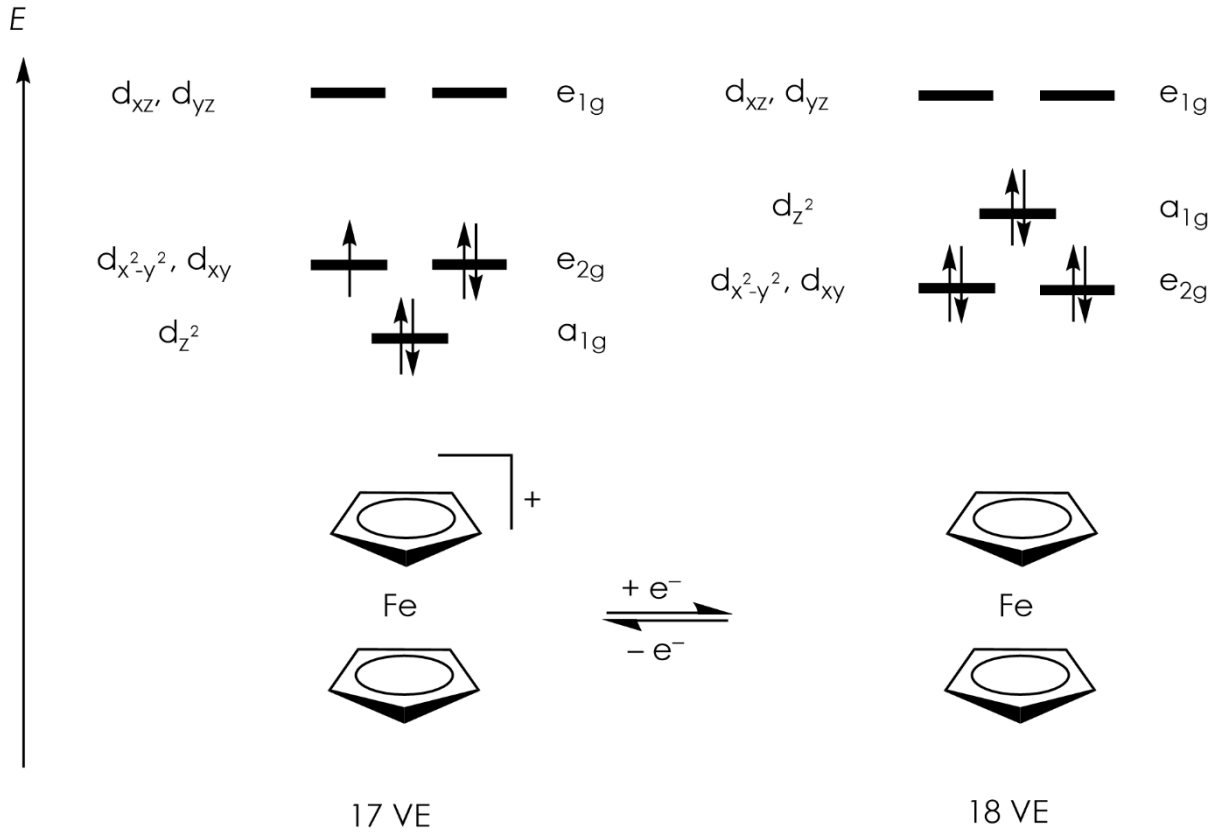

Figure 9: Electron configuration regarding the metal d-orbitals of the ferrocenium cation (left) and ferrocene (right).

Ferrocene and ferrocenium can be distinguished by UV/Vis spectroscopy due to their different electronic configurations. Ferrocene shows an absorption band at 440 nm (≈ 22.700 cm^{-1}) at room temperature in acetonitrile, methanol and tetrahydrofuran (THF).[49,50] This is the commonly observable absorption band, which is responsible for the typical color. It can be assigned as *Laporte* forbidden d-d transition of the ferrocene ligand field, which is the reason for the relatively weak absorption (ε = 91.5 M^{-1} cm^{-1}).[50] Derivatization of ferrocene may result in a shift of the absorption band (λ = 440–490) but does not change the nature of the electron transitions of the ferrocene complexes.[49–52] Since oxidation changes the electronic configuration, the corresponding ferrocenium ion owns different electronic transitions. Ferrocenium itself shows a set of up to four absorption bands at around λ = 485 nm, 560 nm, 600 nm and 640 nm. The energetically lowest transition was proven of being a ligand to metal charge transfer (LMCT).[46,49,53,54] The LMCT is not Laporte forbidden which is the reason of the higher absorption intensity compared to its neutral equivalent (ε ≈ 8.000 M^{-1} cm^{-1}). On the other hand, the first three absorption bands are assigned

to d-d transitions and thus explain the lower intensity compared to the absorption at $\lambda = 640$ nm. Other metallocenes show similar behavior. Cobaltocenium complexes as the 18 electrons equivalent of cobalt metallocenes show absorption bands at $\lambda \approx 420$ nm.[55]

In a mixture of ferrocene and ferrocenium, this couple undergoes electron self exchange with an electron transfer from ferrocene to ferrocenium.[56,57] The self exchange is not much affected by the dielectric properties of the solvent, which is opposing the *Marcus* theoretical model for electron exchange. Even different substitution patterns with different substituents do not have a big effect on the electron exchange.[56] The rate constants k_{ex} for the ferrocene ferrocenium couple can be determined as a function of electrolyte concentration in different solvents like acetonitrile, acetone, nitrobenzene and methanol by ^{1}H NMR line broadening technique.[57] Depending on the solvent and the electrolyte concentration the rate constant for the ferrocene ferrocenium couple lies between $k_{ex} = 5\ 10^6 - 2\ 10^7\ M^{-1}s^{-1}$.[56,57] The electron self exchange can also be seen in the absorption spectra in the NIR region between $\lambda_{max} = 1150–1400$ nm. This absorption band can be assigned as the intervalence charge transfer transition from a ferrocene to a ferrocenium.[52,58,59]

Further metallocenes-analogues of ferrocene with two Cp anions like chromocene and cobaltocene were discovered a few years later[60–68] as well as other "sandwich" type metalorganic compounds with different cyclic ligands, as cyclooctatetraene in uranocene.[39] In a broader sense, also "half sandwich complexes", with only one cyclic ligand,[69–71] can be called metallocenes. Despite, generally only the "sandwich" compounds with two Cp anions are considered to be metallocenes.

Similar to the iron metallocene, all group 8 metal metallocenes are particularly stable due to the 18-electron rule. Electron rich metallocenes from the group 9 to group 12 elements try to reduce their electron richness by oxidation or by lowering the ligand coordination (hapticity). Cobaltocene with its d^7 ion Co^{2+} is a 19 valence electrons compound. Oxidation of cobaltocene leads to the formation of the cobaltocenium ion (18 valence electrons), which is a stable compound (**Figure 10**). Nickelocene with d^8-Ni^{2+} metal center and therefore 20 valence electrons is reacting similar by getting oxidized twice. Both metallocenes are extremely air sensitive because of "extra" electron(s) located in antibonding orbitals (**Figure 10**). Most of the nickelocene chemistry is characterized by its tendency to donate electrons.[72]

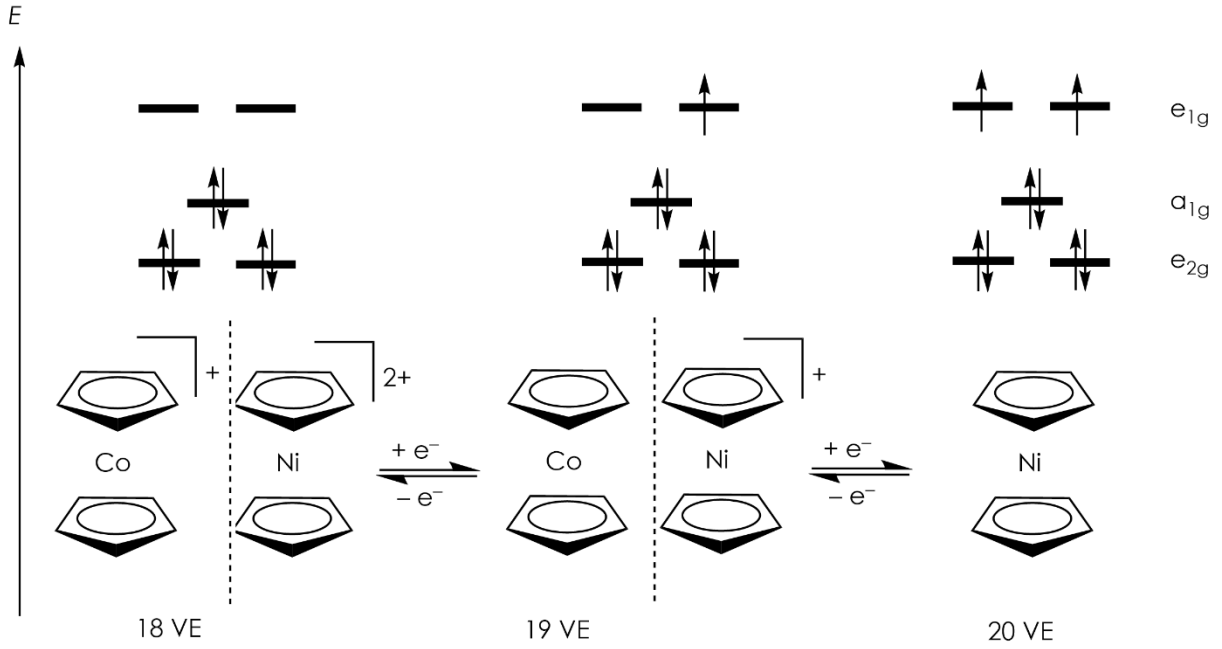

Figure 10: Electronic configuration of cobaltocene/cobaltocenium and nickelocene/nickelocenium.

1.2.1 Ferrocene derivatization

Chemical reactivity of ferrocene shares similarities with the chemical reactivity of aromatic compounds. This is caused by the aromatic caracter of the Cp ligands. Both systems allow to exchange substituents by electrophilic aromatic substitution. Monolithioferrocene and 1,1'-dilithioferrocene can be synthesized selectively by the use of different butyllithium derivatives. Using *n*-butyllithium results in the formation of 1,1'-dilithioferrocene (**Scheme 6** right)[73] because the *n*-butyllithium reacts not selective and therefore lithiates both Cp rings. Otherwise, using *t*-butyllithium results in the formation of monolithioferrocene (**Scheme 6** left).[74]

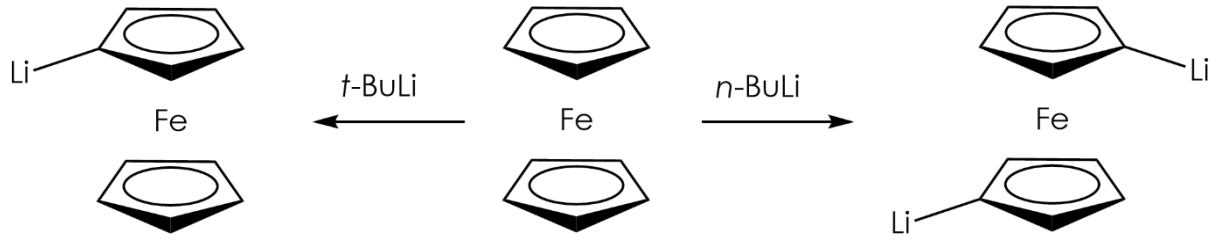

Scheme 6: Regulation of the amount of substitution of Cp rings by the use of different substituted lithium compounds.

Commonly used reactions for the derivatization of ferrocene are the *Friedel-Crafts* reactions to alkylate or acylate the Cp rings by activation with *Lewis* acids like aluminium chloride or iron(III)-chloride. Executing the *Mannich* reaction with ferrocene, formaldehyde and the secondary amine 1,1-dimethyl amine, lead to the formation of *N*,*N*-dimethylaminomethylferrocene (**Scheme 7**a).[75] To circumvent the low C-H acidity, it is necessary to use *Brønsted* acids to activate the ferrocene by protonation of the iron center (**Scheme 7**b).[76] In a non *Mannich* type reaction milieu, the usage of

acetic anhydride or acetyl chloride with the catalyst phosphoric acid gives acetylferrocene or 1,1'-diacetylferrocene (**Scheme 7**c) in a straightforward synthesis.[77–81] Changing the acetic anhydride with another, preferably symmetric organic compound, leads to the formation of different derivatives of alkanoyl ferrocenes.[78] Tributyl borate reacts with monolithioferrocene and 1,1'-lithioferrocene to the ferrocenyl boric acid respective ferrocenyl diboric acid (**Scheme 7**d).[82] Similar to alkyl boric acids, in the presence of basic Ag_2O, the ferrocenyl boric acids "disproportionate" forming ferrocene and biferrocene. The reaction of ferrocenyl boric acid with mercury(II)-chloride leads to the formation of ferrocenylmercurychloride while the reaction with $CuCl_2$ and $CuBr_2$ results in halogen ferrocenes (**Scheme 7**d).[82]

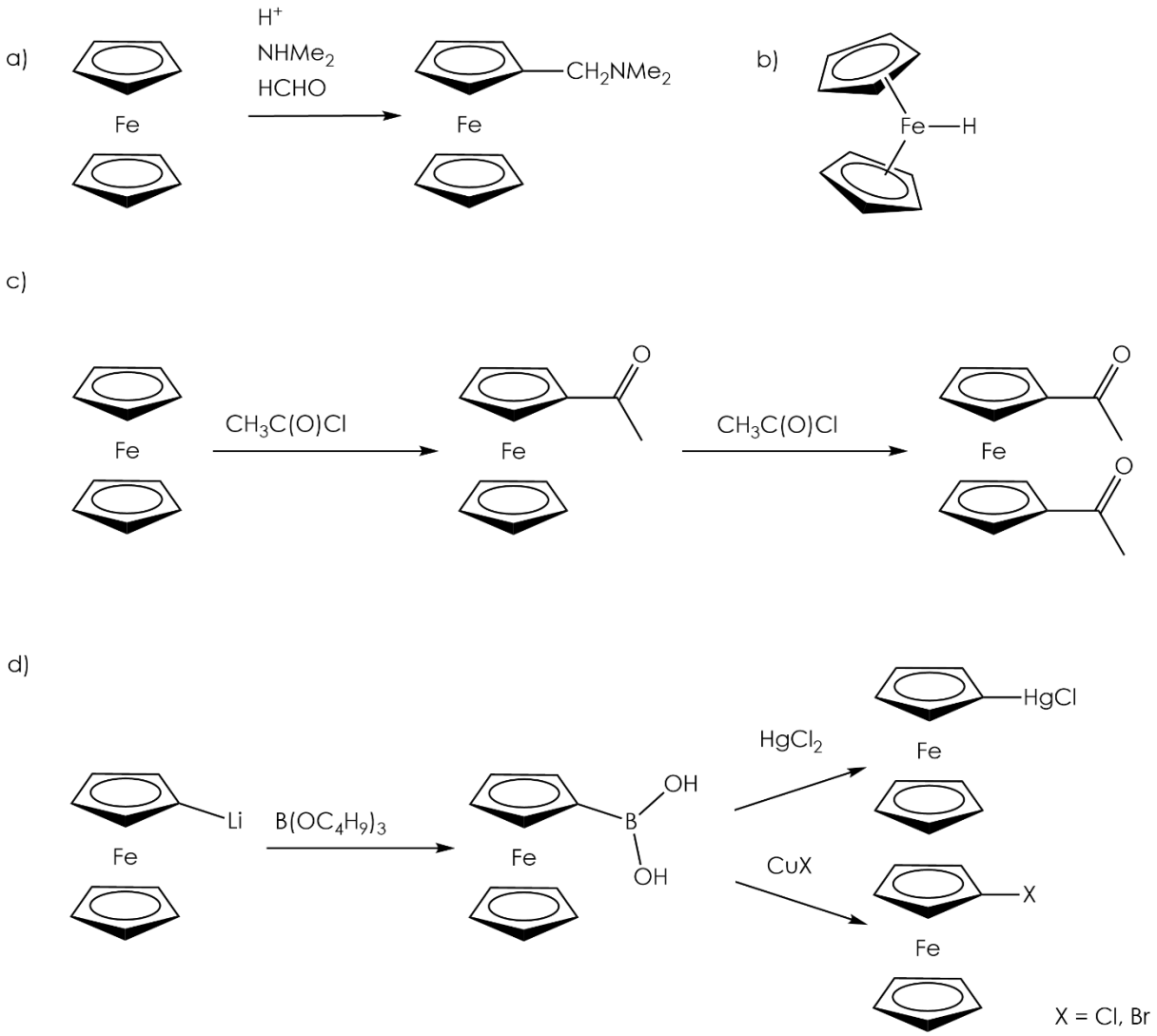

Scheme 7: Reactions of ferrocenes with electrophiles. a) *Mannich* reaction of ferrocene. b) Protonated ferrocene with a metal hydrogen bond at the iron center. c) Acylation of ferrocene with acetic anhydride or acetyl chloride. d) Reaction of lithioferrocene with boric acid and with metalchlorides.

Because of this reactivity, ferrocene has the advantage, that introducing functional groups is straight forward. Introducing one formyl group to synthesize formyl-ferrocene can be achieved in different ways. The formation of formyl-ferrocene by the *Sommelet* method out of ferrocenylmethyltrimethylammonium iodide or the synthesis starting with ferrocene and *N*-

methylformanilide was reported in the 1950s.[83] Despite this, it is also possible to produce formyl-ferrocene from monolithioferrocene and 1,1'-dilithioferrocene by using *N*,*N*-dimethylformamide to introduce the formyl group (**Scheme 8**a).[84–87] With the *Wittig* reaction and the *Horner-Wadsworth-Emmons* reaction the formyl group can be converted to vinyl groups (**Scheme 8**b),[88–91] Glycol as protective group for the formyl-ferrocene can be introduced forming an acetal (**Scheme 8**c).[92,93] If the formyl group is protected, it is possible to synthesize a tri- and tetra- formylated ferrocene derivative. This can be done by using the direct ortho metalation with an aliphatic organolithium reagent and subsequent formylation with *N*,*N*-dimethylformamide. Following deprotection leads to the tri- and tetra- substituted ferrocene (**Scheme 8**d).[92,93] Another possibility to substitute ferrocene with increasing number of the same substituent is the use of the *Lochmann-Schlosser* superbase LiR + 4 $KOCMe_2Et$ with R being either neopentyl or *n*-butyl.[94,95] It is possible to deprotonate the ferrocene up to four times, twice per Cp ring in 1 and 3 position. Following functionalization with a carboxy group by the use of carbondioxide and following protonation leads to carboxylic acids. These acid groups can be methylated to methyl esters (**Scheme 8**e).[94,95] Ferrocene shows to be a versatile compound that can be conjugated to a vast amount of different building blocks.[96–123]

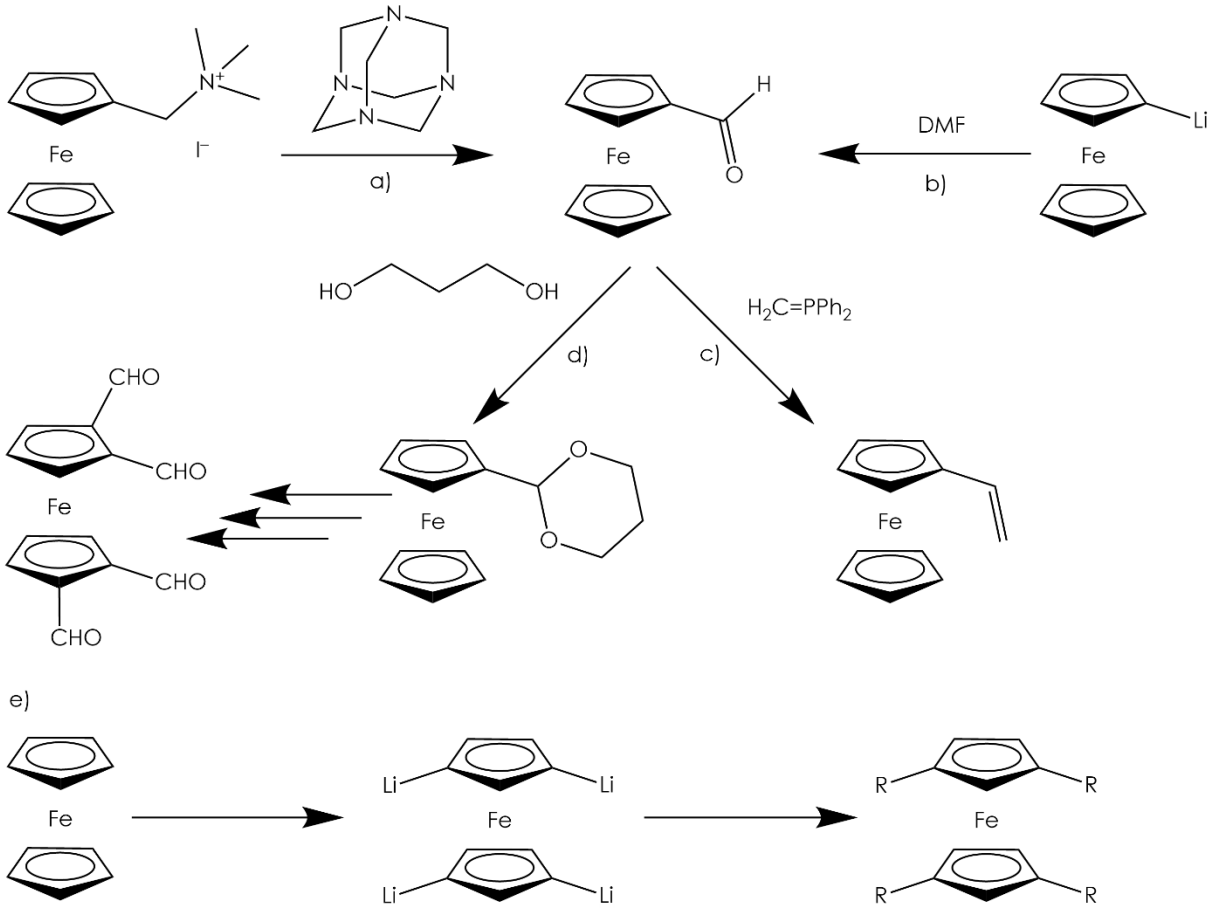

Scheme 8: Functionalization reactions for ferrocene. a) *Sommelet* reaction to synthesize formyl-ferrocene. b) Substitution of monolithioferrocene with formyl group by using DMF. c) Convertion of the formyl group to vinyl group by *Wittig* reaction. d) Introduction of protecting group into formyl group and following formylation. e) Deprotonating ferrocene for times with *Lochmann-Schlosser* superbase and following functionalization.

1.2.2 Cobaltocenium chemistry

Cobaltocene is a 19 valence electrons compound with an electronic configuration of $(e_{2g})^4(a_{1g})^2(e_{1g})^1$ and therefore not stable towards oxidation.[49,124,125] In most cases, to carry out chemical reaction it is necessary to oxidize cobaltocene to the cobaltocenium cation. In case of cobaltocene/ cobaltocenium (CcH/CcH^+) redox couple, the redox potential lies at E^0 = –1.33 V (vs. FcH/FcH^+).[126] The cobaltocenium cation is an 18 valence electrons compound, isolobal to ferrocene with an electronic configuration of $(e_{2g})^4(a_{1g})^2$ and an ^1A_g ground state and therefore stable against further oxidation.[49,124,125] But due to the positive charge, which attracts nucleophiles to attack the Co^{III} center and its high reduction potential, typical ferrocene chemistry does not work with cobaltocenium. This leads to an overall lower number of obtainable substitution patterns for cobaltocenium as well as challenging synthetic routes.[127,128] Hence, there exist just a few applications of the Cc/Cc^+ couple.[55,129–138] In the past decade, the group of *Bildstein* published new possibilities for the synthesis of monosubstituted cobaltocenium compounds (**Scheme 9**). Cobaltocenium derivatives with amino-, carboxy-, halogen- and alkylgroups became accessible.[127,139,140] As a result, *Heck* developed more molecules containing cobaltocenium like nitrocobaltocenium and hydroxycobaltocenium,[141] which can be used for purposes such as redox switchable catalysts[142] or building blocks for metallomacromolecules.[143]

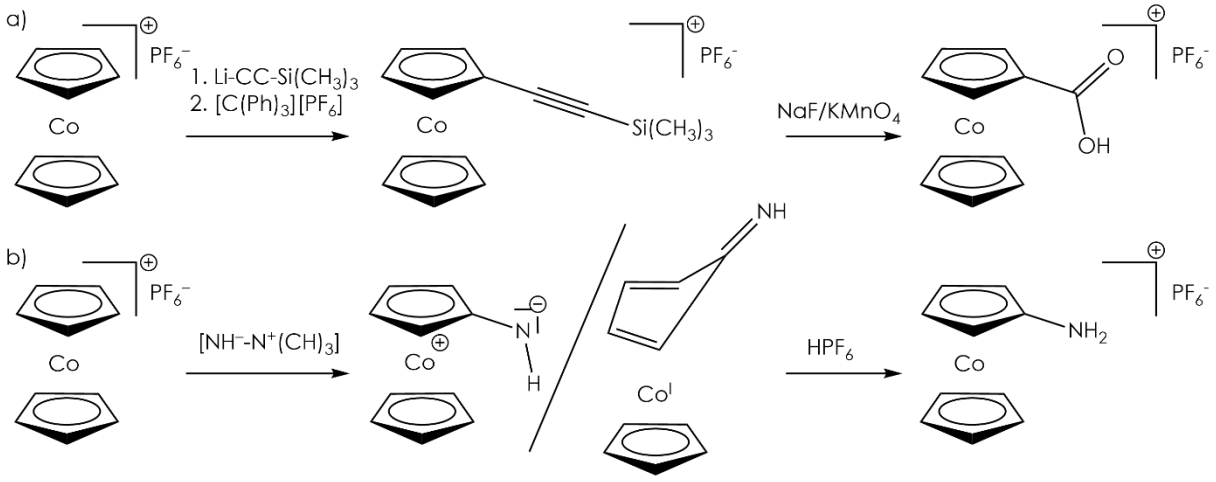

Scheme 9: Bildstein group syntheses of a) carboxycobaltocenium hexafluoridophosphate and b) aminocobaltocenium hexafluoridophosphate.

Previous work of *Heinze* and *coworkers* was focused on ferrocene chemistry, like the progress of redox-active foldamers,[52,58,144–147] ferrocene-based redox switchable catalysts,[148–151] ferrocene amide ion sensors[152,153] and amide-linked ferrocene-chromophore conjugates.[120,121,124,129] Therefore, the transfer of this concepts to cobaltocene due to the extended substituted cobaltocene portfolios is feasible and resulted in the synthesis of an amide-linked zinc(II) porphyrin-cobaltocenium dyad.[55] Substituting the ferrocene moieties by an isoelectronic and isosteric cobaltocenium results in the addition of a positive charge and the adjustment of the redox potential towards a more negative value, which makes this building block attractive for the aformentioned

applications.[139,141,143,154,155] Synthesis of cobaltocenium derivatives from scratch with substituted cyclopentadienides and $CoCl_2$ only leads to 1,1' disubstituted cobaltocenium ions.[156–158] Alternatively, it is possible to insert an isonitrile into a cyclopentadienyl pentadienyl cobalt(III) complex performing a ring closure resulting into the [CpCo(η^5-$C_5Me_4NH^tBu$)] complex.[159] Starting from the nitrocobaltocene $[Cc\text{-}NO_2]^+$ with the substitution of the nitro group with *n*-butyl amine results in the formation of *n*-butyl amino cobaltocenium.[141] By using the optimized procedure from *Bildstein* to synthesize $[Cc\text{-}NH_2]^+$ out of $[Cc\text{-}COCl]^+$ and NaN_3,[139] the amine became available. Thus, it was possible to expand the portfolio of amide bridged bimetallocenes from *N*-ferrocenyl substituted (**Figure 11**a and **Figure 11**b) to *N*-cobaltocenium substituted (**Figure 11**c and **Figure 11**d) bimetallocenes.[160]

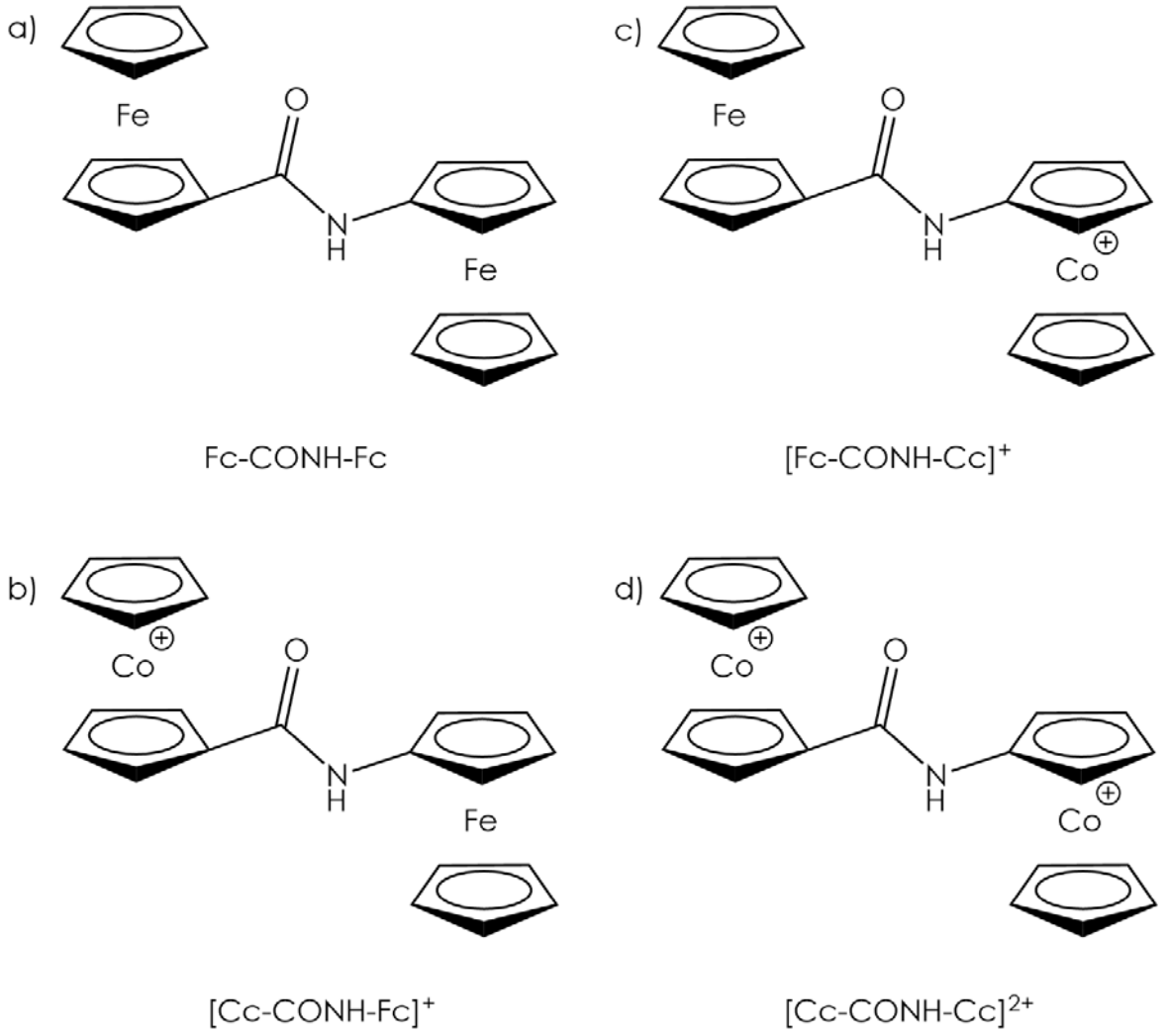

Figure 11: Amide bridged bimetallocenes with Fc and Cc^+ units. a)[145,146,161], b)[129], c)[160], d)[160]

Amino cobaltocenium has to be activated towards acylation due to its low basicity and nucleophilicity (pK_b = 15.6).[128] The activated amine can react with the corresponding acid chlorides to form amides. Several former attempts to couple the cobaltocenium amine with strong electrophiles, by activation of the cobaltocenium amine due to a metal-centered reduction or by deprotonation of the amino group with several bases, failed. The only known pathway to

successfully and reliable activate the amine is deprotonation with sodium hydride.[160,162] Density functional theory (DFT) calculations were performed to gain insight on the structure of the deprotonated amine (B3LYP/def2-TZVP/PCM THF). The calculations suggest an imine structure with a bent Cp ring which is therefore η^4 bonded to a cobalt(I) center (**Scheme 10**).[160]

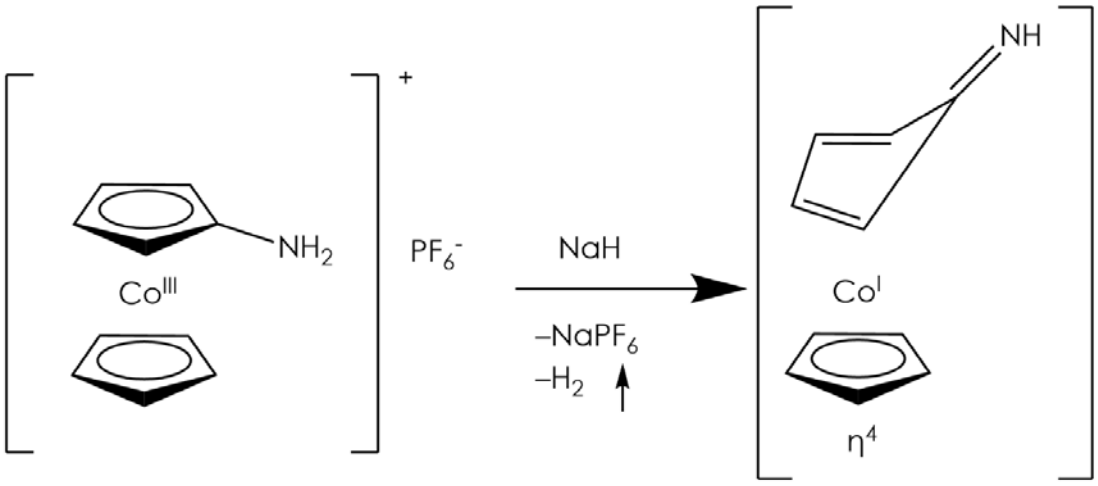

Scheme 10: Deprotonation of the amino cobaltocene forming the imine like structured η^4 compound.

1.3 Carbenes

Carbon is a well known element which affords eight electrons and therefore four electron pair bonds. In difference to the "standard" electron octett carbon atoms, carbenes are neutrally charged carbon atoms with two substituents and two valence electrons forming an electron sextet.[163,164] Despite being postulated by *Curtius* and *Staudinger* between 1885 and 1912,[165,166] carbenes were first used in the 1950s as an *in-situ* C_1-building block in organic synthesis (**Equation 13**).[167,168]

$$CHCl_3 + NaOH \rightarrow :CCl_2 + H_2O + NaCl \qquad \textbf{Equation 13}$$

Due to the electron sextet, carbenes are highly reactive and the isolation of a monomer failed. Promising experiments by *Wanzlick* in the 1960s failed, too, due to small donor substituents, which led to dimerization (**Figure 12**).

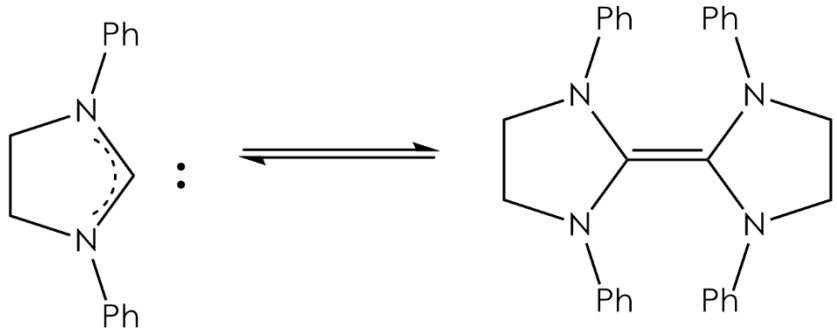

Figure 12: *Wanzlick* equilibrium with the not stable bis(dimethylamino)carbene.

A well known class of carbene complexes are the *Fischer* carbene complexes[169] which reacts as a starting material in the *Dötz* reaction (**Figure 13**a).[170] *Fischer* type carbene complexes are singlet carbenes and contain π-donating organic groups and π-accepting metal ligands due to the weak back bonding metal center.[171] Another class of carbenes are *Schrock* carbene complexes, with the so-called first and second generation *Grubbs* catalysts as prominent examples (**Figure 13**b, **Figure 13**c).[172] *Schrock* type carbenes complexes are triplet carbenes and have a strong back bonding metal center without π-accepting metal ligands. Due to the π-donating groups these carbenes are nucleophiles.[171]

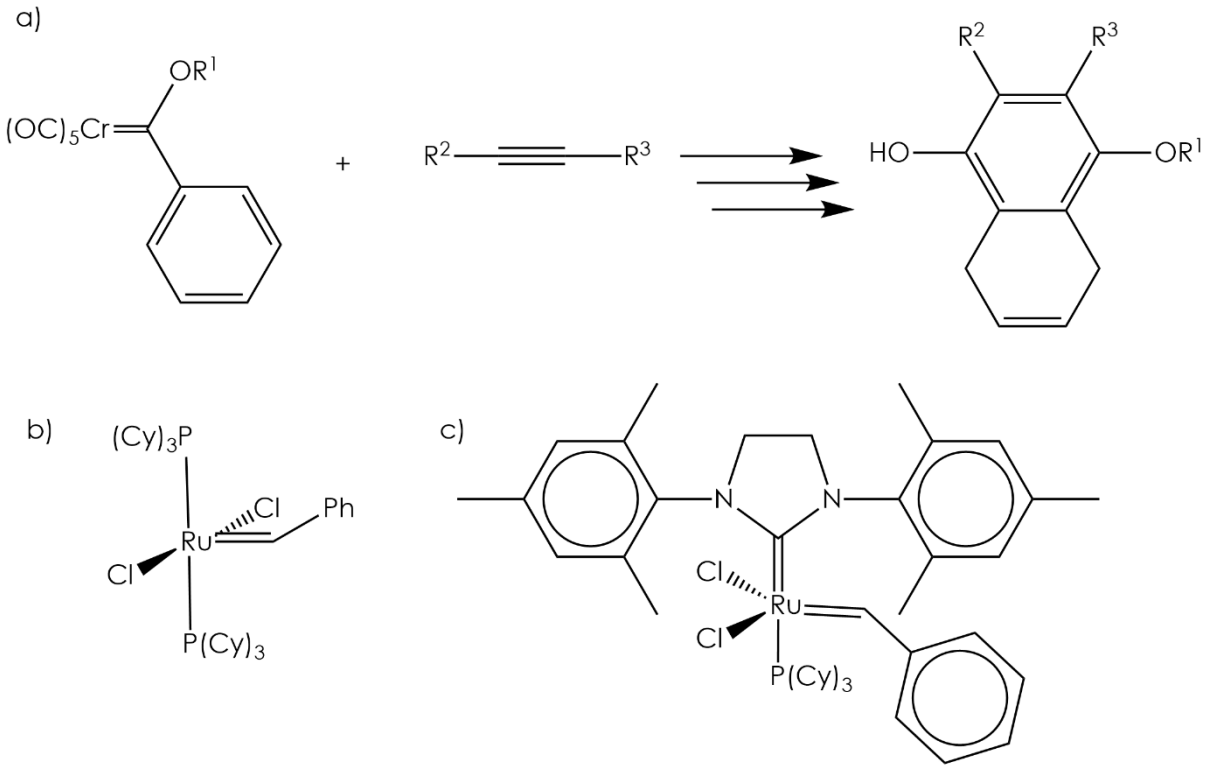

Figure 13: a) *Dötz* reaction to benzo-annulate *Fischer* carbenes. b) *Grubbs* first generation catalyst. *c) Grubbs* second generation catalyst.

1.3.1 Stabilization of carbenes

Electronic and steric effects have a high impact on the multiplicity of the carbene carbon in the ground state. The instability of carbenes origins in the electron sextet, forming electron poor compounds. Stabilization occurs by increasing the electron density at the carbene carbon by inserting π-electron donating substituents in α-position to the carbene carbon. Pnictogenes are suitable elements for this purpose, as they donate electron density to the carbene carbon by its +M-effect. Hitherto, all meanwhile isolated acyclic singlet carbenes possess at least one phosphano or amino group to stabilize the carbene carbon.[173] The main reason for their stabilization is a bigger steric demand (compared to chalcogenes) due to the free electron pair and two more substituents at the pnictogene. A higher steric demand prevents dimerization. Chalcogenes own one additional substituent which leads to a decreased steric demand and are therefore less suitable for stabilization of the carbene carbon.

Based on the substituents, there are two types of acyclic carbenes. The classification depends on the dominant π donor – amino carbenes and phosphano carbenes. A difference in the stabilization between these species originates from the energy needed to achieve planarity for both elements (nitrogen: 21–42 $\frac{kJ}{mol}$; phosphorus: 126–147 $\frac{kJ}{mol}$).[174] That means phosphorus is a worse π-donor than nitrogen and therefore offers less stabilization of the carbene carbon.[175] In the 2000s, *Bertrand* demonstrated that only one of this groups is required to isolate free carbenes. Therefore, it is possible to access different substitution patterns by variation of the second substituent.[173] Because of this variety, there is another classification of carbenes with three stabilization modes. The amino or the phosphano substituents always provide an electron donation effect which is the push effect. The second substituent can be electron withdrawing (pull), electron donating (push) or not being involved electronically (spectator) (**Table 1**).

Table 1: Examples for stabilization modes of acyclic carbenes.

substitution pattern	carbene	substituent	stabilization
phosphano-phosphonio	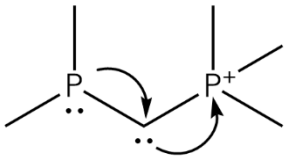	P	push-pull
diamino		N	push-push
amino-aryl	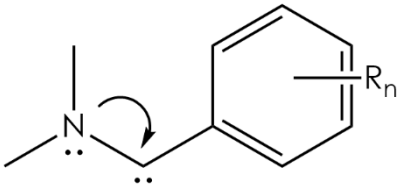	N	push-spectator

Diamino carbenes are notable carbenes because they are stabilized by a push-push effect. They own two strong π-donors which stabilize the carbene, forming a neutral and strong *Lewis* base.[173] An example for this is the *N*-heterocyclic carbene (NHC) 1,3 diisopropyl-4,5-dimethylimidazol-2-ylidene (**Figure 14**) with a pK_a value of 24 in [d_6]-DMSO, which makes it one of the strongest neutral bases known.[176] This carbene is stabilized by the two nitrogen atoms inside an imidazole frame through the push-push effect.

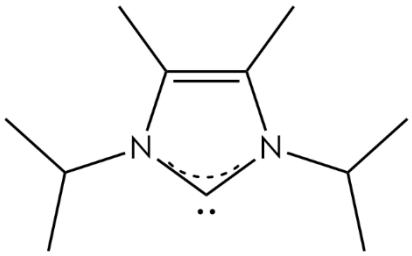

Figure 14: Structure of the 1,3 diisopropyl-4,5-dimethylimidazol-2-ylidene with a pK_a value of 24 in [D_6]-DMSO.

1.3.2 *N*-heterocyclic carbenes

Nowadays there are a lot of applications for carbene complexes in homogeneous catalysis.[163,164] While the first free carbene was synthesized by *Bertrand* in 1988,[177] the first free and stable NHC was synthesized by *Arduengo* in 1993 (**Figure 15**, **Figure 16**a).[178]

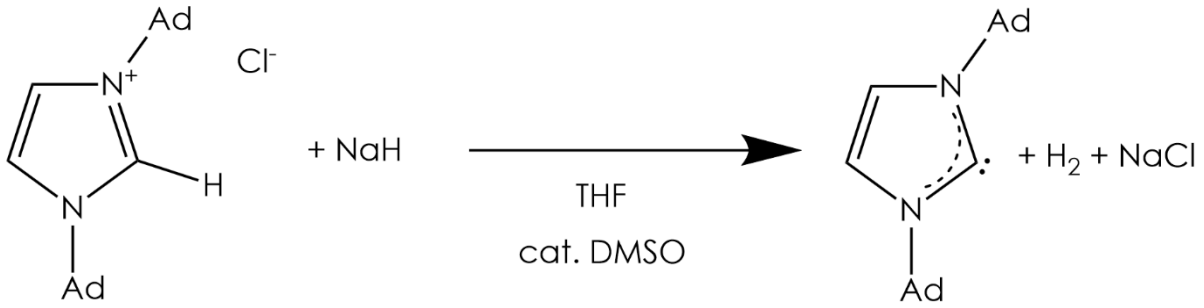

Figure 15: Synthesis of the *Arduengo* carbene.[178]

Bis(diisopropylamine)carbene was not only the starting point of NHCs but also for the development of more stable carbenes. Soon after, the cyclic alkyl amino carbenes (CAACs)[179,180] were synthesized (**Figure 16**b), both types of carbenes have a cyclic structure in common. In 1996, *Alder* published bis(diisopropylamino)carbene (**Figure 16**c) which belongs to the acyclic diamino carbene (ADC) class.[181] In the past decade, the focus of metal organic chemistry shifted to the ADCs as well as acyclic amino carbenes (AACs) (**Figure 16**d).[182–184]

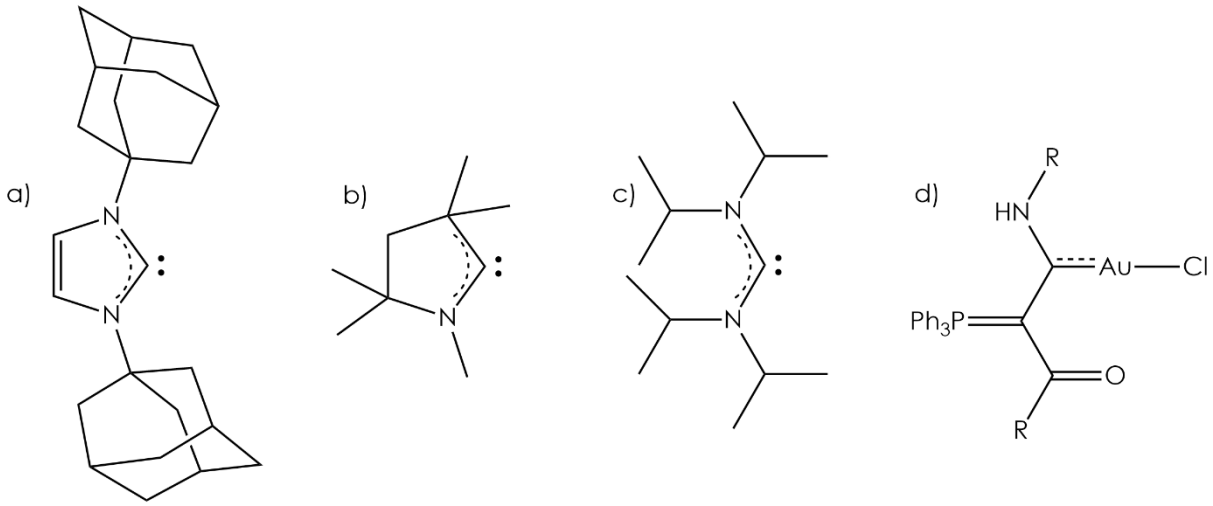

Figure 16: Examples for a) Arduengo carbene (NHC).[178] b) Cyclic alkyl amino carbene (CAAC).[179,180] c) Acyclic diamino carbene (ADC).[181] d) Acyclic amino carbene (AAC) as a ligand in a gold complex.[184]

NHCs base on an imidazolium or benzimidazolium frame.[185] The NHC is stabilized by the cycle and the two amino groups (push-push). Due to the steric demand of the adamantyl substituents, the carbene is even more stabilized.[178] On the one hand, the NHCs are established ligands in organometallic chemistry and homogeneous, transition metal catalyzed, organic synthesis.[186–199] On the other hand, the ADCs are still neglected, although the amount of related publications is increasing. There is big variety of NHC containing transition metal complexes known.[185] By modifying the NHC frame, including four to seven membered rings, the electronic donor properties are drastically influenced as well as the steric demands.[200–205]

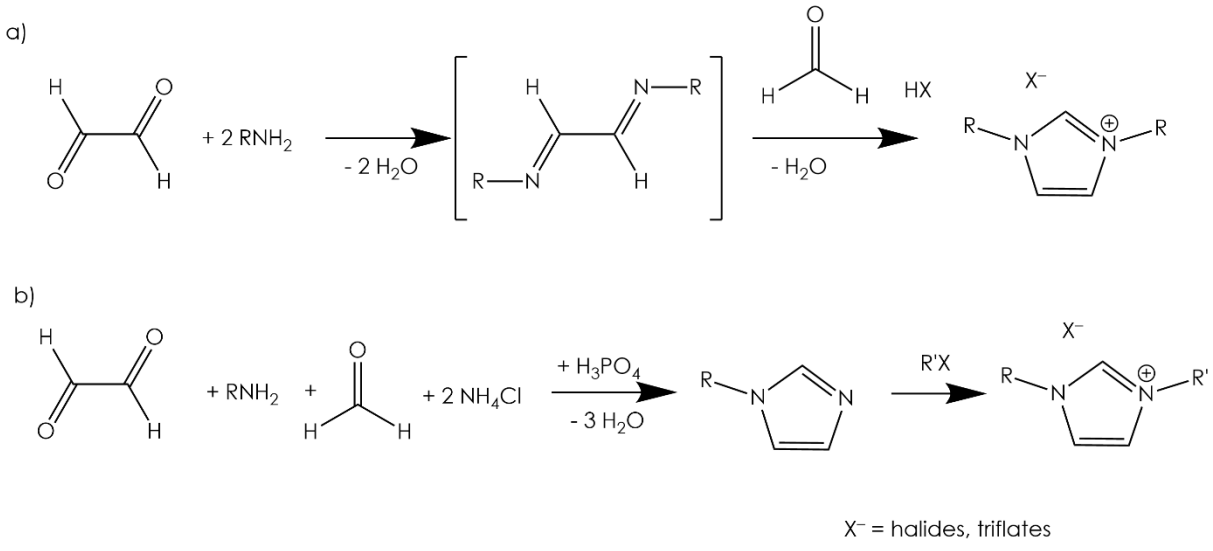

Scheme 11: Synthesis of a) symmetric imidazolium salts, b) unsymmetric imidazolium salts.[206]

Imidazolium salts are common NHC precursor compounds and are synthesized out of a primary amine, formaldehyde and glyoxal via a *Schiff* base intermediate.[206,207] On one hand, this route allows the synthesis of symmetrically *N*,*N'*-substituted imidazolium salts (**Scheme 11**a).[206] It shows issues

with increasing steric demand of the substituents on the other hand, since the formation of the imidazolium salts becomes inhibited. Stepwise alkylation of the nitrogen atoms is possible to synthesize unsymmetrical imidazolium salts.[206] The precursor is deprotonated by bases to form imidazolylidenes (**Scheme 11**b). This procedure requires non-protic solvents and anhydrous conditions.[185]

The high interest in NHCs is described by the difference between the first and the second-generation *Grubbs* catalysts. The first-generation does not contain any NHC ligands (**Figure 13**), while in the second-generation catalyst, one phosphane ligand is replaced by a NHC. The reaction of the NHC containing catalysts is more efficient compared to a catalyst without NHC substituent.[208] Next to an increased efficiency, the second-generation *Grubbs* catalyst has a higher (stereo) selectivity.[172]

1.3.3 Acyclic diamino carbenes

The first acyclic diamino carbene was published by *Alder* in 1996. The deprotonation of the *N*,*N*,*N'*,*N'*-tetramethylformamidinium salt leads to the dimerization of the carbene.[209] *Alder* used steric more demanding substituents and deprotonated the *N*,*N*,*N'*,*N'*-tetraisopropylformamidinium chloride with lithium diisopropylamide in THF (**Figure 17**).[181]

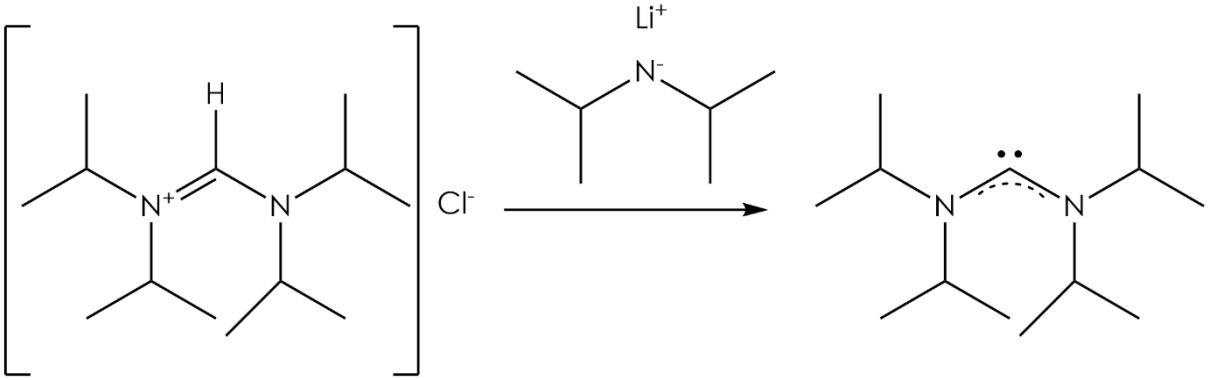

Figure 17: Deprotonation of tetraisopropylformamidinium chloride to bisdiisopropylaminocarbene (*Alder* carbene).[181]

The synthesis gives a yield of about 55%. The carbene is sublimated easily, stable under inert gas atmosphere. By X-ray crystal analysis the molecular structure was determined.[184] The steric interaction of the diisopropyl groups increases the N-C-N angle from NHC-typical 104.5° up to 124° in the case of the acyclic carbene. The deformation leads to a downfield shift of the carbene signal ^{13}C NMR spectroscopy of the *Alder* carbene compared to regular NHCs. The result of the increased angle decreases the energy gap between the singlet and triplet state of the carbene carbon, thus leading to a bigger paramagnetic shielding.[210] *Alder* proved the diamino carbene rotation around the C-N axis to be inhibited by an increased energy barrier resulting in a double bond character. Examples of other crystalline carbenes are bis(piperidino)carbene (**Figure 18**a),[211] bis(4-

methylpiperidino)carbene (**Figure 18**b),[212] bis(pyrrolidino) carbene (**Figure 18**c),[213] diisopropylamino-(2,6-dimethylpiperidino)carbene (**Figure 18**d),[214] bis(*N*-(2,6-diisopropylphenyl)-*N*-methyl) carbene (**Figure 18**e),[215,216] and diisopropylaminodiphenylaminocarbene (**Figure 18**f).[217]

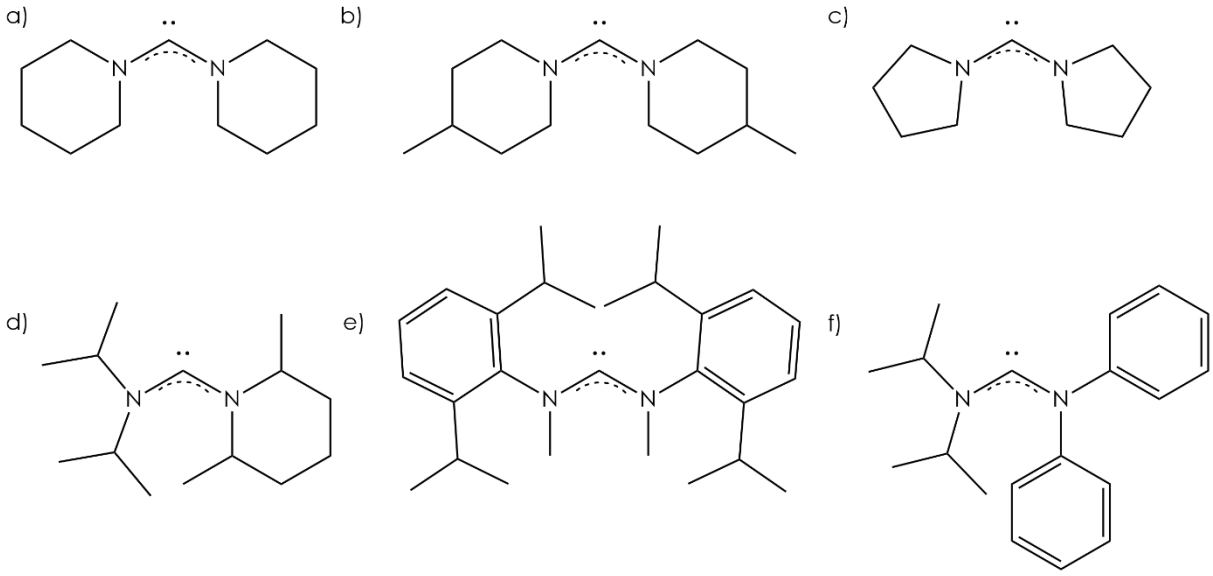

Figure 18: Examples of stable acyclic carbenes.

Possible benefits of ADCs in catalytic applications are, in comparison to NHCs, the increased basicity, nucleophilicity, σ-donating ability and C-N-C angle.[173,182,183] The broader bond angle forces the possibility to localize the substituents closer to the transition metal. The absence of a cyclic backbone adds the possibility of variation of the steric demand by conformation changes and a variation of the donating ability on complexes. Therefore, it is possible to adjust ADC ligands sterically and electronically for different catalytic steps.[215,218]

1.3.4 Ferrocenyl substituted carbenes

Different types of carbene complexes are used in catalysis[163,164] and ferrocene is a widely used redox active building block.[169,170] Combination of carbenes and ferrocenes to upgrade catalysis chemistry is feasible. It is possible to directly control the redox chemistry of a carbene-ferrocene complex by the oxidation state of the ferrocene metal center. By controlling the oxidation state of the ferrocene moiety there might be an option to activate catalytic properties of the carbene complex for homogeneous catalysis. Ferrocene forms a redox switch to activate or deactivate the catalyst by using the electric potential (see 1.4.2).[219] A neutral carbene with a ferrocenyl moiety is soluble in non-polar organic solvents, while a charged carbene containing a ferrocenyl moiety is soluble in aqueous solutions.[220] There are only a few ferrocene containing carbenes known,[221] most of them are NHCs (**Figure 19**).[164,222–224]

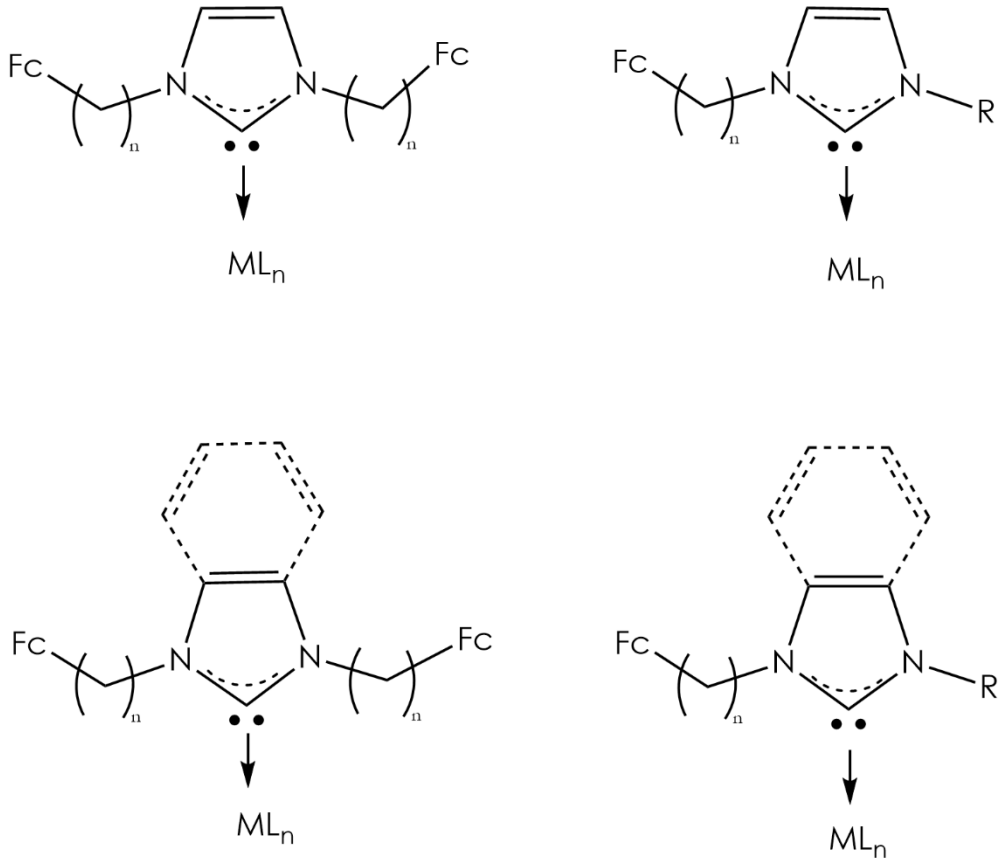

Figure 19: Selection of known N-heterocyclic ferrocenylcarbenes.[164,222–224]

NHCs are stabilized by their cyclic structure. It is possible to introduce a ferrocene backbone like in [3]ferrocenophane *N*-heterocyclic carbenes, mimicing the stabilization of a cyclic structure. The introduced ferrocene is substituted in 1,1' position with nitrogen substituents.[225–227] Differently to imidazole and benzimidazole carbenes, the *N*-heterocycle of ferroceneophanes shows six atoms, also counting the iron atom of the ferrocene (**Figure 20**).

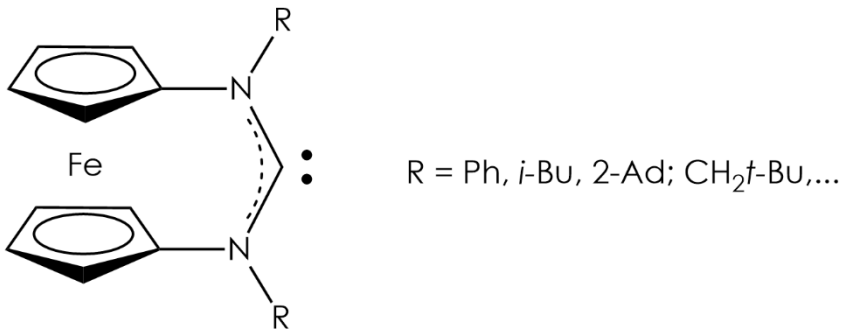

Figure 20: N-heterocyclic carbene with a 1,1´-ferrocenediyl backbone (ferrocenophane).[225–227]

All mentioned ferrocene containing carbenes are cyclic carbenes. There are only two acyclic ferrocenyl substituted aminocarbenes (AFcC) known. α-Ferrocenyl aminocarbene was published by *Bertrand* (**Figure 21**).[228]

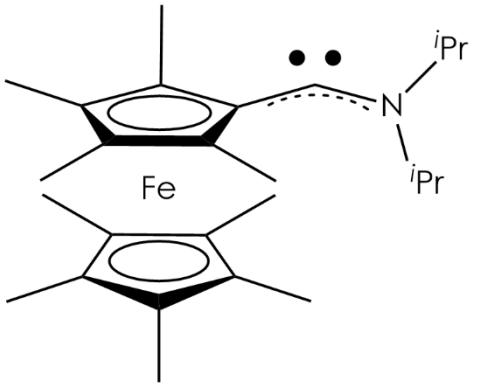

Figure 21: Diisopropylamino-nonamethylferrocenyl carbene.[228]

The nonamethylated ferrocenyl substituent acts as a spectator (Fc*-substituent). Since the other carbene substituent is an amino group, the carbene is stabilized by the push-spectator effect. For stability it is necessary to use fully methylated ferrocene due to the increased electron donating ability. So diisopropylamino ferrocenyl carbene is not known, yet. The second known AFcC was not yet isolated as a free carbene but rather as a palladium coupled complex (**Figure 22**).[229]

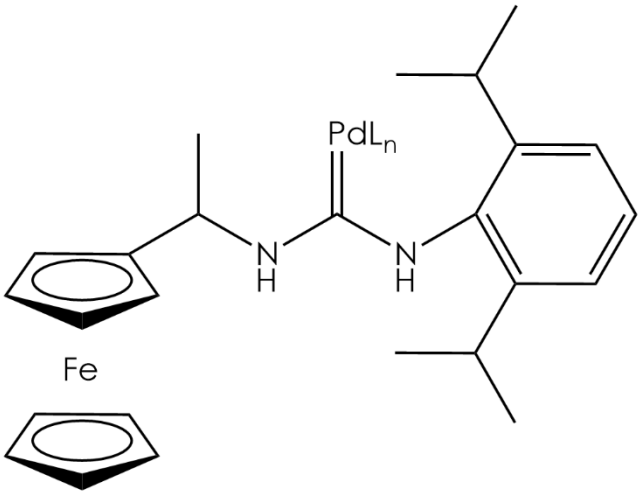

Figure 22: The diamino carbene complex with a ferrocenyl substituent.[229]

Possible substitution patterns for AFcCs are shown in **Figure 23**. Experimental attempts to synthesize **Type A** diferrocenyl carbenes were done by *Bildstein*[230], *Förster* and *Heinze* (**Figure 23**a).[59] *Bildsteins* experiments resulted in the dimerization of the carbene to 1,1,2,2-tetraferrocenylethen (*Wanzlick* equilibrium) (**Figure 23**b). The free diferrocenyl carbene wasn't isolated. The +M-effect of the substituted Cp rings is not sufficient enough to stabilize the free carbene. In comparison to **Type A** compounds, **Type B** compounds use nitrogen as a donor. The nitrogen atom stabilizes the carbene by pushing electron density to the carbene carbon.

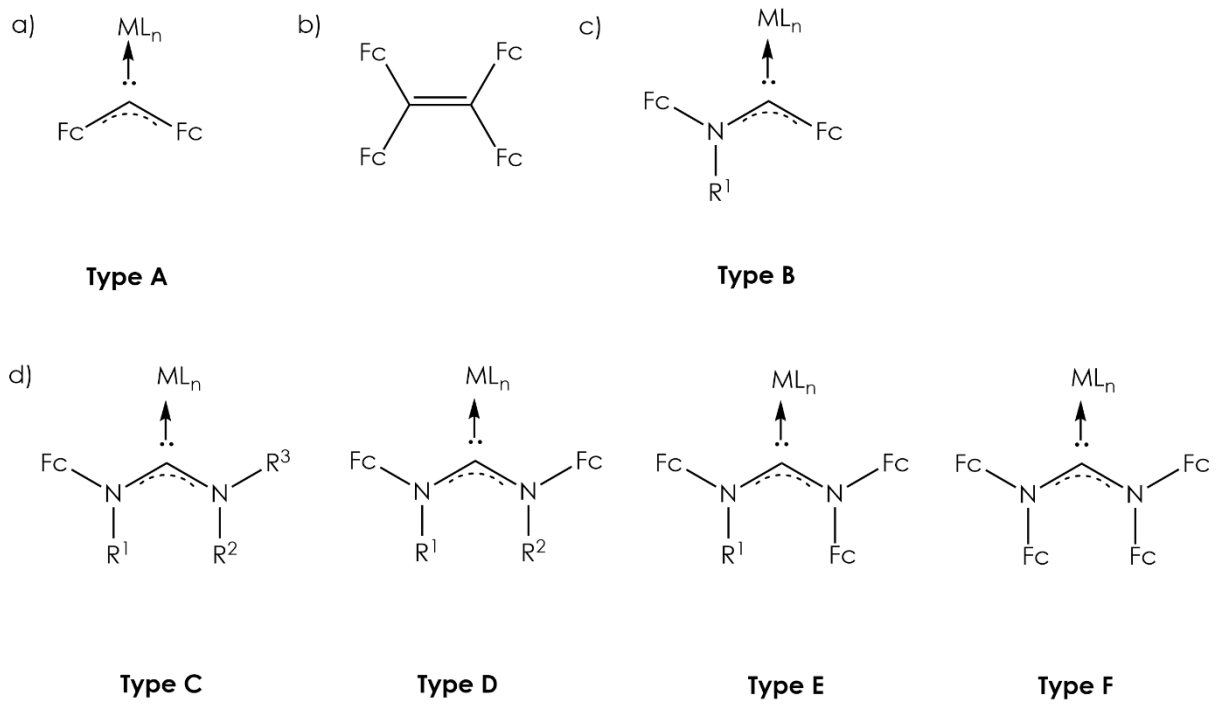

R^1, R^2, R^3 = Alkyl, Aryl
ML$_n$ = /, M(CO)$_5$, Rh(cod)Cl, AuCl, ...

Figure 23: Possible types of substitution patterns for AFcCs. a) Differocenyl carbene. b) Differeocenyl carbene dimerized to 1,1,2,2-tetraferrocenylethen. c) Ferrocenyl substituted acyclic amino carbene. d) Variations of ferrocenylsubstituted acyclic diamino carbenes.

The synthesis of **Type B** complex *a,β*–diferrocenyl carbene pentacarbonyl tungsten(0) and *a,β*–diferrocenyl carbene pentacarbonyl chromium(0) with a proton as R^1 (**Figure 23**c) by *Veit* and *Heinze* was successful.[231] However, the complex decomposes by a 1,2-H shift resulting in the formation of an imine. To prevent the 1,2-H shift, methylation with iodomethane of the tungsten complex led to (*N*-methylaminoferrocenyl)(ferrocenyl)(pentacarbonyl)tungsten(0).[232] This complex is stable towards the imine decomposition pathway. It exists as a 6:1 mixture of *syn/anti* conformers (**Figure 24**). Theoretically ferrocenyl substituted diamino carbenes are substituted by ferrocene up to four times. Complexes of **Type C, D, E** and **F** (**Figure 23**d) are not yet reported.

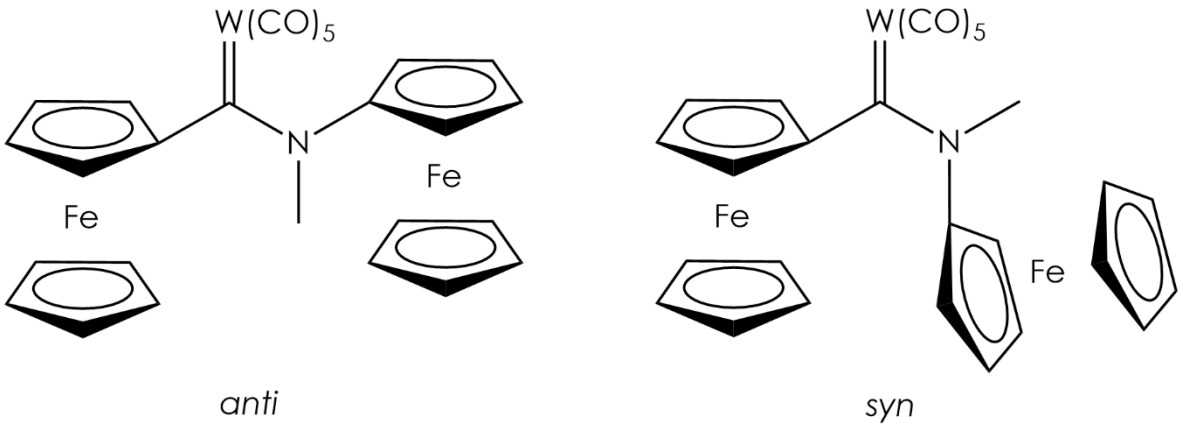

Figure 24: anti- and syn- confomeres of (N-methylaminoferrocenyl)(ferrocenyl)(pentacarbonyl)tungsten(0).

1.4 Gold catalysis

1.4.1 Gold carbenes

The term gold carbene describes compounds that resemble a carbene like structure. This neglects the variety of possible bond orders for this type of complexes. "True" gold carbene complexes possess an Au-C bond order of two. A complex with a small Au-C bond order of one isn't a carbene complex but rather a carbenium complex. Owning an even smaller Au-C bond order of zero describes a so-called carbenoid complex (**Figure 25**).[233,234] The true structure of the Au-C bond in gold carbene complexes is still a highly interesting matter of discussion. This is mainly due to the rather little structural information.[235] Therefore, the main part of this discussion is based on computational chemistry.[236] The most sensible way to describe the "carbene" and "carbenoid" relation is the dependency by the addition or elimination of a halide group.[237]

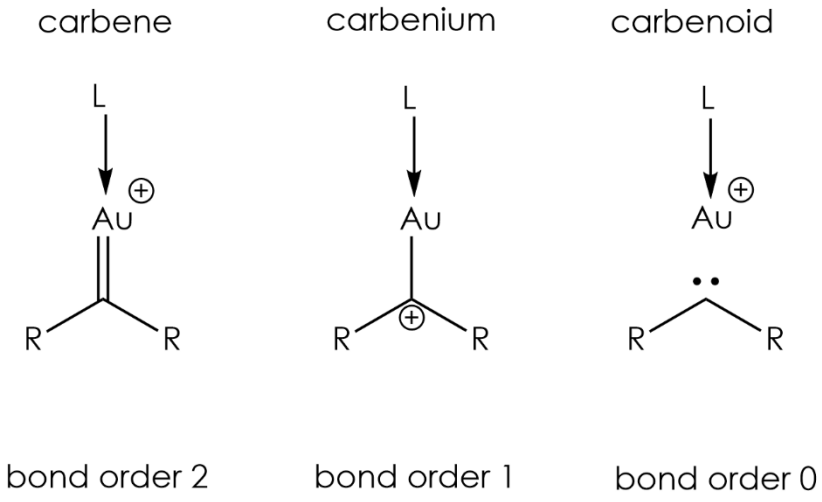

Figure 25: Structure of different Au-C bond orders.

Carbene complexes with a bond order of zero catalyze the cyclopropanation of alkenes which is possible due to the weak metal-carbene bond.[233,234] Due to the strong bond that "bond order two" carbene complexes form, metathesis reaction with alkenes is accessible.[234]

Gold(I) complexes are sometimes stabilized by an extraordinary effect. Physically, two gold(I) atoms are supposed to show repulsive *Coulomb* interaction. Despite this, several gold(I) complexes were reported to show intramolecular (in case of binuclear) or intermolecular Au(I)-Au(I) distances between 2.5 Å and 3.5 Å. The distance is smaller than the sum of the *van der Waals radii* of two gold(I) atoms (3.80 Å), since the resulting force between both gold(I) ions is attractive instead of repulsive. A gold core with an atomic number of 79 accelerate the electrons of the inner orbitals towards the speed of light, which is why relativistic effects have to be considered. This acceleration causes an increase of electron mass and therefore contraction and stabilization of the s- and p-orbitals. Due to the resulting increase in nuclear shielding, the d- and f- orbitals are expanded and get destabilized. With this, the energy gap between the 6s/p and the 5d/f orbitals decrease, enabling an effective overlap and the formation of strong metal-metal interactions get possible.[238]

Combination with the lanthanide contraction that is able do decrease the *van der Waals radii* of gold(I) gives an explanation for this aurophilicity called effect.[239,240]

First gold(I) carbene complexes were described by *Balch* in 1973, using tetra-chloridoaurate(III) for α-addition of amines to isocyanides intermediates forming $[Au^{I}(C(NHMe)(CRMe))_2]$ (**Figure 26**a).[241] *Balch* also reported gold(III) carbene compounds, which form planar biscarbene complexes (**Figure 26**b).[242] Treating a trimeric cyclic gold(0) complex with hydrochloric acid results in the formation of a gold(I) carbene complex with only one carbene ligand and a chloride ligand stabilizing the gold(I) center (**Figure 26**c).[242] These mono carbene complexes are also synthesized by transmetallating a carbene ligand from a tungsten *Fischer* type carbene complex onto tetrachloridoaurate (**Figure 26**d).[243] This can also be done with chromium and molybdenum as metal and several halide ligands to form gold(I) and gold(III) complexes (**Figure 26**e).[244,245] Next to mononuclear complexes, there are also known binuclear gold carbene complexes. *Laguna* described mononuclear gold carbene complexes, binuclear gold carbene complexes and also binuclear biscarbene complexes, where two segments of the binuclear complexes are linked together by diamino groups (**Figure 26**f).[246] .

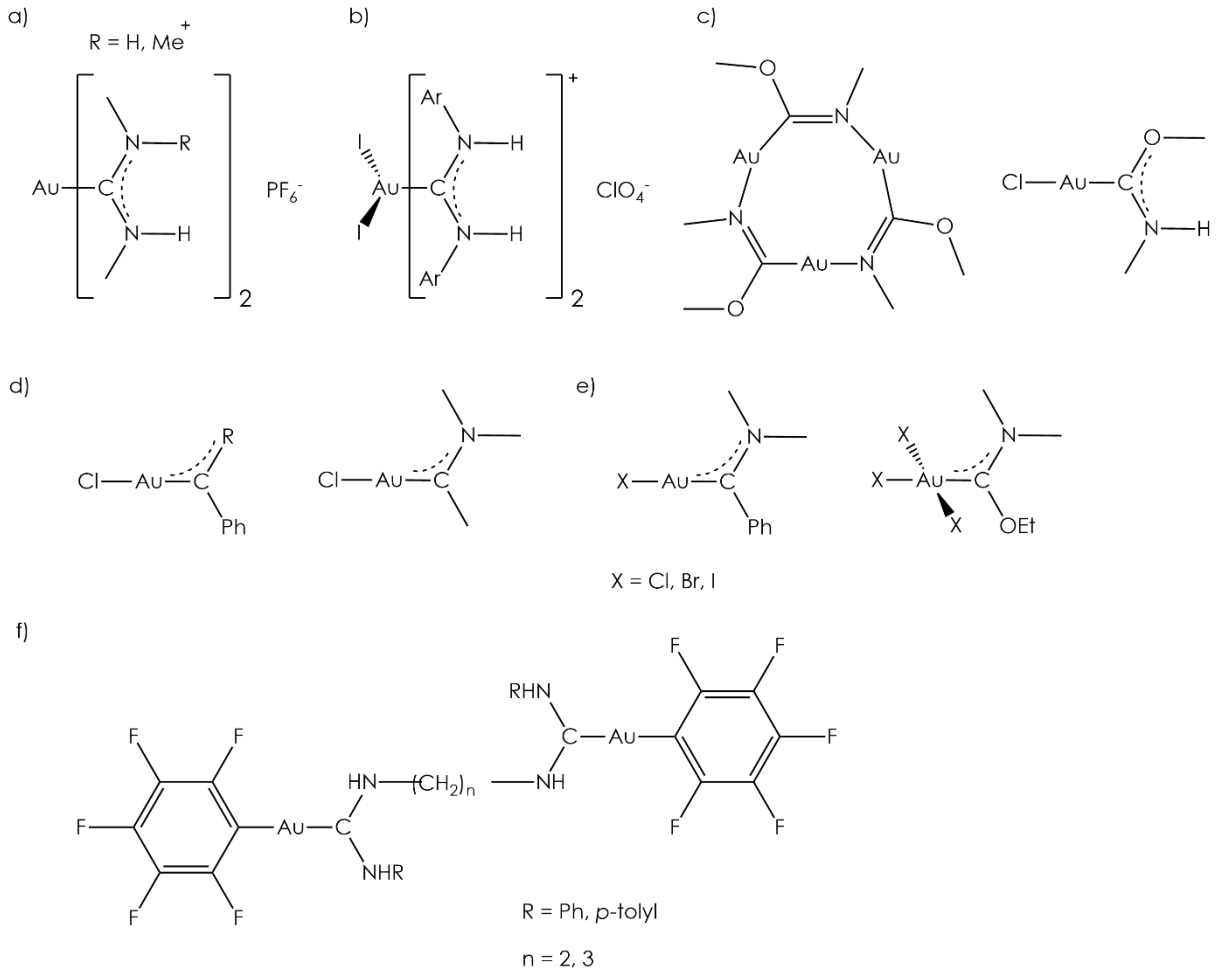

Figure 26: Gold carbene complexes. a) Gold(I) carbene complex reported by *Balch* in 1973.[241] b) Gold(III) carbene complex reported by Balch in 1974.[242] c) Trimeric gold(I) carbene complex and resulting product, gold(I) carbene complex after dissociation, reported by Balch in 1974.[242] d) Gold(I) carbene complex formed by transmetalation from

tungsten Fischer type carbene complexes, reported by Aumann in 1981.[243] e) Gold(I) and gold(III) carbene complexes formed by transmetalation from tungsten, chromium and molybdenum Fischer type carbene complexes. All complexes are having different halide ligands. Reported by Aumann in 1981.[244,245] f) Binuclear gold(I) biscarbene complex reported by Laguna in 1984.[246] All stable gold carbene complexes are either gold(I) complexes or gold(III) complexes.

The oxidation state of a gold center is determined by the use of ^{197}Au *Mössbauer* spectroscopy.[247–249] Today, gold complexes are used as catalysts in organic synthesis. The gold center has the ability to activate C-C multiple bonds. Another typical aspect in gold catalysis is the unchanged oxidation state of the gold metal center during catalysis[250] in contrast to other transition metals such as rhodium[251] or palladium.[252,253] The first step of the catalytic cycle is the activation of the π-bond towards nucleophilic substitution. Therefore, an electrophilic gold complex is η^2-coordinated to the C-C π-bond. This is accompanied by an increase of the π-bond length and a change of the carbon configuration from trigonal planar towards pyramidal.[254] The now activated multiple bond is substituted nucleophilicly by the intermolecular carbonyl group leading to a ring closure. Tautomerisation and the abstraction of the gold complex eventually forms the oxazole and restores the catalytic active gold complex (**Scheme 12**). The reactivity of the catalysts is highly dependent on the steric and electronic behavior of the ligands.[255,256] Recently carbene ligands outdated phosphine ligands as substituents for gold(I) complex catalysis.[257,258]

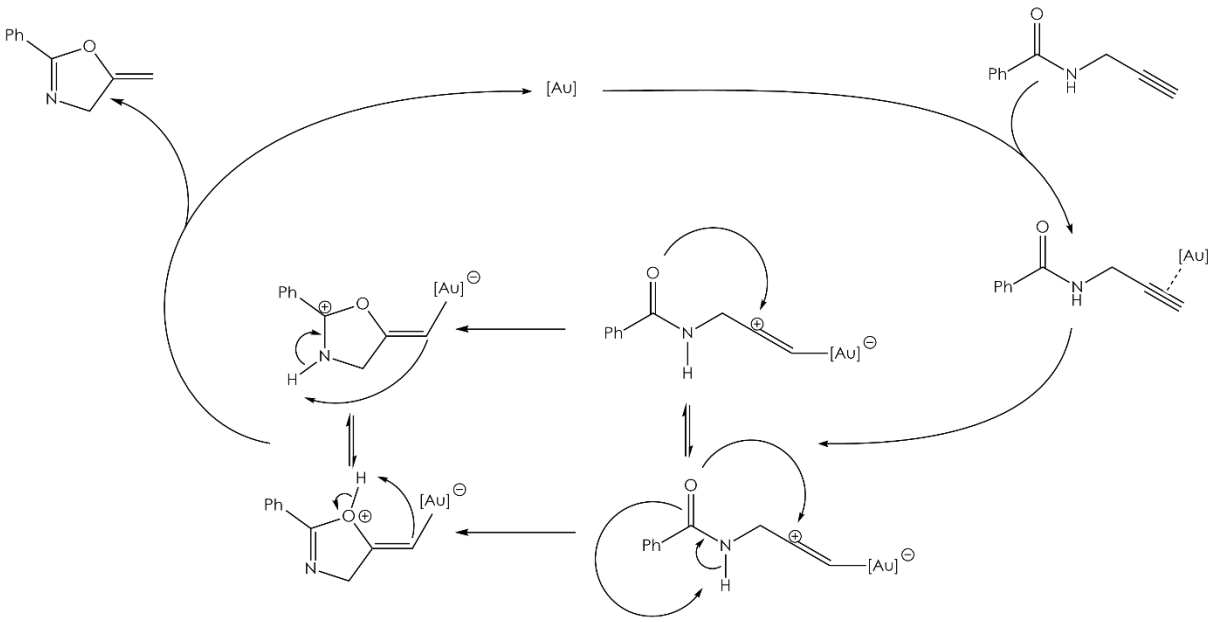

Scheme 12: Mechanism of the gold catalyzed cycloisomerization of *N*-phenyl-propargylamide to 5-methylene-2-phenyl-4,5-dihydroxyoxazole.[250]

The cycloisomerization of propargylamide to oxazole is a benchmark reaction for determining the effectivity of a gold catalyst.[256,259,260] Despite of the big variety of gold carbene complexes, there are nearly no gold(0) and gold(II) carbene complexes known. *Bertrand* was the first to report mononuclear and binuclear gold(0) carbene complexes. He used two strongly donating CAAC ligands to stabilize the paramagnetic gold(0) centers.[261]

1.4.2 Redox switchable catalysis (RSC)

Normally, the generation of the active gold species is done using halide abstraction. Silver salts showed to be the most effective abstraction reagents.[194] Next to silver salts, methyl trifluoromethansulfonate and potassium salts are also used as abstracting agents.[262] Gold carbene complexes with redox active substituents are able to work in redox switchable catalysis (RSC). By adding an oxidant, the activity of the catalyst is increased. A reductive agent reduces the catalyst and deactivates it. *Wrighton* published several rhenium carbonyl complexes with an 1,1'-bis(diphenylphosphino)cobaltocene (dppc) as chelating ligand. The neutral complex shows small carbonyl electrophilicity which results in a slow nucleophilic substitution at the carbonyl ligands. Oxidizing the cobaltocene moiety leads to a higher carbonyl electrophilicity and a faster nucleophilic carbonyl substitution (**Figure 27**a).[263] This is explained by the higher d to π* backbonding of the neutral complex. This backbonding increases the electron density at the carbonyl and lowers its electrophilicity. The oxidized complex has a weaker d to π* backbonding and hence a larger electrophilicity (**Figure 27**b).[263]

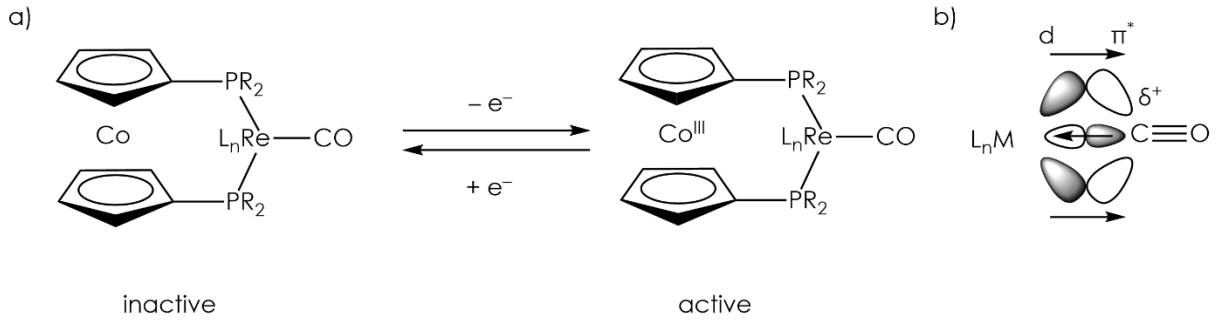

Figure 27: a) Rhenium carbonyl complex with dppc ligand. By changing the oxidation state of the cobaltocene moiety in the dppc ligand the activity towards nucleophilic substitution is controlled. b) Stronger d to π* backbonding leads to a smaller carbonyl electrophilicity and therefore to decreased activity towards nucleophilicity.[263]

The redox switchable catalyst is regenerated after catalysis. *Plenio* was able to regain the redox switchable catalyst in ring closing methathesis (RCM) by phase separation. The homogeneous catalyst was substituted by two ferrocenyl groups. With this substitution pattern it was possible to control the solubility of the catalyst by switching between the neutral and the double oxidized state.[220] Due to this different solution behavior the ferrocenyl moieties are so called phase tags. Separation of the catalyst from the reaction mixture is done with the oxidized species, which is soluble in a polar solvent like water. This second solvent is added to the reaction mixture and dissolves the catalyst but not the product.

Peris used a ferrocenyl-imidazolylidene gold(I) complex for cyclization of alkynes with furanes and the hydroamination of terminal alkynes in a redox switchable catalysis. In the first reaction, the neutral complex is not catalytically active while the oxidized one does. In the later reaction, the difference in catalytical activity between the neutral and oxidized species was not as big as in the first reaction, but still observable.[219] A big advantage of this redox active gold(I) carbene complexe

compared to the non-redox active complexe is the independence of halide abstraction reagents. Due to the redox active moiety it is not necessary to abstract the halide ligand to activate the complex.

Sarkar reported several mesoionic carbene (MIC) gold complexes containing ferrocenyl moieties, based on a 1,2,3-triazol-5ylidene (trz) scaffold. This scaffold is substituted by one to two metallocenes, either ferrocenyl, cobaltocenyl or both (**Figure 28**).[264][265] [266] [142] A possibility to measure the electron donating and withdrawing ability of a NHC ligand is the *Tolman electronic parameter* (TEP). This parameter is determined by IR spectroscopy in the complex *cis*-[LRhCl(CO)$_2$], with L being the investigated ligand.[267] Electron withdrawing ligands decrease the π-backbonding effect of the metal to the carbonyl ligand which increase the CO vibration frequency. Electron donating substituents on the other hand, increase the π-backbonding from the metal to the carbonyl and decrease the CO vibration frequency. All of the ferrocenyl only containing MIC gold(I) complexes show an increased TEP value upon oxidation (around 2045 cm^{-1} to 2053–2057 cm^{-1}). The cobaltoceniumyl containing MIC gold(I) complexes show even higher TEP values of 2078 cm^{-1} (monocobaltoceniumyl) and 2109 cm^{-1} (dicobaltoceniumyl) and are therefore even more electron poor. These complexes show even better catalytic activity due to the increased electrophilicity.

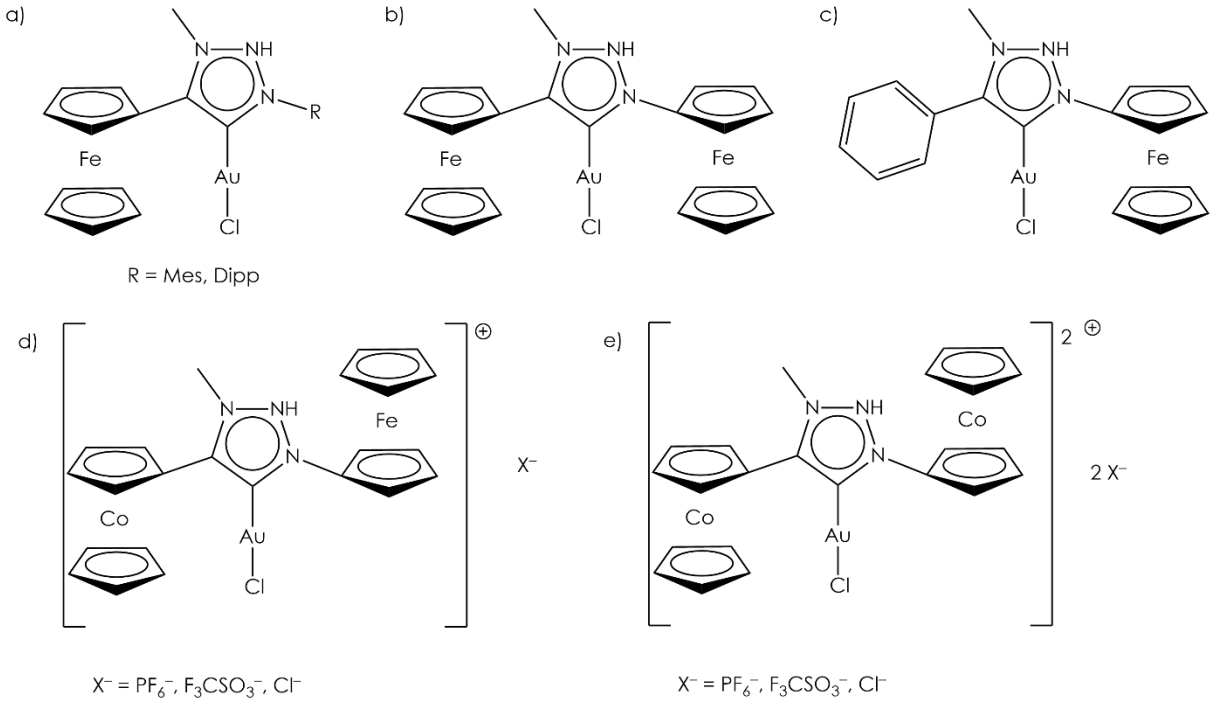

Figure 28: a) 4-ferrocenyl-(1-mesityl)/(1-dipp) triazolylidene gold(I).[264] b) 1,4-diferrocenyl triazolylidene gold(I).[265] c) 4-ferrocenyl-1-phenyl triazolylidene gold(I).[266] d) 1-cobaltoceniumyl-4-ferrocenyl triazolylidene gold(I).[142] e) 1,4-dicobaltoceniumyl triazolylidene gold(I).[142]

Bezuidenhout reported gold(I) carbene complexes with a ferrocenyl substituent in α position towards the carbene carbon atom (**Figure 29**a).[268] These carbene complexes are stabilized by aurophilic interactions, which allows the synthesis of a ferrocenophane like biscarbene complex with two

gold(I) atoms (**Figure 29**b). *Veit* and *Heinze* reported a derivative of the gold(I) carbene complex from *Bezuidenhout* using an ethoxy substituent instead of a methoxy substituent (**Figure 29**c).[269] The ethoxy gold carbene complex shows similar behavior as the previous mentioned ferrocenyl substituted gold(I) carbene complexes. The neutral ethoxy carbene (**Figure 29**c) complex is not able to catalyze a cycloisomerization of *N*-phenyl-propargylamide to 5-methylene-2-phenyl-4,5-dihydroxyoxazole. After oxidation with tris(4-bromophenyl)ammoniumyl hexachloridoantimonate (*magic blue*) the carbene complex is able to catalyze the reaction. It is also possible to stop the catalysis by reducing the complex with decamethylferrocene. It is possible to start and stop the catalytic reaction multiple times. Electron paramagnetic resonance (EPR) studies show the rise of a signal at $g = 2.01$, which correlates with the catalytic activity. This EPR signal has a similar g -value as known gold(II) complexes.[270,271] By oxidation with magic blue, first the ferrocene moiety is oxidized. Over time, there is an intramolecular electron shift with the reduction of the ferroceniumyl moiety and the oxidation of the gold(I) to gold(II). Since the rise of the gold(II) and the conversion of the substrate is correlating, the gold(II) species is suggested to act as catalytic active species.[269]

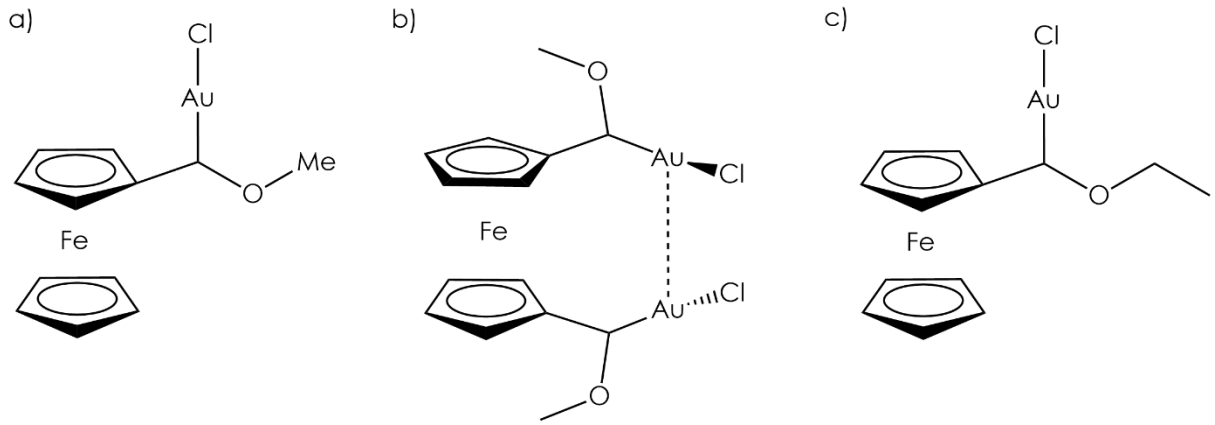

Figure 29: α ferrocenylsubstituted gold(I) carbene complexes. a) Chloride [(methoxy)(ferrocenyl)ylidene] gold(I)derivative by *Bezoidenhout*.[268] b) Ferrocenophane biscarbene complex by *Bezoidenhout*.[268] c) Chloride [(ethoxy)(ferrocenyl)ylidene] gold(I) by *Veit* and *Heinze*.[269]

1.5 Catalyzing Hydrogen Evolution Reaction (HER) with cobalt complexes

1.5.1 Hydrogen Evolution Reaction (HER)

The electrolysis of water consists of two components which are the hydrogen evolution reaction (HER, **Equation 14**) and the oxygen evolution reaction (OER, **Equation 15**).[272]

HER: $2\ H^+ + 2\ e^- \rightarrow H_2$ **Equation 14**

OER: $2\ H_2O \rightarrow O_2 + 4\ H^+ + 4\ e^-$ **Equation 15**

Due to the increasing interest in green energy as well as the already big amount of application possibilities for hydrogen,[273,274] the interest in HER increased in the recent years. Though, the normal HER affords high energy as the minimum potential along the one-electron pathway is 1.8 V.[275] This results in the water electrolysis being nearly insignificant in hydrogen production. More than 95% of the hydrogen is produced out of fossil fuels by steam reforming (**Equation 16**)[276] or by other minor processes like partial oxidation (**Equation 17**)[251] and the water-gas shift reaction (**Equation 18**)[277], while hydrogen production out of water electrolysis represent around 4%.[272]

$$CH_4 + H_2O \rightleftharpoons CO + 3\ H_2 \qquad \textbf{Equation 16}$$

$$CH_4 + ½\ O_2 \rightleftharpoons CO + H_2 \qquad \textbf{Equation 17}$$

$$H_2O + CO \rightleftharpoons H_2 + CO_2 \qquad \textbf{Equation 18}$$

To decrease the amount of the fossile based hydrogen and to increase the amount of green hydrogen, it is necessary to improve the efficiency of the HER by developing cheap and earth abundant catalysts. Therefore it is useful to develop catalysts for multielectron photochemistry[278–280] or proton coupled electron transfer (PCET).[281–284] Basically, there are different possibilities for the metal complex-catalyzed HER (**Scheme 13**).[285,286] The most common way is the twofold reduction of a metal which is then oxidatively protonated forming a hydrogenated metal complex. This intermediate can either react heterolytically with a proton (protonolysis) and release H_2 as well as a regenerated metal catalyst (red path, **Scheme 13**). Or it reacts in a bimolecular homolytic reaction with another hydrogenated metal complex to release one H_2 and two molecules of a singly reduced metal catalyst (blue area, **Scheme 13**). Despite the two possibilities for the hydrogenated metal complex to react, the heterolytic reaction is the preferred path.

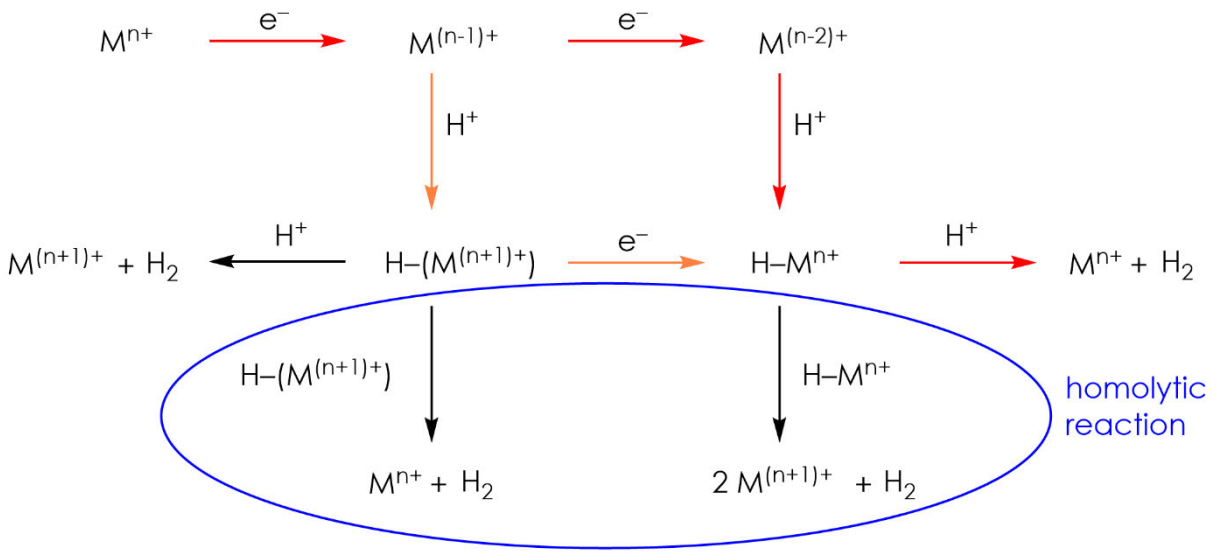

Scheme 13: Pathways for metal complex catalyzed hydrogen revolving reaction (HER).

In addition, there is the possibility for the singly reduced metal catalyst to become protonated oxidatively to form a hydrogenated singly oxidized metal complex (oxidative addition of H^+). This complex can be reduced to give the hydrogenated metal complex (orange path, **Scheme 13**), which has the two already described reaction pathways to produce H_2. Otherwise, the hydrogenated singly oxidized metal complex can react similar to the hydrogenated metal complex. It can either react heterolytically with a proton to release H_2 and the singly oxidized metal catalyst (black path, **Scheme 13**) or in a bimolecular homolytic reaction with another molecule to release H_2 and the metal catalyst (blue circle, **Scheme 13**).

1.5.2 Cobalt Porphyrins

Cobalt complexes like cobalt porphyrins and cobalt corroles show catalytic activity. Already in the last century metal porphyrins showed to be able to catalyze the HER.[287–290] In case of cobalt porphyrins like *meso*-tetrakis (*N*,*N*,*N*-trimethylanilinium-4-yl)porphine chloride (CoTMAP), *meso*-tetrapyrid-4-ylporphine (CoTPyP), *meso*-tetrakis(*N*-methyl-pyridinium-4-yl)porphine chloride (CoTMPyP), *meso*-tetrakis(2-aminophenyl)porphine (CoTAPP) and *meso*-tetraphenylporphine (CoTPP) *Kellet* postulated, that cobalt(III) porphyrin is reduced twice to a cobalt(I) porphyrin and then is protonated oxidatively to form a hydrogenated cobalt(III) porphyrin. *Kellet* thought of this intermediate to be involved in the HER part of the catalytic process.[288] Despite not knowing the actual mechanism, the cobalt complexes were able to catalyze the hydrogen production out of water. The disadvantage of this complexes are the lack of efficiency and stability.[287,291] Later research with cobalt(II) porphyrins pointed out something different. Instead of the need of the hydrogenated cobalt(III) center for the protonolysis reaction, the metal has to be reduced to a hydrogenated cobalt(II) center to allow proton reduction.[292,293] HER in weak acids only occurs from the cobalt(II) species, while in stronger acids, the cobalt(III) species is at least formed but still has to be reduced to the cobalt(II) species.[294] To get more insight into the mechanism, it is crucial to control the proton stoichiometry. With a controlled stoichiometry, it is possible to order the mechanism and get more information about the catalytic cycle. *Lee* used the hanging group effect to access control over the proton stoichiometry. He used an acid-base functionality which was connected to the porphyrin by a xanthene and therefore positioned directly over the redox active metal center of the porphyrin (**Figure 30**, left). The electrochemical results of this hangman cobalt porphyrin was compared to a similar system where the hanging group was substituted by a bromide (**Figure 30**, right) to describe the effect of the hanging group as a hangman effect.[294]

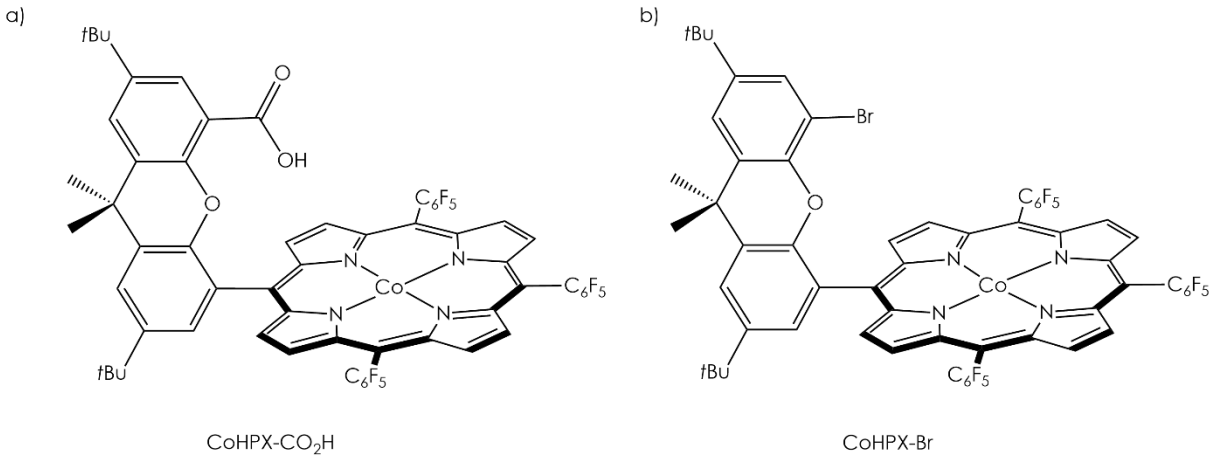

Figure 30: Cobalt porphyrins used by *Lee* to verify the hangman effect. a) With hanging group. b) Without hanging group.

Recently, some cobalt porphyrins with high turnover number (TON) and turnover frequencies (TOF) were reported.[295,296] *Bren* presented a way to a bimolecular water soluble cobalt porphyrin-peptide that can be synthesized by cobalt substitution of the microperoxidase-11.[295] This cobalt-microperoxidase-11 (CoMP11-Ac; **Figure 31**, left) complex can catalyze the HER with a high efficiency. In difference to efficient cobalt complexes with high TONs (up to 9000)[297] and TOFs which are dependent on organic solvents or at least acidic conditions in aqueous solutions,[297–299] CoMP11-Ac can catalyze under aerobic conditions in water.[295] Another advantage of this system is the use of a biosynthetic and biodegradable ligand with five coordination sites for the cobalt(II) center. In the first ten minutes of catalysis, this cobalt porphyrin-peptide has a faradaic efficiency of around 95% and a TOF of ~ 6.7 s^{-1} which was determined by controlled potential electrolysis. The TON was also determined to be 2.5 10^4 under argon atmosphere and 1.9 10^4 under air. The TON under presence of air is comparable to the highest TON of non-noble-metal catalyzed HER in aqueous solution under inert atmosphere.[299] Similar to this complex, *Hung* analyzed cobalt(II) tetrakis-(*p*-sulfonatophenyl)-porphyrin (CoTPPS; **Figure 31**, right) which is an anionic porphyrin and therefore also highly water soluble. CoTPPS showed to be an efficient catalyst for HER out of water without the use of any other additives. With a quantitative faradaic efficiency, in the first hour this system shows a TOF of around ~1.8 s^{-1} and a TON of 1.9 10^4.[296] Following to this results, *Hung* investigated a series of different cobalt porphyrins with electron withdrawing and donating substituents on the *meso* substituted phenyl (**Figure 31**, right). The different catalysts showed faradaic efficiencies between 44% and 99%, TONs from 1.5 up to 104.1 (in ~11 h) and TOFs from 0.23 up to 9.12 h^{-1} (in ~11 h). With this data, it was possible to determine parameters to improve the catalytic activity. The best effect showed a combination of acidic functional groups with an electron withdrawing effect. These cobalt complexes are interesting due to their ability of HER catalysis in water, while being made from earth abundant metal and easy accessible porphyrin derivatives.[300]

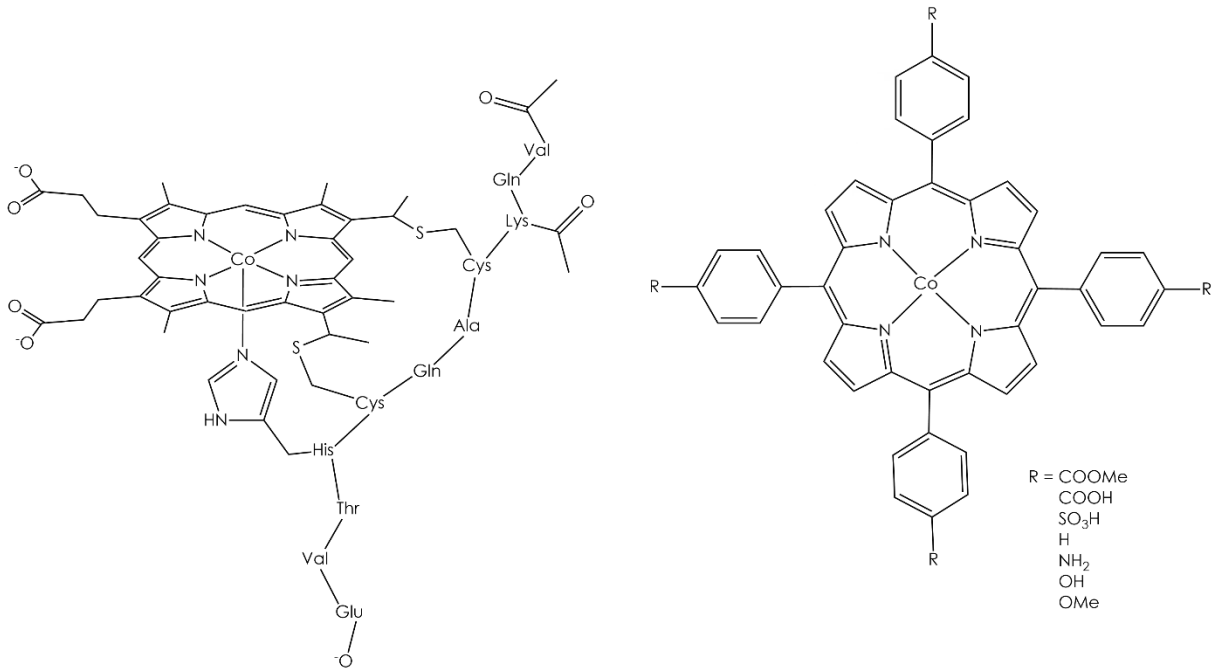

Figure 31: Water soluble cobalt(II) porphyrins with high TON and TOF from *Bren* and *Hung*.[295,296]

1.5.3 Cobalt Corroles

Next to cobalt porphyrines, cobalt corroles are another system of cobalt complexes that show catalyzation abilities for HER. A highly fluorinated cobalt corrole, *β*-octofluoro-cobalt-5,10,15-tris(pentafluorophenyl)corrole (Co(tpfc-F_8)) (**Figure 32**), is able to catalyze HER under ambient conditions.[301] Electrochemical investigations in acetonitrile show reversible redox chemistry with a Co^{II}/Co^{I} redox pair which shows activity by the addition of trifluoroacetic acid (TFA). Under anaerobic conditions at room temperature the corrole has a TOF of 600 s^{-1} at –0.7 V (vs. Ag/AgCl) while at increased negative potential of –0.8 V (vs. Ag/AgCl) the TOF also increases to 1140 s^{-1}. The TON was reported to be over 10^7 in 16 h. *Gross* also checked the HER under aerobic conditions which worked despite reduced efficiency.[302]

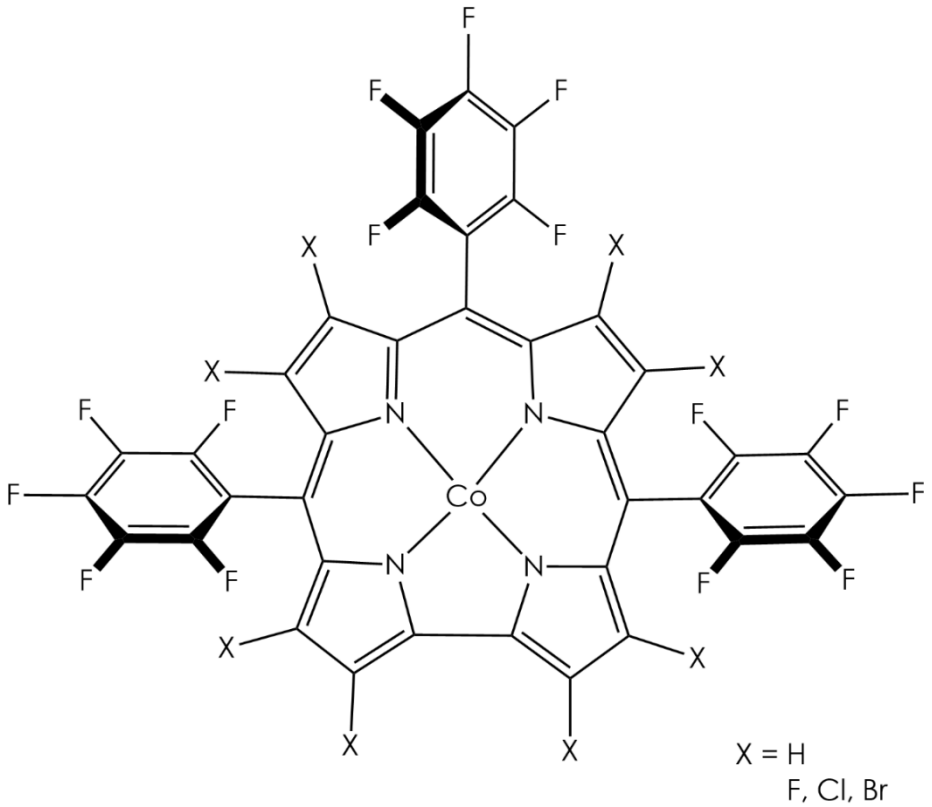

Figure 32: Cobalt-5,10,15-tris(pentafluorophenyl)corrole (Co(tpfc)) with the marked *β*-positions which were halogenated with fluorine, chlorine and bromine.[285,301]

Tpfc-F_8 was also compared to other *β*-halogeneted derivatives (Co(tpfc-X_8)) (**Figure 32**).[302] Although the electrochemical potential for the Co^{II}/Co^{I} reduction of the halogenated complexes shifts to higher potential, the trend from the used halogens fluorine, over chlorine to bromine did not correspond to the electronegativity of the halogens (Co(tpfc) (**Figure 32**): –1.39 V, Co(tpfc-F_8): –0.97 V, Co(tpfc-Cl_8): –0.80 V, Co(tpfc-Br_8): –0.78 V (vs. Ag/AgCl). DFT calculations stated the π-donation of the fluoride to be stronger than the chloride π-donation. This also overcomes the difference in their electron withdrawing effects. The same trend is shown for the onset potentials for the HER catalysis. The most effective derivative was shown to be Co(tpfc-F_8). Co(tpfc-F_8) also catalyzes HER from natural water sources which was demonstrated with water from a tap, a pond, the Ganges and the Dead Sea amongst other sources.[301] Due to the intense analysis of the whole set of derivatives the mechanism for the HER involving cobalt corroles could be formulated (**Scheme 14**).[302]

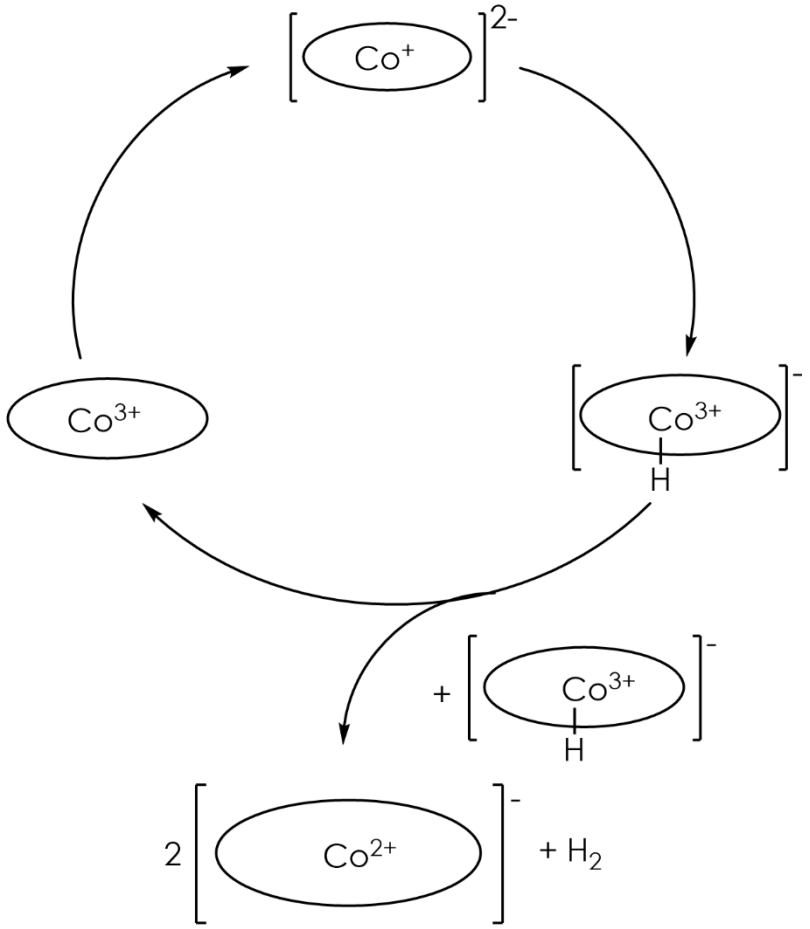

Scheme 14: HER mechanism involving cobalt corroles established by full analysis of Co(tpfc-X_8) derivatives with X being H, F, Cl and Br.[302]

Another cobalt corrole which shows appropriate HER efficiency is [Co(tpfc)$(py)_2$] (py = pyridine).[303] This cobalt corrole was compared with manganese corrole complexes and showed similar oxidizing possibilities as the manganese complexes. But stability during the catalysis was advanced. Next to HER, the cobalt and the manganese corroles were also able to perform oxygen evolution reaction (OER).[303]

1.5.4 Cobaltocene

Next to the large cobalt porphyrins and corroles, cobalt containing metallocenes show HER behavior, too. Cobaltocene is able to reduce protons to molecular hydrogen out of acidic solutions. If hydrochloric acid is used, the catalyst is slowly decomposed, forming tetrachloridocobaltate.[304,305] By using acids with non-coordinating corresponding bases like HBF_4, HPF_6 or even H_2SO_4, cobaltocene reduces protons without decomposition and can be used in a catalytic circle (**Scheme 15**).[306]

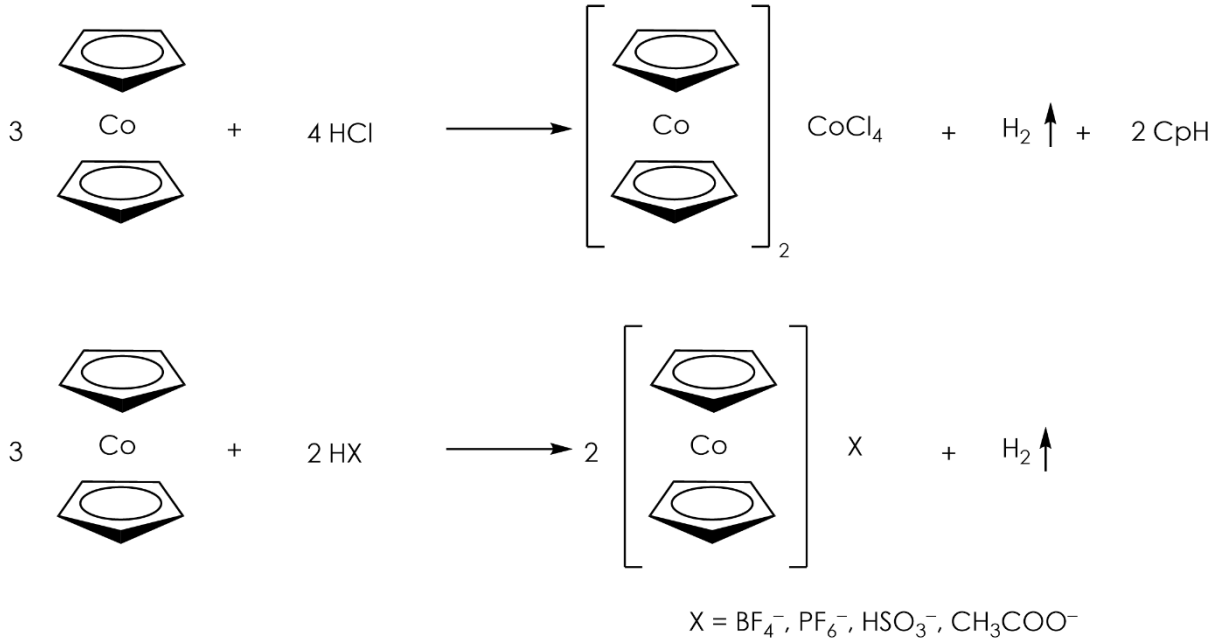

Scheme 15: Reaction of acids with cobaltocene. The reaction with HCl leads to decomposition of cobaltocene due to the nucleophilic character of the chloride anion. Acids with a non-coordinating anion do not decompose cobaltocene.[304–306]

To clarify the reaction pathway, *Grätzel* did protonation and deuteration experiments. He showed, that no protonation of the Cp rings occures. The HER always involves the formation of a cobalt bound hydride which can react in three different ways (**Scheme 16**).[306,307] Two of the cobaltocenium hydrides - formed out of cobaltocene - are able to fulfill the HER in a bimolecular reaction by releasing molecular hydrogen and cobaltocenium salt. Another possibility for the cobaltocenium hydride to be reduced by cobaltocene is forming a cobaltocene hydride which can also react in a bimolecular reaction with a second cobaltocene hydride. In this case, the resulting products will be molecular hydrogen as well as cobaltocene. The last possibility reaction pathway is the reaction of cobaltocene hydride with a proton out of the solution, forming molecular hydrogen and a cobaltocenium salt. The substitution of alkyl groups into the Cp ring leads to an increased protonation rate at the metal center.[306] The steric effects of the alkyl substituents lowers the possibility of reaction of two metallocenes. Additionally, the alkyl groups afford an electron donating effect that results in a higher electron density on the central cobalt atom, which therefore increases the nucleophilicity towards the proton. The homolytic bimolecular reaction of two cobaltocenium hydrides is electronically hindered by two positive charges. Therefore, it is inferior to the reduction with cobaltocene which just needs a small reorganization energy to occur. It is not clear whether the bimolecular reaction or the proton induced reaction is the preferred reaction for the cobaltocene hydride to undergo the HER. The proton induced seems to be the preferred reaction path since only one complex is involved in the reaction.[306,308,309]

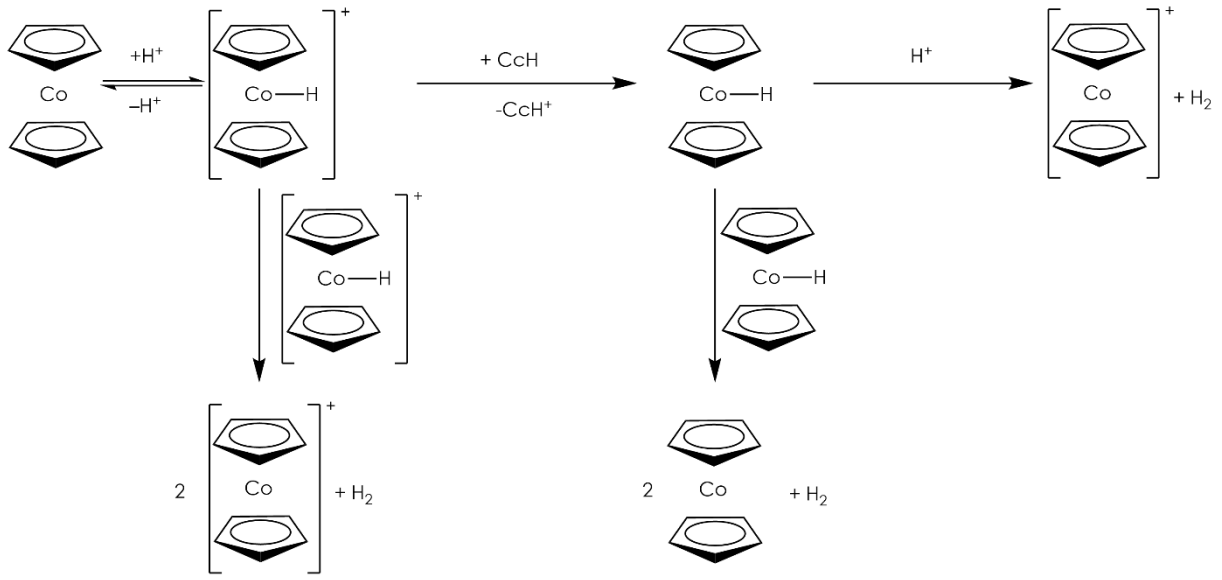

Scheme 16: Possible pathways for the HER to occur starting with cobaltocene.[306]

Cobaltocene is also able to act as a concerted proton-electron transfer (CPET) reagent. The CPET is a competitive reaction towards the HER. A protonation of the Cp ring is necessary to generate the CPET reagent but this results in an anodically shift of the reduction potential and therefore preferation of the HER (ΔG_{HER} = –20 to –60 kcal mol^{-1}) (see **Chapter 1.1.4**).[26] The HER can be attenuated by introducing an aniline substituent to the cobaltocene generating [(Cp)Co(Cp^{N})]. Protonation of the aniline cobaltocene results in a CPET reagent [(Cp)Co(Cp^{NH})]$^+$ with a decreased HER rate. This is because there is only one possibility for the HER which is a bimolecular coupling reaction of two [(Cp)Co(Cp^{NH})]$^+$ to form [(Cp)Co(Cp^{N})]$^+$ and hydrogen gas (**Scheme 17**).[26,310]

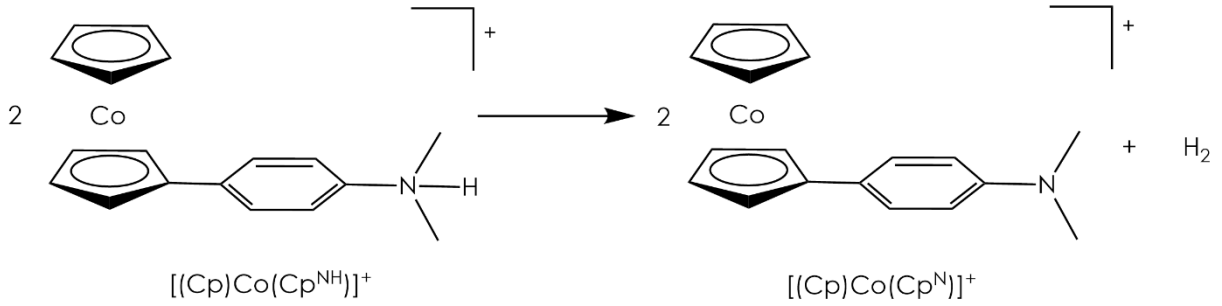

Scheme 17: Bimolecular coupling of [(Cp)Co(Cp^{NH})]$^+$ to [(Cp)Co(Cp^{N})]$^+$.

Bildstein reported the synthesis for a combination of metallocenes with CpCo tetrazenes (**Scheme 18**).[311] Instead of the typical CpCo fragment source dicarbonyl (cyclopentadienyl) cobalt(I), he used cyclooctadiene (cyclopentadienyl)-cobalt(I) as substrate.[312] The cobaltocene tetrazene was analyzed in regard of its catalytic abilities for HER. It showed a catalytic activity which is dependent on the concentration of protons. The maximum TOF was calculated to be ~46.1 s^{-1} (0.05 M acetic acid) and ~59.5 s^{-1} (0.10 M) with a small overpotential of 300 mV. The TON was 2.9 per catalyst molecule and the faradaic efficiency was around 80%. Catalysis experiments including the cobaltocene tetrazene should not exceed a time period of two hours since the faradaic efficiency will decrease, which is an indication for the decomposition of the cobaltocene catalyst. Since the

cobaltocene tetrazene offers three metal centers with two different ligand spheres, the catalytic activities were also analyzed for the ferrocene tetrazene. The voltammograms for the ferrocene derivative showed no reaction upon addition of acetic acid. Therefore the CpCo -tetrazene center can be excluded of being the redox active site in cobaltocene tetracene. This leads to the conclusion that the cobaltocene moieties are the catalytic active sites by binding protons and forming hydrids.[311]

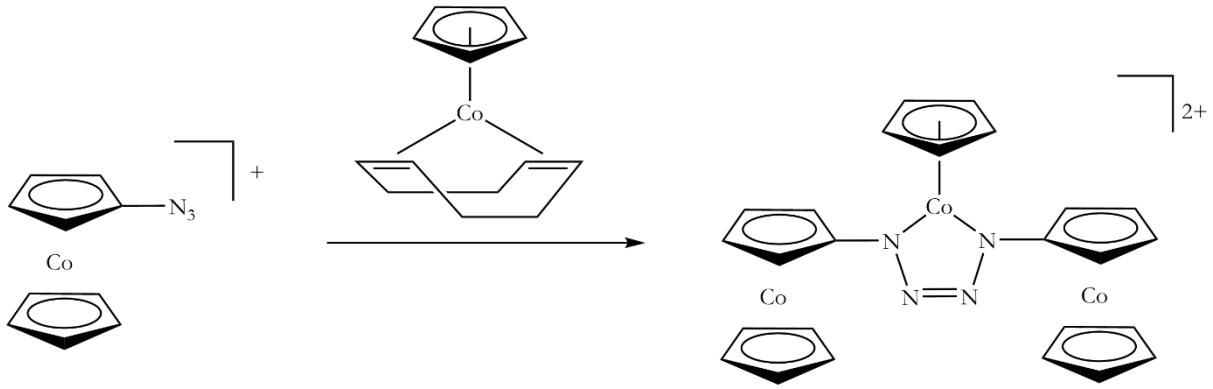

Scheme 18: Synthesis of the trimetallic cobaltocene tetrazene complex reported by *Bildstein*. Changing to azidoferrocene as starting material will lead to ferrocene tetrazene complex.[311]

1.6 Redox mediation

1.6.1 Mediation

Recently, the chemistry community has become more interested in electro(chemical) organic synthesis for manifold reasons.[313] First, there is an ecological aspect. By using electrons (from electricity) in a direct organic synthesis for oxidation or reduction steps, the mostly used redox reagents can be avoided. These redox reagents are typically dangerous and toxic substances, so the use of electricity is more environmental friendly and less energy consuming.[314,315] Secondly, and more significant, is the development of a cost-effective technique.[316] Electrochemical reactions require electrodes inside a solution to form a power circuit. The voltage can be controlled without delay during the reaction. So apart from the substrates an electrochemical synthesis only needs electricity. Compared to the chemicals that can be used as redox reagents in a chemical organic synthesis, electricity is cheap. The electrochemical step often plays a key role in multi-step organic reaction as the base of generating reactive intermediates.[317,318] Next to this, the electric synthesis can be used to produce substances for further reaction steps *in situ* which are possibly instable for storage or transfer.[319] For chemical reactions it is favorable to use the least possible number of substances. The use of electricity circumvents the addition of redox reagents and therefore also a variety of side reactions. There are lots of applications for electro organic synthesis, like the generation and channeling of highly reactive intermediates,[318] construction of complex molecules like peptidomimetics and biomolecules,[317,318] intramolecular control[320] and bond formation.[321] So

electro organic synthesis is already used in a wide field. Despite, the numbers of applications as well as the quality of the electro organic synthesis can still be increased.

Normally, the electro organic synthesis is a direct electrolysis, with a heterogeneous electron transfer at the electrode surface (**Figure 33**).[322] That step produces the (reactive) intermediate for the next step of the multi-step reaction. This type of reaction comes with several disadvantages. First of all, it is a slow reaction due to the heterogeneous nature of the reaction and for it being kinetically hindered by a big reorganization energy for the substrate.[322–324] In addition, normal electrolysis comes with the possibility of overoxidation and overreduction due to local overpotential and therefore to the formation of a large amount of side products.[319] Additionally, by using a direct electrolysis there comes the possibility of electrode passivation by the formation of polymers on the electrode or by precipitation of side products.[322]

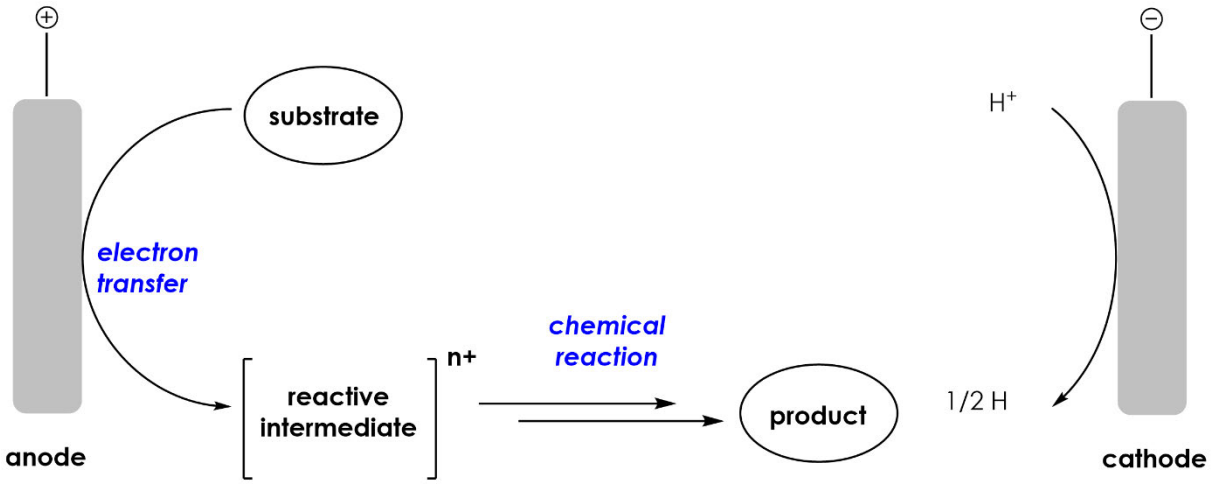

Figure 33: Principle of common electrolysis.[49]

A possibility to avoid some off these problems is the indirect electrolysis, using a so-called mediator.[322] The mediator is a competitor for the electron and has to have a high electron self exchange rate and a small reorganization energy for redox events. That ensures the redox chemistry at the electrode to be done by the mediator. The heterogeneous process that forms the intermediate changes to a homogeneous process while the mediator reacts as a transport agent for the electrons. Optimally, a mediator is a stable redox couple that does not react chemically with the substrate. Instead of the substrate, the mediator undergoes the oxidation or reduction at the electrode avoiding the substrate to get in contact with the electrode surface and thus a possible local overpotential (**Figure 34**). So the mediator inhibits the formation of polymer films or side products resulting in better yields for the organic synthesis.[322]

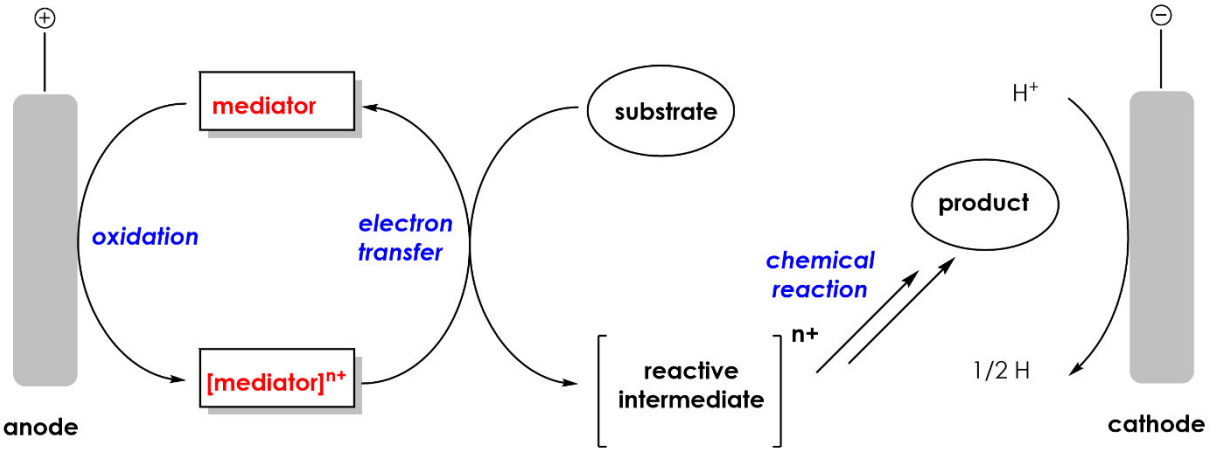

Figure 34: Principle of the redox mediation.[49]

There are a lot of fields in chemistry where the electro organic chemistry is promising and will improve its impact. For example, it is possible to reduce CO_2 indirectly electrochemically to produce fuels.[325–328] A redox mediator can also be used in batteries to protect them from overcharge,[329] and as electron transfer agent for exited states in photoinitiated processes.[330] Due to this, there are some examples for mediators being used in the active layer of dye sensitized solar cells and light emitting diodes.[331–334] Commonly used redox mediator in anodic oxidation are triarylamines (**Figure 35**a) and *N*-oxyl radicals such as 2,2,6,6-Tetramethylpiperidinyloxyl (TEMPO) (**Figure 35**b). The typical reactivity of the triarylamines are electron transfer reactions. They can be used for the oxidation of allylic and benzylic alcohols, the deprotection of thioacetals, functionalization of aromatic side chains and the α-oxidation of aliphatic ethers.[322] Otherwise, the typical reactivity of TEMPO comes from hydrogen abstraction reactions. It can be used for the oxidation of aliphatic, benzylic and allylic alcohols, amines and carbonyl and for the conversion of propargyl acetates and tetrahydroisoquinolines.[322]

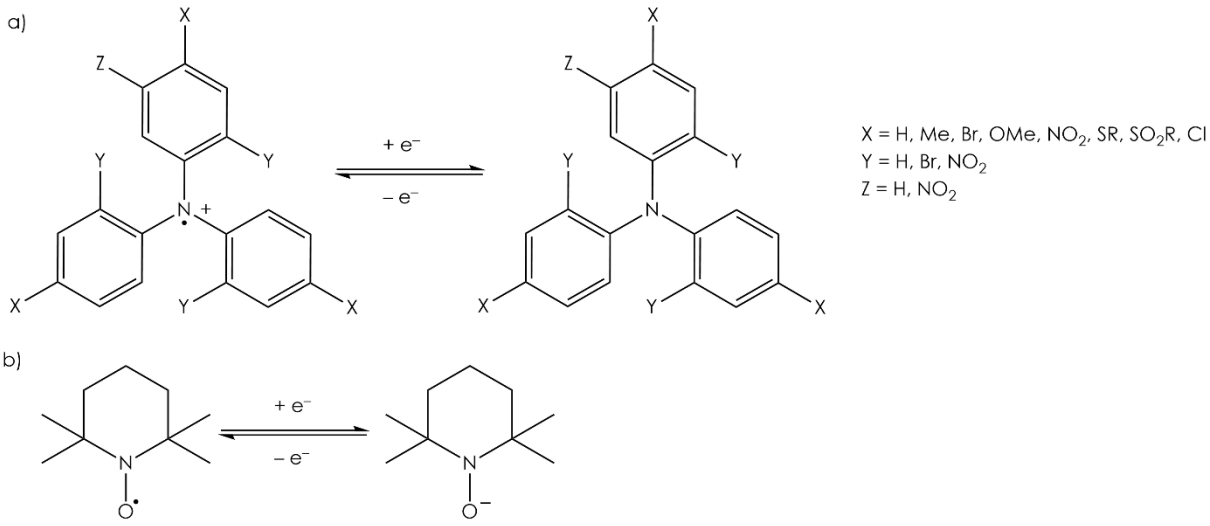

Figure 35: Redox mediator for anodic oxidation. a) Triarylamines. b) TEMPO.

Redox mediators are the crucial part in the indirect electro organic synthesis and therefore need to fulfill certain requirements to be useable as redox mediators. Since the redox potentials of the

mediator need to be close to the redox potential of the catalysts, several classes of mediators have to be tuned to vary their redox potential. In case of metal complexes this can be done by using several metal centers. The change from iron(II) to cobalt(II) as metal center in metallocenes shifts the redox potential to $E^0 = -1.33$ V (vs. FcH/FcH^+). Organic compounds can be tuned by variation of the substituents. Electron donating substituents like the two amino groups in 1,1'-diaminoferrocene shifts the potential to lower values ($E^0 = -0.602$ V vs. FcH/FcH^+).[335] Otherwise, the potential is shifted to higher values by electron accepting substituents like in decachloridoferrocene ($E^0 = 1.246$ V vs. FcH/FcH^+).[336] A theoretical model using the *Hammett* constants (σ) of the substituents was defined to determine compounds for a broad redox potential range. With this, it is possible to find a fitting mediator without extensive tests. The *Hammett* constants are empirical obtained values for the influence of substituents in benzoic acid relating reaction rate and equilibrium constants.[337] The constants are also influenced by their position in the aromatic system resulting in σ_m constants for substituents in meta position and σ_p constants for substituents in para position. Commonly used organic redox mediators are derivatives of triarylamine. The redox potentials of different triarylamine derivatives can be plotted against the sum of the substituents respective *Hammett* constants.[154,338] A linear fit on this data gives a method to predict the redox potential of untested derivatives.[339,340] The redox mediator and its oxidized or reduced counterpart have to be stable under the reaction conditions and inert to side reactions despite the electron transfer. This is necessary to prevent the appearance of side reaction initiated by the redox mediator.

1.6.2 Application

Ferrocenyl derivatives can be used as redox mediators in different ways. They act as catholytes in redox flow batteries[341] and assist in the voltammetric determination of glutathione in hemolized erythrocytes.[342] The most important use is the utilization of ferrocene as single electron transfer (SET) reagent in organic syntheses.[343–353] In case of tandem cyclizations of malonates, adjusting the electrochemical potential of the used ferrocene derivatives supports the selectivity of the reaction (**Scheme 19**a).[354] Ferrocene moieties can also be used as redox catalysts for different reactions like C–H imidation reactions of heteroarenes (**Scheme 19**b),[355] borylation of

arenediazonium salts (**Scheme 19**c)[356] and *Meerwein* arylation reactions (**Scheme 19**d).[357]

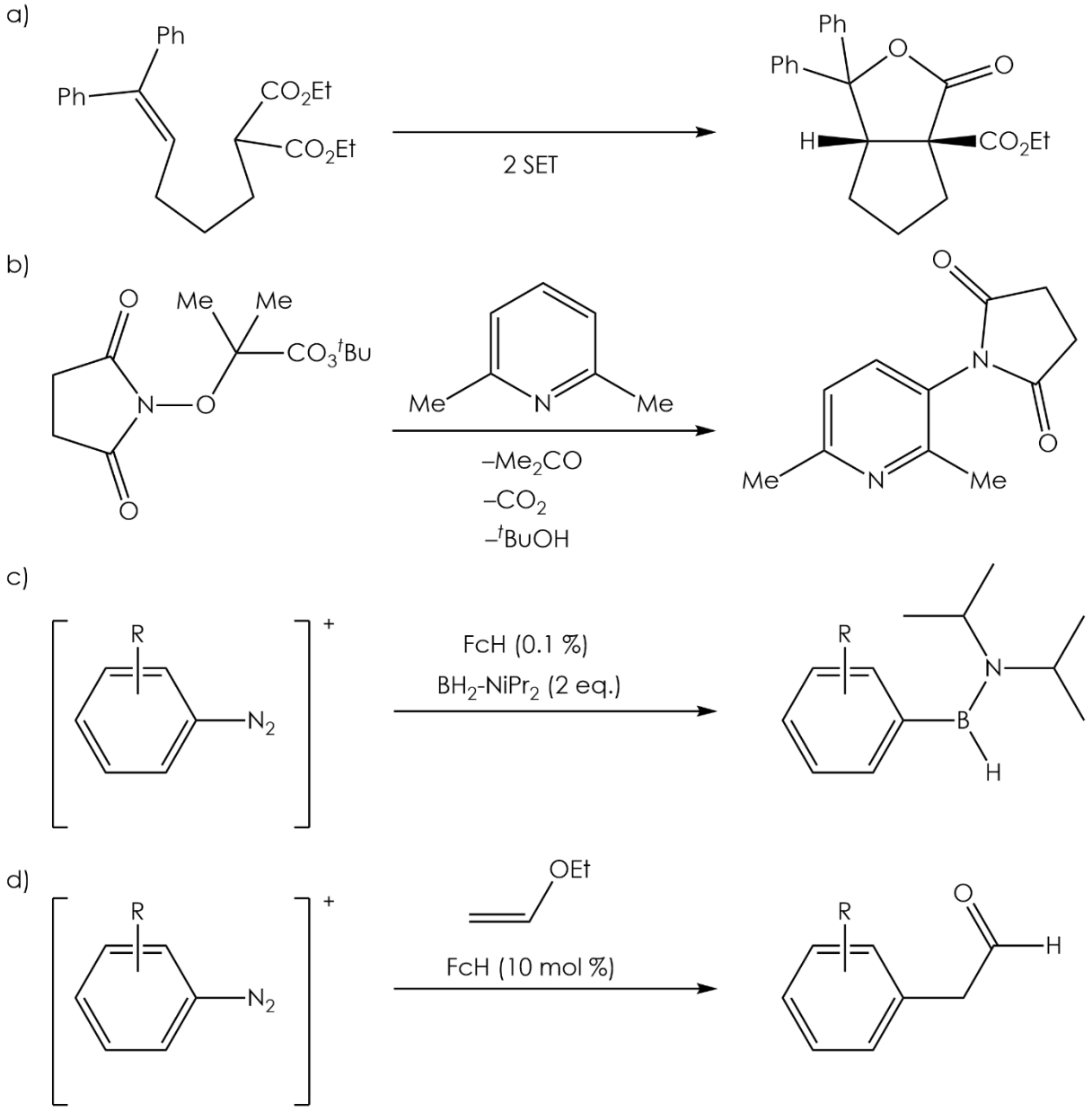

Scheme 19: Several applications for the ferrocene/ferrocenium couple as a) SET reagent. b) redox catalysts for C–H imidation. c) redox catalyst for borylation of arenediazonium salts. d) redox catalyst for *Meerwein* arylation reactions.

Electrochemical oxidation of carboxylates for the electrochemical modification of carbon surfaces,[358,359] dehydrogenative coupling reactions[360,361] and olefin hydroaminations[362] (**Scheme 20**) are conducted with ferrocene (derivatives) as redox mediators. In this reaction, the proton (provided by the solvent) is reduced at the cathode. The methanolate is able to deprotonate the allylic carbamate by self regeneration. The deprotonation of the allylic carbamate forms a substrate, which owns a lower potential for oxidation. So it is oxidized by ferrocenium, which forms ferrocene. Ferrocenium is restored by the oxidation of ferrocene at the anode. The carbamate now exhibits a nitrogen centered radical which performs a ring closure with the olefin. The final step is a hydrogen abstraction of the resulting radical from a solvent molecule. The ferrocene/ferrocenium

redox cycle prevents the need for the deprotonated carbamate to diffuse to the anode to get oxidized. This decreases the reaction time and blocks side reactions.

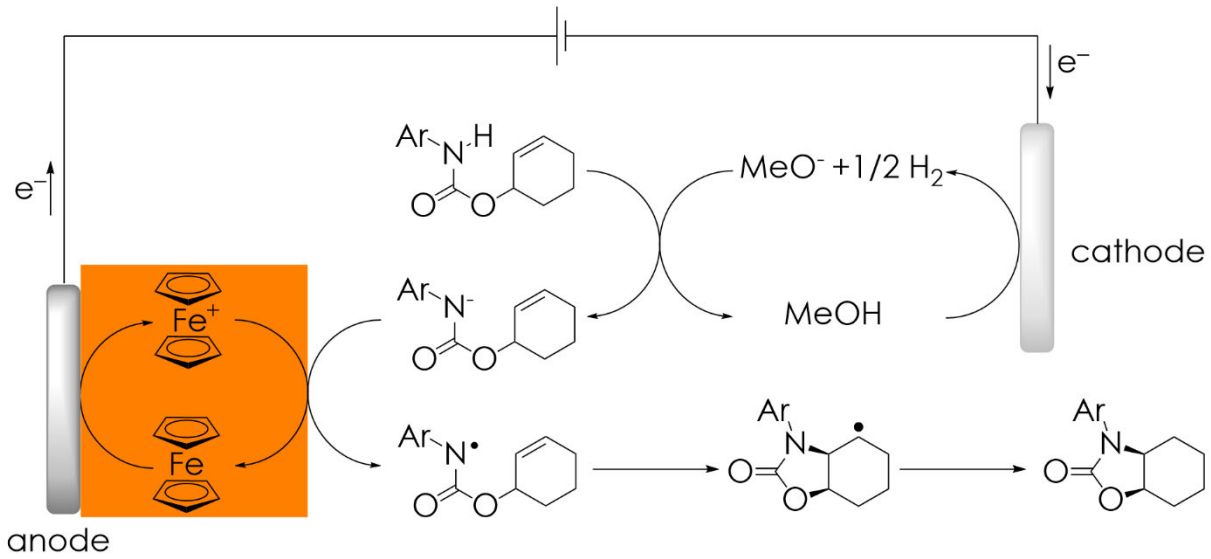

Scheme 20: Mechanism of the ferrocene mediated electrocatalytic hydroamidation of allylic carbamates.[362]

2 Aim of work

Metallocenes as metal organic complexes can be introduced as substituents in organic and metal organic systems. This work considers the extensive involvement of metallocenes feasible due to their electrochemical properties. Several applications of metallocenes depending on their electrochemical potential will be investigated. Therefore, three topics with different types of metallocene participation are processed:

- Metallocenes as redox mediatiors: intermolecular participation as supporting agent
- Metallocenes as redox switchs: intramolecular phase tag as redox support for gold(I)/(II) redox chemistry
- Metallocenes as mediates: Hydrogen Evolution Reaction (HER)

Potential ferrocene/ferrocenium redox mediators:

Metallocenes and their associated metallocenium cations are known to form stable redox couples. In order to be used as redox mediators, it is necessary to adjust the potential of ferrocene derivatives by addition of electron withdrawing substituents. Furthermore, the potential needs to be predictable. A set of similar ferrocenyl ester derivatives is studied. Their redox potentials are determined via cyclic voltammetry (CV) and square wave voltammetry (SWV). Besides the *Hammett* model will be used for the prediction of redox potential of ferrocene derivatives. Since ferrocenium is quite unstable towards nucleophiles, the stability of all ferrocene/ferrocenium couples has to be determined. Substitution of the ferrocene unit may have a big influence on the electron self exchange rate, which is why ^{1}H NMR spectroscopy is used for all derivatives for proof of fast electron self exchange.

Ferrocenyl carbene gold(I) complexes as potential redox switchable catalysts:

Typical catalysis using gold carbene complexes start with abstraction of the halide ligand. Introducing a metallocene into the carbene ligand opens the possibility of redox switchable catalysis (RSC). By changing the oxidation state of the metallocene substituent, the catalyst can be activated or deactivated. This can occur chemically or electrochemically. That allows the option to regenerate the catalyst by using the metallocene as phase tag. Ferrocene is a suitable substituent for RSC complexes. These complexes are originally based on NHC and MICs as ligands. Attempts for acyclic metallocene carbenes succeeded only recently. The acyclic ferrocenylsubstituted diamino carbene shows a different behavior than the NHC based gold(I) carbene complexes. Oxidation of the acyclic complexes leads to the formation of a gold(II) complex, probably supported by a temporarily existing ferrocenium moiety in the acyclic carbene ligand. The gold(II) complex is the active species towards the cycloisomerization of propargylamides. The amino-ferrocenyl carbenes published by *Heinze* offer a push-spectator stabilization. Diamino carbenes are supposed to be more stable due to their push-push stabilization. In this study, the synthesis for acyclic

ferrocenylsubstituted diamino carbene gold(I) complexes is investigated. The synthesis uses chloride(isocyano-ferrocene)gold(I) as flexible precurser for addition of secondary amines to form acyclic ferrocenylsubstituted carbene gold(I) complexes. The stability of these complexes upon oxidation will be observed as well as their electrochemical behavior. Similar to the *Heinze* complexes, the oxidation of the diamino carbene complexes will be followed via EPR spectroscopy to identify a possible formation of gold(II), which would also indicate the ability to perform RSC.

Dicobaltoceniumylamine as potential catalyst for hydrogen evolving reaction:

Complexes like cobalt porphyrins, cobalt corroles and cobaltocenium containing complexes show the ability to catalyze hydrogen evolution reaction (HER). Two metal centers are necessary for HER. Therefore, *N*,*N*-dicobaltoceniumamine with two nitrogen bridged cobaltoceniumyl substituents shall be synthesized and investigated in regard of its electrochemical properties. Deprotonation of the amine leads to the formation of an amide, which is supposed to afford a different electrochemical behavior compared to the amine complex. The pK_a value of this acid-base pair will give information about the equilibrium between both complexes. Using the pK_a value and the electrochemical potential, the BDFE of the nitrogen bridged complex shall be determined. Considering the BDFE, the possibility of the amine and the amide to provide HER catalysis should be investigated in regard to the concerted proton-electron coupling which is a competitive pathway towards the HER.

3 Results and Discussion

Section 3.1, 3.2 and 3.3 of this dissertation have been published/submitted as scientific articles in the peer-reviewed journals *Beilstein Journal of Organic Chemistry*, *European Journal of Inorganic Chemistry* and *Organometallics*.

Section 3.1 was published as: "Sven D. Waniek, Jan Klett, Christoph Förster and Katja Heinze *Beilstein J. Org. Chem.* **2018**, *14*, 1004–1015.*Polysubstituted ferrocenes as tunable redox mediators* in *Beilstein Journal of Organic Chemistry*". It shows the investigation of mono-, di-, tri- and tetrasubstituted ferrocenyl esters with methoxycarbonyl substituents. The redox potential of all four complexes were determined by Cyclic Voltammetry (CV) and Square Wave Voltammetry (SWV) and compared with the theoretical expectations. UV/Vis and IR spectroscopy were performed to verify the stability of all redox pairs. ^{1}H NMR spectroscopy was used to determine the electron self exchange for all esters.

Section 3.2 was published as: "Sven D. Waniek, Christoph Förster and Katja Heinze *Eur. J. Inorg. Chem.* **2022**, e202100905. *Protic Ferrocenyl Acyclic Diamino Carbene Gold(I) Complexes* in *European Journal of Inorganic Chemistry*". In this publication, the synthesis, isolation and characterization of chlorido [(diethylamino)(aminoferrocenyl) methylidene] gold(I) and chloride [(diisopropylamino)(amino-ferrocenyl) methylidene] gold(I) is described. The structure of both carbene complexes was clarified by X-ray diffraction (XRD) while the diisopropyl derivative exhibits aurophilic interaction between two gold atoms. Both complexes were oxidized chemically and investigated by EPR and UV/Vis spectroscopy to monitor electrochemical changes after oxidation.

Section 3.3 was published as: "Sven D. Waniek, Christian Heine, Dimitri Zorn, Taro Lieberth, Maximilian Lauck, Christoph Förster and Katja Heinze *Organometallics*, **2022**, 10.1021/acs.organomet.2c00211. *Dicobaltocenium Amine – Proton, Electron, and H Atom Transfer* in *Organometallics*". A synthesis for *N*,*N*-dicobaltoceniumamine hexafluorophosphat and *N*,*N*-dicobaltoceniumamide hexafluorophosphate was developed. The electronic behavior between two nitrogen bridged cobaltocenium moieties was investigated dependent on the presence and absence of an amine proton. Several electrochemical and spectroelectrochemical measurements were performed to understand the nature of the electronic properties. Attempts to prove hydrogen evolution reaction (HER) being performed by redox chemistry of both complexes were done by EPR and ^{1}H NMR spectroscopy.

3.1 Polysubstituted ferrocenes as tunable redox mediators

Sven D. Waniek, Jan Klett, Christoph Förster and Katja Heinze

Beilstein J. Org. Chem. **2018**, *14*, 1004–1015.

Thematic Series: "Electrosynthesis II"

The standard ferrocene/ferrocenium couple has been used successfully as a redox mediator for organic transformations and electrocatalytic synthesis such as dehydrogenative coupling reactions. For applications of redox mediators, it is crucial to adjust their electrochemical potential $E_{1/2}$ to the potential of the substrate. The potential of ferrocene can be tuned by variation of the number and nature of substituents. A complete series of ferrocene methyl esters (mono to tetra substituted) is investigated, covering a wide potential range from $E_{1/2}$ = 260 mV to $E_{1/2}$ = 900 mV vs. ferrocene. The impact of number and position of substituents of the four pairs was analyzed considering stability and electrochemical properties by Cyclic Voltammetry, Square Wave Voltammetry, IR and UV/Vis spectroelectrochemical methods as well as paramagnetic ^{1}H NMR spectroscopy, supported by detailed Density Functional Theory calculations.

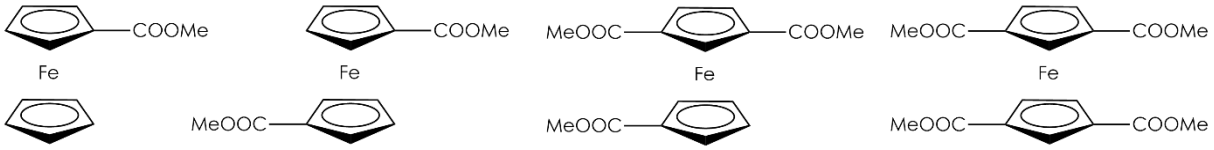

Author contributions

The compounds were synthesized by [redacted]. Purification, (spectro)electrochemical analysis, UV/Vis, IR and ^{1}H NMR spectroscopy and DFT calculations were performed by *Sven D. Waniek*. The manuscript was written by [redacted] and [redacted] and the supporting information was written by *Sven D. Waniek*.

Supporting Information

The Supporting Information is found in Section 6.1 on pp. 102. The Cartesian coordinates from DFT calculations can be found online at

https://doi.org/10.3762/bjoc.14.86

BEILSTEIN JOURNAL OF ORGANIC CHEMISTRY

Polysubstituted ferrocenes as tunable redox mediators

Sven D. Waniek, Jan Klett*, Christoph Förster* and Katja Heinze*

Full Research Paper

Open Access

Address:
Institute of Inorganic Chemistry and Analytical Chemistry, Johannes Gutenberg University Mainz, Duesbergweg 10–14, D-55128 Mainz, Germany

Email:
Jan Klett* - klettj@uni-mainz.de; Christoph Förster* - cfoerster@uni-mainz.de; Katja Heinze* - katja.heinze@uni-mainz.de

* Corresponding author

Keywords:
cyclic voltammetry; ferrocene; paramagnetic NMR spectroscopy; redox mediator; spectroelectrochemistry

Beilstein J. Org. Chem. **2018,** *14,* 1004–1015.
doi:10.3762/bjoc.14.86

Received: 09 February 2018
Accepted: 19 April 2018
Published: 07 May 2018

This article is part of the Thematic Series "Electrosynthesis II".

Guest Editor: S. R. Waldvogel

Abstract

A series of four ferrocenyl ester compounds, 1-methoxycarbonyl- (**1**), 1,1'-bis(methoxycarbonyl)- (**2**), 1,1',3-tris(methoxycarbonyl)- (**3**) and 1,1',3,3'-tetrakis(methoxycarbonyl)ferrocene (**4**), has been studied with respect to their potential use as redox mediators. The impact of the number and position of ester groups present in **1**–**4** on the electrochemical potential $E_{1/2}$ is correlated with the sum of Hammett constants. The **1**/**1**$^+$–**4**/**4**$^+$ redox couples are chemically stable under the conditions of electrolysis as demonstrated by IR and UV–vis spectroelectrochemical methods. The energies of the C=O stretching vibrations of the ester moieties and the energies of the UV–vis absorptions of **1**–**4** and **1**$^+$–**4**$^+$ correlate with the number of ester groups. Paramagnetic ^{1}H NMR redox titration experiments give access to the chemical shifts of **1**$^+$–**4**$^+$ and underline the fast electron self-exchange of the ferrocene/ferrocenium redox couples, required for rapid redox mediation in organic electrosynthesis.

Introduction

Since its discovery, ferrocene (FcH) has been established as versatile redox-active building block [1-3]. Ferrocene can be reversibly oxidized to the 17 valence electron ferrocenium cation (FcH^+) at a useful electrochemical potential (FcH/FcH^+ +630 mV vs NHE; +380 mV vs SCE in CH_3CN) [4]. The 0/+ redox couple of ferrocene and its derivatives possesses high electron self-exchange rates k_{ex} = 10^6–10^7 M^{-1} s^{-1}, remarkably independent on the electrolyte and solvent [5,6]. Both, the ferrocene/ferrocenium and the decamethylferrocene/decamethylferrocenium redox couples are well established as internal reference redox systems for electrochemical analyses in non-aqueous media [7-10]. Important requirements for redox couples with respect to useful applications are: (i) Both components of the redox couple should be soluble. (ii) Homogeneous and heterogeneous electron-transfer (ET) reactions should be fast. (iii) Both components should be stable under the electrolysis conditions and should not react irreversibly with any component of the supporting electrolyte [8]. In general, the redox mediators used as redox catalysts in indirect organic electrosyntheses should comprise the same characteristics [11-14]. A mediator is a reversible redox couple with a fast ET between itself and the electrode (heterogeneous) and between itself and the substrate (homogeneous). The benefit of the presence of a mediator is the switch of the sluggish heterogeneous electron

Beilstein J. Org. Chem. 2018, 14, 1004–1015.

transfer between electrode and substrate to a rapid homogeneous redox reaction between mediator and substrate. Further, the mediator's redox potential must be below or above of that of the substrate for oxidation or reduction processes, respectively. This avoids the often kinetically hindered direct ET between electrode and substrate and diminishes overoxidation or overreduction of the substrate.

Redox-active ferrocenyl derivatives find application in redox flow batteries [15], with water soluble (ferrocenylmethyl)ammonium salts acting as catholytes. Ferrocene dicarboxylic acid has been described as mediator for the voltammetric determination of glutathione in hemolized erythrocytes [16]. (Substituted) ferrocenium salts were successfully employed as single-electron transfer (SET) reagents in organic syntheses [17-28]. Tuning of the electrochemical potential of substituted ferrocenium salts promoted a selective oxidative bicyclization reaction under mild conditions (Scheme 1a) [27]. Ferrocene and decamethylferrocene act as redox catalysts in Meerwein arylation reactions [29], borylations of arenediazonium salts [30]

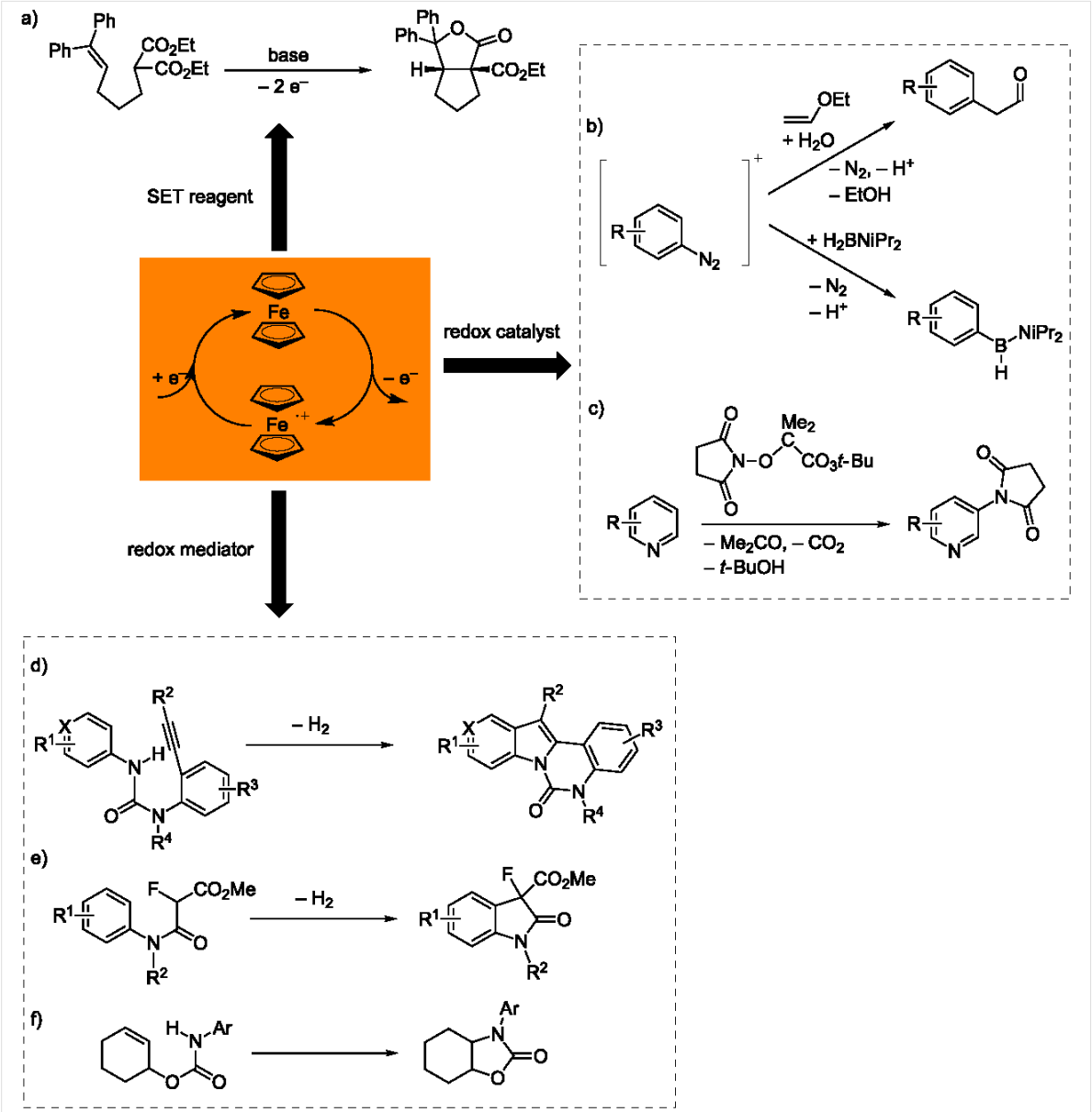

Scheme 1: Selected transformations with ferrocene/ferrocenium as SET reagents (a) [27], catalyzed (b,c) [29-31] and mediated transformations (d–f) [34-36] by the ferrocene/ferrocenium redox couple.

Beilstein J. Org. Chem. **2018,** *14,* 1004–1015.

and in C–H imidation reactions of (hetero)arenes [31] (Scheme 1b,c). Ferrocene has been used as redox mediator for the electrochemical modification of carbon surfaces via electrochemical oxidation of carboxylates [32,33], as mediator for dehydrogenative coupling reactions [34,35] and for olefin hydroamidations [36] (Scheme 1d–f).

For potential applications of ferrocene derivatives as redox mediators or SET reagents, it is crucial to adjust the electrochemical potential to the potential of the substrate. The electrochemical potential of the ferrocene/ferrocenium redox couple strongly depends on the number and types of substituents [27,37-44]. One major drawback of changing the substituents is the dramatic change in chemical reactivity of ferrocene derivatives, e.g., ligand substitutions, apart from the solely intended tuning of the redox potential. A single class of ferrocene compounds with similar chemical and physical characteristics, yet covering a broad range of electrochemical potentials should circumvent this problem. To increase the ferrocene/ferrocenium potential, electron-withdrawing substituents are required. Mono-, 1,1'-diesters and a single 1,1',3-triester of ferrocene are known [45-53]. Elegant routes to 1,1',3-tris(methoxycarbonyl)-ferrocene and 1,1',3,3'-tetrakis(methoxycarbonyl)ferrocene were developed only very recently [54], complementing the series of methyl esters of ferrocene carboxylic acids **1**–**4** (Scheme 2) [45-52].

The extremely bulky and electron-poor pentakis(methoxycarbonyl)cyclopentadienyl ligand gives a pseudo octahedral high-spin iron(II) complex **5**, instead of forming a stable classical low-spin sandwich complex, precluding its application as redox mediator (Scheme 2) [55,56].

Ferrocenyl esters **1**–**4** are synthetically accessible via the acids of **1** [45,46], **2** [57], **3** and **4** [54] in a direct selective metalation of ferrocene [54,57-60], quenching with carbon dioxide, followed by esterification [45-48,54]. The 1,1'-disubstituted ferrocene **2** can also be obtained by direct coordination of the respective substituted cyclopentadienyl ligand (CpR) to iron(II) [49]. An alternative route to the mono-, 1,1'-di- and 1,1',3-tricarboxylic acids of ferrocene is the oxidation of the respective acetylferrocenes [47,48,53]. Ferrocene carboxylic acid is also available via basic hydrolysis of ferrocenyl aryl ketones [61]. Together with the redox potentials of ferrocene, **1** and **2**, the hitherto unknown electrochemical potentials of **3** and **4** should cover a wide potential range. This will meet the requirements of different substrates for the potential application of **1**–**4** and their ferrocenium ions as selective redox mediators or SET reagents. Apart from the redox potentials of the redox mediators FcH and **1**–**4**, the stability of the 18 and 17 valence electron species as well as their solubility and the availability of spectroscopic probes to monitor reaction progress and stability are important issues. These fundamental aspects will be addressed in this study.

Herein, a detailed study of the properties of **1**–**4** and their ferrocenium ions $\mathbf{1}^+$–$\mathbf{4}^+$ in solution is reported including electrochemical methods (cyclic voltammetry and square wave voltammetry; CV, SWV) and covering investigations regarding the stability of **1**–**4**/$\mathbf{1}^+$–$\mathbf{4}^+$ by spectroelectrochemical methods (UV–vis, IR) [62-68]. In addition, the mediators **1**/$\mathbf{1}^+$–**4**/$\mathbf{4}^+$ are probed by paramagnetic NMR spectroscopic methods [69-73]. The results are supported with (time-dependent) density functional theoretical (TD)-DFT methods.

Results and Discussion

Electrochemistry of esters 1–4

The esters **1**–**4** were studied by cyclic and square wave voltammetry in 0.1 M CH_2Cl_2 solutions of [*n*-Bu_4N][$B(C_6F_5)_4$], using platinum working and counter electrodes. All esters **1**–**4** show

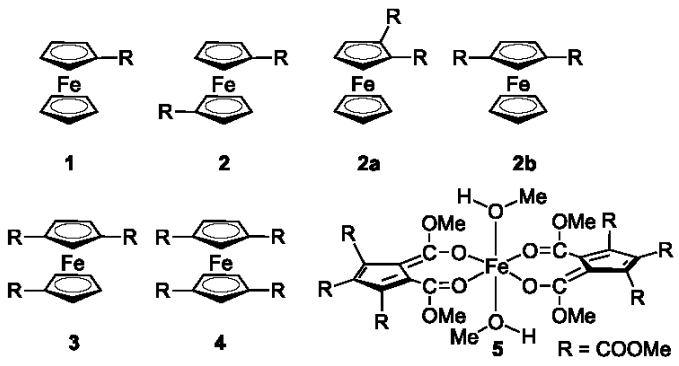

Scheme 2: Methyl esters of ferrocene carboxylic acids **1** [45,46], **2** [47-49], **2a** [50], **2b** [51,52], **3**, **4** [54] and pseudo octahedral high-spin iron(II) complex **5** with pentakis(methoxycarbonyl)cyclopentadienyl ligands [55,56].

Beilstein J. Org. Chem. 2018, 14, 1004–1015.

an essentially reversible behaviour for the ferrocene/ferrocenium oxidation process (Figure 1, Figure S1, Supporting Information File 1). The electrochemical potentials cover a wide range, $E_{1/2}$ = 260–900 mV vs FcH/FcH$^+$ (Figure 1, Table 1).

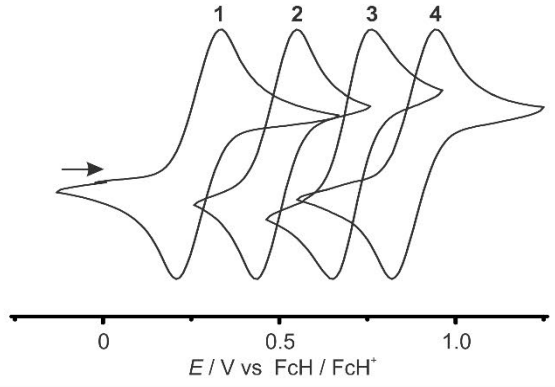

Figure 1: Normalized cyclic voltammograms for anodic sweeps of **1–4** in CH_2Cl_2/[*n*-Bu_4N][$B(C_6F_5)_4$] (scan rate 100 mV s^{-1}).

Table 1: Electrochemical data of esters **1–4** and sum of Hammett substituent constants σ_p[a] and σ_m[a].

	$E_{1/2}$ [mV][b]	$\sum\sigma_{p/m}$	$\sum\sigma_p$
1	260	σ_p = 0.45	0.45
2	495	2 σ_p = 0.90	0.90
3	700	2 σ_p + σ_m = 1.27	1.35
4	900	2 σ_p + 2 σ_m = 1.64	1.80

[a]σ_p = 0.45, σ_m = 0.37 for COOMe substituent [74]. [b]vs FcH/FcH$^+$.

The oxidation potential of the tetraester **4** is very high with $E_{1/2}$ = 900 mV. To the best of our knowledge, higher oxidation potentials (vs FcH/FcH$^+$) have been observed only for 1,1',2,2',4,4'-hexakis(pentafluorophenyl)ferrocene (940 mV in CH_2Cl_2) [40], 1,1',2,2',3,3'-hexakis(pentafluorophenyl)ferrocene (951 mV in CH_2Cl_2) [40], decachloroferrocene (E_p = 1246 mV in MeCN) [37], 1,1',2-tri(formyl)ferrocene (910 mV in CH_2Cl_2 at −40 °C) [38] and 1,1',2,2'-tetra(formyl)ferrocene (1145 mV in CH_2Cl_2 at −40 °C) [38]. The latter three are only irreversibly oxidized at room temperature precluding any application as mediators. The data are in full accordance with the increasing electron-withdrawing character of the cyclopentadienyl ligands from **1** to **4**. The position of the ester groups has a slight influence on the electrochemical potential. 1- or 1'-substitution with a methoxycarbonyl group raises the potential by ca. 250 mV (FcH → **1**, **1** → **2**), while substitution in 3- and 3'-position has only a smaller impact with an increase of the potential by ca. 200 mV (**2** → **3**, **3** → **4**). According to Lever et al. [39], the calculated electrochemical parameters E_L(L) for 1-(methoxycarbonyl)cyclopentadienyl and 1,3-bis(methoxycarbonyl)cyclopentadienyl ligands amount to $E_L(L_1)$ = 250 mV and $E_L(L_2)$ = 450 mV vs FcH/FcH$^+$, respectively. Indeed, the electrochemical potential $E_{1/2}$ = 700 mV of **3** perfectly corresponds to the sum $E_L(L_1) + E_L(L_2)$ = 700 mV. Consequently, the ligand contributions to the electrochemical potential of substituted cyclopentadienyl complexes are essentially additive for **1–4**.

This characteristic relationship is supported by correlating the electrochemical data with the Hammett substituent constants [37,39,74,75]. Typically, the $E_{1/2}$ data of substituted ferrocenes correlate linearly with the sum $\sum\sigma_p$ of the Hammett values σ_p of *para*-substituents [37,39,74].

For esters **1–4**, the electrochemical potentials $E_{1/2}$ (vs FcH/FcH$^+$) versus sum of Hammett values $\sum\sigma_p$ did not give a satisfactory linear relation. Within this approach, the relative positions of ester groups and hence their different electronic influence to the electrochemical potential is not considered. The influence of a methoxycarbonyl substituent in 1- or 1'-position is indeed best described with σ_p = 0.45 [75]. On the other hand, substituents in the 3- or 3'-position require using σ_m = 0.37 [75] for *meta*-substituents, to give an excellent linear correlation of $E_{1/2}$ with $\sum\sigma_{p/m}$ (Figure 2, Table 1).

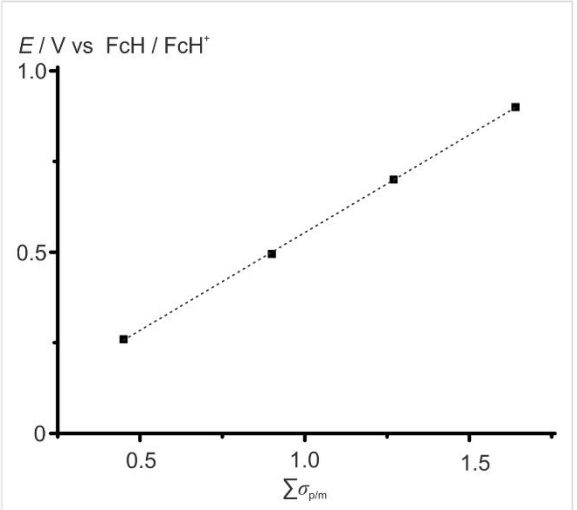

Figure 2: Electrochemical potentials $E_{1/2}$ (vs FcH/FcH$^+$) of esters **1–4** versus sum of Hammett values $\sum\sigma_{p/m}$ with linear regression ($E_{1/2}$ = 0.539 V · $\sum\sigma_{p/m}$ + 0.015 V, R^2 = 0.9999).

The generalizable use of σ_p and especially σ_m to include the effect on the relative positions of substituents for $E_{1/2}$ of polysubstituted ferrocenes has to be further validated with other series of polysubstituted ferrocenes.

Beilstein J. Org. Chem. **2018,** *14,* 1004–1015.

IR spectroelectrochemistry of esters **1–4**

In the attenuated total reflection (ATR) IR spectra of solid samples of esters **1–4**, several overlapping bands for the C=O stretching vibrations of the ester substituents are observed between 1678 and 1730 cm^{-1} (Figure 3a, Figures S2–S6, Table S1, Supporting Information File 1). DFT calculations (B3LYP, def2-TZVP, RIJCOSX, ZORA, CPCM (CH_2Cl_2)) on di-, tri- and tetraesters **2–4** suggest an intramolecular coupling of the C=O vibrations of the ester moieties substantiating the number of observed bands (Table S1, Supporting Information File 1). Furthermore, crystal packing effects with intermolecular C=O···H–C interactions, differing in strengths, can be responsible for the occurrence of distinguishable C=O bands [54,76,77]. For example, two different molecules of monoester **1** are present in the asymmetric unit of the solid-state structure [76], leading to different C=O stretching vibration bands (Figure 3a).

In contrast to the solid-state IR spectra, only a single broad C=O band is observed for **1–4** in solution (Figure 3, Figure 4, Figures S7–S14, Supporting Information File 1). In the series **1–4**, the C=O bands shift to higher wavenumbers in solution $\tilde{\nu}_{CO}$ = 1712–1724 cm^{-1} with increasing number of electron-withdrawing COOMe groups (Figure 3b). The DFT calculated IR spectra with unscaled energies of the C=O vibrations $\tilde{\nu}_{max(CO)}$ = 1710–1724 cm^{-1} fully support these findings (Table S1, Figures S15–S22, Supporting Information File 1).

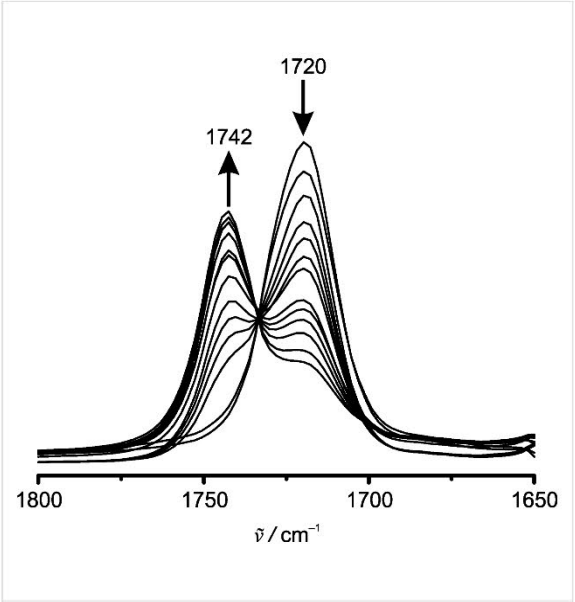

Figure 4: IR spectroelectrochemical oxidation of **3** to $\mathbf{3}^+$ in CH_2Cl_2/[*n*-Bu_4N][$B(C_6F_5)_4$] (C=O stretching vibration region, 0.4–1.1 V vs Ag pseudo reference electrode).

Compounds **1–4** can be reversibly oxidized to $\mathbf{1}^+$–$\mathbf{4}^+$ in dichloromethane and [*n*-Bu_4N][$B(C_6F_5)_4$] as supporting electrolyte in an IR spectroelectrochemical (SEC) cell, confirming

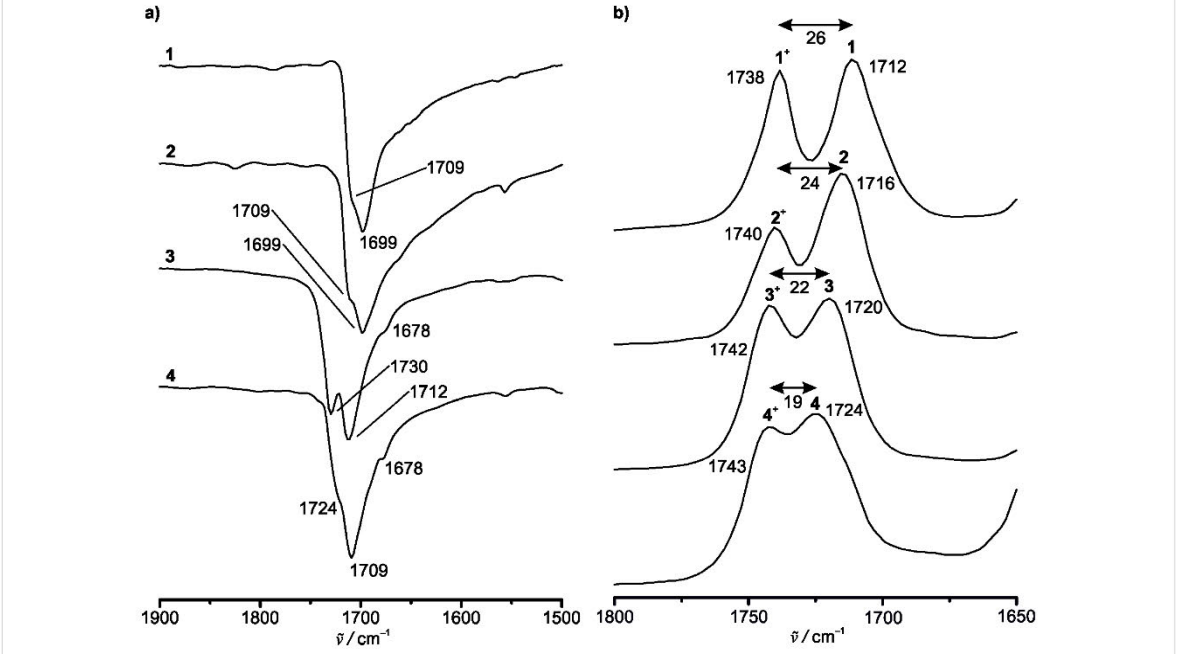

Figure 3: a) Partial ATR IR spectra (transmission normalized, C=O stretching vibration region) of solids **1–4**. b) Partial spectroelectrochemical IR spectra (absorption normalized, C=O stretching vibration region) of mixtures of the $\mathbf{1/1}^+$–$\mathbf{4/4}^+$ redox couples in dichloromethane/[*n*-Bu_4N][$B(C_6F_5)_4$].

Beilstein J. Org. Chem. 2018, 14, 1004–1015.

the chemical stability of the ferrocenyl esters under the conditions of electrolysis (Figure 3b, Figure 4, Figures S7–S14, Table S1, Supporting Information File 1).

Triester **3** and tetraester **4** cannot be quantitatively oxidized to $\mathbf{3}^+$ and $\mathbf{4}^+$ in the SEC cell up to a potential of 1.1 V and 1.4 V, respectively, probably due to a fast diffusion of **3** and **4** to the anode in the beam path (Figure 4, Figures S11–S14, Supporting Information File 1). In addition, precipitation of some poorly soluble **[4][X]** also occurs. During oxidation to the respective ferrocenium cations, the C=O stretching vibration bands of **1**–**4** decrease in intensity, while the C=O bands of $\mathbf{1}^+$–$\mathbf{4}^+$ appear, crossing in clean isosbestic points. Expectedly, the C=O stretching vibrations of $\mathbf{1}^+$–$\mathbf{4}^+$ are shifted to higher wavenumbers by 26–19 cm^{-1} ($\tilde{\nu}_{CO}$ = 1738–1743 cm^{-1}) with an increasing electron-withdrawing character of the Cp ligands. The substituent effect is attenuated by the positive charge at the iron atom in $\mathbf{1}^+$–$\mathbf{4}^+$ ($\Delta\tilde{\nu}_{CO}$ = 5 cm^{-1}), compared to **1**–**4** ($\Delta\tilde{\nu}_{CO}$ = 12 cm^{-1}), respectively (Figure 3b, Table S1, Figures S7–S14, Supporting Information File 1) [78]. The unscaled energies of the DFT calculated C=O bands of $\mathbf{1}^+$–$\mathbf{3}^+$ fit very well to the experimental observations of $\mathbf{1}^+$–$\mathbf{3}^+$ (Figures S7–S12, S16, S18, S20, Table S1, Supporting Information File 1). Unexpectedly, the calculated $\tilde{\nu}_{CO}$ data of $\mathbf{4}^+$ are significantly lower than the experimental ones, which remain unexplained at the moment.

For all redox couples of the ferrocenyl esters, the C=O stretching vibration delivers a useful in operando probe substantiating the stability of the redox mediator and enabling quantification of both redox partners and hence estimation of the actual concentration-dependent redox potential in solution.

UV–vis spectroelectrochemistry of esters 1–4

Analogous to the IR-SEC experiments, the esters **1**–**4** were also probed by UV–vis-SEC investigations. The UV–vis spectra of **1**–**4** recorded in dichloromethane show the ferrocene ligand field absorption band at λ_{max} = 444, 449, 455 and 457 nm, which is typically around $\lambda_{max} \approx$ 440–490 nm [66,70,79,80] (Figure 5a).

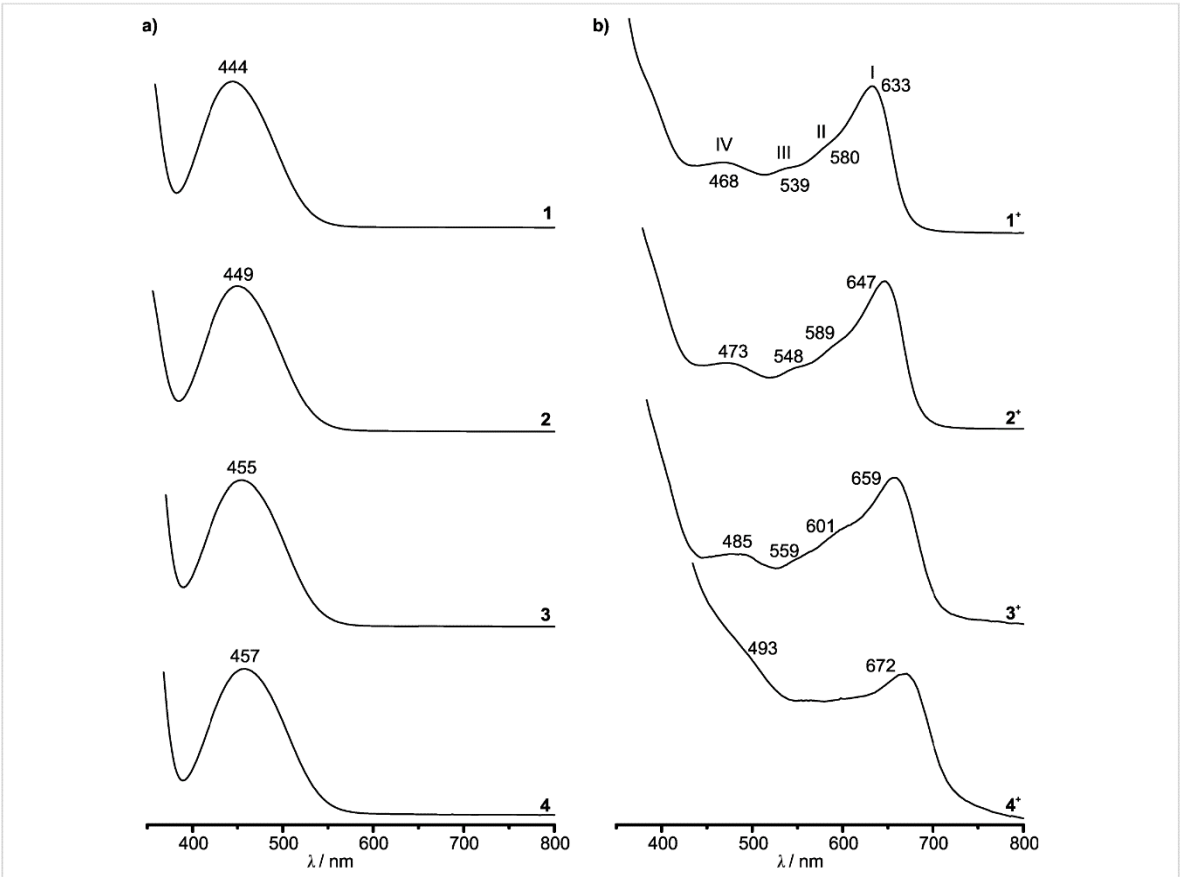

Figure 5: a) Normalized UV–vis spectra of **1**–**4** in CH_2Cl_2. b) Normalized UV–vis absorptions of $\mathbf{1}^+$–$\mathbf{4}^+$ in CH_2Cl_2/[*n*-Bu_4N][$B(C_6F_5)_4$] after spectroelectrochemical oxidation of **1**–**4**.

Beilstein J. Org. Chem. 2018, 14, 1004–1015.

The energy of the absorption bands decreases almost linearly with the number *n* of the electron-withdrawing COOMe substituents for **1**–**4** (Figure 6a).

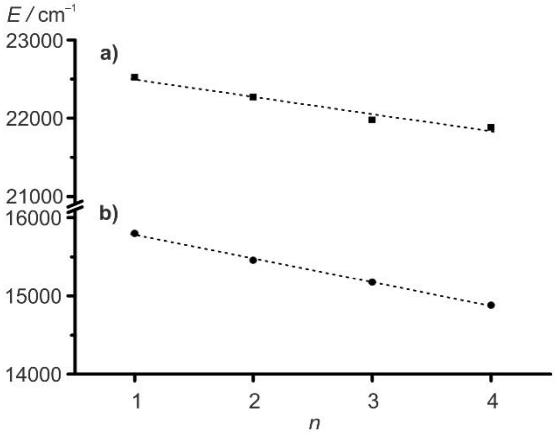

Figure 6: Absorption energy *E* of ferrocene bands of **1**–**4** (a) and energies of the low energy absorption maxima at around λ_{max} ≈ 630–670 nm of $\mathbf{1}^+$–$\mathbf{4}^+$ (b) versus number of methoxycarbonyl substituents *n* with regression lines
a) $E = -222\ cm^{-1} \cdot n + 22700\ cm^{-1}$, $R^2 = 0.9824$;
b) $E = -303\ cm^{-1} \cdot n + 16100\ cm^{-1}$, $R^2 = 0.9991$.

The reversible oxidation of **1**–**4** in UV–vis-SEC experiments in CH_2Cl_2/[*n*-Bu_4N][$B(C_6F_5)_4$] is monitored by the decreasing band intensity of the ferrocene absorption and the appearance of a set of four partially resolved characteristic ferrocenium absorptions (bands I–IV) responsible for the blue color (Figure 5b and Figure 7, Figures S23–S31, Supporting Information File 1).

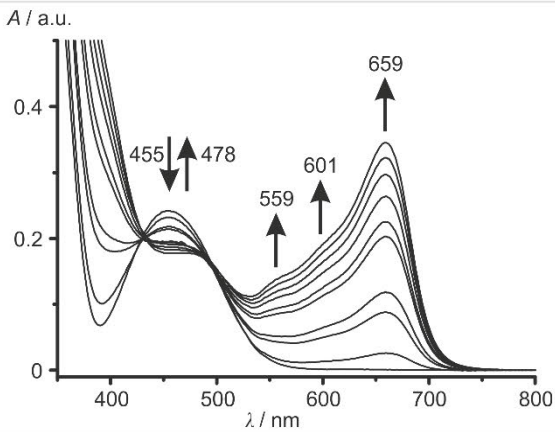

Figure 7: UV–vis spectroelectrochemical oxidation of **3** in CH_2Cl_2/[*n*-Bu_4N][$B(C_6F_5)_4$] (0–1.1 V vs Ag pseudo reference electrode).

Isosbestic points indicate clean conversions of **1** → $\mathbf{1}^+$, **2** → $\mathbf{2}^+$ and **3** → $\mathbf{3}^+$, respectively. For example, this set of bands and shoulders (sh) IV–I is observed at λ_{max} = 485 nm (IV), λ_{sh} = 559 nm (III), 601 nm (II) and λ_{max} = 659 nm (I) for $\mathbf{3}^+$. During oxidation of **4** to $\mathbf{4}^+$, isosbestic points between the absorption bands of **4** and $\mathbf{4}^+$ cannot be observed (Figures S29 and S30, Supporting Information File 1). Probably, precipitation of the poorly soluble tetraester $\mathbf{4}^+$ could be responsible for this effect, as already suggested for the IR-SEC experiments of **4**/$\mathbf{4}^+$. On the other hand, isosbestic points are observed in the UV–vis spectra upon re-reduction of $\mathbf{4}^+$ to **4** (Figure S31, Supporting Information File 1). The energy of the absorptions of the ferrocenium cations $\mathbf{1}^+$–$\mathbf{4}^+$ decreases with the electron-withdrawing nature of the Cp ligands in the series $\mathbf{1}^+$–$\mathbf{4}^+$, similar to the vis absorption maxima of the neutral ferrocenes **1**–**4**. For the prominent band I of the cations $\mathbf{1}^+$–$\mathbf{4}^+$, a linear and stronger dependency of the energy on the number *n* of methoxycarbonyl substituents can be found than for the ligand field band of the ferrocenes **1**–**4** (Figure 6b). The lowest energy band (band I) in the UV–vis spectra of $\mathbf{1}^+$–$\mathbf{4}^+$ is assigned to ligand-to-metal charge transfer (LMCT) transitions [79,81-83]. The bands II–IV are assigned to mainly d–d transitions [79]. TD-DFT calculations on the B3LYP, def2-TZVP, RIJCOSX, ZORA, CPCM (CH_2Cl_2) level do not give satisfactory results concerning energy, number of bands and oscillator strength of electronic transitions (Figures S32–S35, Supporting Information File 1). The poor agreement of TD-DFT calculated electronic spectra of metallocenes and derivatives with experimental data has been noted before. Improvements have been achieved by testing different functionals [84,85] and by including vibrational distortions of the ferrocene geometry into the calculations [86]. Nevertheless, the LMCT character of the prominent band I is confirmed by the calculations. The intensity of band I scales with the amount of the corresponding ferrocenium ion present and consequently the actual potential in solution can be estimated by UV–vis spectroscopy.

NMR spectroscopy of esters 1–4 and $\mathbf{1}^+$–$\mathbf{4}^+$

In contrast to typical organic paramagnetic redox mediators, the relaxation properties of proton nuclei of paramagnetic ferrocenium derivatives allow the observation of reasonable sharp resonances [87]. The fast electron self-exchange of the ferrocene/ferrocenium redox couple and derivatives on the NMR timescale leads to the observation of resonances with averaged chemical shifts δ in the ^{1}H NMR spectra of ferrocene/ferrocenium mixtures [5,6,70-72]. The molar fraction of FcH/FcH^+ can be calculated from the averaged ^{1}H NMR resonance frequencies of a mixture and the known resonance frequencies of FcH and FcH^+, respectively [6]. This relation gives $\chi_P = (\delta - \delta_D)/(\delta_P - \delta_D)$ for the molar fraction of the paramagnetic species, expressed in the chemical shift scale with δ_D being the chemical shift of the diamagnetic species, δ_P being the

Beilstein J. Org. Chem. 2018, 14, 1004–1015.

resonance of the paramagnetic species and δ being the averaged chemical shift of the mixture.

The detection of the resonances of **1**/**1**$^+$–**4**/**4**$^+$ should allow for determining the ratio of **1**:**1**$^+$–**4**:**4**$^+$ by in situ NMR experiments. Thus, titration of **1**–**4** with Magic Green, tris(2,4-dibromophenyl)ammoniumyl hexachloroantimonate [10], as a strong oxidant ($E_{1/2}$ = 1140 mV in MeCN vs FcH/FcH^+) in CD_2Cl_2 under NMR monitoring shows that the Cp proton resonances broaden upon oxidation and shift to lower field, while the methyl proton resonances of the ester substituents shift to higher field and remain much sharper (Figure 8, Table 2, Figures S36–S38, Supporting Information File 1).

In some cases, e.g., **3**$^+$, the different Cp protons can still be distinguished in spite of the broadened resonances (Figure 8). The broadening is much more severe for the Cp proton resonances, while the methyl proton resonances are still rather sharp allowing the discrimination and assignment of the different methyl protons of **3**$^+$ (Figure 8).

With an increasing number of ester groups, the proton resonances of the mono- and disubstituted Cp ligands and of the methyl groups shift to lower field for **1**–**4** (CpR: **1** → **2** → **3**, CpR_2: **3** → **4**), while for **1**$^+$–**4**$^+$, the Cp ligand proton resonances shift to lower field and the methyl proton resonances shift to higher field (CpR: **1**$^+$ → **2**$^+$ → **3**$^+$, CpR_2: **3**$^+$ → **4**$^+$). This substituent effect is larger for the paramagnetically shifted resonances of **1**$^+$–**4**$^+$ than for the diamagnetic complexes **1**–**4**.

In CD_3CN, the treatment of **3** with Magic Green led to the disappearance of the resonances of **3**. However, paramagnetically shifted resonances of **3**$^+$ are absent suggesting that the initially formed **3**$^+$ undergoes further reactions with the coordinating solvent CD_3CN (Figure S39, Supporting Information File 1). This finding underscores that the solvent has to be carefully chosen with respect to the mediated reaction and stability of the mediator.

From the observed ^{1}H NMR chemical shifts – either of the cyclopentadienyl or methyl resonances – the relative concentrations of the ferrocene and ferrocenium ion can be extracted, again allowing the estimation of the actual potential in solution by spectroscopic techniques.

Conclusion

Ferrocenyl esters **1**–**4** with one to four ester substituents are reversibly oxidized to the respective ferrocenium cations **1**$^+$–**4**$^+$, spanning a broad electrochemical potential range from 260 mV for **1** to 900 mV for **4** vs the ferrocene/ferrocenium redox couple. The electrochemical potentials $E_{1/2}$ of **1**–**4** correlate linearly with the sum of Hammett substituent parameters $\sum\sigma_{p/m}$. However, the position of ester substituents has to be taken into account by employing σ_p for 1- and 1'-substituents and σ_m for

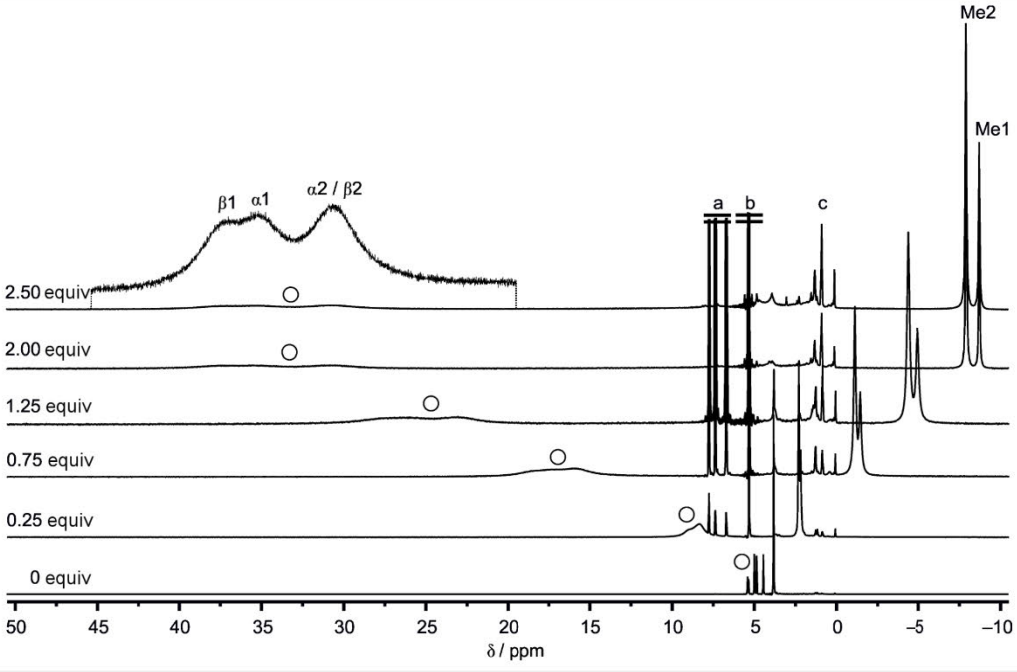

Figure 8: ^{1}H NMR oxidation titration of **3** in CD_2Cl_2 with $[N(2,4\text{-}C_6H_3Br_2)_3]^+$ as oxidant. [a]$[N(2,4\text{-}C_6H_3Br_2)_3]$. [b]$CDHCl_2$. [c]Residual solvents and grease.

Beilstein J. Org. Chem. **2018,** *14,* 1004–1015.

Table 2: ^{1}H NMR data (δ [ppm])[a] of **1–4** and **1**$^+$**–4**$^+$ in CD_2Cl_2.

	H^{Cp}	$H^{\alpha1}/H^{\beta1}$	$H^{\alpha2}/H^{\beta2}$	H^{Me1}	H^{Me2}
1	4.20	4.40/4.77		3.76	
1$^+$	37.0	30.1/32.3		−8.34	
2		4.42/4.79		3.78	
2$^+$		34.0[b]		−8.51	
3		4.43/4.84	4.97/5.39	3.79	3.80
3$^+$		35.3/37.5	30.7[b]	−8.75	−7.94
4			4.98/5.42		3.87
4$^+$			33.6[b]		−8.26

[a]Numbering scheme: 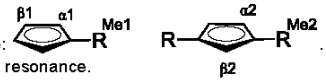

.
[b]Only a single broad resonance.

3- and 3'-substituents, respectively. Complexes **1**–**4** and **1**$^+$–**4**$^+$ are stable under conditions of electrolysis (CH_2Cl_2, [*n*-Bu_4N][$B(C_6F_5)_4$]) as demonstrated by IR and UV–vis spectroelectrochemical experiments and ^{1}H NMR spectroscopy. The C=O stretching vibrations of the ester substituents as characteristic probes in the IR spectra are consistently shifted to higher energies from **1** to **4** and from **1**$^+$ to **4**$^+$. Upon oxidation of **1**–**4** to **1**$^+$–**4**$^+$ in solution, the ferrocene bands in the UV–vis spectra of **1**–**4** at λ_{max} = 444–457 nm and the LMCT bands of **1**$^+$–**4**$^+$ at λ_{max} = 633–672 nm bathochromically shift linearly with increasing number of ester groups. The ^{1}H NMR paramagnetic chemical shifts of **1**$^+$–**4**$^+$ have been determined by redox titration experiments.

With all the data in hand, the molar fraction of the ester-substituted redox couples **1**/**1**$^+$–**4**/**4**$^+$ can be accessed a) from the C=O stretching vibrations of the ester groups, b) the ferrocenium CT bands or c) from the averaged ^{1}H NMR chemical shifts of the Cp or ester methyl protons. Ongoing investigations focus on the spectroscopic monitoring of **1–4** as redox mediators in selected electrosynthetic transformations.

Experimental

Dichloromethane, CD_2Cl_2 and CD_3CN were distilled from calcium hydride. Electrochemical experiments were carried out on a BioLogic SP-50 voltammetric analyzer using a platinum working electrode, a platinum wire as counter electrode, and a 0.01 M $Ag/AgNO_3$ CH_3CN electrode as reference electrode. The measurements were carried out at a scan rate of 100 mV s^{-1} for cyclic voltammetry experiments and 100 mV s^{-1} for square wave voltammetry experiments using 0.1 M [*n*-Bu_4N][$B(C_6F_5)_4$] as supporting electrolyte and 0.001 M of the sample in dichloromethane. Potentials are given relative to the ferrocene/ferrocenium couple.

Spectroelectrochemical experiments were performed using a Specac omni-cell liquid transmission cell with CaF_2 windows equipped with a Pt-gauze working electrode, a Pt-gauze counter electrode and an Ag wire as pseudo-reference electrode, melt-sealed in a polyethylene spacer (approximate path length 0.5 mm) in dichloromethane (68, 35, 13, 2 mM solutions of **1**–**4** in CH_2Cl_2, containing 0.1 M [*n*-Bu_4N][$B(C_6F_5)_4$]) [88]. UV–vis/near-IR spectra were recorded on a Varian Cary 5000 spectrometer using 1.0 cm cells (Hellma, Suprasil). IR spectra were recorded on a Bruker Alpha FTIR spectrometer with ATR unit, containing a diamond crystal.

NMR spectra were recorded on a Bruker Avance DRX 400 spectrometer at 400.31 MHz (^{1}H) at 25 °C. All resonances are reported in ppm versus the solvent signal as internal standard: CD_2Cl_2 (^{1}H, δ = 5.32 ppm), CD_3CN (^{1}H, δ = 1.94 ppm) [89].

DFT calculations were carried out using the ORCA program package (version 4.0.1) [90]. All calculations were performed using the B3LYP functional [91-93] and employ the RIJCOSX approximation [94,95]. Relativistic effects were calculated at the zeroth order regular approximation (ZORA) level [96]. The ZORA keyword automatically invokes relativistically adjusted basis sets. To account for solvent effects, a conductor-like screening model (CPCM) modeling dichloromethane was used in all calculations [97]. Geometry optimizations and TD-DFT calculations (50 vertical transitions) were performed using Ahlrichs' split-valence triple-ξ basis set def2-TZVP which comprises polarization functions for all non-hydrogen atoms [98,99]. The presence of energy minima was checked by numerical frequency calculations. Explicit counterions and/or solvent molecules were not taken into account.

Supporting Information

The Supporting Information file contains square wave voltammograms, IR and UV–vis spectra of the spectroelectrochemical experiments, (TD)-DFT calculated IR and UV–vis spectra, a table with IR data, ^{1}H NMR spectra of the oxidation titration experiments and Cartesian coordinates of DFT calculated structures of **1**–**4**.

Supporting Information File 1

Mediators measured and calculated spectra, IR data and Cartesian coordinates.
[https://www.beilstein-journals.org/bjoc/content/supplementary/1860-5397-14-86-S1.pdf]

Acknowledgements

Financial support from the Rhein-Main-Universities initiative "Novel Concepts in Selective Electro-conversions for Added-value Chemicals" is gratefully acknowledged.

ORCID® iDs

Jan Klett - https://orcid.org/0000-0002-0055-5335
Katja Heinze - https://orcid.org/0000-0003-1483-4156

References

1. Togni, A.; Hayashi, T. *Ferrocenes;* Wiley-VCH Verlag GmbH: Weinheim, Germany, 1994.
2. Štěpnička, P., Ed. *Ferrocenes. Ligands, materials and biomolecules;* J. Wiley: Chichester, England, 2008.
3. Astruc, D. *Eur. J. Inorg. Chem.* **2017,** 6–29. doi:10.1002/ejic.201600983
4. Pavlishchuk, V. V.; Addison, A. W. *Inorg. Chim. Acta* **2000,** *298*, 97–102. doi:10.1016/S0020-1693(99)00407-7
5. Yang, E. S.; Chan, M.-S.; Wahl, A. C. *J. Phys. Chem.* **1980,** *84*, 3094–3099. doi:10.1021/j100460a025
6. Nielson, R. M.; McManis, G. E.; Safford, L. K.; Weaver, M. J. *J. Phys. Chem.* **1989,** *93*, 2152–2157. doi:10.1021/j100342a086
7. Gagne, R. R.; Koval, C. A.; Lisensky, G. C. *Inorg. Chem.* **1980,** *19*, 2854–2855. doi:10.1021/ic50211a080
8. Gritzner, G.; Kuta, J. *Pure Appl. Chem.* **1984,** *56*, 461–466. doi:10.1351/pac198456040461
9. Noviandri, I.; Brown, K. N.; Fleming, D. S.; Gulyas, P. T.; Lay, P. A.; Masters, A. F.; Phillips, L. *J. Phys. Chem. B* **1999,** *103*, 6713–6722. doi:10.1021/jp991381+
10. Connelly, N. G.; Geiger, W. E. *Chem. Rev.* **1996,** *96*, 877–910. doi:10.1021/cr940053x
11. Steckhan, E. *Angew. Chem., Int. Ed. Engl.* **1986,** *25*, 683–701. doi:10.1002/anie.198606831
12. Francke, R.; Little, R. D. *Chem. Soc. Rev.* **2014,** *43*, 2492–2521. doi:10.1039/c3cs60464k
13. Wiebe, A.; Gieshoff, T.; Möhle, S.; Rodrigo, E.; Zirbes, M.; Waldvogel, S. R. *Angew. Chem., Int. Ed.* **2018,** *57*, 2–28. doi:10.1002/anie.201711060
14. Jiang, Y.; Xu, K.; Zeng, C. *Chem. Rev.* **2018,** in press. doi:10.1021/acs.chemrev.7b00271
15. Ding, Y.; Yu, G. *Angew. Chem., Int. Ed.* **2017,** *56*, 8614–8616. doi:10.1002/anie.201701254
16. Raoof, J. B.; Ojani, R.; Karimi-Maleh, H.; Hajmohamadi, M. R.; Biparva, P. *Anal. Methods* **2011,** *3*, 2637–2643. doi:10.1039/c1ay05031a
17. Jahn, U. *J. Org. Chem.* **1998,** *63*, 7130–7131. doi:10.1021/jo981180m
18. Langer, T.; Illich, M.; Helmchen, G. *Synlett* **1996,** *1996*, 1137–1139. doi:10.1055/s-1996-5668
19. Jahn, U.; Müller, M.; Aussieker, S. *J. Am. Chem. Soc.* **2000,** *122*, 5212–5213. doi:10.1021/ja000565v
20. Jahn, U.; Hartmann, P.; Dix, I.; Jones, P. G. *Eur. J. Org. Chem.* **2001,** 3333–3355. doi:10.1002/1099-0690(200109)2001:17<3333::aid-ejoc3333>3.0.co;2-a
21. Pigge, F. C.; Coniglio, J. J.; Rath, N. P. *J. Org. Chem.* **2004,** *69*, 1161–1168. doi:10.1021/jo035058l
22. Sibi, M. P.; Hasegawa, M. *J. Am. Chem. Soc.* **2007,** *129*, 4124–4125. doi:10.1021/ja069245n
23. Goddard, J.-P.; Gomez, C.; Brebion, F.; Beauvière, S.; Fensterbank, L.; Malacria, M. *Chem. Commun.* **2007,** 2929–2931. doi:10.1039/b705284g
24. Richter, J. M.; Whitefield, B. W.; Maimone, T. J.; Lin, D. W.; Castroviejo, M. P.; Baran, P. S. *J. Am. Chem. Soc.* **2007,** *129*, 12857–12869. doi:10.1021/ja074392m
25. Krygowski, E. S.; Murphy-Benenato, K.; Shair, M. D. *Angew. Chem., Int. Ed.* **2008,** *47*, 1680–1684. doi:10.1002/anie.200704830
26. Jahn, U.; Dinca, E. *Chem. – Eur. J.* **2009,** *15*, 58–62. doi:10.1002/chem.200802139
27. Khobragade, D. A.; Mahamulkar, S. G.; Pospíšil, L.; Císařová, I.; Rulíšek, L.; Jahn, U. *Chem. – Eur. J.* **2012,** *18*, 12267–12277. doi:10.1002/chem.201201499
28. Holan, M.; Pohl, R.; Císařová, I.; Klepetářová, B.; Jones, P. G.; Jahn, U. *Chem. – Eur. J.* **2015,** *21*, 9877–9888. doi:10.1002/chem.201500424
29. Chernyak, N.; Buchwald, S. L. *J. Am. Chem. Soc.* **2012,** *134*, 12466–12469. doi:10.1021/ja305660a
30. Marciasini, L. D.; Richy, N.; Vaultier, M.; Pucheault, M. *Adv. Synth. Catal.* **2013,** *355*, 1083–1088. doi:10.1002/adsc.201200942
31. Foo, K.; Sella, E.; Thomé, I.; Eastgate, M. D.; Baran, P. S. *J. Am. Chem. Soc.* **2014,** *136*, 5279–5282. doi:10.1021/ja501879c
32. Hernández-Muñoz, L. S.; Fragoso-Soriano, R. J.; Vázquez-López, C.; Klimova, E.; Ortiz-Frade, L. A.; Astudillo, P. D.; González, F. J. *J. Electroanal. Chem.* **2010,** *650*, 62–67. doi:10.1016/j.jelechem.2010.09.006
33. Hernández-Muñoz, L. S.; Galano, A.; Astudillo-Sánchez, P. D.; Abu-Omar, M. M.; González, F. J. *Electrochim. Acta* **2014,** *136*, 542–549. doi:10.1016/j.electacta.2014.04.189
34. Hou, Z.-W.; Mao, Z.-Y.; Zhao, H.-B.; Melcamu, Y. Y.; Lu, X.; Song, J.; Xu, H.-C. *Angew. Chem., Int. Ed.* **2016,** *55*, 9168–9172. doi:10.1002/anie.201602616
35. Wu, Z.-J.; Xu, H.-C. *Angew. Chem., Int. Ed.* **2017,** *56*, 4734–4738. doi:10.1002/anie.201701329
36. Zhu, L.; Xiong, P.; Mao, Z.-Y.; Wang, Y.-H.; Yan, X.; Lu, X.; Xu, H.-C. *Angew. Chem., Int. Ed.* **2016,** *55*, 2226–2229. doi:10.1002/anie.201510418
37. Brown, K. N.; Gulyas, P. T.; Lay, P. A.; McAlpine, N. S.; Masters, A. F.; Phillips, L. *J. Chem. Soc., Dalton Trans.* **1993,** 835–840. doi:10.1039/DT9930000835
38. Hildebrandt, A.; Khalyfeh, K. A.; Schaarschmidt, D.; Korb, M. *J. Organomet. Chem.* **2016,** *804*, 87–94. doi:10.1016/j.jorganchem.2015.12.027
39. Lu, S.; Strelets, V. V.; Ryan, M. F.; Pietro, W. J.; Lever, A. B. P. *Inorg. Chem.* **1996,** *35*, 1013–1023. doi:10.1021/ic950620e
40. Thornberry, M. P.; Slebodnick, C.; Deck, P. A.; Fronczek, F. R. *Organometallics* **2000,** *19*, 5352–5369. doi:10.1021/om000798v
41. Rhode, C.; Lemke, J.; Lieb, M.; Metzler-Nolte, N. *Synthesis* **2009,** *2009*, 2015–2018. doi:10.1055/s-0029-1216812
42. Nieto, D.; Bruña, S.; Montero-Campillo, M. M.; Perles, J.; González-Vadillo, A. M.; Méndez, J.; Mo, O.; Cuadrado, I. *Chem. Commun.* **2013,** *49*, 9785–9787. doi:10.1039/c3cc44619k
43. Sünkel, K.; Weigand, S.; Hoffmann, A.; Blomeyer, S.; Reuter, C. G.; Vishnevskiy, Y. V.; Mitzel, N. W. *J. Am. Chem. Soc.* **2015,** *137*, 126–129. doi:10.1021/ja511588p
44. Inkpen, M. S.; Du, S.; Hildebrand, M.; White, A. J. P.; Harrison, N. M.; Albrecht, T.; Long, N. J. *Organometallics* **2015,** *34*, 5461–5469. doi:10.1021/acs.organomet.5b00811

45. Benkeser, R. A.; Goggin, D.; Schroll, G. *J. Am. Chem. Soc.* **1954,** *76,* 4025–4026. doi:10.1021/ja01644a047
46. Witte, P.; Lal, T. K.; Waymouth, R. M. *Organometallics* **1999,** *18,* 4147–4155. doi:10.1021/om990083w
47. Woodward, R. B.; Rosenblum, M.; Whiting, M. C. *J. Am. Chem. Soc.* **1952,** *74,* 3458–3459. doi:10.1021/ja01133a543
48. Sonoda, A.; Moritani, I. *J. Organomet. Chem.* **1971,** *26,* 133–140. doi:10.1016/S0022-328X(00)80600-2
49. Petrov, A. R.; Jess, K.; Freytag, M.; Jones, P. G.; Tamm, M. *Organometallics* **2013,** *32,* 5946–5954. doi:10.1021/om4004972
50. Werner, G.; Butenschön, H. *Eur. J. Inorg. Chem.* **2017,** 378–387. doi:10.1002/ejic.201600766
51. Hisatome, M.; Tachikawa, O.; Sashō, M.; Yamakawa, K. *J. Organomet. Chem.* **1981,** *217,* C17–C20. doi:10.1016/S0022-328X(00)86033-7
52. Kasahara, A.; Izumi, T.; Yoshida, Y.; Shimizu, I. *Bull. Chem. Soc. Jpn.* **1982,** *55,* 1901–1906. doi:10.1246/bcsj.55.1901
53. Deschenaux, R.; Kosztics, I.; Nicolet, B. *J. Mater. Chem.* **1995,** *5,* 2291–2295. doi:10.1039/jm9950502291
54. Klett, J. *Chem. – Eur. J.* **2018,** in press. doi:10.1002/chem.201800608.
55. Bruce, M. I.; Skelton, B. W.; Wallis, R. C.; Walton, J. K.; White, A. H.; Williams, M. L. *J. Chem. Soc., Chem. Commun.* **1981,** 428–430. doi:10.1039/C39810000428
56. Bruce, M. I.; Walton, J. K.; Williams, M. L.; Patrick, J. M.; Skelton, B. W.; White, A. H. *J. Chem. Soc., Dalton Trans.* **1983,** 815–821. doi:10.1039/dt9830000815
57. Rausch, M. D.; Ciappenelli, D. J. *J. Organomet. Chem.* **1967,** *10,* 127–136. doi:10.1016/S0022-328X(00)81725-8
58. Sanders, R.; Mueller-Westerhoff, U. T. *J. Organomet. Chem.* **1996,** *512,* 219–224. doi:10.1016/0022-328X(95)05914-B
59. Bishop, J. J.; Davison, A.; Katcher, M. L.; Lichtenberg, D. W.; Merrill, R. E.; Smart, J. C. *J. Organomet. Chem.* **1971,** *27,* 241–249. doi:10.1016/S0022-328X(00)80571-9
60. Butler, I. R.; Cullen, W. R.; Ni, J.; Rettig, S. J. *Organometallics* **1985,** *4,* 2196–2201. doi:10.1021/om00131a023
61. Reeves, P. C. *Org. Synth.* **1977,** *56,* 28. doi:10.15227/orgsyn.056.0028
62. Kaim, W.; Klein, A. *Spectroelectrochemistry;* Royal Society of Chemistry: Cambridge, 2008.
63. Kaim, W.; Fiedler, J. *Chem. Soc. Rev.* **2009,** *38,* 3373–3382. doi:10.1039/b504286k
64. Siebler, D.; Linseis, M.; Gasi, T.; Carrella, L. M.; Winter, R. F.; Förster, C.; Heinze, K. *Chem. – Eur. J.* **2011,** *17,* 4540–4551. doi:10.1002/chem.201002101
65. Neidlinger, A.; Ksenofontov, V.; Heinze, K. *Organometallics* **2013,** *32,* 5955–5965. doi:10.1021/om400498h
66. Kienz, T.; Förster, C.; Heinze, K. *Organometallics* **2014,** *33,* 4803–4812. doi:10.1021/om500052k
67. Hüttinger, K.; Förster, C.; Heinze, K. *Chem. Commun.* **2014,** *50,* 4285–4288. doi:10.1039/C3CC46919K
68. Preiß, S.; Melomedov, J.; Wünsche von Leupoldt, A.; Heinze, K. *Chem. Sci.* **2016,** *7,* 596–610. doi:10.1039/C5SC03429A
69. Bertini, I.; Luchinat, C.; Parigi, G. *Solution NMR of paramagnetic molecules. Applications to metallobiomolecules and models. Current methods in inorganic chemistry 2,* 1st ed.; Elsevier, 2001.
70. Siebler, D.; Förster, C.; Gasi, T.; Heinze, K. *Organometallics* **2011,** *30,* 313–327. doi:10.1021/om1010808
71. Siebler, D.; Förster, C.; Heinze, K. *Dalton Trans.* **2011,** *40,* 3558–3575. doi:10.1039/c0dt01528h
72. Förster, C.; Veit, P.; Ksenofontov, V.; Heinze, K. *Chem. Commun.* **2015,** *51,* 1514–1516. doi:10.1039/C4CC08868A
73. Preiß, S.; Förster, C.; Otto, S.; Bauer, M.; Müller, P.; Hinderberger, D.; Haeri, H. H.; Carella, L.; Heinze, K. *Nat. Chem.* **2017,** *9,* 1249–1255. doi:10.1038/nchem.2836
74. Gubin, S. P. *Pure Appl. Chem.* **1970,** *23,* 463–488. doi:10.1351/pac197023040463
75. Hansch, C.; Leo, A.; Taft, R. W. *Chem. Rev.* **1991,** *91,* 165–195. doi:10.1021/cr00002a004
76. Beck,, W.; Woisetschläger, O. E.; Mayer, P. *Z. Kristallogr. - New Cryst. Struct.* **2001,** *216,* 403–404. doi:10.1524/ncrs.2001.216.14.425
77. Cetina, M.; Jukić, M.; Rapic, V.; Golobic, A. *Acta Crystallogr., Sect. C: Struct. Chem.* **2003,** *59,* m212–m214. doi:10.1107/S0108270103008503
78. For the redox couple **4**/**4**+, an additional shoulder at $\tilde{\nu}_{CO}$ = 1710 cm^{-1} is observed during oxidation (Figure S13, Supporting Information File 1). The intensity of this shoulder also increases upon re-reduction (Figure S14, Supporting Information File 1) and hence is tentatively assigned to the C=O stretching vibration of solid **4** (Figure 3a), as a consequence of precipitation due to the lower solubility of **4** in CH_2Cl_2.
79. Gray, H. B.; Sohn, Y. S.; Hendrickson, N. *J. Am. Chem. Soc.* **1971,** *93,* 3603–3612. doi:10.1021/ja00744a011
80. Yamaguchi, Y.; Ding, W.; Sanderson, C. T.; Borden, M. L.; Morgan, M. J.; Kutal, C. *Coord. Chem. Rev.* **2007,** *251,* 515–524. doi:10.1016/j.ccr.2006.02.028
81. Sohn, Y. S.; Hendrickson, D. N.; Gray, H. B. *J. Am. Chem. Soc.* **1970,** *92,* 3233–3234. doi:10.1021/ja00713a079
82. Hendrickson, D. N.; Sohn, Y. S.; Duggan, D. M.; Gray, H. B. *J. Chem. Phys.* **1973,** *58,* 4666–4675. doi:10.1063/1.1679029
83. Fulara, J.; Filipkowski, K.; Maier, J. P. *J. Phys. Chem. C* **2017,** *121,* 10694–10697. doi:10.1021/acs.jpcc.6b10391
84. Li, Y. L.; Han, L.; Mei, Y.; Zhang, J. Z. H. *Chem. Phys. Lett.* **2009,** *482,* 217–222. doi:10.1016/j.cplett.2009.10.026
85. Yáñez-S, M.; Moya, S. A.; Zúñiga, C.; Cárdenas-Jirón, G. *Comput. Theor. Chem.* **2017,** *1118,* 65–74. doi:10.1016/j.comptc.2017.08.032
86. Salzner, U. *J. Chem. Theory Comput.* **2013,** *9,* 4064–4073. doi:10.1021/ct400322v
87. Bluemel, J.; Hebendanz, N.; Hudeczek, P.; Koehler, F. H.; Strauss, W. *J. Am. Chem. Soc.* **1992,** *114,* 4223–4230. doi:10.1021/ja00037a028
88. Krejčik, M.; Daněk, M.; Hartl, F. *J. Electroanal. Chem. Interfacial Electrochem.* **1991,** *317,* 179–187. doi:10.1016/0022-0728(91)85012-E
89. Fulmer, G. R.; Miller, A. J. M.; Sherden, N. H.; Gottlieb, H. E.; Nudelman, A.; Stoltz, B. M.; Bercaw, J. E.; Goldberg, K. I. *Organometallics* **2010,** *29,* 2176–2179. doi:10.1021/om100106e
90. Neese, F. *Wiley Interdiscip. Rev.: Comput. Mol. Sci.* **2012,** *2,* 73–78. doi:10.1002/wcms.81
91. Becke, A. D. *J. Chem. Phys.* **1993,** *98,* 5648–5652. doi:10.1063/1.464913
92. Lee, C.; Yang, W.; Parr, R. G. *Phys. Rev. B* **1988,** *37,* 785–789. doi:10.1103/PhysRevB.37.785
93. Miehlich, B.; Savin, A.; Stoll, H.; Preuss, H. *Chem. Phys. Lett.* **1989,** *157,* 200–206. doi:10.1016/0009-2614(89)87234-3
94. Neese, F.; Wennmohs, F.; Hansen, A.; Becker, U. *Chem. Phys.* **2009,** *356,* 98–109. doi:10.1016/j.chemphys.2008.10.036
95. Izsák, R.; Neese, F. *J. Chem. Phys.* **2011,** *135,* 144105. doi:10.1063/1.3646921
96. Pantazis, D. A.; Chen, X.-Y.; Landis, C. R.; Neese, F. *J. Chem. Theory Comput.* **2008,** *4,* 908–919. doi:10.1021/ct800047t

97. Sinnecker, S.; Rajendran, A.; Klamt, A.; Diedenhofen, M.; Neese, F. *J. Phys. Chem. A* **2006,** *110,* 2235–2245. doi:10.1021/jp056016z
98. Weigend, F.; Ahlrichs, R. *Phys. Chem. Chem. Phys.* **2005,** *7,* 3297–3305. doi:10.1039/b508541a
99. Weigend, F. *Phys. Chem. Chem. Phys.* **2006,** *8,* 1057–1065. doi:10.1039/b515623h

3.2 Protic Ferrocenyl Acyclic Diamino Carbene Gold(I) Complexes

Sven D. Waniek, Christoph Förster and Katja Heinze

Eur. J. Inorg. Chem. **2022**, e202100905.

Dedicated to the memory of Prof. Dr. Gottfried Huttner

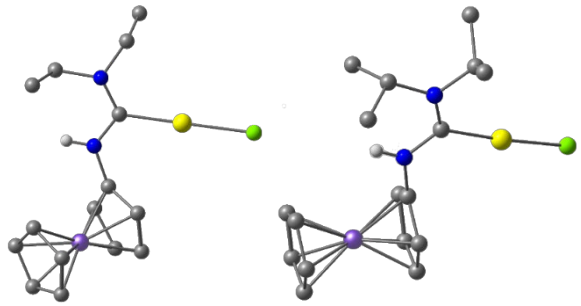

Acyclic ferrocenylsubstituted diamino carbene gold(I) complexes are synthesized via isonitrile route by linking isocyanoferrocene and chlorido(dimethylsulfide)gold(I). The molecular structure of the linear coordinated gold(I) complexes is verified by XRD measurements which shows aurophilic interactions and intermolecular NH Cl hydrogen bonding. Redox activity induced by the ferrocenyl substituents is monitored by voltammetric methods. Intramolecular electron transfer between ferroceniumyl and gold(I) is shown to occur by the formation of gold(II).

Author contributions

The synthesis and characterization of the isocyanoferrocene gold complex and the two gold(I) carbene complexes were done by *Sven D. Waniek*. The crystal structures were solved by [redacted]. All DFT calculations were performed by *Sven D. Waniek*. The manuscript was written by [redacted] and [redacted] and the supporting information was written by *Sven D. Waniek*.

Supporting Information

The Supporting Information is found in **Section 6.2** on pp. 127. The Cartesian coordinates from DFT calculations can be found online at

https://doi.org/10.1002/ejic.202100905

Reprinted with permission from

EurJIC
European Journal of Inorganic Chemistry

Research Article
doi.org/10.1002/ejic.202100905

Chemistry Europe
European Chemical Societies Publishing

www.eurjic.org

Protic Ferrocenyl Acyclic Diamino Carbene Gold(I) Complexes

Sven D. Waniek,[a] Christoph Förster,*[a] and Katja Heinze*[a]

Dedicated to the memory of Prof. Dr. Gottfried Huttner

Two mononuclear protic ferrocenyl acyclic diamino carbene gold(I) complexes AuCl[C(NHFc)(NR_2)] were prepared by nucleophilic attack of diethylamine (R = Et) and diisopropylamine (R = ^{i}Pr) at the ferrocenyl substituted isocyanide complex chlorido (isocyanoferrocene)gold(I) AuCl(CN–Fc). In the solid state, the multifunctional protic carbene gold(I) complexes display intermolecular aurophilic interactions or intermolecular NH···Cl hydrogen bonding in addition to intramolecular non-classical NH···Fe hydrogen bonds. Oxidation of the AuCl[C(NHFc)(NR_2)] complexes initially takes place at the iron centres giving highly coloured ferrocenium ions, which subsequently likely undergo electron transfer from gold(I) to iron(III) yielding putative EPR-active gold(II) species.

Introduction

The multifaceted coordination chemistry[1,2] of gold makes gold complexes play a vital role in catalysis[3–6] in their typical oxidation states I[7–9] and III.[10] In gold(I) catalysis, typically precatalysts of the type AuCl(L) are employed with phosphanes or carbenes as ligands L (Scheme 1), well suited to stabilise the reactive cationic species [Au(L)]$^+$.[7,9] Beside N-heterocyclic carbenes in gold catalysis,[11,12] cyclic amino alkyl carbenes (CAAC)[13] and acyclic diamino carbenes (ADC)[14–19] with their stronger donicity and differing steric bulk[20,21] have demonstrated to be promising candidates. Complexes Au(CAAC)Cl enable new catalytic applications, e.g. the direct hydroamination of alkynes or allenes with hydrazine.[22] The gold(I) catalysed addition of indole to 1,6-enynes yields the cyclopropane product with AuCl(NHC) as pre-catalyst, while Au(ADC)Cl with similar steric bulk shows a different selectivity, giving the alkene as main product.[19] Gold(I) complexes with hydrogen-bond supported heterocyclic carbenes (HBHC), ADCs with intramolecular hydrogen bonding (Scheme 1),[18,23,24] can also show differences in selectivity to their NHC counterparts, e.g. in the cyclization of 1,6-enynes with the *endo* form as preferred product, while the *exo* product is obtained from the NHC complex.[24] Gold(I) complexes with ADC ligands are acessible from gold(I) isonitriles with primary or secondary amines.[16–18,25–28] These ADCs with N(H)R substituents can be viewed as protic ADCs, similar to protic NHCs,[29–31] which are also decribed as ligands in gold complexes.[32–35]

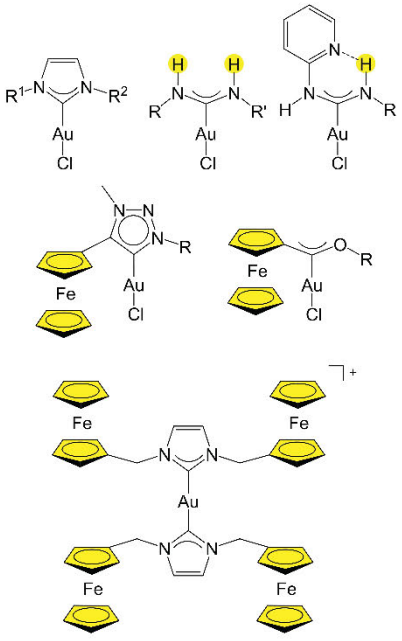

Scheme 1. Schematic representation of gold(I) complexes with N-heterocyclic carbene (NHC), protic acyclic diamino carbene ligands (ADC), hydrogen bond supported heterocyclic carbene (HBHC) (top), ferrocenyl substituted mesoionic carbene, Fischer carbene and NHC ligands (center/bottom).

[a] S. D. Waniek, Dr. C. Förster, Prof. Dr. K. Heinze
Department of Chemistry
Johannes Gutenberg University of Mainz
Duesbergweg 10–14, 55128 Mainz, Germany
E-mail: cfoerster@uni-mainz.de
katja.heinze@uni-mainz.de
www.ak-heinze.chemie.uni-mainz.de

Supporting information for this article is available on the WWW under https://doi.org/10.1002/ejic.202100905

Part of the https://chemistry-europe.onlinelibrary.wiley.com/doi/toc/10.1002/(ISSN)1099-0682c. Ferrocene-Chemistry Ferrocene Chemistry Special Collection.

EurJIC
European Journal of Inorganic Chemistry

Research Article
doi.org/10.1002/ejic.202100905

Chemistry Europe
European Chemical Societies Publishing

Commonly, the use of activators, halide scavengers like silver(I) salts, fascilitating the dissociation of the chlorido ligand from AuCl(L) are necessesary to form the active catalyst $[Au(L)]^+$. Also silver-free activation by e.g. in situ replacing the chlorido ligand using alkali metal salts, copper(II) triflate or methyl triflate is possible.[36–40] Alternatively, introducing ferrocenyl (Fc) as redox-active moiety in carbene[41–44] (Scheme 1) or phosphane ligands[45] and oxidizing the ferrocene to ferrocenium can initiate catalysis. The reversible on/off switching of the catalyst leads to redox-switchable gold catalysis. Recently, the combination of redox- and proton-switchable moieties in a gold(I) complex has been reported.[46] Ferrocenyl substituted carbenes, typically NHCs,[47,48] mesoionic carbenes[42–44,49–51] and Fischer-type carbenes[41,52] have been coordinated to gold(I). To the best of our knowledge, gold(I) complexes with ferrocenyl substituted ADCs have not been reported up to now.

One-electron oxidation of the Fischer-type ferrocenyl carbene complex AuCl[C(OEt)Fc] to $\{AuCl[C(OEt)Fc]\}^+$ has been suggested to yield a mononuclear gold(II) complex as catalytically competent species.[41] Beside the EPR spectroscopic detection of the final Fe^{II}/Au^{II} valence isomer, the postulated initially formed intermediate Fe^{III}/Au^{I} species could not been detected in this case. However, counter ion and solvent dependent $Au^{III}(porph^{\bullet})\rightarrow Au^{II}(porph)$ valence isomerization equilibria have been observed for porphyrinato gold complexes ($porph^{2-}$ = substituted porphyrinato(2-)).[53–55]

Here we combine protic ADCs with redox-active ferrocenyl substituents coordinated to gold(I). We describe the synthesis of protic ferrocenyl ADC gold(I) complexes starting from an isocyanoferrocene gold(I) complex, their solid state structures and their redox properties using cyclic voltammetry, square wave voltammetry, chemical oxidation followed by UV/Vis/NIR and X-band EPR spectroscopy and density functional theory (DFT) calculations. We discuss the potential electron transfer chain in the cationic ADC gold complexes, prepared by chemical oxidation, as monitored by UV/Vis/NIR and X-band EPR spectroscopy.

Results and Discussion

Synthesis and Characterization

Addition of secondary amines to isocyanide gold(I) complexes yields the corresponding protic acyclic diamino carbene gold(I) complexes.[16–18,25–28] To install the redox-active ferrocene unit, we first coordinated isocyanoferrocene Fc–NC[56] to gold(I) chloride via chlorido(dimethylsulfide)gold(I) as gold(I) precursor giving the heterobimetallic complex chlorido (isocyanoferrocene)gold(I) **1** in 27% isolated yield (Scheme 2). The conceivable inverse route to the envisioned ADC gold(I) complexes starting from an (alkylisocyano) chlorido gold(I) complex and aminoferrocene was unsuccessful due to the low nucleophilicity of aminoferrocene.[57,58]

While the reaction of 1,1′-diisocyanoferrocene and chlorido (dimethylsulfide) gold(I) affords an insoluble coordination polymer with aurophilic interactions,[59] the mono(isocyano)

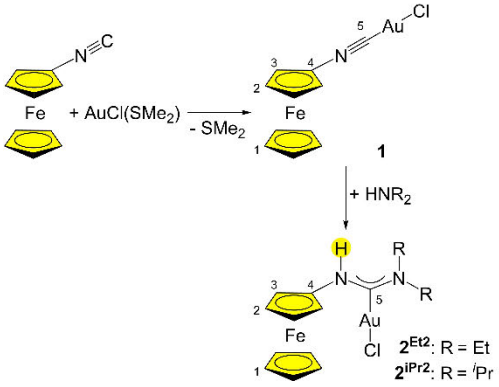

Scheme 2. Synthesis of isocyanoferrocene complex **1** and protic ferrocenyl acyclic diamino carbene complexes $\mathbf{2}^{Et2}$ and $\mathbf{2}^{iPr2}$. Atom numbering for NMR assignments indicated. Ferrocenyl substituents and NH proton highlighted in yellow.

complex 1 is well soluble in common organic solvents. **1** is characterized by its CN stretching vibration at 2225 cm^{-1} (Supporting Information, Figure S1) shifted by 101 cm^{-1} to higher energy as compared to Fc–NC (2124 cm^{-1})[56] and similar to the shift difference of the pair AuCl(4-CN-C_6H_4OMe)/4-CN-C_6H_4OMe (2123/2221 cm^{-1}).[17] The ^{1}H NMR spectrum of **1** displays the expected three resonances in a 2:5:2 ratio for the ferrocenyl substituent (Supporting Information, Figure S2). The ^{13}C NMR resonance of the coordinated isocyanide in **1** in CD_2Cl_2 is observed at δ = 164.7 ppm as a triplet with $^1J_{NC}$ = 5.7 Hz due to coupling to ^{14}N (Supporting Information, Figure S3), slightly shifted to lower field as compared to that of Fc–NC with δ = 163.9 ppm (t, 5.6 Hz).[56] The $APCI^+$ mass spectrum of **1** indicates facile dissociation of chloride and coordination of CH_3CN (m/z = 449, Supporting Information, Figure S4).

ADC gold(I) complexes $\mathbf{2}^{Et2}$ and $\mathbf{2}^{iPr2}$ were formed by nucleophilic attack of the secondary amines $HNEt_2$ and $HN(^iPr_2)$ at the isocyanide complex **1** in 67% and 55% isolated yields, respectively (Scheme 2). Expectedly, the IR band for the CN stretching vibration of **1** has vanished in the carbene complexes $\mathbf{2}^{Et2}$ and $\mathbf{2}^{iPr2}$ (Supporting Information, Figures S5–S6). The NH stretching vibration of the protic diaminocarbene ligands in $\mathbf{2}^{Et2}$ and $\mathbf{2}^{iPr2}$ appear in the ATR IR spectra at 3270 and 3268 cm^{-1}, respectively. The ^{1}H NMR resonances of the NH units turn up at 7.03 and 7.20 ppm in CD_2Cl_2, respectively (Supporting Information, Figures S7–S8). The ^{13}C NMR resonances of the gold coordinated carbon atoms shift to δ = 190.5 and 191.6 ppm in $\mathbf{2}^{Et2}$ and $\mathbf{2}^{iPr2}$, respectively (Supporting Information, Figures S9-S11), a range expected for coordinated diaminocarbenes, e.g. δ = 190.0 ppm was found for chlorido[(diethylamino)(4-methoxyphenylamino) methylidene]gold(I).[17] The chlorido ligand easily dissociates in ESI^+ mass spectra of $\mathbf{2}^{Et2}$ and $\mathbf{2}^{iPr2}$ (m/z = 481 and 509, respectively) and is partially replaced by a solvent molecule CH_3CN (m/z = 522 and 550, respectively) or another intact gold(I) complex (m/z = 997 and 1053, respectively),

EurJIC
European Journal of Inorganic Chemistry

Research Article
doi.org/10.1002/ejic.202100905

Chemistry Europe
European Chemical Societies Publishing

presumably forming a bridging chlorido ligand (Supporting Information, Figures S12–S13).[60]

Structure Determination

Single crystals of $\mathbf{2}^{Et2}$ and $\mathbf{2}^{iPr2}$ suitable for X-ray diffraction analyses were obtained by recrystallization from THF/petroleum ether. While both complexes display the expected linear coordination at the gold(I) ion, a *syn* conformation and unremarkable bond lengths and angles around the gold and ferrocene units (Supporting Information, Table S1), the packing in the crystalline state strongly differs (Figure 1). In principle, several intermolecular interactions are conceivable in these multifunctional complexes, namely classical NH···Cl hydrogen bonding, non-classical NH···Fe hydrogen bonding[58,61,62] and aurophilic interactions.[63–65] The ethyl derivative $\mathbf{2}^{Et2}$ displays a NH···Cl hydrogen bonding motif with a N···Cl distance of 3.402(4) Å giving chains of complexes along the crystallographic *b* axis (Figure 1a). This motif is similar to NH···O/S hydrogen bonds of ferrocenyl amides, ferrocenyl thioamides, ferrocenyl ureas and ferrocenyl (thio)ureas in the solid state.[66–68] On the other hand, isopropyl derivative $\mathbf{2}^{iPr2}$ realizes aurophilic interactions with an Au···Au distance of 3.1897(3) Å in a centrosymmetric dimer (Figure 1b), while chlorido diaminocarbene gold(I) complexes with dialkylamino and arylamino substituents display no aurophilic interactions[17] except of chloride [(diethylamino)(pyridylamino)methylidene] gold(I) forming a dimer with an Au···Au distance of 3.3107(14) Å.[23] The observed Au···Au distance of $\mathbf{2}^{iPr2}$ in the solid state correlates to a bond dissociation energy $D_e = 12.7 \times 10^5\ e^{-3.5d(Au-Au)} = 18\ kJ\,mol^{-1}$ (*d* in Å, D_e in $kJ\,mol^{-1}$) according to an equation derived by Schwerdtfeger.[69,70]

In addition to the intermolecular NH···Cl hydrogen bonding ($\mathbf{2}^{Et2}$) or aurophilic interaction in the centrosymmetric dimer ($\mathbf{2}^{iPr2}$), the iron centers of the ferrocene units in $\mathbf{2}^{Et2}$ and $\mathbf{2}^{iPr2}$ engage in weak intramolecular non-classical NH···Fe hydrogen bonds with N···Fe distances of 3.0760(34) Å and 3.0629(27) Å, respectively (Figure 1).[58,61,62] The strong non-classical NH···Fe hydrogen bond with an N···Fe distance of 3.46 Å in a ferrocenyl hydrazone exhibits a dissociation energy of 13 $kJ\,mol^{-1}$.[61] Clearly, the energetics of the observed intra- and intermolecular interactions of the protic ferrocenyl acyclic diamino carbene gold(I) complexes $\mathbf{2}^{Et2}$ and $\mathbf{2}^{iPr2}$ – hydrogen bonding and aurophilicity – are of similar magnitude.

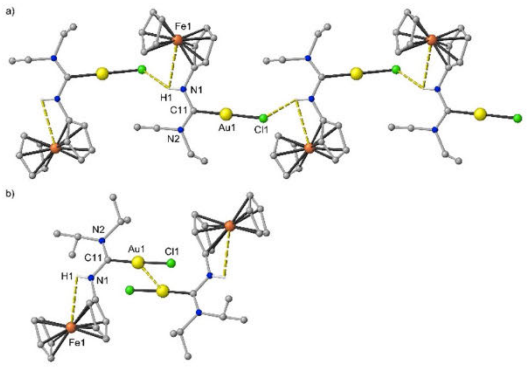

Figure 1. Molecular structures and intermolecular interactions of a) $\mathbf{2}^{Et2}$ and b) $\mathbf{2}^{iPr2}$ in the crystal as determined by X-ray diffraction.

Redox and Optical Properties

Fc–NC is oxidized to $[Fc–NC]^+$ at 350 mV vs. ferrocene[71] while the redox potential of the isocyano gold(I) complex pair $[\mathbf{1}]^+/\mathbf{1}$ amounts to $E_{1/2} = 540$ mV (Supporting Information, Figures S14–S15). On the other hand, the diaminocarbene complexes $\mathbf{2}^{Et2}$ and $\mathbf{2}^{iPr2}$ are oxidized reversibly to $[\mathbf{2}^{Et2}]^+$ and $[\mathbf{2}^{iPr2}]^+$ at 105 and 115 mV vs. ferrocene in $CH_2Cl_2/[^nBu_4N][B(C_6F_5)_4]$, respectively (Supporting Information, Figures S16–S19). These values are lower by 440–475 mV compared to that of the $[\mathbf{1}]^+/\mathbf{1}$ and chlorido (ferrocenyl Fischer carbene) gold(I) redox couples,[41] but at typical potentials of N-substituted ferrocenes,[68] N-ferrocenyl amides, thioamides,[72] ureas, thioureas[73] or chlorido Fc-MIC gold(I) complexes.[44]

Consequently, the oxidation process is assigned to the ferrocene/ferrocenium redox couple, rather than an $Au^{II/I}$ couple.[41,55,74–76] Geometry optimizations of the $\mathbf{2}^{Et2}/[\mathbf{2}^{Et2}]^+$ and $\mathbf{2}^{iPr2}/[\mathbf{2}^{iPr2}]^+$ redox pairs on the DFT level of theory (CPCM (CH_2Cl_2)-(U)B3LYP-D3BJ/def2-TZVPP) corroborate this assignment based on Fe–C distances and Mulliken spin densities at the metal ions (Supporting Information, Tables S2–S5). In both complexes $[\mathbf{2}^{Et2}]^+$ and $[\mathbf{2}^{iPr2}]^+$, the Mulliken spin densities at the iron and gold centers amount to 1.25 and 0.00, respectively, suggesting a negligible spin delocalization onto the gold center. This spin localization at the iron centers fits to the low $Fe^{III/II}$ redox potential precluding any gold(II) contribution.

The UV/Vis/NIR spectra of the yellow complexes **1**, $\mathbf{2}^{Et2}$ and $\mathbf{2}^{iPr2}$ in CH_2Cl_2 display the characteristic ferrocene bands at 434, 439 and 438 nm, respectively (Supporting Information, Figures S20–S22). Although many carbene gold(I) complexes can be luminescent,[23] ferrocene typically quenches luminescence, either via energy transfer or via electron transfer.[77,78] Expectedly, both ferrocenyl complexes $\mathbf{2}^{Et2}$ and $\mathbf{2}^{iPr2}$ are non-emissive at room temperature and at 77 K with excitation at 254 nm.

The cations $[\mathbf{2}^{Et2}]^+$ and $[\mathbf{2}^{iPr2}]^+$, prepared by chemical oxidation with one equivalent of $[N(4\text{-}C_6H_4Br)_3][SbCl_6]$ (magic blue, $E_{1/2} = 700$ mV vs. ferrocene in CH_2Cl_2)[79] in THF are strongly colored with absorption bands at 573/759 and 535/759 nm, respectively (Figure 2). These weakly solvatochromic bands (Experimental Section, Supporting Information Figures S23, S24) are tentatively assigned to transitions with nitrogen lone pairs to iron(III) charge transfer character according to time-dependent DFT (TDDFT) calculations and analyses of the electron density difference maps (Supporting Information, Figures S25–S28). The higher energy transition in $[\mathbf{2}^{iPr2}]^+$ possesses some additional $[Au^I–Cl]$ to iron(III) character, while the analogous transitions in $[\mathbf{2}^{Et2}]^+$ are of negligibly small oscillator strength. The rather poor agreement of TDDFT calculated spectra with

EurJIC
European Journal of Inorganic Chemistry

Research Article
doi.org/10.1002/ejic.202100905

Chemistry Europe
European Chemical Societies Publishing

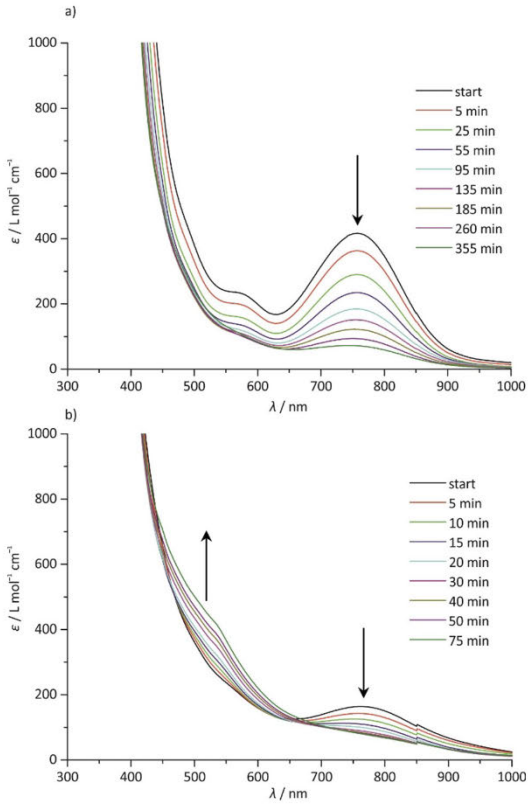

Figure 2. UV/Vis/NIR spectra in THF of a) $[\mathbf{2}^{Et2}]^+$ prepared by oxidation with $[N(4\text{-}C_6H_4Br)_3][SbCl_6]$ from $\mathbf{2}^{Et2}$ and b) $[\mathbf{2}^{iPr2}]^+$ prepared by oxidation with $[N(4\text{-}C_6H_4Br)_3][SbCl_6]$ from $\mathbf{2}^{iPr2}$ over time.

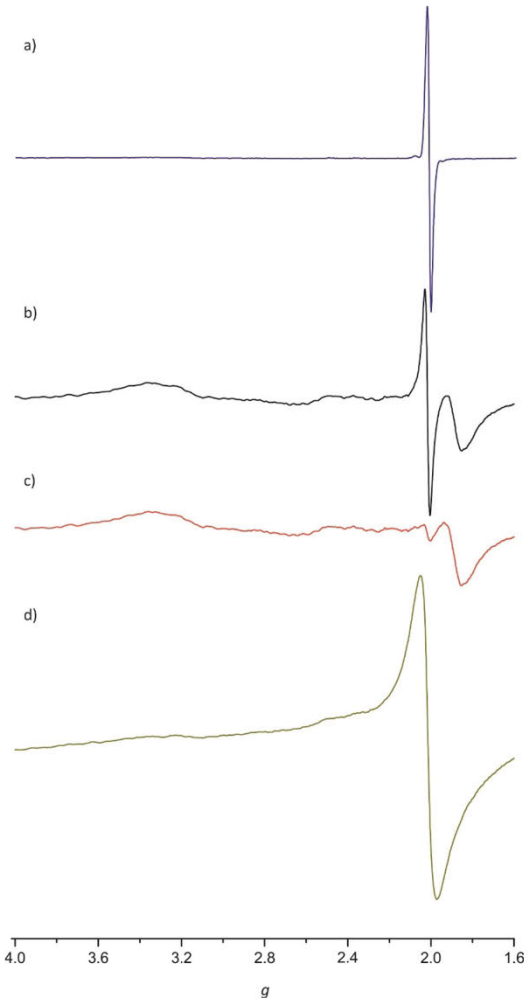

Figure 3. X-band EPR spectra of a) magic blue $[N(4\text{-}C_6H_4Br)_3][SbCl_6]$, b) a mixture of $\mathbf{2}^{iPr2}$ with one equivalent of magic blue rapidly frozen, c) after storing the mixture for 30 min. at 195 K and d) followed by storing the mixture at 295 K for 3.5 h. All spectra were recorded in THF at 77 K.

experimental spectra of metallocenes has been noted before, allowing only a qualitative description.[80,81]

Both cationic complexes are stable on the time scale of the voltammetric experiments. However, $[\mathbf{2}^{Et2}]^+$ and $[\mathbf{2}^{iPr2}]^+$ further react on the time scale of hours after chemical oxidation (Figure 2). Several possibilities can be suggested, namely deprotonation at the amine after oxidation of the ferrocene,[82,83] slow electron transfer from gold(I) to iron(III)[41] followed by dimerization of the gold(II) radical,[84,85] formation of gold(III) via disproportionation or chlorine radical/Cl_2 formation followed by oxidative addition,[86–89] or chloride loss from gold(I)[60] followed by chloride attack on iron(III) of the multifunctional open-shell complexes $[\mathbf{2}^{Et2}]^+$ and $[\mathbf{2}^{iPr2}]^+$.

To experimentally confirm the thermodynamically and kinetically feasible initial oxidation of the iron(II) center, pre-cooled solutions of $\mathbf{2}^{Et2}$ and $\mathbf{2}^{iPr2}$ with one equivalent of magic blue ($[N(4\text{-}C_6H_4Br)_3][SbCl_6]$) in THF were rapidly frozen to 77 K and X-band EPR spectra were recorded (Figure 3, Supporting Information Figure S29). Besides the resonance of residual magic blue at $g \approx 2.016$ (Figure 3a), resonances at $g \approx 3.36$ and $g \approx 1.89$ (inflexion point), typical for the low- and high-field tensor components of N-substituted ferrocenium ions are observed (Figure 3b; Supporting Information Figures S29b).[82,83] Upon warming to 195 K, the resonance of magic blue decreases rapidly in intensity, while the ferrocenium resonance persists (Figure 3c, Supporting Information Figure S29c). Further warming to room temperature results in the appearance of a new very broad resonance at $g \approx 2.014$ and in disappearing of the ferrocenium resonances (Figure 3d, Supporting Information Figure S29d). The broad resonance is similar to the Au^{II} resonance with unresolved hyperfine coupling to the gold nucleus (^{197}Au: $I = {}^3/_2$) at $g_{iso} = 2.017$ observed for the species formed from the cationic ferrocenyl Fischer-type gold complex $\{AuCl[C(Fc)OEt]\}^+$.[41] Hence, we assign these final broad resonances to gold

EurJIC
European Journal of Inorganic Chemistry

Research Article
doi.org/10.1002/ejic.202100905

Chemistry Europe
European Chemical Societies Publishing

(II)-centered radical species after oxidation of 2^{Et2} and 2^{iPr2}, which could form via an $Fe^{III}/Au^{I} \rightarrow Fe^{II}/Au^{II}$ intramolecular electron transfer (IET) after the initial Fc/Fc^{+} oxidation. Unfortunately, the exact nature of the final species after oxidation of 2^{Et2} and 2^{iPr2} observed by EPR spectroscopy remains unclear. The EPR resonances of these species are even observable at room temperature and increase over time at room temperature (Supporting Information, Figures S30-S31), reaching a maximum intensity after ca. 23 h. Concomitantly, the characteristic UV/Vis/NIR absorption bands of the ferrocenium complexes $[2^{Et2}]^{+}$ and $[2^{iPr2}]^{+}$ at 759 nm decrease in intensity at room temperature (Figure 2). The decay of the Fc^{+} absorption bands and the parallel rise of the putative gold(II) EPR resonances (Supporting Information, Figure S32) give spectroscopic evidence of the $Fe^{III}/Au^{I} \rightarrow Fe^{II}/Au^{II}$ IET in $[2^{Et2}]^{+}$ and $[2^{iPr2}]^{+}$ or in respective follow-up products. The EPR active species from the reaction of the closely related carbene gold(I) complex AuCl[C(Fc)OEt] with magic blue formed with 75% yield obtained almost quantitatively, supporting the $Fe^{III}/Au^{I} \rightarrow Fe^{II}/Au^{II}$ IET.[41] The rather slow electron transfer from gold(I) to iron(III) likely occurs with small reorganization at the iron center but with large structural reorganization at the gold ion. For example, $[SbCl_6]^{-}$ anion and/or solvent could coordinate to the gold ion under expansion of the coordination sphere from linear for gold(I) to square planar for gold(II),[74] stabilizing the Fe^{II}/Au^{II} species.[41] The absence of a well resolved ^{197}Au hyperfine coupling pattern may be due to spin delocalization over the gold(II) bonded ligands, as calculated for $Au^{II}Cl$[C(Fc)OEt]$(SbCl_6)$.[41] Alternatively, spin exchange interactions of distant Au^{II} centers in oligonuclear aggregates could be responsible as observed for mononuclear gold(II) complex compounds in the solid.[74b]

While the Fc/Fc^{+} oxidation is more facile in $2^{Et2}/2^{iPr2}$ than in the Fischer carbene complex AuCl[C(Fc)OEt][41] and with the assumption that the redox potentials for the Au^{I}/Au^{II} oxidation are rather similar for all these gold(I) complexes, the driving force for the proposed IET might be lower in the ADC complexes $2^{Et2}/2^{iPr2}$. This lower driving force should increase the electron transfer barrier for the IET in $2^{Et2}/2^{iPr2}$, which allows the spectroscopic detection of the ferrocenium valence isomers of $[2^{Et2}]^{+}$ and $[2^{iPr2}]^{+}$ before formation of the putative gold(II) species.

The redox chemistry of AuCl[C(Fc)OEt][41] and the ADC gold (I) complexes 2^{Et2} and 2^{iPr2} makes these complexes potential candidates as pre-catalysts without the necessity for halide abstraction for activation but oxidative activation instead, e.g. in catalyzed phenol synthesis, hydration of alkynes,[17] methoxycyclization of 1,6-enynes[18] or cyclisation of *N*(2-propyn-1-yl) benzamide.[41–44] Catalysis experiments with 2^{Et2}, 2^{iPr2} and derivatives as pre-catalysts under oxidative conditions and redox-switchable catalysis will be addressed in future studies.

Conclusion

Protic ferrocenyl acyclic diamino carbene gold(I) complexes have been prepared from chlorido(isocyanoferrocene)gold(I) and secondary amines NHR_2 (R = Et, ^{i}Pr). The complexes were characterized structurally and spectroscopically. The multifunctionality enables various structural motifs in the solid state, namely NH···Cl and NH···Fe hydrogen bonds as well as aurophilic interactions. Reversible oxidation to the respective cations is feasible on the time scale of cyclic and square wave voltammetry. The initial formation of ferrocenium ions was verified EPR spectroscopically for the first time. Slow follow-up, possibly intramolecular, electron transfer yields persistent EPR-active species, likely with gold(II) character. Their potential in redox-switchable gold catalysis will be exploited in the future.

Experimental Section

Reactions and measurements were performed under argon atmosphere unless otherwise noted using Gloveboxes (*UniLab/MBraun* – Ar 4.8, $O_2 < 1$ ppm, $H_2O < 0.1$ ppm) or Schlenk techniques. Dichloromethane and acetonitrile were dried and distilled from calcium hydride. THF and petroleum ether were dried and distilled from potassium and sodium, respectively. Dry methanol was purchased from *Acros Organics*. Deuterated solvents were purchased from *Deutero GmbH*. Other reagents were used as received from commercial suppliers (*Strem Chemicals*, *Apollo Scientific* and *Acros Organics*). Fc–NC was prepared according to a literature method.[56]

Crystal Structure Determinations. Data for 2^{Et2} were collected with an *IPDS 2T* single crystal x-ray diffractometer from *STOE & CIE GmbH* and corrected for absorption and other effects using Mo K_α radiation ($\lambda = 0.71073$ Å). The diffraction frames were integrated using the *STOE X-Area* software package,[90] and most were corrected for absorption with *MULABS*[91] of the *PLATON* software package.[92] Crystal structure data for 2^{iPr2} were collected with a *STADIVARI* diffractometer from *STOE & CIE GmbH* using Mo K_α radiation ($\lambda = 0.71073$ Å). The diffraction frames were integrated using the *STOE X-Area* software package[90] and were corrected for absorption with *STOE LANA*.[93] The structures were solved by direct methods and refined by the full-matrix method based on F^2 using the *SHELX* software package[94–96] and the *ShelXle* graphical interface.[97] All non-hydrogen atoms were refined anisotropically, while the position of hydrogen atoms were generated with appropriate geometric constraints and allowed to ride on their respective parent atoms with fixed isotropic thermal parameters.

Crystallographic Data of 2^{Et2}×THF. $C_{15}H_{20}AuClFeN_2 \times THF$ (588.70); monoclinic; $P2_1/n$; $a = 9.2897(19)$ Å, $b = 14.204(3)$ Å, $c = 15.637(3)$ Å, $\beta = 98.66(3)°$; $V = 2039.8(7)$ Å^3; $Z = 4$; density, calcd. = 1.917 g cm^{-3}, $T = 120(2)$ K, $\mu = 8.035$ mm^{-1}; F(000) = 1144; crystal size 0.160 × 0.110 × 0.050 mm; $\theta = 2.403$ to 27.891 deg.; $-10 \le h \le 12$, $-16 \le k \le 18$, $-20 \le l \le 20$; rfln collected = 12268; rfln unique = 4853 [R(int) = 0.0411]; completeness to $\theta = 25.242$ deg. = 99.8%; semi empirical absorption correction from equivalents; max. and min. transmission 1.30375 and 0.77806; data 4853; restraints 0, parameters 228; goodness-of-fit on $F^2 = 1.061$; final indices [$I > 2\sigma(I)$] $R_1 = 0.0278$, $wR_2 = 0.0612$; R indices (all data) $R_1 = 0.0373$, $wR_2 = 0.0653$; largest diff. peak and hole 0.765 and −0.889 e Å^{-3}.

Crystallographic Data of 2^{iPr2}. $C_{17}H_{24}AuClFeN_2$ (544.65); triclinic; $P\bar{1}$; $a = 7.7203(3)$ Å, $b = 9.8414(3)$ Å, $c = 12.5908(4)$ Å, $\alpha = 69.153(3)°$; $\beta = 79.014(3)°$; $\gamma = 83.656(4)°$; $V = 876.67(5)$ Å^3; $Z = 2$; density, calcd. = 2.063 g cm^{-3}, $T = 120(2)$ K, $\mu = 9.335$ mm^{-1}; F(000) = 524; crystal size 0.200 × 0.138 × 0.075 mm; $\theta = 2.217$ to 30.734 deg.; $-10 \le h \le 10$, $-12 \le k \le 14$, $-17 \le l \le 17$; rfln collected = 12307; rfln unique = 4804 [R(int) = 0.0230]; completeness to $\theta = 25.242$ deg. = 100.0%; semi empirical absorption correction from equivalents; max. and min. transmission 0.4826 and 0.1426; data 4804; restraints 0, parameters 203; goodness-of-fit on $F^2 = 1.037$; final indices [$I > 2\sigma(I)$] $R_1 = 0.0263$,

EurJIC
European Journal of Inorganic Chemistry

Research Article
doi.org/10.1002/ejic.202100905

Chemistry Europe
European Chemical Societies Publishing

$wR_2 = 0.0645$; R indices (all data) $R_1 = 0.0284$, $wR_2 = 0.0654$; largest diff. peak and hole 1.219 and −3.258 e Å^{-3}.

Density functional theory calculations were performed with Orca 4.1.1[98] using the high performance computing cluster *ELWE-TRITSCH*. The B3LYP[99–101] formulation of DFT and Def2-tzvpp[102,103] as basis set which uses polarization functions for non-hydrogen atoms were used. For solvent modelling keyword *CPCM*[104,105] in CH_2Cl_2 was applied. The *"zeroth order regular approximation"* (keyword *ZORA*)[106–108] was used for relativistic corrections. For the gold atom the segmented all-electron relativistically contracted (SARC) basis set (SARC-ZORA-TZVPP) by Pantazis et al. was employed.[106] The RIJCOSX[109–111] approximation was used to accelerate the calculations. Atom-pairwise dispersion correction was performed with the Becke-Johnson damping scheme (keyword D3BJ).[112,113] The energy of the electronic states and presence of energy minima were checked by numerical frequency calculations. Explicit counter ions and/or solvent molecules were not taken into account

NMR spectra were recorded on a *Bruker Avance DRX 400* spectrometer at 400 MHz (^{1}H) and 100 MHz (^{13}C) at 25 °C. All resonances are reported in ppm versus the solvent signal as internal standard: CD_2Cl_2 (^{1}H, $\delta = 5.32$; ^{13}C, $\delta = 54.24$ ppm).[114] **ESI and APCI mass spectra** were recorded with an *Agilent 6545 QTOF mass spectrometer*. **UV/Vis/NIR spectra** were recorded on a *Varian Cary 5000* or a *Jasco V770* spectrometer using 1.0 cm quartz cells with a Schott valve. **ATR IR spectra** were recorded on a Bruker ALPHA II FT-IR spectrometer with a Platinum DI-ATR module under ambient conditions. **Electrochemical experiments** were carried out on a *BioLogic SP-200* voltammetric analyzer using platinum wires as counter and working electrodes and 0.01 M $Ag/AgNO_3$ as the reference electrode. The measurements were carried out at a scan rate of 100 mV s^{-1} for cyclic voltammetry experiments and at 50 mV s^{-1} for square-wave voltammetry experiments using [^{n}Bu$_4$N][B(C$_6$F$_5$)$_4$] as the supporting electrolyte in CH_2Cl_2. Potentials are referenced to the ferrocene/ferrocenium couple by using ferrocene as a standard for the isocyano complex **1** ($E_{1/2} = 260$ mV under the experimental conditions) and decamethylferrocene as a standard for the carbene complexes **2** ($E_{1/2} = -590$ mV under the experimental conditions). **X-band EPR spectra** were recorded on a *Miniscope MS 300* (Magnettech GmbH, Germany) with a frequency counter *FC 400* (Magnettech GmbH, Germany) or *HewlettPackard 5340A* at a microwave frequency of 9.39 GHz at room temperature or 77 K, Mn^{2+} in ZnS was used as external standard ($g = 2.118$, 2.066, 2.027, 1.986, 1.946, 1.906). **Elemental analyses** were performed by the central analytic service of the department of chemistry of the University of Mainz with an *Vario El cube* from *Elementar*.

Synthesis of AuCl(CN-Fc) 1 [similar to a literature procedure for (1'-(diphenylphosphino)-1-isocyanoferrocene)(AuCl)$_2$].[115,116] 200 mg (0.68 mmol, 1 eq) of chlorido(dimethyl sulfide)gold(I) was dissolved in CH_2Cl_2 (15 mL). Isocyanoferrocene (143.3 mg, 0.68 mmol, 1 eq) was added as solid and the solution was stirred for 10–15 minutes. The solvent was removed under reduced pressure. Recrystallization from THF/petroleum ether yielded **1** as yellow powder in 27 % yield (81 mg, 0.18 mmol). Elemental analysis calcd. (%) for $C_{11}H_9ClFeAuN$ (443.64) + 0.25 C_4H_7O (THF): C 31.25, H 2.35, N 3.04; found C 31.05, H 2.50, N 3.19. ^{1}H NMR (400.31 MHz, CD_2Cl_2): $\delta = 4.81$ (pt, 2H, H^3), 4.40 (s, 5 H, H^1), 4.35 (pt, 2 H, H^2) ppm. ^{13}C{^{1}H} NMR (100.66 MHz, CD_2Cl_2): $\delta = 164.7$ (t, C^5, $^1J_{NC} = 5.7$ Hz), 79.3 (t, C^4, $^1J_{NC} = 15.8$ Hz), 71.2 (C^1), 67.4 (C^2), 67.3 (C^3) ppm. MS (APCI, CH_3CN): m/z (%) = 449.00 (100), 450.00 (16), 451.01 (2) [**1**-Cl + CH_3CN]$^+$. IR (ATR): $\tilde{\nu} = 3099$ (w, CH), 2225 (s, C≡N), 1409 (m), 1240 (w), 1104 (m), 1023 (m), 999 (m), 923 (m), 813 (s), 484 (vs) cm^{-1}. CV (CH_2Cl_2/[^{n}Bu$_4$N][B(C$_6$F$_5$)$_4$]): $E_{1/2}$ = 540 mV vs. ferrocene/ferrocenium. UV/Vis/NIR (CH_2Cl_2): λ (ε/M^{-1} cm^{-1}) = 434 (430) nm.

Synthesis of 2^{Et2}. Chlorido(isocyanoferrocene) gold(I) **1** (133.0 mg, 0.30 mmol, 1 eq) was dissolved in CH_2Cl_2 (25 mL). Diethylamine (0.15 mL, 1.50 mmol, 5 eq, 109.7 mg) was added under exclusion of light and the solution was stirred for one hour at room temperature. The solvent was removed under reduced pressure. Recrystallization from THF/petroleum ether yielded 2^{Et2} as yellow crystals in 67 % yield (104 mg, 0.20 mmol). Elemental analysis calcd. (%) for $C_{15}H_{20}ClFeAuN_2$ (516.60 g mol^{-1}): C 34.88, H 3.90, N 5.42; found C 34.76, H 4.01, N 5.45. ^{1}H NMR (400.31 MHz, CD_2Cl_2): $\delta = 7.03$ (s, 1 H, NH), 4.71 (pt, 2 H, H^3), 4.26 (s, 5 H, H^1), 4.13 (pt, 2 H, H^2), 3.98 (q, $^3J_{HH} = 7.1$ Hz, 2 H, CH_2), 3.42 (q, 2 H, $^3J_{HH} = 7.3$ Hz, CH_2), 1.31 (m, 6 H, CH_3) ppm. ^{13}C{^{1}H} NMR (100.66 MHz, CD_2Cl_2): $\delta = 190.5$ (C^5), 98.5 (C^2), 70.1 (C^1), 66.3 (C^4), 65.7 (C^3), 54.8 (CH_2), 41.9 (CH_2), 14.9 (CH_3), 12.7 (CH_3) ppm. MS (ESI$^+$, CH_3CN): m/z (%) = 481.06 (79), 482.07 (14), 483.07 (2) [2^{Et2}-Cl]$^+$, 520.09 (6), 521.09 (1), 522.09 (100), 523.09 (21), 524.09 (24) [2^{Et2}-Cl + CH_3CN]$^+$, 997.10 (10), 998.10 (4), 999.10 (4), 1000.10 (2) [(2^{Et2}-Cl)$_2$Cl]$^+$. IR (ATR): $\tilde{\nu} = 3270$ (w, NH), 2963 (w, CH), 1545 (vs), 1368 (s), 1139 (m), 1104 (s), 811 (m), 486 (vs) cm^{-1}. CV (CH_2Cl_2/[^{n}Bu$_4$N][B(C$_6$F$_5$)$_4$]): $E_{1/2} = 105$ mV vs. ferrocene/ferrocenium. UV/Vis/NIR (THF): λ (ε/M^{-1} cm^{-1}) = 435 (309) nm. UV/Vis/NIR (CH_2Cl_2): λ (ε/M^{-1} cm^{-1}) = 439 (210) nm. UV/Vis/NIR (CH_3CN): λ (ε/M^{-1} cm^{-1}) = 433 (255) nm.

Synthesis of 2^{iPr2}. Chlorido(isocyanoferrocene) gold(I) **1** (215.4 mg, 0.49 mmol, 1 eq) was dissolved in CH_2Cl_2 (25 mL). Diisopropylamine (0.34 mL, 2.43 mmol, 5 eq, 245.7 mg) was added under exclusion of light and the solution was stirred for one hour at room temperature. The solvent was removed under reduced pressure. Recrystallization from THF/petroleum ether yielded 2^{iPr2} as yellow crystals in 55 % yield (146 mg, 0.27 mmol). Elemental analysis calcd. (%) for $C_{17}H_{24}ClFeAuN_2$ (544.65 g mol^{-1}): C 37.49, H 4.44, N 5.14; found C 37.60, H 4.62, N 5.31. ^{1}H NMR (400.31 MHz, CD_2Cl_2): $\delta = 7.18$ (s, 1 H, NH), 4.65 (pt, 2 H, H^3), 4.25 (s, 5 H, H^1), 4.16 (pt, 2 H, H^2), 3.92 (m, 1 H, CH) 1.51 (d, 6 H, CH_3), 1.51–1.30 (m, 1 H, CH), 1.30 (d, 6 H, CH_3) ppm. ^{13}C{^{1}H} NMR (100.66 MHz, CD_2Cl_2): $\delta = 191.6$ (C^5), 98.1 (C^2), 69.8 (C^1), 66.5 (C^4), 62.4 (C^3), 46.8 (CH), 21.4 (CH_3), 21.0 (CH_3) ppm. MS (ESI$^+$, CH_3CN): m/z (%) = 509.10 (78), 510.10 (16), 511.10 (2) [2^{iPr2}–Cl]$^+$, 548.13 (6), 549.13 (1), 550.13 (100), 551.13 (23), 552.13 (3) [2^{iPr2}-Cl + CH_3CN]$^+$, 1053.16 (16), 1054.16 (7), 1055.16 (6), 1056.16 (2) [(2^{iPr2}-Cl)$_2$Cl]$^+$. IR (ATR): $\tilde{\nu} = 3268$ (w, NH), 2969 (w, CH), 1547 (vs), 1370 (s), 1139 (s), 1104 (m), 813 (m), 486 (vs) cm^{-1}. CV (CH_2Cl_2/[^{n}Bu$_4$N][B(C$_6$F$_5$)$_4$]): $E_{1/2} = 115$ mV vs. ferrocene/ferrocenium. UV/Vis/NIR (THF): λ (ε/M^{-1} cm^{-1}) = 432 (336) nm. UV/Vis/NIR (CH_2Cl_2): λ (ε/M^{-1} cm^{-1}) = 438 (220) nm. UV/Vis/NIR (CH_3CN): λ (ε/M^{-1} cm^{-1}) = 433 (256) nm.

Oxidation of 2^{Et2} and 2^{iPr2} – UV/Vis/NIR spectroscopic monitoring. The complexes (2^{Et2}: 1.49 mg, 0.0029 mmol; 2^{iPr2}: 1.58 mg, 0.0029·mmol) were dissolved under inert atmosphere at room temperature in THF, CH_3CN, CH_2Cl_2 or CH_3OH (3 mL), respectively. A UV/Vis/NIR spectrum was recorded. The oxidant [N(4-C$_6$H$_4$Br)$_3$][SbCl$_6$] (2.36 mg, 0.0029 mmol) was added as a solid and UV/Vis/NIR spectra were recorded after the indicated time intervals.

Oxidation of 2^{iPr2} – EPR spectroscopic monitoring. To pre-cooled (dry ice/ethanol) solutions of 2^{Et2} or 2^{iPr2} (1.72 mg/1.82 mg, 0.0033 mmol) in THF (0.5 mL) was added a solution of magic blue [N(4-C$_6$H$_4$Br)$_3$][SbCl$_6$] (2.36 mg, 0.0029 mmol) in THF (0.3 mL) under inert atmosphere. The EPR tubes were immediately cooled to 77 K in the EPR spectrometer. Analogous experiments and spectroscopic monitoring were performed at room temperature under inert atmosphere. EPR spectra of magic blue (1.06 mg, 0.0013 mmol) in THF (0.5 mL) were recorded at room temperature and at 77 K for comparison.

Deposition Numbers 2107165 (for 2^{Et2}×THF) and 2107164 (for 2^{iPr2}) contain the supplementary crystallographic data for this paper. These data are provided free of charge by the joint Cambridge

EurJIC
European Journal of Inorganic Chemistry

Research Article
doi.org/10.1002/ejic.202100905

Chemistry Europe
European Chemical Societies Publishing

Crystallographic Data Centre and Fachinformationszentrum Karlsruhe Access Structures service www.ccdc.cam.ac.uk/structures.

Acknowledgements

Financial support from the Deutsche Forschungsgemeinschaft HE 2778/16-1 is gratefully acknowledged. Parts of this research were conducted using the supercomputer ELWETRITSCH and advisory services offered by the Technical University of Kaiserslautern (https://elwe.rhrk.uni-kl.de/), which is a member of the AHRP. We thank Dr. Dieter Schollmeyer and Dr. Luca M. Carrella for collection of the diffraction data. Open Access funding enabled and organized by Projekt DEAL.

Conflict of Interest

The authors declare no conflict of interest.

Data Availability Statement

The data that support the findings of this study are available in the supplementary material of this article.

Keywords: Acyclic carbenes · Diamino carbenes · Ferrocene ligands · Gold · Redox properties

[1] R. P. Herrera, M. C. Gimeno, *Chem. Rev.* **2021**, *121*, 8311–8363.
[2] G. J. Hutchings, M. Brust, H. Schmidbaur, *Chem. Soc. Rev.* **2008**, *37*, 1759–1765.
[3] P. Font, X. Ribas, *Eur. J. Inorg. Chem.* **2021**, *2021*, 2556–2569.
[4] A. S. K. Hashmi, *Acc. Chem. Res.* **2014**, *47*, 864–876.
[5] A. S. K. Hashmi, *Angew. Chem. Int. Ed.* **2010**, *49*, 5232–5241; *Angew. Chem.* **2010**, *122*, 5360–5369.
[6] A. Fürstner, *Chem. Soc. Rev.* **2009**, *38*, 3208–3221.
[7] A. Collado, D. J. Nelson, S. P. Nolan, *Chem. Rev.* **2021**, *121*, 8559–8612.
[8] R. Dorel, A. M. Echavarren, *Chem. Rev.* **2015**, *115*, 9028–9072.
[9] C. Obradors, A. M. Echavarren, *Chem. Commun.* **2014**, *50*, 16–28.
[10] L. Rocchigiani, M. Bochmann, *Chem. Rev.* **2021**, *121*, 8364–8451.
[11] D. Gatineau, J.-P. Goddard, V. Mouriès-Mansuy, L. Fensterbank, *Isr. J. Chem.* **2013**, *53*, 892–900.
[12] N. Marion, S. P. Nolan, *Chem. Soc. Rev.* **2008**, *37*, 1776–1782.
[13] R. Jazzar, M. Soleilhavoup, G. Bertrand, *Chem. Rev.* **2020**, *120*, 4141–4168.
[14] L. M. Slaughter, *ACS Catal.* **2012**, *2*, 1802–1816.
[15] V. P. Boyarskiy, K. V. Luzyanin, V. Y. Kukushkin, *Coord. Chem. Rev.* **2012**, *256*, 2029–2056.
[16] A. A. Ruch, M. C. Ellison, J. K. Nguyen, F. Kong, S. Handa, V. N. Nesterov, L. M. Slaughter, *Organometallics* **2021**, *40*, 1416–1433.
[17] A. S. K. Hashmi, T. Hengst, C. Lothschütz, F. Rominger, *Adv. Synth. Catal.* **2010**, *352*, 1315–1337.
[18] C. Bartolomé, Z. Ramiro, D. García-Cuadrado, P. Pérez-Galán, M. Raducan, C. Bour, A. M. Echavarren, P. Espinet, *Organometallics* **2010**, *29*, 951–956.
[19] H. Seo, B. P. Roberts, K. A. Abboud, K. M. Merz, S. Hong, *Org. Lett.* **2010**, *12*, 4860–4863.
[20] C. Singh, A. Kumar, H. V. Huynh, *Inorg. Chem.* **2020**, *59*, 8451–8460.
[21] M. Soleilhavoup, G. Bertrand, *Acc. Chem. Res.* **2015**, *48*, 256–266.
[22] R. Kinjo, B. Donnadieu, G. Bertrand, *Angew. Chem. Int. Ed.* **2011**, *50*, 5560–5563; *Angew. Chem.* **2011**, *123*, 5674–5677.
[23] C. Bartolomé, M. Carrasco-Rando, S. Coco, C. Cordovilla, J. M. Martín-Alvarez, P. Espinet, *Inorg. Chem.* **2008**, *47*, 1616–1624.
[24] C. Bartolomé, Z. Ramiro, P. Pérez-Galán, C. Bour, M. Raducan, A. M. Echavarren, P. Espinet, *Inorg. Chem.* **2008**, *47*, 11391–11397.
[25] V. Vethacke, V. Claus, M. C. Dietl, D. Ehjeij, A. Meister, J. F. Huber, L. K. Paschai Darian, M. Rudolph, F. Rominger, A. S. K. Hashmi, *Adv. Synth. Catal.* **2021**, *363*, DOI: 10.1002/adsc.202101000.
[26] R. Usón, A. Laguna, J. Vicente, J. García, B. Bergareche, *J. Organomet. Chem.* **1979**, *173*, 349–355.
[27] J. E. Parks, A. L. Balch, *J. Organomet. Chem.* **1974**, *71*, 453–463.
[28] F. Bonati, G. Minghetti, *J. Organomet. Chem.* **1973**, *59*, 403–410.
[29] S. Kuwata, F. E. Hahn, *Chem. Rev.* **2018**, *118*, 9642–9677.
[30] M. C. Jahnke, F. E. Hahn, *Coord. Chem. Rev.* **2015**, *293–294*, 95–115.
[31] M. C. Jahnke, F. E. Hahn, *Chem. Lett.* **2015**, *44*, 226–237.
[32] J. Ruiz, M. A. Mateo, *Organometallics* **2021**, *40*, 1515–1522.
[33] J. Ruiz, L. García, D. Sol, M. Vivanco, *Angew. Chem. Int. Ed.* **2016**, *55*, 8386–8390; *Angew. Chem.* **2016**, *128*, 8526–8530.
[34] P. C. Kunz, C. Wetzel, S. Kögel, M. U. Kassack, B. Spingler, *Dalton Trans.* **2011**, *40*, 35–37.
[35] H. G. Raubenheimer, L. Lindeque, S. Cronje, *J. Organomet. Chem.* **1996**, *511*, 177–184.
[36] A. Franchino, M. Montesinos-Magraner, A. M. Echavarren, *Bull. Chem. Soc. Jpn.* **2021**, *94*, 1099–1117.
[37] R. Pretorius, M. R. Fructos, H. Müller-Bunz, R. A. Gossage, P. J. Pérez, M. Albrecht, *Dalton Trans.* **2016**, *45*, 14591–14602.
[38] L. Hettmanczyk, D. Schulze, L. Suntrup, B. Sarkar, *Organometallics* **2016**, *35*, 3828–3836.
[39] H. Schmidbaur, A. Schier, *Z. Naturforsch. B* **2011**, *66*, 329–350.
[40] S. Gaillard, J. Bosson, R. S. Ramón, P. Nun, A. M. Z. Slawin, S. P. Nolan, *Chem. Eur. J.* **2010**, *16*, 13729–13740.
[41] P. Veit, C. Volkert, C. Förster, V. Ksenofontov, S. Schlicher, M. Bauer, K. Heinze, *Chem. Commun.* **2019**, *55*, 4615–4618.
[42] S. Klenk, S. Rupf, L. Suntrup, M. van der Meer, B. Sarkar, *Organometallics* **2017**, *36*, 2026–2035.
[43] L. Hettmanczyk, L. Suntrup, S. Klenk, C. Hoyer, B. Sarkar, *Chem. Eur. J.* **2017**, *23*, 576–585.
[44] L. Hettmanczyk, S. Manck, C. Hoyer, S. Hohloch, B. Sarkar, *Chem. Commun.* **2015**, *51*, 10949–10952.
[45] A. Straube, P. Coburger, L. Dütsch, E. Hey-Hawkins, *Chem. Sci.* **2020**, *11*, 10657–10668.
[46] B. S. Birenheide, F. Krämer, L. Bayer, P. Mehlmann, F. Dielmann, F. Breher, *Chem. Eur. J.* **2021**, *27*, DOI: 10.1002/chem.202101969.
[47] J. F. Arambula, R. McCall, K. J. Sidoran, D. Magda, N. A. Mitchell, C. W. Bielawski, V. M. Lynch, J. L. Sessler, K. Arumugam, *Chem. Sci.* **2016**, *7*, 1245–1256.
[48] J. K. Muenzner, B. Biersack, A. Albrecht, T. Rehm, U. Lacher, W. Milius, A. Casini, J.-J. Zhang, I. Ott, V. Brabec, O. Stuchlikova, I. C. Andronache, L. Kaps, D. Schuppan, R. Schobert, *Chem. Eur. J.* **2016**, *22*, 18953–18962.
[49] C. Hoyer, P. Schwerk, L. Suntrup, J. Beerhues, M. Nössler, U. Albold, J. Dernedde, K. Tedin, B. Sarkar, *Eur. J. Inorg. Chem.* **2021**, *2021*, 1373–1382.
[50] K. Škoch, P. Vosáhlo, I. Císařová, P. Štěpnička, *Dalton Trans.* **2020**, *49*, 1011–1021.
[51] D. Aucamp, S. V. Kumar, D. C. Liles, M. A. Fernandes, L. Harmse, D. I. Bezuidenhout, *Dalton Trans.* **2018**, *47*, 16072–16081.
[52] D. I. Bezuidenhout, B. van der Westhuizen, A. J. Rosenthal, M. Wörle, D. C. Liles, I. Fernández, *Dalton Trans.* **2014**, *43*, 398–401.
[53] S. Preiß, J. Melomedov, A. Wünsche von Leupoldt, K. Heinze, *Chem. Sci.* **2016**, *7*, 596–610.
[54] Z. Ou, K. M. Kadish, W. E. J. Shao, P. J. Sintic, K. Ohkubo, S. Fukuzumi, M. J. Crossley, *Inorg. Chem.* **2004**, *43*, 2078–2086.
[55] K. Heinze, *Angew. Chem. Int. Ed.* **2017**, *56*, 16126–16134; *Angew. Chem.* **2017**, *129*, 16342–16350.
[56] G. R. Knox, P. L. Pauson, D. Willison, E. Solčániová, Š. Toma, *Organometallics* **1990**, *9*, 301–306.
[57] P. Veit, S. Seibert, C. Förster, K. Heinze, *Z. Anorg. Allg. Chem.* **2020**, *646*, 940–947.
[58] P. Veit, C. Förster, S. Seibert, K. Heinze, *Z. Anorg. Allg. Chem.* **2015**, *641*, 2083–2092.
[59] U. Siemeling, D. Rother, C. Bruhn, H. Fink, T. Weidner, F. Träger, A. Rothenberger, D. Fenske, A. Priebe, J. Maurer, R. Winter, *J. Am. Chem. Soc.* **2005**, *127*, 1102–1103.
[60] S. F. Hartlaub, N. K. Lauricella, C. N. Ryczek, A. G. Furneaux, J. D. Melton, N. A. Piro, W. S. Kassel, C. Nataro, *Eur. J. Inorg. Chem.* **2017**, *2017*, 424–432.

EurJIC
European Journal of Inorganic Chemistry

Research Article
doi.org/10.1002/ejic.202100905

Chemistry Europe
European Chemical Societies Publishing

[61] C. Förster, P. Veit, V. Ksenofontov, K. Heinze, *Chem. Commun.* **2015**, *51*, 1514–1516.
[62] P. Veit, E. Prantl, C. Förster, K. Heinze, *Organometallics* **2016**, *35*, 249–257; in Druck.
[63] N. Mirzadeh, S. H. Privér, A. J. Blake, H. Schmidbaur, S. K. Bhargava, *Chem. Rev.* **2020**, *120*, 7551–7591.
[64] H. Schmidbaur, A. Schier, *Chem. Soc. Rev.* **2012**, *41*, 370–412.
[65] H. Schmidbaur, *Gold Bull.* **2000**, *33*, 3–10.
[66] D. Siebler, C. Förster, K. Heinze, *Dalton Trans.* **2011**, *40*, 3558–3575.
[67] D. Siebler, M. Linseis, T. Gasi, L. M. Carrella, R. F. Winter, C. Förster, K. Heinze, *Chem. Eur. J.* **2011**, *17*, 4540–4551.
[68] K. Heinze, M. Schlenker, *Eur. J. Inorg. Chem.* **2004**, 2974–2988.
[69] P. Pyykkö, *Angew. Chem. Int. Ed.* **2004**, *43*, 4412–4456; *Angew. Chem.* **2004**, *116*, 4512–4557.
[70] P. Schwerdtfeger, A. E. Bruce, M. R. M. Bruce, *J. Am. Chem. Soc.* **1998**, *120*, 6587–6597.
[71] T. El-Shihi, F. Siglmüller, R. Herrmann, M. Fernanda, N. N. Carvalho, A. J. Pombeiro, *J. Organomet. Chem.* **1987**, *335*, 239–247.
[72] T. Kienz, C. Förster, K. Heinze, *Organometallics* **2014**, *33*, 4803–4812.
[73] K. Hanauer, M. T. Pham, C. Förster, K. Heinze, *Eur. J. Inorg. Chem.* **2017**, *2017*, 433–445.
[74] a) S. Preiß, C. Förster, S. Otto, M. Bauer, P. Müller, D. Hinderberger, Haeri, Haleh, Hashemi, L. Carella, K. Heinze, *Nat. Chem.* **2017**, *9*, 1249–1255; b) R. Kirmse, M. Kampf, R.-M. Olk, M. Hildebrand, H. Krautscheid, *Z. Anorg. Allg. Chem.* **2004**, *630*, 1433–1436.
[75] T. Drews, S. Seidel, K. Seppelt, *Angew. Chem. Int. Ed.* **2002**, *41*, 454–456; *Angew. Chem.* **2002**, *114*, 470–473.
[76] A. J. Blake, J. A. Greig, A. J. Holder, T. I. Hyde, A. Taylor, M. Schröder, *Angew. Chem. Int. Ed. Engl.* **1990**, *29*, 197–198; *Angew. Chem.* **1990**, *102*, 203–204.
[77] S. Fery-Forgues, B. Delavaux-Nicot, *J. Photochem. Photobiol. A* **2000**, *132*, 137–159.
[78] J. Melomedov, J. R. Ochsmann, M. Meister, F. Laquai, K. Heinze, *Eur. J. Inorg. Chem.* **2014**, *2014*, 2902–2915.
[79] N. G. Connelly, W. E. Geiger, *Chem. Rev.* **1996**, *96*, 877–910.
[80] S. D. Waniek, J. Klett, C. Förster, K. Heinze, *Beilstein J. Org. Chem.* **2018**, *14*, 1004–1015.
[81] M. Yáñez-S, S. A. Moya, C. Zúñiga, G. Cárdenas-Jirón, *Comput. Theor. Chem.* **2017**, *1118*, 65–74.
[82] A. Neidlinger, T. Kienz, K. Heinze, *Organometallics* **2015**, *34*, 5310–5320.
[83] A. Neidlinger, V. Ksenofontov, K. Heinze, *Organometallics* **2013**, *32*, 5955–5965.
[84] J. Holz, M. Ayerbe García, W. Frey, F. Krupp, R. Peters, *Dalton Trans.* **2018**, *47*, 3880–3905.
[85] M. R. Ringenberg, J. Holz, R. Peters, *Dalton Trans.* **2018**, *47*, 12873–12878.
[86] S. Vanicek, J. Beerhues, T. Bens, V. Levchenko, K. Wurst, B. Bildstein, M. Tilset, B. Sarkar, *Organometallics* **2019**, *38*, 4383–4386.
[87] M. Pažický, A. Loos, M. J. Ferreira, D. Serra, N. Vinokurov, F. Rominger, C. Jäkel, A. S. K. Hashmi, M. Limbach, *Organometallics* **2010**, *29*, 4448–4458.
[88] P. de Frémont, R. Singh, E. D. Stevens, J. L. Petersen, S. P. Nolan, *Organometallics* **2007**, *26*, 1376–1385.
[89] P. Kühlkamp, H. G. Raubenheimer, J. S. Field, M. Desmet, *J. Organomet. Chem.* **1998**, *552*, 69–74.
[90] STOE & Cie, *X-Area*, STOE & Cie, Darmstadt, Germany.
[91] R. H. Blessing, *Acta Crystallogr. Sect. A* **1995**, *51*, 33–38.
[92] A. L. Spek, *Acta Crystallogr. Sect. D* **2009**, *65*, 148–155.
[93] J. Koziskova, F. Hahn, J. Richter, J. Kožíšek, *Acta Chim. Slov.* **2016**, *9*, 136–140.
[94] G. M. Sheldrick, *Acta Crystallogr. Sect. A* **2015**, *71*, 3–8.
[95] G. M. Sheldrick, *Acta Crystallogr. Sect. C* **2015**, *71*, 3–8.
[96] G. M. Sheldrick, *SHELXL-2018/3*, University of Göttingen, Göttingen, Germany, **2018**.
[97] C. B. Hübschle, G. M. Sheldrick, B. Dittrich, *J. Appl. Crystallogr.* **2011**, *44*, 1281–1284.
[98] F. Neese, *WIREs Comput. Mol. Sci.* **2018**, *8*.
[99] A. D. Becke, *J. Chem. Phys.* **1993**, *98*, 5648–5652.
[100] C. Lee, W. Yang, R. G. Parr, *Phys. Rev. B* **1988**, *37*, 785–789.
[101] B. Miehlich, A. Savin, H. Stoll, H. Preuss, *Chem. Phys. Lett.* **1989**, *157*, 200–206.
[102] A. Schäfer, H. Horn, R. Ahlrichs, *J. Chem. Phys.* **1992**, *97*, 2571–2577.
[103] A. Schäfer, C. Huber, R. Ahlrichs, *J. Chem. Phys.* **1994**, *100*, 5829–5835.
[104] S. Miertuš, E. Scrocco, J. Tomasi, *Chem. Phys.* **1981**, *55*, 117–129.
[105] V. Barone, M. Cossi, *J. Phys. Chem. A* **1998**, *102*, 1995–2001.
[106] D. A. Pantazis, X.-Y. Chen, C. R. Landis, F. Neese, *J. Chem. Theory Comput.* **2008**, *4*, 908–919.
[107] E. van Lenthe, E. J. Baerends, J. G. Snijders, *J. Chem. Phys.* **1993**, *99*, 4597–4610.
[108] C. van Wüllen, *J. Chem. Phys.* **1998**, *109*, 392–399.
[109] F. Neese, F. Wennmohs, A. Hansen, U. Becker, *Chem. Phys.* **2009**, *356*, 98–109.
[110] R. Izsák, F. Neese, *J. Chem. Phys.* **2011**, *135*, 144105.
[111] S. Kossmann, F. Neese, *Chem. Phys. Lett.* **2009**, *481*, 240–243.
[112] S. Grimme, J. Antony, S. Ehrlich, H. Krieg, *J. Chem. Phys.* **2010**, *132*, 154104.
[113] S. Grimme, S. Ehrlich, L. Goerigk, *J. Comput. Chem.* **2011**, *32*, 1456–1465.
[114] G. R. Fulmer, A. J. M. Miller, N. H. Sherden, H. E. Gottlieb, A. Nudelman, B. M. Stoltz, J. E. Bercaw, K. I. Goldberg, *Organometallics* **2010**, *29*, 2176–2179.
[115] K. Škoch, I. Císařová, J. Schulz, U. Siemeling, P. Štěpnička, *Dalton Trans.* **2017**, *46*, 10339–10354.
[116] K. Škoch, I. Císařová, P. Štěpnička, *Chem. Eur. J.* **2018**, *24*, 13788–13791.

Manuscript received: October 19, 2021
Revised manuscript received: November 4, 2021
Accepted manuscript online: November 9, 2021

3.3 Dicobaltocenioum Amine – Proton, Electron, and H atom Transfer

Sven D. Waniek, Christian Heine, Dimitri Zorn, Taro Lieberth, Maximilian Lauck, Christoph Förster and Katja Heinze

Organometallics, **2022**. 10.1021/acs.organomet.2c00211

N,*N*-dicobaltoceniumamine hexafluorophosphat and *N*,*N*-dicobaltoceniumamide hexafluorophosphate are synthesized by amide linkage. Amine and amide form an acid-base pair as well as a redox pair on longer time-scales than voltammetric ones. Reversible reduction on the amine performs hydrogen abstraction. The nature of the redox reversibility is proved by EPR and ^{1}H NMR spectroscopy.

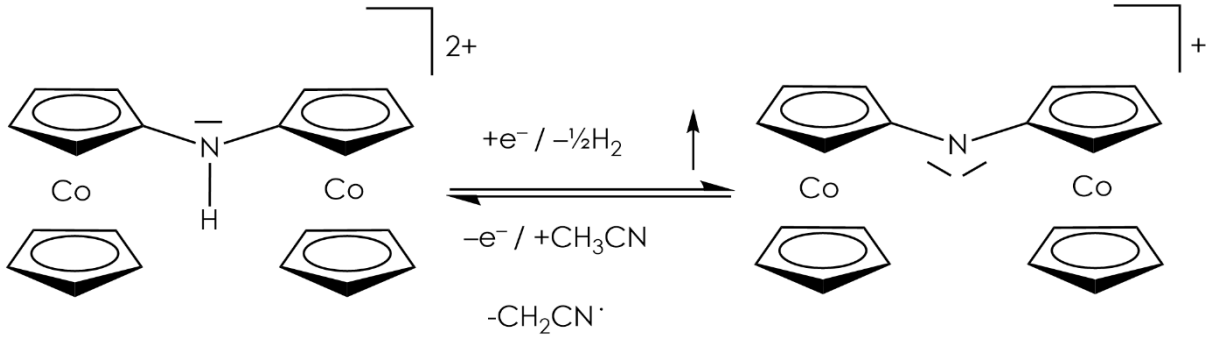

Author contributions

The synthesis of the diaminocobaltocenium complexes were done by *Sven D. Waniek*, [redacted], [redacted] and [redacted] who was under the supervision of [redacted]. The crystal structures were solved by [redacted]. Purification, (spectro)electrochemical analysis, UV/Vis, IR, EPR and NMR spectroscopy and DFT calculations were performed by *Sven D. Waniek*. The manuscript was written by [redacted] and [redacted] and the supporting information was written by *Sven D. Waniek*.

Supporting Information

The Supporting Information is found in Section 6.3 on pp. 127. The Cartesian coordinates from DFT calculations can be found online at

https://pubs.acs.org/doi/10.1021/acs.organomet.2c00211

Reprinted with permission from

Sven D. Waniek, Christian Heine, Dimitri Zorn, Taro Lieberth, Maximilian Lauck, Christoph Förster and Katja Heinze .

ORGANOMETALLICS

pubs.acs.org/Organometallics Article

Dicobaltocenium Amine–Proton, Electron, and H Atom Transfer

Sven D. Waniek, Christian Heine, Dimitri Zorn, Taro Lieberth, Maximilian Lauck, Christoph Förster,* and Katja Heinze*

Cite This: https://doi.org/10.1021/acs.organomet.2c00211 Read Online

ACCESS | Metrics & More | Article Recommendations | Supporting Information

ABSTRACT: The dicobaltocenium ion $[Cc_2NH]^{2+}$ $[\mathbf{H-1}]^{2+}$ was obtained via nucleophilic substitution of the nitro group of $[Cc-NO_2]^+$ by amino cobaltocenium $[Cc-NH_2]^+$ (Cc = Co(η^5-C_5H_4)(η^5-C_5H_5)). $[\mathbf{H-1}]^{2+}$ is moderately acidic, giving the conjugate base $\mathbf{1}^+$ after deprotonation (pK_a = 16.36 in acetonitrile). Single-crystal X-ray diffraction analyses and quantum chemical calculations of the $[\mathbf{H-1}]^{2+}/\mathbf{1}^+$ acid/base pair show only minor geometric changes during the proton transfer. One-electron reduction of $[\mathbf{H-1}]^{2+}$ at −1.32 V versus ferrocene furnishes $[\mathbf{H-1}]^+$, which is a strong hydrogen atom donor with a bond dissociation free energy (BDFE) of the NH group of only 44.6 kcal mol^{-1}. Hydrogen gas evolves from $[\mathbf{H-1}]^+$, generating cation $\mathbf{1}^+$. One-electron oxidation of $\mathbf{1}^+$ at E_p = +0.47 V gives the highly reactive aminyl radical $\mathbf{1}^{2+}$. The BDFE of the NH group of $[\mathbf{H-1}]^{2+}$ amounts to 85.9 kcal mol^{-1}. Spin trapping experiments confirm that $\mathbf{1}^{2+}$ abstracts a hydrogen atom from the CH_3CN solvent, regenerating $[\mathbf{H-1}]^{2+}$. Consequently, the $[\mathbf{H-1}]^{2+/+}$ redox couple is competent in the hydrogen evolution reaction and the $[\mathbf{H-1}]^{2+}/\mathbf{1}^{2+}$ pair enables hydrogen atom abstraction from CH_3CN. The $[\mathbf{H-1}]^{2+}/[\mathbf{H-1}]^+/\mathbf{1}^{2+}$ ions exhibit a unique proton, electron, and hydrogen atom transfer reactivity.

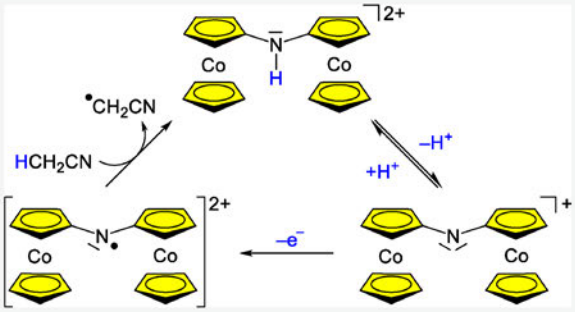

■ INTRODUCTION

Cobaltocene CcH (CcH = cobaltocene Co(η^5-C_5H_5)$_2$) is protonated by acids such as H_2SO_4, CH_3COOH, CF_3COOH, HBF_4, or HPF_6 to $[Co(\eta^4\text{-}C_5H_6)(\eta^5\text{-}C_5H_5)]^+$, which subsequently forms H_2 and $[Co(\eta^5\text{-}C_5H_5)(\eta^5\text{-}C_5H_5)]^+$.[1] In 2017/2019, Peters et al. demonstrated that decamethylobaltocene Cc* (Cc* = decamethylcobaltocene Co(η^5-C_5Me_5)$_2$) can be protonated to $[Co(\eta^4\text{-}C_5Me_5H)(\eta^5\text{-}C_5Me_5)]^+$, which transfers a hydrogen atom to iron complexes capable of reducing N_2 to NH_3 (Scheme 1a).[2,3] Consequently, $[Co(\eta^4\text{-}C_5Me_5H)(\eta^5\text{-}C_5Me_5)]^+$ acts as a competent reagent for proton-coupled electron transfer (PCET;[4] concerted proton electron transfer CPET). Its bond dissociation free energy BDFE(CH) is below 29 kcal mol^{-1}.[3] Later, an anilinium-based Brønstedt acid was attached to cobaltocenium ions, giving $[Cc-C_6H_4-NMe_2]^+$ as a molecular mediator for reductive CPET via electrocatalysis (Scheme 1b).[5]

Directly linking nitrogen-based substituents to cobaltocenium ions was recently successful thanks to reliable synthetic pathways to $[Cc-NH_2]^+$, $[Cc-N_2]^{2+}$, $[Cc-N_3]^+$, and $[Cc-NO_2]^+$, developed by Bildstein and Heck (Scheme 1c).[6−8] The amino cobaltocenium ion $[Cc-NH_2]^+$ can be deprotonated by NaH to give Cc–NH.[9] These basis compounds $[Cc-NH_2]^+$, $[Cc-N_3]^+$, and $[Cc-NO_2]^+$ already enabled the preparation of dicobaltocenium complexes with an amide bridge,[9] an azo bridge,[10] and a triazole bridge (Scheme 1c).[11] However, a dicobaltocenium complex $[Cc_2NH]^{2+}$ (Scheme 1d) with the smallest conceivable nitrogen-based bridge and hence the smallest distance between redox-active and Brønstedt acidic sites involved in CPET has not yet been reported.

We surmised that the dicobaltocenium dication $[Cc_2NH]^{2+}$ $[\mathbf{H-1}]^{2+}$ could deprotonate to $[Cc_2N]^+$ $\mathbf{1}^+$ similar to the $[Cc-NH_2]^+$/Cc–NH pair and that $[Cc_2NH]^+$ could enable the loss of a hydrogen atom after one-electron reduction of $[Cc_2NH]^{2+}$ (Scheme 1d), rendering $[\mathbf{H-1}]^+$ a possible PCET mediator with a small BDFE(NH). We report here the synthesis, structure, acid/base, and redox properties of $[Cc_2NH]^{2+}$ $[\mathbf{H-1}]^{2+}$ and its conjugate base $[Cc_2N]^+$ $\mathbf{1}^+$. Electrochemical and chemical oxidation of base $\mathbf{1}^+$ furnishes $\mathbf{1}^{2+}$, which is expected to be a highly reactive species with a high hydrogen atom affinity, that is, a high BDFE(NH) of $[\mathbf{H-1}]^{2+}$.

■ RESULTS AND DISCUSSION

The targeted dicobaltocenium amine $[Cc_2NH]^{2+}$ $[\mathbf{H-1}]^{2+}$ is accessible by nucleophilic substitution of the nitro group of $[Cc-NO_2]^+$[8] by amino cobaltocenium $[Cc-NH_2]^+$[6] deproto-

Received: May 6, 2022

https://doi.org/10.1021/acs.organomet.2c00211
Organometallics XXXX, XXX, XXX−XXX

Scheme 1. (a) Cobaltocenium Ions Showing CPET at the Metallocene and (b) at the NMe_2 Group; (c) Cobaltocenium Ions with N-Substituents and Dicobaltocenium Ions with N-Bridges and (d) Dicobaltocenium Amine $[H-1]^{2+}$ and Its Conjugate Base 1^+

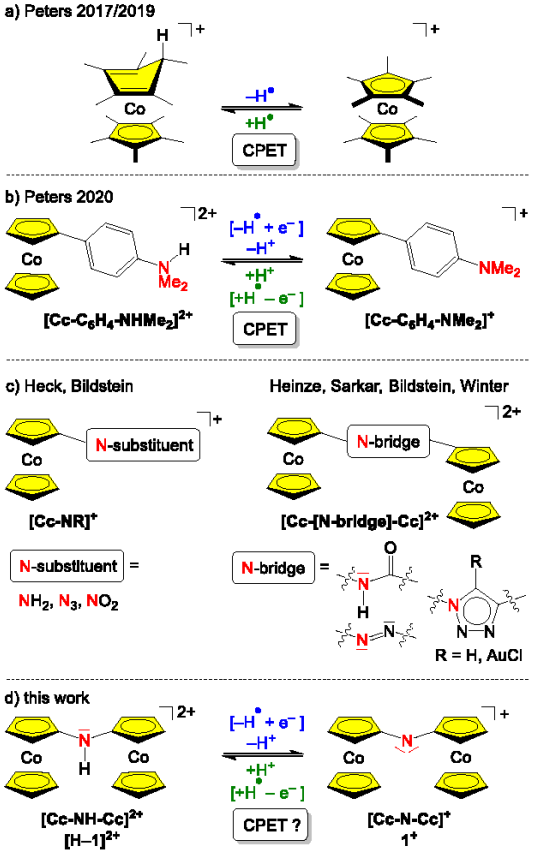

Scheme 2. Synthesis of Dicobaltocenium Amine $[H-1][PF_6]_2$ and Its Conjugate Base $1[PF_6]$

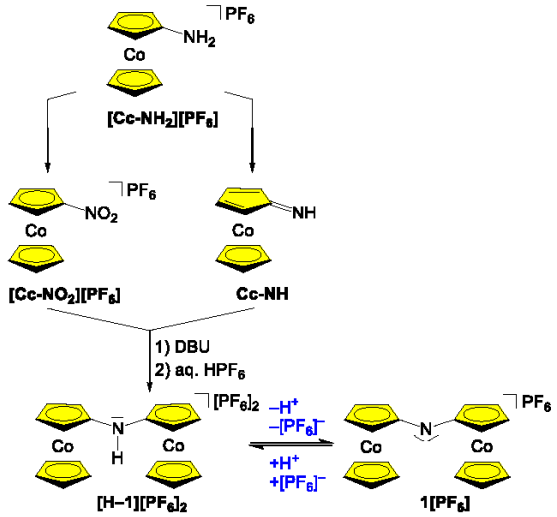

nated by NaH to the neutral Cc−NH[9] (Scheme 2), similar to the reaction of $[Cc-NO_2]^+$ with organic primary amines, hydroxide, or alkoxides.[8] This procedure initially yields a mixture of $[H-1]^{2+}$ and its conjugate base 1^+. Quantitative deprotonation to 1^+ by DBU (1,8-diazabicyclo(5.4.0)undec-7-ene) allows chromatographic separation from starting materials. Reprotonation with aqueous hexafluorophosphoric acid furnishes $[H-1][PF_6]_2$ (Scheme 2). Recrystallization of $[H-1][PF_6]_2$ or $1[PF_6]$ from acetonitrile/*tert*-butyl methyl ether yields yellow and red crystals, respectively.

During the various crystallization attempts with different counterions, crystals of $[H-1]Cl_2 \times 2\ H_2O$ suitable for X-ray diffraction were obtained in one instance. This salt crystallized in the orthorhombic space group *Fdd*2 along with two water molecules. The cobaltocenium moieties are oriented in a *syn* fashion with a Co···Co distance of 5.39 Å (Figure 1a). One chloride counterion is hydrogen-bonded to the NH group and to two water molecules being part of a hydrogen-bonded water/chloride chain ···[Cl1···O1(water)···Cl2···O2(water)]··· (Supporting Information, Figure S1). After salt metathesis, twinned crystals of $[H-1][PF_6]_2$ were obtained. The structure solution and refinement was sufficient to confirm the identity of the complex salt, but the crystal quality was too poor to allow detailed discussion of metrical data. The structure determination clearly shows that the cobaltocenium ions are oriented in an *anti* fashion and that the NH moiety is hydrogen-bonded to a hexafluorophosphate counterion (Figure 1b). The presence of *syn* and *anti* orientations in the different salts suggests that both orientations are energetically similar. This negligible energy difference is also confirmed by density functional theory (DFT) calculations of *syn* and *anti* conformers of $[H-1]^{2+}$ and 1^+ on the ((CPCM-(acetonitrile)-RIJCOSX-B3LYP-ZORA/def2-TZVP)) level of theory (Supporting Information).

Before chromatographic workup, crystals of the mixed salt $[1]_2[CcNH_2][PF_6]_3$ (triclinic $P\bar{1}$) were obtained in one instance. The two crystallographically independent cations 1^+ are orientated *syn* and *anti* with respect to the approximate Cp−N−Cp planes with Co···Co distances of 5.18 and 5.53 Å, respectively (Figure 1c). The amine substituent of $[CcNH_2]^+$ is disordered over two positions (N3/N3A with occupancy factors 0.54/0.46) forming hydrogen bonds to the bridging nitrogen atoms of the two cations 1^+ (Supporting Information, Figure S2). The hydrogen bonding and the different orientations might account for the crystallization of the mixed salt. The C−N−C angles decrease only slightly upon deprotonation of $[H-1]^{2+}$ to 1^+ from 125.6(6)° (*syn*) to 121.8(4)°/122.3(4)° (*syn*/*anti*). Similarly, the C−N distances decrease marginally from 1.378(9)/1.392(9) Å to 1.344(7)/1.355(7) Å, demonstrating a small reorganization at nitrogen upon deprotonation.

DFT calculations on *syn*/*anti*-$[H-1]^{2+}$ and *syn*/*anti*-1^+ reproduce the slight decrease of the C−N−C angles from 128.8°/129.8° (*syn*/*anti*) to 123.2°/124.3° (*syn*/*anti*) and C−N distances from 1.351/1.400//1.372/1.372 (*syn*//*anti*) to 1.341/1.337//1.338/1.339 Å (*syn*//*anti*). The calculations suggest only minor energy differences for the two conformations in both dicobaltocenium ions $[H-1]^{2+}$ and 1^+. Consequently, no strong preference for a particular conformation is expected in solution.

The ^1H NMR spectra of $[H-1][PF_6]_2$ and $1[PF_6]$ in CD_3CN exhibit the characteristic resonance pattern for the protons H^1, H^2, and H^3 of monosubstituted cobaltocenium ions between δ = 5.7 and 5.2 ppm in a 2:2:5 integral ratio

https://doi.org/10.1021/acs.organomet.2c00211
Organometallics XXXX, XXX, XXX−XXX

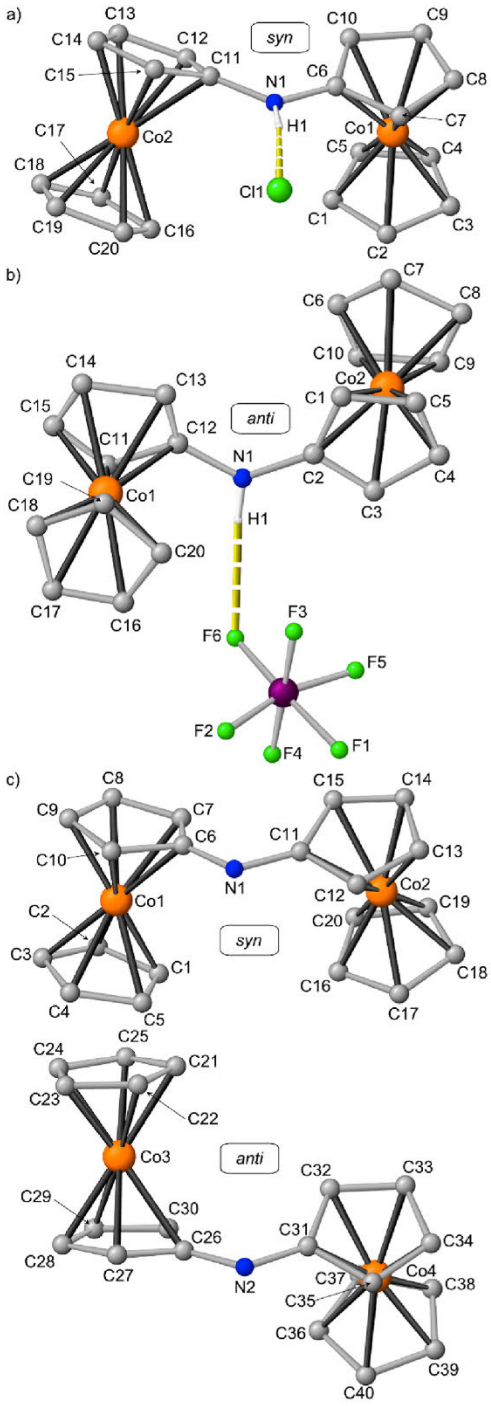

Figure 1. Molecular structures of (a) dication of $[\mathbf{H-1}]Cl_2 \times 2\ H_2O$ H-bonded to a chloride ion, (b) dication of $[\mathbf{H-1}][PF_6]_2$ H-bonded to a $[PF_6]^-$ ion, and (c) $\mathbf{1}^+$ of $[\mathbf{1}]_2[\mathbf{CcNH_2}][PF_6]_3$ featuring *syn* and *anti* conformations. CH hydrogen atoms, solvent molecules, and further counterions are omitted.

(Figure 2; Supporting Information, Figures S3–S4). Deprotonation of $[\mathbf{H-1}]^{2+}$ at the amine shifts all cyclopentadienyl proton resonances to a higher field by 0.2–0.3 ppm. This is similar to the shift experienced by Cp protons upon deprotonation of $[CcNH_2]^+$ to CcNH.[9] Expectedly, the NH proton resonance H^4 of $[\mathbf{H-1}]^{2+}$ at δ = 7.62 ppm vanishes upon deprotonation to $\mathbf{1}^+$ (Figure 2). Deprotonation shifts the ^{13}C NMR resonances to a higher field as well by 1.4 to 2.3 ppm (Supporting Information, Figures S5–S6). The presence of the $[PF_6]^-$ counterions is confirmed by the septet resonance at $\delta(^{31}P) = -144.6$ in the ^{31}P NMR spectra and the doublet resonance at $\delta(^{19}F) = -73.3$ in the ^{19}F NMR spectra ($^1J_{PF}$ = 706 Hz) (Supporting Information, Figures S7–S10).

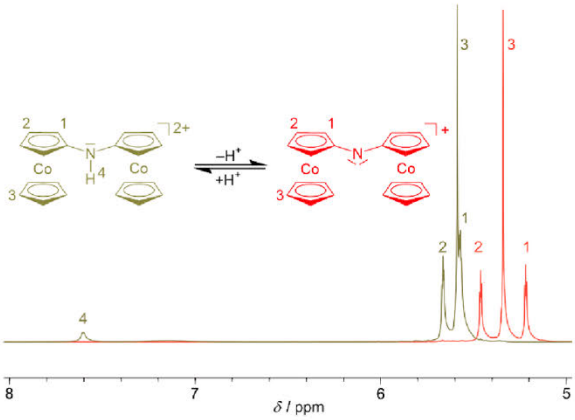

Figure 2. ^1H NMR spectra of $[\mathbf{H-1}][PF_6]_2$ (beige) and $\mathbf{1}[PF_6]$ (red) in CD_3CN.

IR spectra of $[\mathbf{H-1}][PF_6]_2$ and $\mathbf{1}[PF_6]$ display the characteristic T_{1u} bands of the $[PF_6]^-$ counterion at 825/795 and 557 cm^{-1} in addition to the bands of the C–C, C–N, and C–H stretching vibrations of the cobaltocenium moieties (Supporting Information, Figure S11). The symmetric and antisymmetric C–N stretching vibrations of $[\mathbf{H-1}][PF_6]_2$ are strongly split by Δ = 78 cm^{-1} (1497/1575 cm^{-1}) due to coupling with the NH bending vibration. The splitting is much weaker in $\mathbf{1}^+$ (1492 cm^{-1}; Δ < 10 cm^{-1}) due to the absence of the N–H proton. DFT calculations and numerical frequency calculations confirm this weaker splitting in $\mathbf{1}^+$ (*syn*/*anti*-$[\mathbf{H-1}]^{2+}$: Δ = 75/61 cm^{-1}; *syn*-/*anti*-$\mathbf{1}^+$: Δ = 10/4 cm^{-1}). The N–H stretching vibration of $[\mathbf{H-1}][PF_6]_2$ gives a sharp absorption band at 3400 cm^{-1} (Supporting Information, Figure S11).

The UV–visible (UV/vis) absorption spectrum of $[\mathbf{H-1}][PF_6]_2$ shows two bands at λ = 385 nm (ε = 1985 M^{-1} cm^{-1}) and λ = 452 nm (ε = 1665 M^{-1} cm^{-1}) accounting for the yellow color (Figure 3). Time-dependent (TD) DFT calculations of *syn*- and *anti*-$[\mathbf{H-1}]^{2+}$ assign LMCT (nitrogen lone pair to cobalt) and some dd character to the bands. Upon deprotonation, these bands bathochromically shift to λ = 409 nm (ε = 1285 M^{-1} cm^{-1}) and λ = 527 nm (ε = 3795 M^{-1} cm^{-1}), respectively, giving amide $\mathbf{1}^+$. TD-DFT calculations confirm the bathochromic shift (Supporting Information, Figures S12–S13). An analogous bathochromic shift occurs upon deprotonation of $[CcNH_2]^+$ to CcNH.[9]

Deprotonation with NEt_3, NaOH, or NaH and reprotonation with HOAc or HCl are highly reversible reactions confirming the stability of $[\mathbf{H-1}]^{2+}$ and $\mathbf{1}^+$. The pK_a value of the acid was determined spectrophotometrically in water to 9.56, close to the value of 9.2 of the ammonium ion $[NH_4]^+$ (Supporting Information, Figures S14–S15). The substituted

https://doi.org/10.1021/acs.organomet.2c00211
Organometallics XXXX, XXX, XXX–XXX

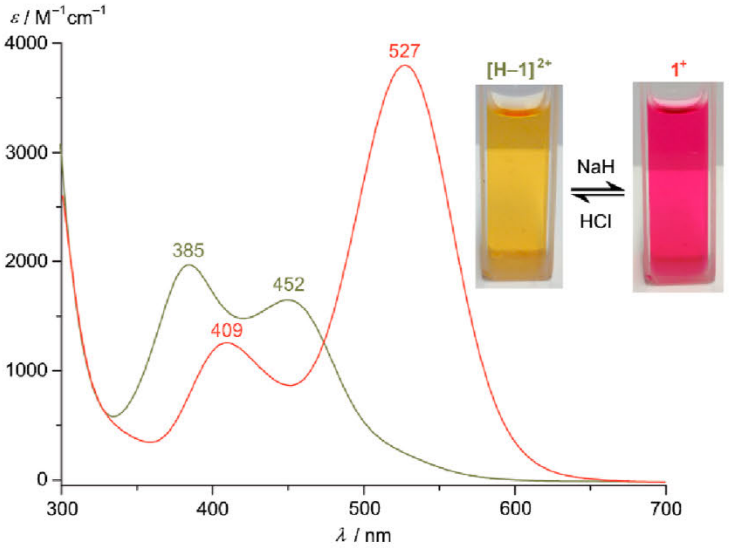

Figure 3. UV/vis spectra of $[\mathbf{H-1}][PF_6]_2$ (beige) and $\mathbf{1}[PF_6]$ (red) in CH_3CN. The inset shows photographs of solutions of $[\mathbf{H-1}]^{2+}$ and $\mathbf{1}^+$.

dimethyl aniline $[Cc-C_6H_4-NMe_2H]^{2+}$ (Scheme 1b) possesses pK_a = 8.6 in acetonitrile.[5] Assuming that $[\mathbf{H-1}]^{2+}$ possesses a similar acidic character as an aniline, a pK_a of 16.36 in acetonitrile is obtained after empirical conversion from water to acetonitrile as a solvent.[12]

The dication $[\mathbf{H-1}]^{2+}$ is reversibly reduced on the cyclic voltammetry time scale within the solvent window to the Co^{II}/Co^{III} mixed-valent cation $[\mathbf{H-1}]^+$ and the neutral dicobaltocene **H−1** at −1.32 and −1.54 V versus ferrocene, respectively (Figure 4; Supporting Information, Figures S16−S17).

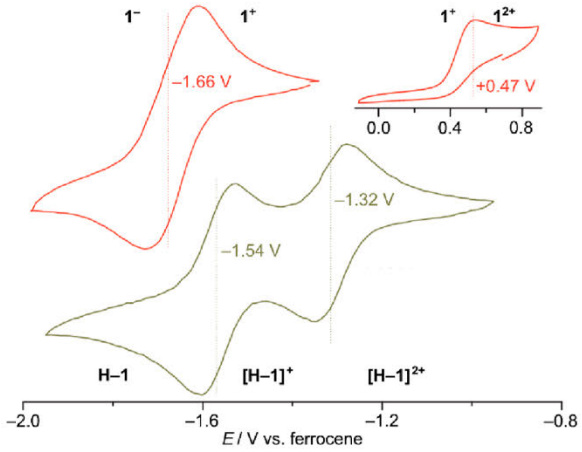

Figure 4. Cyclic voltammograms of $\mathbf{1}[PF_6]$ (red) and $[\mathbf{H-1}][PF_6]_2$ (beige) in $CH_3CN/[^nBu_4N][PF_6]$. $E_{1/2}$ and E_p values of reversible reductions and irreversible oxidation are indicated.

According to unrestricted DFT calculations, the mixed-valent cation $[\mathbf{H-1}]^+$ is localized with a cobalt(II) and a cobalt(III) moiety both in the *syn* and *anti* conformers (Figure 5; Supporting Information, Figure S20). **H−1** is a dicobaltocene with two cobalt(II) moieties (Figure 5; Supporting Information, Figure S20).

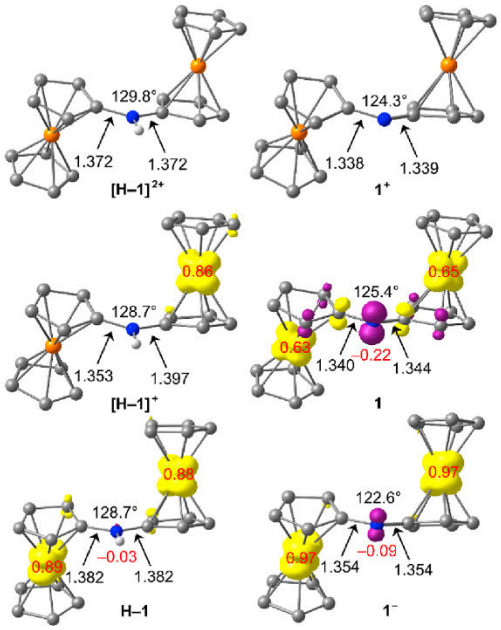

Figure 5. DFT-optimized geometries of the three acid/base pairs $[\mathbf{H-1}]^{2+}/\mathbf{1}^+$, $[\mathbf{H-1}]^+/\mathbf{1}$, and $[\mathbf{H-1}]/\mathbf{1}^-$ in *anti* conformations. Spin densities of open shell species are displayed in yellow/purple with an isosurface value of 0.01. CH hydrogen atoms are omitted. C−N distances/Å and C−N−C angles/deg are indicated. For *syn* conformations, see Supporting Information, Figure S20.

In contrast, monocation $\mathbf{1}^+$ displays only a single reversible two-electron reduction wave at −1.66 V under our conditions in the solvent window (Figure 4; Supporting Information, Figures S18−S19). According to unrestricted DFT calculations, spins and charges in the resulting intermediate mixed-valent complex *anti*-**1** are delocalized over both cobalt centers and the nitrogen bridge is spin-polarized (Figure 5), while the *syn* conformer *syn*-**1** is valence-localized (Supporting Informa-

https://doi.org/10.1021/acs.organomet.2c00211
Organometallics XXXX, XXX, XXX−XXX

tion, Figure S20). This intermediate **1** is unstable toward disproportionation 1^+ and 1^- as seen from the 2e$^-$ reduction wave under our conditions.[13,14] The doubly reduced complex 1^- possesses two cobalt(II) centers and spin polarization at the nitrogen bridge (Figure 5; Supporting Information, Figure S20). In addition to the 2e$^-$ reductive wave, 1^+ displays an irreversible 1e$^-$ oxidative wave at E_p = +0.47 V (Figure 4), which can be assigned to the $1^{2+/+}$ redox event. The electrochemically formed dication 1^{2+} undergoes a subsequent chemical reaction. The observed high reactivity of 1^{2+} likely arises from the high Mulliken spin density of 0.47 and 0.45 at the bridging nitrogen center of *anti*-1^{2+} and *syn*-1^{2+}, respectively, as calculated by DFT methods (Figure 6; Supporting Information, Figure S21).

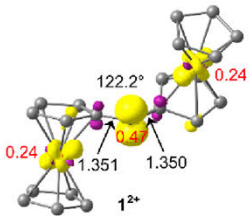

Figure 6. DFT-optimized geometry of the reactive dicationic aminyl radical *anti*-1^{2+} (S = 1/2). Spin densities are displayed in yellow/purple with an isosurface value of 0.01. CH hydrogen atoms are omitted. C–N distances/Å and C–N–C angles/deg are indicated. For *syn* conformations, see Supporting Information, Figure S21.

In order to access the mixed-valent complex $[\mathbf{H-1}]^+$ spectroscopically, we conducted UV/vis spectroelectrochemical (SEC) experiments in dry $CH_3CN/[^nBu_4N][PF_6]$. To our surprise, reduction of $[\mathbf{H-1}]^{2+}$ (at −1.0 V vs Ag pseudoelectrode) furnishes the characteristic UV/vis absorption spectrum of 1^+ instead of the expected $[\mathbf{H-1}]^+$ with an isosbestic point at 462 nm (Supporting Information, Figure S22). On the time scale of the SEC experiments, the initially formed complex $[\mathbf{H-1}]^+$ obviously formally expels a hydrogen atom H$^\bullet$ to form 1^+. During the SEC electrolysis, gas bubbles form in the SEC cell. It is tempting to assign these to H_2. With the converted pK_a and $E_{1/2}$ values of $[\mathbf{H-1}]^{2+}$ in acetonitrile, the BDFE of the NH bond of $[\mathbf{H-1}]^+$ is estimated according to eq 1 to BDFE($[\mathbf{H-1}]^+$) = 44.6 kcal mol^{-1} (186 kJ mol^{-1}) using the solvent-dependent thermodynamic constant $C_G(CH_3CN)$ = 52.6 kcal mol^{-1} (Scheme 3a, square scheme[4]).[15,16] This low BDFE supports the suggested facile formation of H_2 from $[\mathbf{H-1}]^+$. For comparison, the reported BDFE of the substituted dimethyl anilinium $[Cc-C_6H_4-NHMe_2]^+$ amounts to 36.5 kcal mol^{-1} (using the corrected C_G value[15,16]) (Scheme 1b)[5]

$$\mathrm{BDFE} = 1.37 \times \mathrm{p}K_a + 23.06 \times E_{1/2} + C_G \qquad (1)$$

Electrochemical oxidation of the thus generated 1^+ under SEC conditions in $CH_3CN/[^nBu_4N][PF_6]$ reforms $[\mathbf{H-1}]^{2+}$ according to the UV/vis spectroscopic data (Supporting Information, Figure S23). Analogous spectra are obtained by oxidizing $\mathbf{1}[\mathbf{PF_6}]$ generated by deprotonation of $[\mathbf{H-1}]^{2+}$ with NaH (Supporting Information, Figure S24). Similarly, oxidation of 1^+ (generated by deprotonation of $[\mathbf{H-1}]^{2+}$ with NaH) with ferrocenium ions as the chemical oxidant in CD_3CN cleanly produces the characteristic CH proton resonances of $[\mathbf{H-1}]^{2+}$ yet lacking the NH resonance (Supporting Information, Figure S25). These observations

Scheme 3. (a) PCET Square Scheme of the Thermochemistry of $[\mathbf{H-1}]^{2+}$, Its Conjugate Base 1^+, and Their Reduced Mixed-Valent Complexes $[\mathbf{H-1}]^+$ and 1 (Lower Part) and the Thermodynamical Properties of 1^{2+} (Upper Part). pK_a($[\mathbf{H-1}]^{2+}$), $E_{1/2}$($[\mathbf{H-1}]^{2+/+}$), $E_{1/2}$($1^{+/0}$), and $E_{1/2}$($1^{2+/+}$) Were Determined Experimentally, While pK_a($[\mathbf{H-1}]^+$), BDFE($[\mathbf{H-1}]^+$), and BDFE($[\mathbf{H-1}]^{2+}$) (in kcal mol^{-1}) Were Determined by eq 1; (b) Reductively Induced Chemistry of $[\mathbf{H-1}]^{2+}$ in CH_3CN and Indirect Experimental Observation of the Initial $^\bullet CH_2CN$ and H$^\bullet$ Products

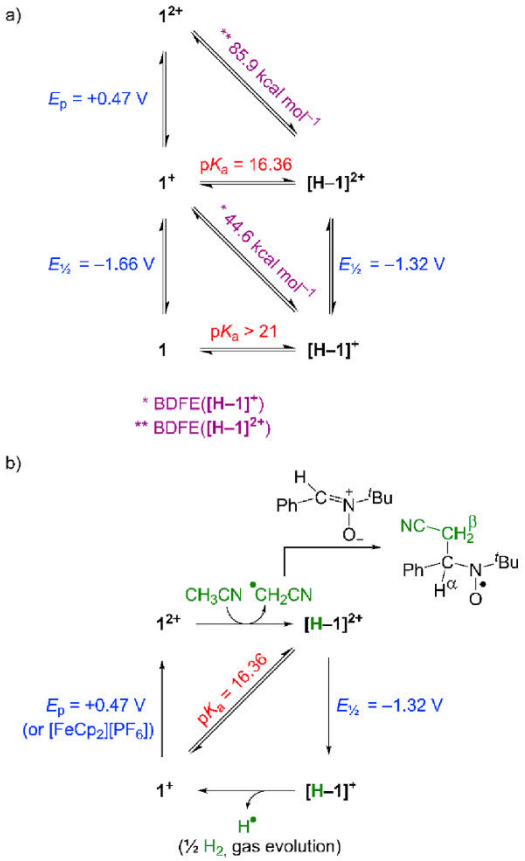

suggest that a very reactive aminyl radical 1^{2+} is initially formed by one-electron oxidation of 1^+. This short-lived radical abstracts a hydrogen atom from CH_3CN (HAT, hydrogen atom transfer) or a deuterium atom from CD_3CN. Dimerization[17,18] of 1^{2+} to a highly charged and sterically crowded hydrazine $[\mathbf{1-1}]^{4+}$ in the absence of a catalyst appears unfavorable, and hence, HAT/PCET from the solvent becomes competitive. From the thermochemical cycle (Scheme 3a), a BDFE($[\mathbf{H-1}]^{2+}$) ≈ 85.9 kcal mol^{-1} (359 kJ mol^{-1}) is estimated as an upper limit by using the peak potential E_p of the irreversible oxidation (instead of $E_{1/2}$) in eq 1. The BDFE($[\mathbf{H-1}]^{2+}$) of $[\mathbf{H-1}]^{2+}$ with two 18 valence electron complex units is almost twice as large as that of the mixed-valent cation $[\mathbf{H-1}]^+$ with 18/19 valence electron moieties with 44.6 kcal mol^{-1}. A similar trend was observed for the C–H BDEs of benzylic iron(II/I) metallocenes with 18 and 19 valence electrons, respectively.[19]

https://doi.org/10.1021/acs.organomet.2c00211
Organometallics XXXX, XXX, XXX−XXX

The BDE of a C–H bond of the employed CH_3CN has been reported as 93 kcal mol^{-1}.[20] With eq 2 and $TS^0(H^\bullet)$ = 6.37 kcal mol^{-1} (for CH_3CN at 298 K), the BDFE(CH, CH_3CN) amounts to 86.6 kcal mol^{-1}. Although this value is slightly higher than the estimated BDFE of $[\mathbf{H-1}]^{2+}$, the large excess of CH_3CN and the absence of other suitable H atom donors seem to enable the reaction of the aminyl radical $\mathbf{1}^{2+}$ with CH_3CN giving the cyanomethyl radical $^\bullet CH_2CN$[16]

$$\mathrm{BDFE(XH)} = \mathrm{BDE(XH)} - TS^0(\mathrm{H}^\bullet) \quad (2)$$

The dicationic aminyl radical $\mathbf{1}^{2+}$ was calculated by DFT methods (Figure 6). According to the calculations, this species is best described as two cobaltocenium substituents bound to the spin-carrying aminyl unit with a C–N–C angle of 122.2°. With a smaller Mulliken spin density shared between the cobalt centers (0.24 each) and a larger Mulliken spin density of 0.47 at the nitrogen atom, $\mathbf{1}^{2+}$ might attack the C–H bond of a solvent molecule via the aminyl nitrogen atom. DFT calculations (CPCM-(acetonitrile)-RIJCOSX-B3LYP-ZORA/def2-TZVP) of the $[\mathbf{H-1}]^{2+}/\mathbf{1}^{2+}$ pair estimate the BDE as 86 kcal mol^{-1}. With eq 2, the calculated BDFE($[\mathbf{H-1}]^{2+}$) equals 80 kcal mol^{-1} in good agreement with the experimentally estimated value. A BDE($[\mathbf{H-1}]^{+}$) = 55 kcal mol^{-1} is obtained computationally for the $[\mathbf{H-1}]^{+}/\mathbf{1}^{+}$ pair. The resulting BDFE($[\mathbf{H-1}]^{+}$) = 49 kcal mol^{-1} reasonably matches the experimental one. The calculated BDE and BDFE(CH_3CN) of acetonitrile amount to 92 and 86 kcal mol^{-1}, respectively, in very good agreement with the experimentally estimated value.[20] Overall, the calculated values agree well with the experimental ones. The calculated structures of the $[\mathbf{H-1}]^{2+}/\mathbf{1}^{2+}$ and $[\mathbf{H-1}]^{+}/\mathbf{1}^{+}$ pairs suggest only small changes in metrical data. The same holds for the $[\mathbf{H-1}]^{+}/\mathbf{1}^{2+}$ pair, connected via hydride abstraction, with a hydricity of 55.4 kcal mol^{-1}, lying in a similar range of hydrido phosphane cobalt(II) and nickel(II) complexes.[21] Hence, these structural changes contribute only marginally to the reorganization energy in the HAT/PCET and potential hydride transfer steps (Figures 5 and 6).

In order to find evidence for the proposed cyanomethyl radical generated by the aminyl radical $\mathbf{1}^{2+}$, a spin trapping experiment was performed (Scheme 3b). Electrochemical oxidation of $\mathbf{1}^{+}$ in the presence of phenyl *N-tert*-butylnitrone (PBN) as a spin trapping agent in CH_3CN furnishes the room-temperature X-band EPR spectrum shown in Figure 7. The characteristic triplet resonance of the nitroxide-based radical (A_N = 1.462 mT) is split into doublets by superhyperfine coupling to a single proton ($A_{H\alpha}$ = 0.381 mT) and importantly split into triplets by coupling to two protons ($A_{H\beta}$ = 0.064 mT) stemming from the trapped $^\bullet CH_2CN$ radical (Scheme 3b, Figure 7). These values match literature data of the cyanomethyl adduct of PBN (A_N = 1.485 mT; $A_{H\alpha}$ = 0.400 mT; $A_{H\beta}$ = 0.055 mT in aqueous CH_3CN) and unambiguously confirm the intermediate formation of the cyanomethyl radical.[22]

■ CONCLUSIONS

The dicobaltocenium amine $[\mathbf{H-1}]^{2+}$ is a weak acid with pK_a = 9.56 in water and 16.36 in acetonitrile. One-electron reduction to $[\mathbf{H-1}]^{+}$ at −1.32 V transforms $[\mathbf{H-1}]^{2+}$ into a good hydrogen atom donor thanks to a small BDFE of the NH group of $[\mathbf{H-1}]^{+}$ of 44.6 kcal mol^{-1} in acetonitrile. This leads to hydrogen evolution from $[\mathbf{H-1}]^{2+}$ and the formation of the conjugate base $\mathbf{1}^{+}$.

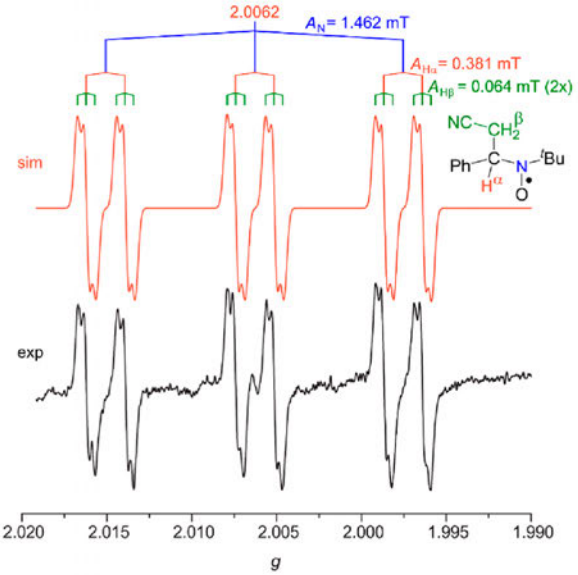

Figure 7. X-band EPR spectrum of $\mathbf{1}^{+}$ oxidized by ferrocenium hexafluorophosphate in CH_3CN in the presence of PBN shown in black (temperature = 298 K, field = 335.5 mT, sweep = 5 mT, sweep time = 300 s (20×), modulation = 0.025 mT, and MW attenuation = 5 dB) demonstrating the formation of a nitroxide-based radical. Simulation is displayed in red with g_{iso} = 2.0062, A_N = 1.462 mT, $A_{H\alpha}$ = 0.381 mT, $A_{H\beta}$ = 0.064 mT (2×), Gaussian linewidth 0.067, and Lorentzian linewidth 0.0.

One-electron oxidation of $\mathbf{1}^{+}$ generates the highly reactive aminyl radical $\mathbf{1}^{2+}$ competent to abstract a hydrogen atom from CH_3CN thanks to the larger BDFE of the NH group of $[\mathbf{H-1}]^{2+}$ of ≈85.9 kcal mol^{-1}. With these thermodynamic properties, the pairs $[\mathbf{H-1}]^{+}/\mathbf{1}^{+}$ and $[\mathbf{H-1}]^{2+}/\mathbf{1}^{2+}$ might be competent for electrocatalytic or photocatalytic HAT/PCET reactions, for example, HAT/PCET to ketones after reductive activation of $[\mathbf{H-1}]^{2+}$ in the presence of H^+[5] or cyanomethylation of arenes after oxidative activation of $\mathbf{1}^{+}$ in the presence of CH_3CN and a base.[22] Exploiting the biscobaltocenium amine $[\mathbf{H-1}]^{2+}$ presented in this study as a potential PCET mediator in electro- or photocatalytic[23,24] scenarios will be conducted in the future.

■ EXPERIMENTAL SECTION

General Procedures. All reactions and measurements were performed under an argon atmosphere unless otherwise noted. Gloveboxes (UniLab/MBraun—Ar 4.8, O_2 < 1 ppm, H_2O < 0.1 ppm) were used to store and weigh sensitive compounds for synthesis as well as to prepare samples that require the absence of oxygen and water. Dichloromethane, acetonitrile, and CD_3CN were dried and distilled from calcium hydride. THF was dried and distilled from potassium. Deuterated solvents were purchased from euriso-top and Deutero GmbH. Other reagents were used as received from commercial suppliers (ABCR, Acros Organics, Alfa Aesar, Fischer Scientific, Fluka, and Sigma-Aldrich). Cobaltocenium salt precursors were synthesized according to literature procedures.[6,8]

Intensity Data of Single-Crystal Structures. CCDC-2157935 and CCDC-2157936 were collected with a STOE IPDS-2T diffractometer from STOE & CIE GmbH with an Oxford cooling system using Mo K_α radiation (λ = 0.71073 Å). The diffraction frames were integrated using the STOE X-area[25] software package and were

https://doi.org/10.1021/acs.organomet.2c00211
Organometallics XXXX, XXX, XXX−XXX

corrected for absorption with MULABS[26] of the PLATON software package.[27] Intensity data of single-crystal structure CCDC-2157937 were collected with a STADIVARI diffractometer from STOE & CIE GmbH using Mo K_α radiation (λ = 0.71073 Å). The diffraction frames were integrated using the STOE X-Area[25] software package and were corrected for absorption with STOE LANA[28,29] of the STOE X-Area software package.[25] The structures were solved with SHELXT[30] and refined by the full-matrix method based on F^2 using SHELXL[31] of the SHELX[32] software package and the ShelXle[33] graphical interface. All non-hydrogen atoms were refined anisotropically, while the positions of all hydrogen atoms were generated with appropriate geometric constraints and allowed to ride on their respective parent atoms with fixed isotropic thermal parameters. Crystallographic data for the structures reported in this paper have been deposited with the Cambridge Crystallographic Data Centre as supplementary publication no. CCDC-2157935−2157937.

DFT Calculations. All calculations were performed using the quantum computing suite ORCA[34] 4.0.1. Geometry optimization was performed using (un-)restricted Kohn−Sham orbitals DFT (UKS) and the B3LYP functional[35−37] in combination with Ahlrichs' split-valence triple-ζ basis set def2-TZVP for all atoms.[38,39] Tight convergence criteria were chosen for DFT-UKS calculations (keywords *tightscf* and *tightopt*). All DFT-UKS calculations make use of the resolution of identity (Split-RI-J) approach for the Coulomb term in combination with the chain-of-spheres approximation for the exchange term (keyword *RIJCOSX*).[40,41] The zeroth order regular approximation was used to describe relativistic effects (keyword *ZORA*).[42] To account for solvent effects, a conductor-like screening model (keyword *CPCM* acetonitrile) modeling acetonitrile was used in all calculations.[43,44] A numerical frequency calculation confirmed that the optimized geometry corresponds to a minimum structure. Explicit counterions and/or solvent molecules were neglected. A total of 70 vertical spin-allowed transitions were calculated by TD-DFT.

NMR Spectra. NMR spectra were recorded on a Bruker Avance DRX 400 spectrometer at 400.31 MHz (^{1}H), 100.68 MHz (^{13}C), 377.63 MHz (^{19}F), and 162.04 MHz (^{31}P) at 25 °C. All resonances are reported in ppm versus the solvent signal as the internal standard CD_3CN (^{1}H, δ = 1.94 ppm; ^{13}C, δ = 1.94 ppm)[45] or external standards for ^{31}P (H_3PO_4 (85%), δ = 0 ppm) and ^{19}F (CCl_3F, δ = 0 ppm).

UV/vis Spectra. UV/vis spectra were recorded on a Varian Cary 5000 spectrometer or a Jasco V770 spectrometer using 1.0 cm cells (Hellma, Suprasil).

pH Measurements. pH measurements were performed with an Orion 3-Star Benchtop pH Meter from Thermo Scientific.

ESI Mass Spectra. ESI mass spectra were recorded with a 6545 QTOF-HRAM mass spectrometer from Agilent.

Elemental Analyses. Elemental analyses were performed by the Mikroanalytisches Labor Kolbe, c/o Fraunhofer Institut UMSICHT, Oberhausen, Germany.

IR Spectra. IR spectra were recorded on a Bruker Alpha FTIR spectrometer with an ATR unit, containing a diamond crystal.

Electrochemical Experiments. Electrochemical experiments were carried out on a BioLogic SP-200 voltammetric analyzer using a platinum working electrode, a platinum wire as the counter electrode, and a 0.01 M Ag/$AgNO_3$ reference electrode in CH_3CN. All potentials were referenced versus the FcH/FcH^+ couple (E° = 0.4 V vs SCE).[46] The measurements were carried out at a scan rate of 100 mV s^{-1} for cyclic voltammetry experiments and at 5−100 mV s^{-1} for square wave voltammetry experiments using 0.1 M [^{n}Bu$_4$N][PF_6] as the supporting electrolyte and 0.001 M of the sample in acetonitrile.

Spectroelectrochemical Measurements. Spectroelectrochemical measurements were performed with a Biologic SP-50 voltammetric analyzer using a Specac omni-cell liquid transmission cell[47] with CaF_2 windows equipped with a Pt-gauze working electrode and a Ag wire as a pseudo-reference electrode, melt-sealed in a self-made polyethylene spacer (approximate 0.5 mm path length) in 0.1 M [^{n}Bu$_4$N][PF_6]/acetonitrile (20 mM solutions of [**H−1**][PF_6]$_2$ or **1**[**PF6**]).

X-Band EPR Spectra. X-band EPR spectra were recorded on a Miniscope MS 300 (Magnettech GmbH, Germany) with a frequency counter FC 400 (Magnettech GmbH, Germany) at a microwave frequency of 9.39 GHz in acetonitrile (295 K). Mn^{2+} in ZnS was used as the external standard (g = 2.118, 2.066, 2.027, 1.986, 1.946, 1.906). Simulations were performed with the program package Easyspin for MatLab (R2016b).[48]

Synthesis of [H−1][PF_6]$_2$. Amino cobaltocenium hexafluorphosphate [Cc−NH_2][PF_6] (32.4 mg, 93.0 μmol, 1 equiv) was dissolved in THF (6 mL). Sodium hydride (9.2 mg, 372.0 μmol, 4 equiv) was added as a solid. The solution was stirred for 10 min. The color changed from yellow to red. This solution was transferred within ca. 30 s via a syringe filter into a solution of nitro cobaltocenium hexafluorphosphate [Cc−NO_2][PF_6] (36.6 mg, 96.8 μmol, 1.04 equiv) in acetonitrile (6 mL). DBU (14.1 mg, 93.0 μmol, 13.9 μL, 1 equiv) was added to ensure full deprotonation. The reaction mixture was stirred for 15 min. After evaporation of the solvents under reduced pressure, the crude product was isolated by column chromatography (aluminum oxide, acetonitrile/acetic acid 98:2 v/v) to give a yellow to red oil. This oily product mixture contains [**H−1**][PF_6]$_2$, **1**[PF_6] and the corresponding acetate salts. The oil was dissolved in ethanol (5 mL). Adding concentrated aqueous hexafluorophosphoric acid (0.2 mL) precipitates [**H−1**][PF_6]$_2$ as a yellow solid. Yield: 12.1 mg (17.8 mmol, 19.1%). Further purification can be achieved by recrystallization from acetonitrile via diffusion of diethyl ether. Elem. anal. calcd. for $C_{20}H_{19}NCo_2P_2F_{12}$: C, 35.27; H, 2.81; N, 2.06. Found: C, 35.32; H, 2.80; N, 2.06. ^{1}H NMR (CD_3CN): δ 7.62 (s, 1H, H^4), 5.66 (pt, 4H, H^2), 5.57 (s, 10H, H^3), 5.56 (pt, 4H, H^1) ppm. ^{13}C{^{1}H} NMR (CD_3CN): δ 85.8 (s, C^3), 80.9 (s, C^1), 71.1 (s, C^2). ppm. ^{31}P{^{1}H} NMR (CD_3CN): δ −144.6 (sept., $^1J_{PF}$ = 706 Hz). ^{19}F NMR (CD_3CN): δ −73.3 (d, $^1J_{PF}$ = 706 Hz). ESI$^+$ (CH_3CN): m/z = 390.0 (100, % **1**$^+$). IR (ATR): $\tilde{\nu}$ = 3400 (w, NH), 3120 (w, CH), 1575 (m, CN), 1497 (m, CN), 825 (s, PF), 557 (s, PF_2). UV/Vis (CH_3CN): λ (ε) = 385 (1985), 452 nm (1665 M^{-1} cm^{-1}). UV/Vis (H_2O): λ (ε) = 380 (5730), 441 nm (4005 M^{-1} cm^{-1}). CV (CH_3CN/[^{n}Bu$_4$N][PF_6]): $E_{1/2}$ = −1.32, −1.54 V versus FcH/FcH^+.

Synthesis of 1[PF_6]. To a solution of [**H−1**][PF_6]$_2$ (10 mg, 14.7 μmol, 1 equiv) in acetonitrile (3 mL) was added trimethylamine (2 μL, 1.49 mg, 14.7 μmol, 1 equiv), resulting in a color change to red. The solution was filtered via syringe filtration, and the solvent was removed under reduced pressure. The conversion is quantitative. Further purification can be achieved by recrystallizing from acetonitrile via diffusion of diethyl ether. Yield: 1.3 mg (2.43 mmol, 16.5%). Recrystallization from acetonitrile via diffusion of diethyl ether gives red crystals. Elem. anal. calcd. for $C_{20}H_{18}NCo_2PF_6$: C, 44.88; H, 3.39; N, 2.62. Found: C, 44.67; H, 3.41; N, 2.61. ^{1}H NMR (CD_3CN): δ 5.45 (pt, 4H, H^2), 5.34 (s, 10H, H^3), 5.22 (pt, 4H, H^1) ppm. ^{13}C{^{1}H} NMR (CD_3CN): δ 83.5 (s, C^3), 79.5 (s, C^1), 69.0 (s, C^2). ppm. ^{31}P{^{1}H} NMR (CD_3CN): δ −144.6 (sept., $^1J_{PF}$ = 706 Hz). ^{19}F NMR (CD_3CN): δ −73.3 (d, $^1J_{PF}$ = 706 Hz). IR (ATR): $\tilde{\nu}$ = 1492 (m, CN), 1413 (w), 1260 (m), 1067 (s), 1021 (s), 795 (s, PF), 557 (s, PF_2). UV/Vis (CH_3CN): λ (ε) = 409 (1285), 527 nm (3795 M^{-1} cm^{-1}). UV/Vis (H_2O): λ (ε) = 401 (3870), 501 nm (8890 M^{-1} cm^{-1}). CV (CH_3CN/[^{n}Bu$_4$N][PF_6]): $E_{1/2}$ = −1.66 V (2 e$^-$), E_p = +0.47 versus FcH/FcH^+.

Spin Trapping Experiment. To a solution of [**H−1**][PF_6]$_2$ (0.85 mg, 1.25 μmol, 1 equiv) in acetonitrile (0.5 mL) was added sodium hydride (0.15 mg, 6.25 μmol, 5 equiv). The solution was stirred for 5 min and filtered via syringe filtration. [^{n}Bu$_4$N][PF_6] (96.86 mg, 2.5 mmol) as the supporting electrolyte and PBN (221.55 mg, 1.25 mmol, 1000 equiv) were added to the solution. This solution (0.5 mL) was oxidized using spectroelectrochemical methods (60 min, 1 V vs silver wire reference). After electrolysis, the solution was subjected to X-band EPR spectroscopy at 298 K. EPR (CH_3CN): g_{iso} = 2.0062, A_N = 1.462 mT, $A_{H\alpha}$ = 0.381 mT, $A_{H\beta}$ = 0.064 mT (2H).

https://doi.org/10.1021/acs.organomet.2c00211
Organometallics XXXX, XXX, XXX−XXX

■ ASSOCIATED CONTENT

Supporting Information

The Supporting Information is available free of charge at https://pubs.acs.org/doi/10.1021/acs.organomet.2c00211.

Structural and spectroscopic data and energies of all computed structures (PDF)

Cartesian Coordinates of all computed structures (XYZ)

Accession Codes

CCDC 2157935−2157937 contain the supplementary crystallographic data for this paper. These data can be obtained free of charge via www.ccdc.cam.ac.uk/data_request/cif, or by emailing data_request@ccdc.cam.ac.uk, or by contacting The Cambridge Crystallographic Data Centre, 12 Union Road, Cambridge CB2 1EZ, UK; fax: +44 1223 336033.

■ AUTHOR INFORMATION

Corresponding Authors

Christoph Förster − *Department of Chemistry, Johannes Gutenberg University Mainz, D-55128 Mainz, Germany;* orcid.org/0000-0003-4971-5368; Email: katja.heinze@uni-mainz.de

Katja Heinze − *Department of Chemistry, Johannes Gutenberg University Mainz, D-55128 Mainz, Germany;* orcid.org/0000-0003-1483-4156; Email: cristoph.foerster@uni-mainz.de

Authors

Sven D. Waniek − *Department of Chemistry, Johannes Gutenberg University Mainz, D-55128 Mainz, Germany*

Christian Heine − *Department of Chemistry, Johannes Gutenberg University Mainz, D-55128 Mainz, Germany*

Dimitri Zorn − *Department of Chemistry, Johannes Gutenberg University Mainz, D-55128 Mainz, Germany*

Taro Lieberth − *Department of Chemistry, Johannes Gutenberg University Mainz, D-55128 Mainz, Germany*

Maximilian Lauck − *Department of Chemistry, Johannes Gutenberg University Mainz, D-55128 Mainz, Germany*

Complete contact information is available at: https://pubs.acs.org/10.1021/acs.organomet.2c00211

Notes

The authors declare no competing financial interest.

■ ACKNOWLEDGMENTS

Parts of this research were conducted using the supercomputer Elwetritsch and advisory services offered by the TU Kaiserslautern (https://elwe.rhrk.uni-kl.de), which is a member of the Allianz für Hochleistungsrechnen Rheinland-Pfalz (AHRP). We thank Dr. Dieter Schollmeyer and Dr. Luca M. Carrella for collecting the XRD data.

■ REFERENCES

(1) Koelle, U.; Infelta, P. P.; Graetzel, M. Kinetics and Mechanism of the Reduction of Protons to Hydrogen by Cobaltocene. *Inorg. Chem.* **1988**, *27*, 879−883.

(2) Chalkley, M. J.; Del Castillo, T. J.; Matson, B. D.; Roddy, J. P.; Peters, J. C. Catalytic N_2-to-NH_3 Conversion by Fe at Lower Driving Force: A Proposed Role for Metallocene-Mediated PCET. *ACS Cent. Sci.* **2017**, *3*, 217−223.

(3) Chalkley, M. J.; Oyala, P. H.; Peters, J. C. Cp* Noninnocence Leads to a Remarkably Weak C−H Bond via Metallocene Protonation. *J. Am. Chem. Soc.* **2019**, *141*, 4721−4729.

(4) Tyburski, R.; Liu, T.; Glover, S. D.; Hammarström, L. Proton-Coupled Electron Transfer Guidelines, Fair and Square. *J. Am. Chem. Soc.* **2021**, *143*, 560−576.

(5) Chalkley, M. J.; Garrido-Barros, P.; Peters, J. C. A molecular mediator for reductive concerted proton-electron transfers via electrocatalysis. *Science* **2020**, *369*, 850−854.

(6) Jochriem, M.; Bosch, D.; Kopacka, H.; Bildstein, B. Direct Amination of Cobaltocenium Hexafluoridophosphate via Vicarious Nucleophilic Substitution. *Organometallics* **2019**, *38*, 2278−2279.

(7) Vanicek, S.; Kopacka, H.; Wurst, K.; Müller, T.; Hassenrück, C.; Winter, R. F.; Bildstein, B. Monofunctionalized Cobaltocenium Compounds by Dediazoniation Reactions of Cobaltoceniumdiazonium Bis(hexafluorophosphate). *Organometallics* **2016**, *35*, 2101−2109.

(8) Wolter-Steingrube, A.; Cordsen, K.; Heck, J. Nucleophilic Substitution in the Nitrocobaltocenium Ion. *Eur. J. Inorg. Chem.* **2017**, 1314−1319.

(9) Lauck, M.; Förster, C.; Heinze, K. *N*-Cobaltocenium Amide as Reactive Nucleophilic Reagent for Donor−Acceptor Bimetallocenes. *Organometallics* **2017**, *36*, 4968−4978.

(10) Vanicek, S.; Jochriem, M.; Hassenrück, C.; Roy, S.; Kopacka, H.; Wurst, K.; Müller, T.; Winter, R. F.; Reisner, E.; Bildstein, B. Redox-Rich Metallocene Tetrazene Complexes: Synthesis, Structure, Electrochemistry, and Catalysis. *Organometallics* **2019**, *38*, 1361−1371.

(11) Vanicek, S.; Podewitz, M.; Stubbe, J.; Schulze, D.; Kopacka, H.; Wurst, K.; Müller, T.; Lippmann, P.; Haslinger, S.; Schottenberger, H.; Liedl, K. R.; Ott, I.; Sarkar, B.; Bildstein, B. Highly Electrophilic, Catalytically Active and Redox-Responsive Cobaltoceniumyl and Ferrocenyl Triazolylidene Coinage Metal Complexes. *Chem.—Eur. J.* **2018**, *24*, 3742−3753.

(12) Rossini, E.; Bochevarov, A. D.; Knapp, E. W. Empirical Conversion of pK_a Values between Different Solvents and Interpretation of the Parameters: Application to Water, Acetonitrile, Dimethyl Sulfoxide, and Methanol. *ACS Omega* **2018**, *3*, 1653−1662.

(13) Evans, D. H. One-Electron and Two-Electron Transfers in Electrochemistry and Homogeneous Solution Reactions. *Chem. Rev.* **2008**, *108*, 2113−2144.

(14) Sampson, M. D.; Nguyen, A. D.; Grice, K. A.; Moore, C. E.; Rheingold, A. L.; Kubiak, C. P. Manganese Catalysts with Bulky Bipyridine Ligands for the Electrocatalytic Reduction of Carbon Dioxide: Eliminating Dimerization and Altering Catalysis. *J. Am. Chem. Soc.* **2014**, *136*, 5460−5471.

(15) Agarwal, R. G.; Wise, C. F.; Warren, J. J.; Mayer, J. M. Correction to Thermochemistry of Proton-Coupled Electron Transfer Reagents and its Implications. *Chem. Rev.* **2022**, *122*, 1482.

(16) Agarwal, R. G.; Coste, S. C.; Groff, B. D.; Heuer, A. M.; Noh, H.; Parada, G. A.; Wise, C. F.; Nichols, E. M.; Warren, J. J.; Mayer, J. M. Free Energies of Proton-Coupled Electron Transfer Reagents and Their Applications. *Chem. Rev.* **2022**, *122*, 1−49.

(17) Zhu, Y.; Shi, Y. Facile Cu(I)-Catalyzed Oxidative Coupling of Anilines to Azo Compounds and Hydrazines with Diaziridinone under Mild Conditions. *Org. Lett.* **2013**, *15*, 1942−1945.

(18) Reddy, C. B. R.; Reddy, S. R.; Naidu, S. Cu(I) catalyzed dehydrogenative homo coupling of aromatic amines under simple and mild reaction conditions. *Catal. Commun.* **2014**, *56*, 50−54.

(19) Trujillo, H. A.; Casado, C. M.; Ruiz, J.; Astruc, D. Thermodynamics of C-H Activation in Multiple Oxidation States: Comparison of Benzylic C-H Acidities and C-H Bond Dissociation Energies in the Isostructural 16-20-Electron Complexes $[Fe^x(\eta^5\text{-}C_5R_5)(\eta^6\text{-arene})]^n$, x = 0-IV, R = H or Me, n = −1 to +3. *J. Am. Chem. Soc.* **1999**, *121*, 5674−5686.

(20) Naguib, Y. M. A.; Steel, C.; Cohen, S. G.; Young, M. A. Photoreduction of Benzophenone by Acetonitrile: Correlation of Rates of Hydrogen Abstraction from RH with the Ionization Potentials of the Radicals $R^{\bullet}$. *J. Phys. Chem.* **1987**, *91*, 3033−3036.

(21) Wiedner, E. S.; Chambers, M. B.; Pitman, C. L.; Bullock, R. M.; Miller, A. J. M.; Appel, A. M. Thermodynamic Hydricity of Transition Metal Hydrides. *Chem. Rev.* **2016**, *116*, 8655−8692.

https://doi.org/10.1021/acs.organomet.2c00211
Organometallics XXXX, XXX, XXX−XXX

(22) Yoshida, H.; Fujimura, Y.; Yuzawa, H.; Kumagai, J.; Yoshida, T. A heterogeneous palladium catalyst hybridised with a titanium dioxide photocatalyst for direct C−C bond formation between an aromatic ring and acetonitrile. *Chem. Commun.* **2013**, *49*, 3793−3795.
(23) Kwon, K.; Simons, R. T.; Nandakumar, M.; Roizen, J. L. Strategies to Generate Nitrogen-centered Radicals That May Rely on Photoredox Catalysis: Development in Reaction Methodology and Applications in Organic Synthesis. *Chem. Rev.* **2022**, *122*, 2353−2428.
(24) Derosa, J.; Garrido-Barros, P.; Peters, J. C. Electrocatalytic Ketyl-Olefin Cyclization at a Favorable Applied Bias Enabled by a Concerted Proton−Electron Transfer Mediator. *Inorg. Chem.* **2022**, *61*, 6672−6678.
(25) STOE & Cie. *X-Area*; STOE & Cie GmbH: Darmstadt, Germany.
(26) Blessing, R. H. An empirical correction for absorption anisotropy. *Acta Crystallogr., Sect. A: Found. Crystallogr.* **1995**, *51*, 33−38.
(27) Spek, A. L. Structure validation in chemical crystallography. *Acta Crystallogr., Sect. D: Biol. Crystallogr.* **2009**, *65*, 148−155.
(28) Koziskova, J.; Hahn, F.; Richter, J.; Kožíšek, J. Comparison of different absorption corrections on the model structure of tetrakis(μ_2-acetato)-diaqua-di-copper(II). *Acta Chim. Slovaca* **2016**, *9*, 136−140.
(29) STOE & Cie. *X-Area LANA*; STOE & Cie GmbH: Darmstadt, Germany.
(30) Sheldrick, G. M. SHELXT- Integrated space-group and crystal-structure determination. *Acta Crystallogr., Sect. A: Found. Crystallogr.* **2015**, *71*, 3−8.
(31) Sheldrick, G. M. Crystal structure refinement with SHELXL. *Acta Crystallogr., Sect. C: Struct. Chem.* **2015**, *71*, 3−8.
(32) Sheldrick, G. M. A short history of SHELX. *Acta Crystallogr., Sect. A: Found. Crystallogr.* **2008**, *64*, 112−122.
(33) Hübschle, C. B.; Sheldrick, G. M.; Dittrich, B. ShelXle: a Qt graphical user interface for SHELXL. *J. Appl. Crystallogr.* **2011**, *44*, 1281−1284.
(34) Neese, F. Software update: the ORCA program system, version 4.0. *Wiley Interdiscip. Rev.: Comput. Mol. Sci.* **2018**, *8*, No. e1327.
(35) Becke, A. D. Density-functional thermochemistry. III. The role of exact exchange. *J. Chem. Phys.* **1993**, *98*, 5648−5652.
(36) Lee, C.; Yang, W.; Parr, R. G. Development of the Colle-Salvetti correlation-energy formula into a functional of the electron density. *Phys. Rev. B: Condens. Matter Mater. Phys.* **1988**, *37*, 785−789.
(37) Miehlich, B.; Savin, A.; Stoll, H.; Preuss, H. Results obtained with the correlation energy density functionals of Becke and Lee, Yang and Parr. *Chem. Phys. Lett.* **1989**, *157*, 200−206.
(38) Weigend, F.; Ahlrichs, R. Balanced basis sets of split valence, triple zeta valence and quadruple zeta valence quality for H to Rn: Design and assessment of accuracy. *Phys. Chem. Chem. Phys.* **2005**, *7*, 3297−3305.
(39) Weigend, F. Accurate Coulomb-fitting basis sets for H to Rn. *Phys. Chem. Chem. Phys.* **2006**, *8*, 1057−1065.
(40) Neese, F.; Wennmohs, F.; Hansen, A.; Becker, U. Efficient, approximate and parallel Hartree−Fock and hybrid DFT calculations. A 'chain-of-spheres' algorithm for the Hartree−Fock exchange. *Chem. Phys.* **2009**, *356*, 98−109.
(41) Izsák, R.; Neese, F. An overlap fitted chain of spheres exchange method. *J. Chem. Phys.* **2011**, *135*, 144105.
(42) Pantazis, D. A.; Chen, X.-Y.; Landis, C. R.; Neese, F. All-Electron Scalar Relativistic Basis Sets for Third-Row Transition Metal Atoms. *J. Chem. Theory Comput.* **2008**, *4*, 908−919.
(43) Miertuš, S.; Scrocco, E.; Tomasi, J. Electrostatic interaction of a solute with a continuum: A direct utilization of ab initio molecular potentials for the prevision of solvent effects. *Chem. Phys.* **1981**, *55*, 117−129.
(44) Barone, V.; Cossi, M. Quantum Calculation of Molecular Energies and Energy Gradients in Solution by a Conductor Solvent Model. *J. Phys. Chem. A* **1998**, *102*, 1995−2001.
(45) Fulmer, G. R.; Miller, A. J. M.; Sherden, N. H.; Gottlieb, H. E.; Nudelman, A.; Stoltz, B. M.; Bercaw, J. E.; Goldberg, K. I. NMR Chemical Shifts of Trace Impurities: Common Laboratory Solvents, Organics, and Gases in Deuterated Solvents Relevant to the Organometallic Chemist. *Organometallics* **2010**, *29*, 2176−2179.
(46) Connelly, N. G.; Geiger, W. E. Chemical Redox Agents for Organometallic Chemistry. *Chem. Rev.* **1996**, *96*, 877−910.
(47) Krejčik, M.; Daněk, M.; Hartl, F. Simple construction of an infrared optically transparent thin-layer electrochemical cell. *J. Electroanal. Chem. Interfacial Electrochem.* **1991**, *317*, 179−187.
(48) Stoll, S.; Schweiger, A. EasySpin, a comprehensive software package for spectral simulation and analysis in EPR. *J. Magn. Reson.* **2006**, *178*, 42−55.

https://doi.org/10.1021/acs.organomet.2c00211
Organometallics XXXX, XXX, XXX−XXX

4 Summary and Outlook

In this work, metallocenes were used in three different ways in catalysis (**Section 3.1**). Ferrocene showed to be a reliable structural motif to be used as redox mediator. Redox mediators are working as intermolecular supporting agents in electrochemical catalysis. The actual potential of ferrocene derivatives can be tuned by addition of electron withdrawing or donating substituent. With increasing number of electron withdrawing methoxycarbonyl substituents, the redox potential is changed to higher values (**Figure 36**). There is a difference in the extent of the potential change depending on the amount of already connected substituents on a Cp ring. With rising number of substituents, the individual impact of the substituents decreases. Nevertheless, the potential of the derivatives can be calculated by an empirically derived equation considering the kind of substitution and based on this, the *Hammett* constant σ_p and σ_m. All four derivatives are stable during electrolysis and can be oxidized reversibly. This was proven by UV/Vis and IR spectroscopy. The electron self exchange reactions between the neutral ferrocene complexes and their corresponding ferrocenium complex are fast, compared to the timescale of ^{1}H NMR spectroscopy. That is demonstrated by a combined signal in a ferrocene/ferrocenium mixture which make both components indistinguishable. Therefore, ferrocene moieties are good redox mediators due to them satisfying all necessary conditions.

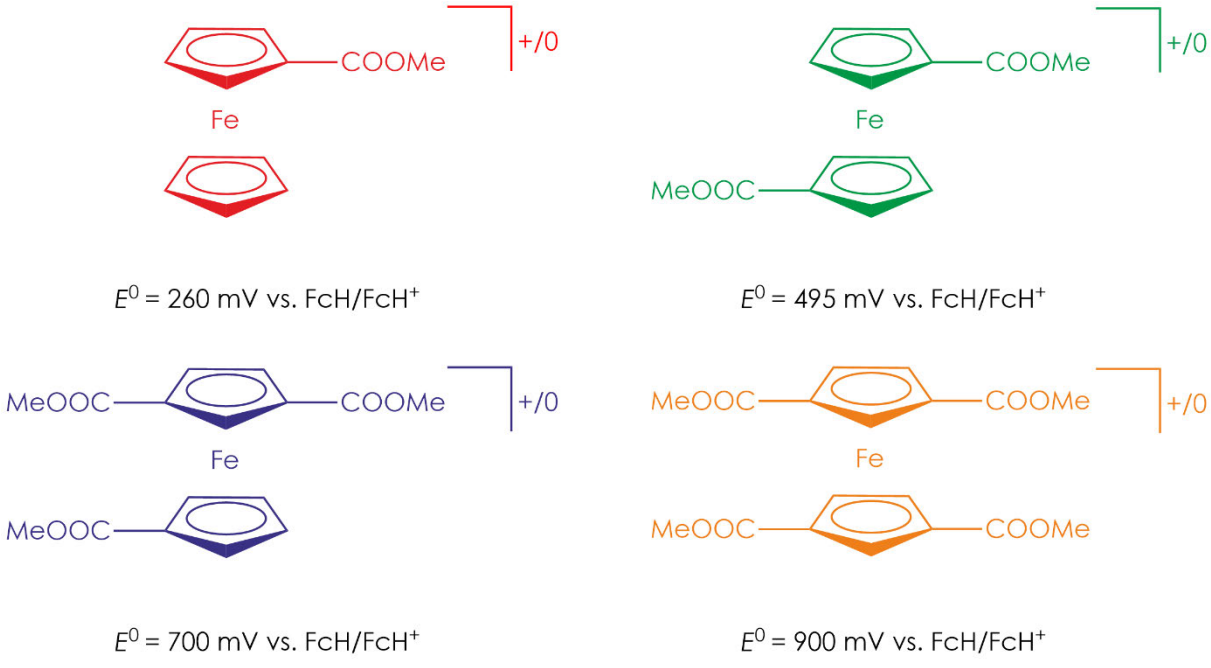

Figure 36: Mono- to tetra- substituted ferrocenyl esters and their redox potentials vs. the ferrocene/ ferrocenium couple.

To complete the set of methoxycarbonyl substituted ferrocenes, the 1,3-dimethoxycarbonyl ferrocene has to be synthesized and analyzed. The electrochemical potential should be around 450 mV to 460 mV which would be less than the electrochemical potential of 1,1'-dimethoxycarbonyl ferrocene. In case of redox stability and self exchange rate, no deviation is expected compared to

its derivatives. Nevertheless, the redox stability has to be verified by UV/Vis and IR spectroscopy as well as the existence of a fast electron self exchange by ^{1}H NMR spectroscopy. Mono- to tetrasubstituted methoxycarbonyl substituted ferrocenes cover a broad potential range from 0 mV to 900 mV (including ferrocene itself). Next to methoxycarbonyl substitutents, also other substituents should be analyzed to increase the accessible potential range of ferrocene derivatives even more. For example, amino groups as substituents would lower the electrochemical potential due to its electron donating nature. 1,1'-Diaminoferrocene offers a potential of –602 mV vs. FcH/FcH^+.[335] The redox stability of the aminoferrocenes and their electron self exchange rate have to be verified by UV/Vis-, IR- and ^{1}H NMR spectroscopy. Therefore, a combination of methoxycarbonyl ferrocenes and aminoferrocenes would be a suitable set of metallocenes to become reliable single electron transfer (SET) reagents for redox mediation.

The synthesis and characterization of two ferrocenyl substituted acyclic diamino carbene gold(I) complexes are reported (**Section 3.2**). Isocyanoferrocene and chlorido(dimethylsulfide)gold(I) were used to form the carbene precursor chlorido(isocyanoferrocene)gold(I). In the presence of the secondary amines diisopropylamine and diethylamine, the formation of the corresponding carbene gold(I) complexes occurs. The formation of the precursor and the following carbene formation was monitored by IR spectroscopy. The CN stretching vibration shifts by 101 cm^{-1} to higher energy by the addition of chlorido(dimethyl-sulfide)gold(I). Since the CN triple bond is broken during the formation of the carbene, the stretching vibration at 2225 cm^{-1} disappears as well. The complexe structures were verified by XRD measurements. Both complexes show weak intramolecular non-classical NH Fe hydrogen bonds with distances of 3.0760(34) Å and 3.0629(27) Å between nitrogen and iron. They are comparable to non-classical NH Fe hydrogen bonds in ferrocenyl hydrazone with a dissociation energy of 13 kJ mol^{-1}.[59] The diethyl derivative exhibits classical NH Cl hydrogen bonding. This results in the formation of complex chains along the *b* axis (**Figure 37**a). Aurophilic interactions between two gold atoms with an Au Au distance of 3.1897(3) Å are shown within the diisopropyl complex (**Figure 37**b). All three complexes (including the chlorido(isocyanoferrocene) gold(I)) were oxidized reversibly. The diaminocarbene complexes have lower oxidation potentials than the isocyanide complexes but therefore fit in the typical range for *N*-substituted ferrocenes. The oxidized species are stable on short timescales, like the one for voltammetric experiments. On contrast to this, the oxidized species are not stable for several hours. This is shown by decreasing absorption bands in the UV/Vis spectrum. First, ferrocene seems to be oxidized chemically or electrochemically. Then, an intramolecular electron transfer from ferrocenium to gold occurs to oxidize the gold(I) center to gold(II). By EPR spectrometry, the rise of a gold(II) signal over time is observed.

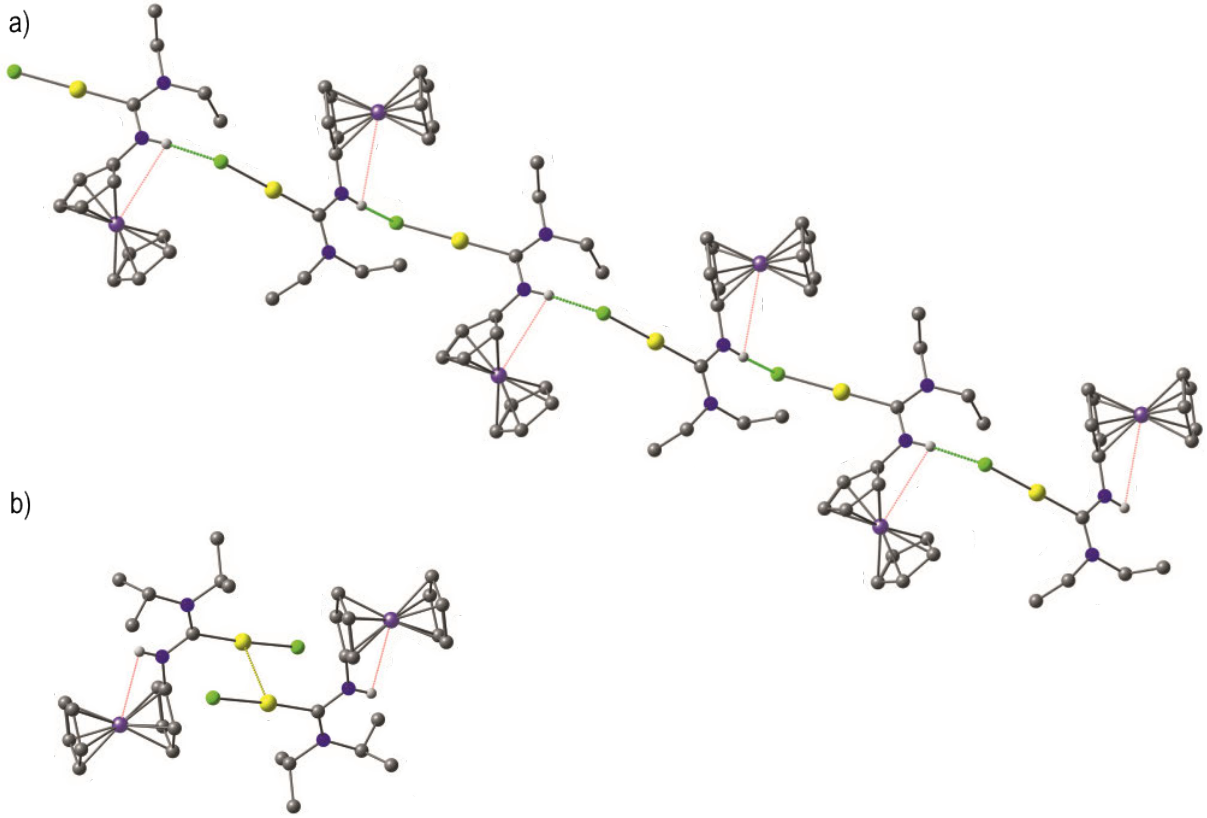

Figure 37: Crystal structures of a) [(diethylamino)(aminoferrocenyl) methylidene] gold(I) and b) [(diisopropylamino)-(aminoferrocenyl) methylidene] gold(I).

This behaviour is similar to ferrocenylsubstituted *Fischer* carbene gold(I) complexes. Therefore, the formation of the gold(II) should be investigated. If the synthesis of the gold(II) species is reversible the diamino carbene gold(I) complexes may be suitable catalysts for redox switchable catalysis (RSC). Afterwards, the activity of the diamino carbene complexes towards the cyclization of *N*-(2-propyn-1-yl) benzamide has to be determined. In case of activity towards RSC, other alkynes have to be used for the synthesis of different diamino carbene gold(I) complexes. The chlorido(isocyanoferrocene)gold(I) carbene is a useable precursor for acyclic diamino carbene gold(I) complexes. Despite diisopropyl amine and diethyl amine, other (asymmetrical) secondary amines can be used to increase the diversity of acyclic diamino carbene gold(I) complexes. Using aminoferrocene derivatives may result in the formation of diamino carbene complexes with two or three ferrocenyl substituents, which would offer the possibility of double and triple oxidation (**Scheme 21**). This may lead to an even further increase on catalytic activity and may facilitate the recovery of the catalyst by phase separation due to an increased phase tag. In addition, the NH may be substituted by other organic substituents. One example would be the methylation or alkylation with methyl iodide or alkyl iodide. Crystallization attempts of the oxidized species should be performed to gain the molecular structure and evidence for the formation of gold(II) complexes.

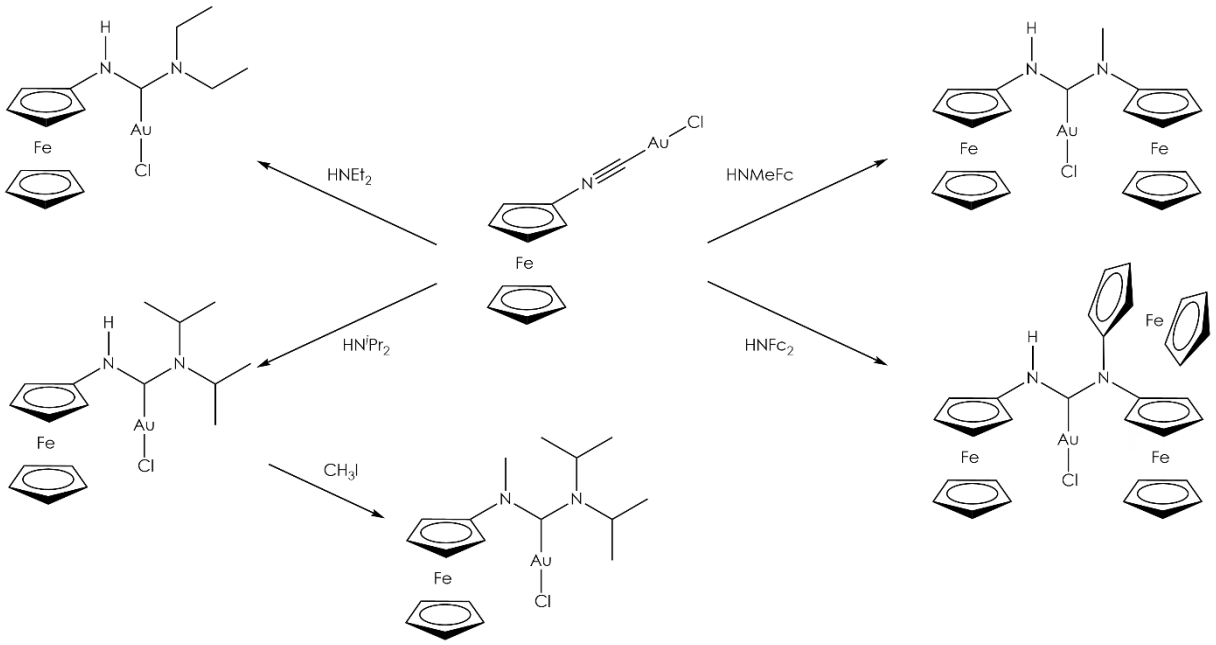

Scheme 21: Proposed reactions for the synthesis of different diamino carbene gold(I) complexes with up to three ferroecene substituents and following methylation.

The coupling of cobaltocenium amine with nitro cobaltocenium to build a *N*,*N*-dicobaltocenium substituted amine and purification of the complex was successful (**Section 3.3**). Cobaltocenium amine has to be deprotonated to an imine intermediate to get activated for the reaction. The desired product is a weak acid with a pK_a value of 9.56 (comparable to hydrogen cyanide with 9.40 and ammonium chloride with 9.25), so the imine intermediate is reprotonated easily. Deprotonation of *N*,*N*-dicobaltoceniumamine hexafluorophosphate forms the corresponding base *N*,*N*-dicobaltoceniumamide hexafluorophosphate (**Scheme 22**). To investigate the deprotonated product, the use of a non-nucleophilic base like diazabicycloundecene (DBU) is essential to gain reasonable yields. Amine and amide are colored differently and can be distinguished by ^{1}H NMR spectroscopy easily. Both complexes also form a redox pair on a bigger timescale than voltammetric ones. On one hand, the reduction of the amine leads to a proton abstraction and release of molecular hydrogen while the amide is formed. On the other hand, oxidation of the amide results in the formation of the amine. The required hydrogen radical to regain the amine is provided by the acetonitrile solvent, proved by EPR and ^{1}H NMR spectroscopy. Abstraction of the hydrogen radical from acetonitrile results in the formation of a radical which can be spin trapped with *N*-tertiary-butyl-nitrone (PBN) and detected by EPR spectroscopy. ^{1}H NMR experiments show no N-H signal in the ^{1}H NMR spectrum after the oxidation of the amine in deuterated acetonitrile. Nevertheless, the amine emerges during the oxidation. This is confirmed by the ^{1}H NMR signals for the Cp rings which are quite different for the amine and amide. Oxidation in deuterated acetonitrile lead to the formation of N-D which gives no signal in the ^{1}H NMR spectrum. The redox pair *N*,*N*-dicobaltoceniumamine and *N*,*N*-dicobaltocenium-amide hexafluorophosphate is therefore able to perform hydrogen evolution reaction (HER) since molecular hydrogen is released upon reduction. While oxidation reproduces the starting product by proton abstraction from the solvent.

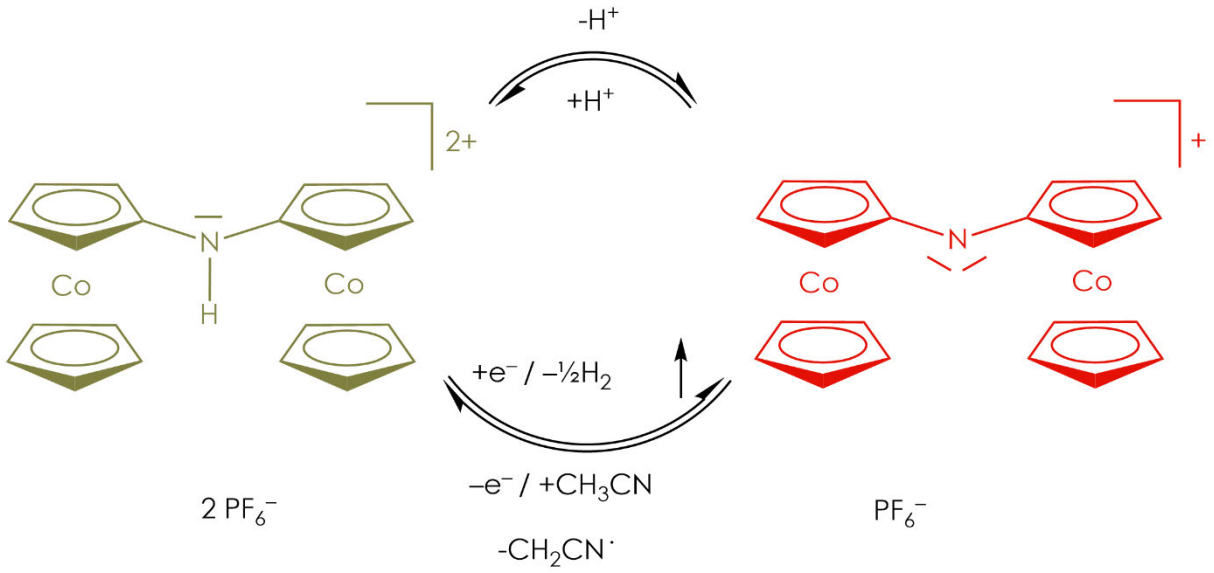

Scheme 22: Acid-base and redox equilibrium of *N*,*N*-dicobaltoceniumamine hexafluorophosphate and *N*,*N*-di-cobaltocenium-amide hexafluorophosphate.

More insight is necessary for the cobaltocenium induced HER. The absolute yield of hydrogen needs to be verified. With this, the *Faraday* efficiency of the HER can be determined. The quantification can only be achieved by thermal conductivity detection (TCD) due to the small molecular weight of molecular hydrogen. Since hydrogen is the typical reference gas in TCD, the reference needs to be changed to argon or nitrogen to analyze hydrogen itself. Next, an enhanced reaction atmosphere and build-up may be developed to increase the efficiency of catalysis and the amount of produced molecular hydrogen. The necessary reaction potential for the reduction and oxidation may be tuned by the introduction of substituents to the cobaltocenium Cp rings.

5 References

[1] R. A. Marcus, *Angew. Chem.* **1993**, *105*, 1161–1172; *Angew. Chem. Int. Ed.* **1993**, *32*, 1111–1121.

[2] R. A. Marcus, *Annu. Rev. Phys. Chem.* **1964**, *15*, 155–196.

[3] J. W. Gryder, R. W. Dodson, *J. Am. Chem. Soc.* **1949**, *71*, 1894–1895.

[4] R. C. Thompson, *J. Am. Chem. Soc.* **1948**, *70*, 1045–1046.

[5] G. T. Seaborg, *Chemical reviews* **1940**, *27*, 199–285.

[6] R. A. Marcus, P. Siddarth (Hrsg.) *Theory of Electron Transfer Reactions and Comparison with Experiments*, Springer, Netherlands, **1992**.

[7] J. Franck, E. G. Dymond, *Trans. Faraday Soc.* **1926**, *21*, 536.

[8] E. Condon, *Phys. Rev.* **1926**, *28*, 1182–1201.

[9] E. U. Condon, *Phys. Rev.* **1928**, *32*, 858–872.

[10] R. A. Marcus, *The Journal of Chemical Physics* **1956**, *24*, 966–978.

[11] T. J. Meyer, *Acc. Chem. Res.* **1978**, *11*, 94–100.

[12] N. S. Hush, *Trans. Faraday Soc.* **1961**, *57*, 557.

[13] B. S. Brunschwig, N. Sutin, *Coordination Chemistry Reviews* **1999**, *187*, 233–254.

[14] M. B. Robin, P. Day in *Advances in Inorganic Chemistry and Radiochemistry* (Hrsg.: H. J. Emeléus, A. G. Sharpe), Academic Press, **1968**, S. 247–422.

[15] P. Day, N. S. Hush, R. J. H. Clark, *Philosophical transactions. Series A, Mathematical, physical, and engineering sciences* **2008**, *366*, 5–14.

[16] M. H. V. Huynh, T. J. Meyer, *Chemical reviews* **2007**, *107*, 5004–5064.

[17] J. J. Warren, T. A. Tronic, J. M. Mayer, *Chemical reviews* **2010**, *110*, 6961–7001.

[18] H. N. Po, N. M. Senozan, *J. Chem. Educ.* **2001**, *78*, 1499.

[19] A. J. Bard, L. R. Faulkner, *Electrochemical Methods: Fundamentals and Applications,* 2. Aufl., John Wiley & Sons, Hoboken, NJ, **2011**.

[20] E. A. Mader, E. R. Davidson, J. M. Mayer, *J. Am. Chem. Soc.* **2007**, *129*, 5153–5166.

[21] E. A. Mader, A. S. Larsen, J. M. Mayer, *J. Am. Chem. Soc.* **2004**, *126*, 8066–8067.

[22] E. A. Mader, V. W. Manner, T. F. Markle, A. Wu, J. A. Franz, J. M. Mayer, *J. Am. Chem. Soc.* **2009**, *131*, 4335–4345.

[23] M. Tilset in *Comprehensive Organometallic Chemistry III*, Elsevier, **2007**, S. 279–305.

[24] M. J. Chalkley, T. J. Del Castillo, B. D. Matson, J. P. Roddy, J. C. Peters, *ACS central science* **2017**, *3*, 217–223.

[25] M. J. Chalkley, P. H. Oyala, J. C. Peters, *J. Am. Chem. Soc.* **2019**, *141*, 4721–4729.

[26] M. J. Chalkley, P. Garrido-Barros, J. C. Peters, *Science (New York, N.Y.)* **2020**, *369*, 850–854.

[27] Y. Peng, M. V. Ramos-Garcés, D. Lionetti, J. D. Blakemore, *Inorg. Chem.* **2017**, *56*, 10824–10831.

[28] T. H. Parsell, M.-Y. Yang, A. S. Borovik, *J. Am. Chem. Soc.* **2009**, *131*, 2762–2763.

[29] S. Pattanayak, A. J. Jasniewski, A. Rana, A. Draksharapu, K. K. Singh, A. Weitz, M. Hendrich, L. Que, A. Dey, S. Sen Gupta, *Inorg. Chem.* **2017**, *56*, 6352–6361.

[30] T. J. Kealy, P. L. Pauson, *Nature* **1951**, *168*, 1039–1040.

[31] P. L. Pauson, *J. Organomet. Chem.* **2001**, *637-639*, 3–6.
[32] S. A. Miller, J. A. Tebboth, J. F. Tremaine, *J. Chem. Soc.* **1952**, 632.
[33] C. Czekelius, *Cyclopentadienyl*, Thieme Gruppe, **2010**.
[34] J. D. Dunitz, L. E. Orgel, A. Rich, *Acta Cryst.* **1956**, *9*, 373–375.
[35] *The Nobel Prize in Chemistry 1973*, **1973**.
[36] G. Wilkinson, M. Rosenblum, M. C. Whiting, R. B. Woodward, *J. Am. Chem. Soc.* **1952**, *74*, 2125–2126.
[37] E. O. Fischer, W. Pfab, *Z. Naturforsch. B* **1952**, *7*, 377–379.
[38] F. A. Cotton, *J. Am. Chem. Soc.* **1968**, *90*, 6230–6232.
[39] A. Streitwieser, U. Mueller-Westerhoff, *J. Am. Chem. Soc.* **1968**, *90*, 7364.
[40] D. Seyferth, *Organometallics* **2004**, *23*, 3562–3583.
[41] I. Langmuir, *Science* **1921**, *54*, 59–67.
[42] W. B. Jensen, *J. Chem. Educ.* **2005**, *82*, 28.
[43] C. A. Tolman, *Chem. Soc. Rev.* **1972**, *1*, 337.
[44] H.-M. Koepp, H. Wendt, H. Stkehlow, *Ber. Bunsenge. Phys. Chemie* **1960**, *64*.
[45] C. E. Housecroft, *Inorganic chemistry. Solutions manual*, Pearson, Harlow, England, London, New York, Boston, San Francisco, Toronto, Sydney, Dubai, Singapore, Hong Kong, Tokyo, **2018**.
[46] Y. S. Sohn, D. N. Hendrickson, H. B. Gray, *J. Am. Chem. Soc.* **1970**, *92*, 3233–3234.
[47] G. Gritzner, J. Kuta, *Pure Appl. Chem.* **1982**, *54*, 1527–1532.
[48] G. Gritzner, J. Kuta, *Pure Appl. Chem.* **1984**, *56*, 461–466.
[49] H. B. Gray, Y. S. Sohn, N. Hendrickson, *J. Am. Chem. Soc.* **1971**, *93*, 3603–3612.
[50] Y. Yamaguchi, W. Ding, C. T. Sanderson, M. L. Borden, M. J. Morgan, C. Kutal, *Coord. Chem. Rev.* **2007**, *251*, 515–524.
[51] T. Kienz, C. Förster, K. Heinze, *Organometallics* **2014**, *33*, 4803–4812.
[52] D. Siebler, C. Förster, T. Gasi, K. Heinze, *Organometallics* **2011**, *30*, 313–327.
[53] D. N. Hendrickson, Y. S. Sohn, D. M. Duggan, H. B. Gray, *J. Chem. Phys.* **1973**, *58*, 4666–4675.
[54] J. Fulara, K. Filipkowski, J. P. Maier, *J. Phys. Chem. C* **2017**, *121*, 10694–10697.
[55] M. Lauck, C. Förster, D. Gehrig, K. Heinze, *J. Organomet. Chem.* **2017**, *847*, 33–40.
[56] E. S. Yang, M.-S. Chan, A. C. Wahl, *J. Phys. Chem.* **1980**, *84*, 3094–3099.
[57] R. M. Nielson, G. E. McManis, L. K. Safford, M. J. Weaver, *J. Phys. Chem.* **1989**, *93*, 2152–2157.
[58] D. Siebler, C. Förster, K. Heinze, *Dalton trans.* **2011**, *40*, 3558–3575.
[59] C. Förster, P. Veit, V. Ksenofontov, K. Heinze, *Chem. Commun.* **2015**, *51*, 1514–1516.
[60] G. Wilkinson, *J. Am. Chem. Soc.* **1952**, *74*, 6146–6147.
[61] G. Wilkinson, P. L. Pauson, J. M. Birmingham, F. A. Cotton, *J. Am. Chem. Soc.* **1953**, *75*, 1011–1012.
[62] E. O. Fischer, R. Jira, *Z. Naturforsch. B* **1953**, *8*, 217–219.
[63] E. O. Fischer, W. Hafner, *Z. Naturforsch. B* **1953**, *8*, 444–445.

[64] F. A. Cotton, R. O. Whipple, G. Wilkinson, *J. Am. Chem. Soc.* **1953**, *75*, 3586–3587.
[65] G. Wilkinson, *J. Am. Chem. Soc.* **1954**, *76*, 209–211.
[66] L. Friedman, A. P. Irsa, G. Wilkinson, *J. Am. Chem. Soc.* **1955**, *77*, 3689–3692.
[67] G. Wilkinson, J. M. Birmingham, *J. Am. Chem. Soc.* **1954**, *76*, 6210.
[68] J. M. Birmingham, G. Wilkinson, *J. Am. Chem. Soc.* **1956**, *78*, 42–44.
[69] C. Elschenbroich, *Organometallics,* 3. Aufl., Wiley-VCH, Weinheim, **2016**.
[70] J. C. Huffman, L. N. Lewis, K. G. Caulton, *Inorg. Chem.* **1980**, *19*, 2755–2762.
[71] H. E. Abdou, A. A. Mohamed, J. P. Fackler, M. M. Ghimire, M. A. Omary, D. Schilter, T. B. Rauchfuss, J. A. Denny, M. Y. Darensbourg, M. Morshedi et al. **2018**, *37*, 155–204.
[72] W. L. Jolly (Hrsg.) *Inorganic Syntheses*, McGraw-Hill, New York, **1968**.
[73] J. J. Bishop, A. Davison, M. L. Katcher, D. W. Lichtenberg, R. E. Merrill, J. C. Smart, *J. Organomet. Chem.* **1971**, *27*, 241–249.
[74] F. Rebiere, O. Samuel, H. Kagan, *Tetrahedron Lett.* **1990**, *31*, 3121–3124.
[75] D. Lednicer, C. R. Hauser, *Org. Synth.* **1960**, *40*, 31.
[76] M. Malischewski, K. Seppelt, J. Sutter, F. W. Heinemann, B. Dittrich, K. Meyer, *Angew. Chem. Int. Ed.* **2017**, *56*, 13372–13376.
[77] R. E. Bozak, *J. Chem. Educ.* **1966**, *43*, 73.
[78] C. J. Donahue, E. R. Donahue, *J. Chem. Educ.* **2013**, *90*, 1688–1691.
[79] Y. T. Liu, H. L. Guo, W. Da Yin, *Adv. Mat. Res.* **2011**, *396-398*, 1875–1878.
[80] J. Zhang, R. Liu, *J. Chem. Soc. Pak.* **2011**, *33*, 356–359.
[81] H. M. A. Abood, A. P. Abbott, A. D. Ballantyne, K. S. Ryder, *Chem. Commun.* **2011**, *47*, 3523–3525.
[82] A. N. Nesmejanow, W. A. Ssasonowa, V. N. Drosd, *Chem. Ber.* **1960**, *93*, 2717–2729.
[83] G. D. Broadhead, J. M. Osgerby, P. L. Pauson, *J. Chem. Soc.* **1958**, 650.
[84] U. T. Mueller-Westerhoff, Y. Zheng, G. Ingram, *J. Organomet. Chem.* **1993**, *463*, 163–167.
[85] A. Connell, P. J. Holliman, I. R. Butler, L. Male, S. J. Coles, P. N. Horton, M. B. Hursthouse, W. Clegg, L. Russo, *J. Organomet. Chem.* **2009**, *694*, 2020–2028.
[86] R. Claus, J. P. Lewtak, T. J. Muller, J. C. Swarts, *J. Organomet. Chem.* **2013**, *740*, 61–69.
[87] J. Jia, Y. Cui, Y. Li, W. Sheng, L. Han, J. Gao, *Dyes Pigment.* **2013**, *98*, 273–279.
[88] M. I. Reyes Valderrama, R. A. Vázquez García, T. Klimova, E. Klimova, L. Ortiz-Frade, M. M. García, *Inorg. Chim. Acta* **2008**, *361*, 1597–1605.
[89] X. Wang, G. Kehr, C. G. Daniliuc, G. Erker, *J. Am. Chem. Soc.* **2014**, *136*, 3293–3303.
[90] L. Horner, H. Hoffmann, H. G. Wippel, *Chem. Ber.* **1958**, *91*, 64–67.
[91] W. S. Wadsworth, W. D. Emmons, *J. Am. Chem. Soc.* **1961**, *83*, 1733–1738.
[92] W. Steffen, M. Laskoski, G. Collins, U. Bunz, *J. Organomet. Chem.* **2001**, *630*, 132–138.
[93] A. Hildebrandt, K. Al Khalyfeh, D. Schaarschmidt, M. Korb, *J. Organomet. Chem.* **2016**, *804*, 87–94.
[94] B. Jennewein, S. Kimpel, D. Thalheim, J. Klett, *Chem. Eur. J.* **2018**, *24*, 7605–7609.
[95] J. Hein, J. Klett, *Synthesis* **2019**, *51*, 407–413.
[96] D. Astruc, *Eur. J. Inorg. Chem.* **2017**, *2017*, 6–29.

[97] P. Štěpnička, *Eur. J. Inorg. Chem.* **2017**, *2017*, 215–216.

[98] K. Heinze, H. Lang, *Organometallics* **2013**, *32*, 5623–5625.

[99] P. Štěpnička (Hrsg.) *Ferrocenes [Elektronische Ressource]. Ligands, materials and biomolecules*, J. Wiley, Chichester, England, **2008**.

[100] A. Togni, T. Hayashi (Hrsg.) *Ferrocenes [Elektronische Ressource]. Homogeneous catalysis, organic synthesis, materials science*, VCH Publishers, Weinheim, **1995**.

[101] R. L. N. Hailes, A. M. Oliver, J. Gwyther, G. R. Whittell, I. Manners, *Chem. Soc. Rev.* **2016**, *45*, 5358–5407.

[102] P. Molina, A. Tárraga, M. Alfonso, *Dalton trans.* **2014**, *43*, 18–29.

[103] H.-B. Kraatz, J. Lusztyk, G. D. Enright, *Inorg. Chem.* **1997**, *36*, 2400–2405.

[104] O. Brosch, T. Weyhermüller, N. Metzler-Nolte, *Inorg. Chem.* **1999**, *38*, 5308–5313.

[105] D. R. van Staveren, N. Metzler-Nolte, *Chem. Rev.* **2004**, *104*, 5931–5985.

[106] T. Moriuchi, T. Hirao, *Chem. Soc. Rev.* **2004**, *33*, 294–301.

[107] K. Heinze, M. Beckmann, *Eur. J. Inorg. Chem.* **2005**, *2005*, 3450–3457.

[108] K. Heinze, U. Wild, M. Beckmann, *Eur. J. Inorg. Chem.* **2007**, *2007*, 617–623.

[109] S. Djaković, D. Siebler, M. Č. Semenčić, K. Heinze, V. Rapić, *Organometallics* **2008**, *27*, 1447–1453.

[110] A. Lataifeh, S. Beheshti, H.-B. Kraatz, *Eur. J. Inorg. Chem.* **2009**, *2009*, 3205–3218.

[111] M. Č. Semenčić, D. Siebler, K. Heinze, V. Rapić, *Organometallics* **2009**, *28*, 2028–2037.

[112] C. Förster, M. Kovačević, L. Barišić, V. Rapić, K. Heinze, *Organometallics* **2012**, *31*, 3683–3694.

[113] H. Mansour, M. E. El-Khouly, S. Y. Shaban, O. Ito, N. Jux, *J. Porphyr. Phthalocyanines* **2007**, *11*, 719–728.

[114] P. K. Poddutoori, A. S. D. Sandanayaka, T. Hasobe, O. Ito, A. van der Est, *J. Phys. Chem. B* **2010**, *114*, 14348–14357.

[115] M. A. Bakar, N. N. Sergeeva, T. Juillard, M. O. Senge, *Organometallics* **2011**, *30*, 3225–3228.

[116] B. M. J. M. Suijkerbuijk, R. J. M. Klein Gebbink, *Angew. Chem.* **2008**, *120*, 7506–7532; *Angew. Chem. Int. Ed.* **2008**, *47*, 7396–7421.

[117] S. J. Dammer, P. V. Solntsev, J. R. Sabin, V. N. Nemykin, *Inorg. Chem.* **2013**, *52*, 9496–9510.

[118] A. Vecchi, E. Gatto, B. Floris, V. Conte, M. Venanzi, V. N. Nemykin, P. Galloni, *Chem. Commun.* **2012**, *48*, 5145–5147.

[119] V. N. Nemykin, G. T. Rohde, C. D. Barrett, R. G. Hadt, C. Bizzarri, P. Galloni, B. Floris, I. Nowik, R. H. Herber, A. G. Marrani et al., *J. Am. Chem. Soc.* **2009**, *131*, 14969–14978.

[120] J. Melomedov, J. R. Ochsmann, M. Meister, F. Laquai, K. Heinze, *Eur. J. Inorg. Chem.* **2014**, *2014*, 2902–2915.

[121] J. Melomedov, J. R. Ochsmann, M. Meister, F. Laquai, K. Heinze, *Eur. J. Inorg. Chem.* **2014**, *2014*, 1984–2001.

[122] U. Siemeling, J. Vor der Brüggen, U. Vorfeld, B. Neumann, A. Stammler, H.-G. Stammler, A. Brockhinke, R. Plessow, P. Zanello, F. Laschi et al., *Chem. Eur. J.* **2003**, *9*, 2819–2833.

[123] K. Heinze, K. Hempel, M. Beckmann, *Eur. J. Inorg. Chem.* **2006**, *2006*, 2040–2050.

[124] R. T. Roginski, A. Moroz, D. N. Hendrickson, H. G. Drickamer, *J. Phys. Chem.* **1988**, *92*, 4319–4323.

[125] J. H. Ammeter, J. D. Swalen, *J. Chem. Phys.* **1972**, *57*, 678–698.

[126] N. G. Connelly, W. E. Geiger, *Chem. Rev.* **1996**, *96*, 877–910.

[127] S. Vanicek, H. Kopacka, K. Wurst, T. Müller, H. Schottenberger, B. Bildstein, *Organometallics* **2014**, *33*, 1152–1156.

[128] J. E. Sheats, M. D. Rausch, *J. Org. Chem.* **1970**, *35*, 3245–3249.

[129] H. Huesmann, C. Förster, D. Siebler, T. Gasi, K. Heinze, *Organometallics* **2012**, *31*, 413–427.

[130] K.-E. Schwarzhans, W. Stolz, *Monatsh. Chem.* **1987**, *118*, 875–878.

[131] P. D. Beer, Z. Chen, A. J. Goulden, A. Graydon, S. E. Stokes, T. Wear, *J. Chem. Soc., Chem. Commun.* **1993**, 1834.

[132] S. Barlow, *Inorg. Chem.* **2001**, *40*, 7047–7053.

[133] G. Laus, C. E. Strasser, M. Holzer, K. Wurst, G. Pürstinger, K.-H. Ongania, M. Rauch, G. Bonn, H. Schottenberger, *Organometallics* **2005**, *24*, 6085–6093.

[134] R. Warratz, G. Peters, F. Studt, R.-H. Römer, F. Tuczek, *Inorg. Chem.* **2006**, *45*, 2531–2542.

[135] C. Ornelas, J. Ruiz, D. Astruc, *Organometallics* **2009**, *28*, 2716–2723.

[136] D. Astruc, C. Ornelas, J. Ruiz, *Chem. Eur. J.* **2009**, *15*, 8936–8944.

[137] J. B. Gilroy, S. K. Patra, J. M. Mitchels, M. A. Winnik, I. Manners, *Angew. Chem.* **2011**, *123*, 5973–5977; *Angew. Chem. Int. Ed.* **2011**, *50*, 5851–5855.

[138] C. M. Casado, B. González, I. Cuadrado, B. Alonso, M. Morán, J. Losada, *Angew. Chem.* **2000**, *112*, 2219–2222; *Angew. Chem. Int. Ed.* **2000**, *39*, 2135–2138.

[139] S. Vanicek, H. Kopacka, K. Wurst, T. Müller, C. Hassenrück, R. F. Winter, B. Bildstein, *Organometallics* **2016**, *35*, 2101–2109.

[140] M. Jochriem, D. Bosch, H. Kopacka, B. Bildstein, *Organometallics* **2019**, *38*, 2278–2279.

[141] A. Wolter-Steingrube, K. Cordsen, J. Heck, *Eur. J. Inorg. Chem.* **2017**, *2017*, 1314–1319.

[142] S. Vanicek, M. Podewitz, J. Stubbe, D. Schulze, H. Kopacka, K. Wurst, T. Müller, P. Lippmann, S. Haslinger, H. Schottenberger et al., *Chem. Eur. J.* **2018**, *24*, 3742–3753.

[143] L. Zhao, X. Liu, L. Zhang, G. Qiu, D. Astruc, H. Gu, *Coord. Chem. Rev.* **2017**, *337*, 34–79.

[144] K. Heinze, M. Schlenker, *Eur. J. Inorg. Chem.* **2004**, *2004*, 2974–2988.

[145] K. Heinze, D. Siebler, *Z. anorg. allg. Chem.* **2007**, *633*, 2223–2233.

[146] D. Siebler, M. Linseis, T. Gasi, L. M. Carrella, R. F. Winter, C. Förster, K. Heinze, *Chem. Eur. J.* **2011**, *17*, 4540–4551.

[147] D. Siebler, K. Heinze, *J. Organomet. Chem.* **2016**, *821*, 19–24.

[148] P. Veit, C. Förster, S. Seibert, K. Heinze, *Z. anorg. allg. Chem.* **2015**, *641*, 2083–2092.

[149] P. Veit, E. Prantl, C. Förster, K. Heinze, *Organometallics* **2016**, *35*, 249–257.

[150] K. Hanauer, M. T. Pham, C. Förster, K. Heinze, *Eur. J. Inorg. Chem.* **2017**, *2017*, 433–445.

[151] T. Kienz, C. Förster, K. Heinze, *Organometallics* **2016**, *35*, 3681–3691.

[152] K. Heinze, M. Schlenker, *Eur. J. Inorg. Chem.* **2005**, *2005*, 66–71.

[153] D. Siebler, C. Förster, K. Heinze, *Eur. J. Inorg. Chem.* **2010**, *2010*, 523–527.

[154] S. Lu, V. V. Strelets, M. F. Ryan, W. J. Pietro, A. B. P. Lever, *Inorg. Chem.* **1996**, *35*, 1013–1023.

[155] A. Wolter-Steingrube, B. E. C. Bugenhagen, C. Herrmann, J. Heck, *Eur. J. Inorg. Chem.* **2014**, *2014*, 4115–4122.

[156] G. R. Knox, J. D. Munro, P. L. Pauson, G. H. Smith, W. E. Watts, *J. Chem. Soc.* **1961**, 4619.

[157] P. L. Pauson, G. Knox, **1962**.

[158] K.-P. Stahl, G. Boche, W. Massa, *J. Organomet. Chem.* **1984**, *277*, 113–125.

[159] M. V. Butovskii, U. Englert, G. E. Herberich, U. Koelle, *Eur. J. Inorg. Chem.* **2005**, *2005*, 971–980.

[160] M. Lauck, C. Förster, K. Heinze, *Organometallics* **2017**, *36*, 4968–4978.

[161] E. M. Acton, R. M. Silverstein, *J. Org. Chem.* **1959**, *24*, 1487–1490.

[162] B. Enk, H. Kopacka, K. Wurst, T. Müller, B. Bildstein, *Organometallics* **2009**, *28*, 5575–5586.

[163] D. Bourissou, O. Guerret, F. P. Gabbaï, G. Bertrand, *Chem. Rev.* **2000**, *100*, 39–92.

[164] U. Siemeling, *Eur. J. Inorg. Chem.* **2012**, *2012*, 3523–3536.

[165] E. Buchner, T. Curtius, *Ber. Dtsch. Chem. Ges.* **1885**, *18*, 2377–2379.

[166] H. Staudinger, O. Kupfer, *Ber. Dtsch. Chem. Ges.* **1912**, *45*, 501–509.

[167] W. v. E. Doering, L. H. Knox, *J. Am. Chem. Soc.* **1953**, *75*, 297–303.

[168] W. von E. Doering, A. K. Hoffmann, *J. Am. Chem. Soc.* **1954**, *76*, 6162–6165.

[169] E. O. Fischer, A. Maasböl, *Angew. Chem.* **1964**, *76*, 645; *Angew. Chem. Int. Ed.* **1964**, *3*, 580–581.

[170] K. H. Dötz, *Angew. Chem.* **1975**, *87*, 672–673; *Angew. Chem. Int. Ed. Engl.* **1975**, *14*, 644–645.

[171] C. D. Montgomery, *J. Chem. Educ.* **2015**, *92*, 1653–1660.

[172] R. H. Grubbs, T. M. Trnka (Hrsg.) *Ruthenium-Catalyzed Olefin Metathesis. Ruthenium-Catalyzed Olefin Metathesis*, Wiley-VCH, Weilheim, **2004**.

[173] J. Vignolle, X. Cattoën, D. Bourissou, *Chem. Rev.* **2009**, *109*, 3333–3384.

[174] G. Bouhadir, D. Bourissou, *Chem. Soc. Rev.* **2004**, *33*, 210–217.

[175] J. Kapp, C. Schade, A. M. El-Nahasa, P. von Ragué Schleyer, *Angew. Chem. Int. Ed.* **1996**, *35*, 2236–2238.

[176] R. W. Alder, P. R. Allen, S. J. Williams, *J. Chem. Soc., Chem. Commun.* **1995**, 1267.

[177] A. Igau, H. Grutzmacher, A. Baceiredo, G. Bertrand, *J. Am. Chem. Soc.* **1988**, *110*, 6463–6466.

[178] A. J. Arduengo, R. L. Harlow, M. Kline, *J. Am. Chem. Soc.* **1991**, *113*, 361–363.

[179] M. Soleilhavoup, G. Bertrand, *Acc. Chem. Res.* **2015**, *48*, 256–266.

[180] V. Lavallo, Y. Canac, C. Präsang, B. Donnadieu, G. Bertrand, *Angew. Chem.* **2005**, *117*, 5851–5855; *Angew. Chem. Int. Ed.* **2005**, *44*, 5705–5709.

[181] R. W. Alder, P. R. Allen, M. Murray, A. G. Orpen, *Angew. Chem. Int. Ed.* **1996**, *35*, 1121–1123.

[182] L. M. Slaughter, *ACS Catal.* **2012**, *2*, 1802–1816.

[183] V. P. Boyarskiy, K. V. Luzyanin, V. Y. Kukushkin, *Coord. Chem. Rev.* **2012**, *256*, 2029–2056.

[184] E. González-Fernández, J. Rust, M. Alcarazo, *Angew. Chem.* **2013**, *125*, 11603–11606; *Angew. Chem. Int. Ed.* **2013**, *52*, 11392–11395.

[185] P. de Frémont, N. Marion, S. P. Nolan, *Coord. Chem. Rev.* **2009**, *253*, 862–892.

[186] S. Díez-González, S. P. Nolan, *Annu. Rep. Prog. Chem. B* **2005**, *101*, 171.
[187] H. Clavier, S. P. Nolan, *Annu. Rep. Prog. Chem. B* **2007**, *103*, 193.
[188] R. E. Douthwaite, *Coord. Chem. Rev.* **2007**, *251*, 702–717.
[189] S. Díez-González, S. Nolan, *Synlett* **2007**, *2007*, 2158–2167.
[190] L. H. Gade, S. Bellemin-Laponnaz, *Coord. Chem. Rev.* **2007**, *251*, 718–725.
[191] V. Dragutan, I. Dragutan, L. Delaude, A. Demonceau, *Coord. Chem. Rev.* **2007**, *251*, 765–794.
[192] W. J. Sommer, M. Weck, *Coord. Chem. Rev.* **2007**, *251*, 860–873.
[193] P. Bazinet, T.-G. Ong, J. S. O'Brien, N. Lavoie, E. Bell, G. P. A. Yap, I. Korobkov, D. S. Richeson, *Organometallics* **2007**, *26*, 2885–2895.
[194] N. Marion, S. P. Nolan, *Chem. Soc. Rev.* **2008**, *37*, 1776–1782.
[195] D. Enders, T. Balensiefer, *Acc. Chem. Res.* **2004**, *37*, 534–541.
[196] N. Marion, S. Díez-González, S. P. Nolan, *Angew. Chem. Int. Ed.* **2007**, *46*, 2988–3000.
[197] D. Enders, O. Niemeier, A. Henseler, *Chem. Rev.* **2007**, *107*, 5606–5655.
[198] K. Zeitler, *Angew. Chem.* **2005**, *117*, 7674–7678; *Angew. Chem. Int. Ed.* **2005**, *44*, 7506–7510.
[199] E. A. B. Kantchev, C. J. O'Brien, M. G. Organ, *Angew. Chem.* **2007**, *119*, 2824–2870; *Angew. Chem. Int. Ed.* **2007**, *46*, 2768–2813.
[200] E. Despagnet-Ayoub, R. H. Grubbs, *J. Am. Chem. Soc.* **2004**, *126*, 10198–10199.
[201] P. L. Arnold, S. Pearson, *Coord. Chem. Rev.* **2007**, *251*, 596–609.
[202] D. Pugh, A. A. Danopoulos, *Coord. Chem. Rev.* **2007**, *251*, 610–641.
[203] E. Colacino, J. Martinez, F. Lamaty, *Coord. Chem. Rev.* **2007**, *251*, 726–764.
[204] J. A. Mata, M. Poyatos, E. Peris, *Coord. Chem. Rev.* **2007**, *251*, 841–859.
[205] F. E. Hahn, M. C. Jahnke, *Angew. Chem.* **2008**, *120*, 3166–3216; *Angew. Chem. Int. Ed.* **2008**, *47*, 3122–3172.
[206] W. A. Herrmann, *Angew. Chem.* **2002**, *114*, 1342; *Angew. Chem. Int. Ed.* **2002**, *41*, 1290–1309.
[207] A. A. Gridnev, I. M. Mihaltseva, *Synth. Commun.* **1994**, *24*, 1547–1555.
[208] A. Fürstner, O. R. Thiel, L. Ackermann, *Org. Lett.* **2001**, *3*, 449–451.
[209] N. Wiberg, J. W. Buchler, *Z. Naturforsch. B* **1964**, *19*, 953–955.
[210] J. Mason (Hrsg.) *Multinuclear NMR*, Plenum Press, New York, **1987**.
[211] R. W. Alder, M. E. Blake, *Chem. Commun.* **1997**, 1513–1514.
[212] W. A. Herrmann, J. Schütz, G. D. Frey, E. Herdtweck, *Organometallics* **2006**, *25*, 2437–2448.
[213] G. D. Frey, C. F. Rentzsch, D. von Preysing, T. Scherg, M. Mühlhofer, E. Herdtweck, W. A. Herrmann, *J. Organomet. Chem.* **2006**, *691*, 5725–5738.
[214] G. D. Frey, W. A. Herrmann, *J. Organomet. Chem.* **2005**, *690*, 5876–5880.
[215] M. S. Collins, E. L. Rosen, V. M. Lynch, C. W. Bielawski, *Organometallics* **2010**, *29*, 3047–3053.
[216] E. L. Rosen, M. D. Sanderson, S. Saravanakumar, C. W. Bielawski, *Organometallics* **2007**, *26*, 5774–5777.
[217] S. Conejero, Y. Canac, F. S. Tham, G. Bertrand, *Angew. Chem.* **2004**, *116*, 4181–4185; *Angew. Chem. Int. Ed.* **2004**, *43*, 4089–4093.
[218] G. Altenhoff, R. Goddard, C. W. Lehmann, F. Glorius, *Angew. Chem.* **2003**, *115*, 3818–3821; *Angew. Chem. Int. Ed.* **2003**, *42*, 3690–3693.

[219] S. Ibáñez, M. Poyatos, L. N. Dawe, D. Gusev, E. Peris, *Organometallics* **2016**, *35*, 2747–2758.
[220] M. Süßner, H. Plenio, *Angew. Chem.* **2005**, *117*, 7045–7048; *Angew. Chem. Int. Ed.* **2005**, *44*, 6885–6888.
[221] T. Schulz, D. Weismann, L. Wallbaum, R. Guthardt, C. Thie, M. Leibold, C. Bruhn, U. Siemeling, *Chem. Eur. J.* **2015**, *21*, 14107–14121.
[222] A. Bertogg, F. Camponovo, A. Togni, *Eur. J. Inorg. Chem.* **2005**, *2005*, 347–356.
[223] F. Demirhan, Ö. Yıldırım, B. Çetinkaya, *Transit. Met. Chem.* **2003**, *28*, 558–562.
[224] A. Dallas, H. Kuhtz, A. Farrell, B. Quilty, K. Nolan, *Tetrahedron Lett.* **2007**, *48*, 1017–1021.
[225] U. Siemeling, C. Färber, C. Bruhn, *Chem. Commun.* **2009**, 98–100.
[226] U. Siemeling, C. Färber, M. Leibold, C. Bruhn, P. Mücke, R. F. Winter, B. Sarkar, M. von Hopffgarten, G. Frenking, *Eur. J. Inorg. Chem.* **2009**, *2009*, 4607–4612.
[227] D. M. Khramov, E. L. Rosen, V. M. Lynch, C. W. Bielawski, *Angew. Chem.* **2008**, *120*, 2299–2302; *Angew. Chem. Int. Ed.* **2008**, 47, 2267–2270.
[228] A. Dehope, D. Mendoza-Espinosa, B. Donnadieu, G. Bertrand, *New J. Chem.* **2011**, *35*, 2037–2042.
[229] A. S. K. Hashmi, C. Lothschütz, C. Böhling, F. Rominger, *Organometallics* **2011**, *30*, 2411–2417.
[230] B. Bildstein, *J. Organomet. Chem.* **2001**, *617-618*, 28–38.
[231] P. Veit, C. Förster, K. Heinze, *Beilstein J. Org. Chem.* **2016**, *12*, 1322–1333.
[232] P. Veit, *Dissertation*, Johannes Gutenberg-Universität, Mainz, **2020**.
[233] Y. Wang, M. E. Muratore, A. M. Echavarren, *Chem. Eur. J.* **2015**, *21*, 7332–7339.
[234] M. W. Hussong, F. Rominger, P. Krämer, B. F. Straub, *Angew. Chem.* **2014**, *126*, 9526–9529.
[235] G. Seidel, A. Fürstner, *Angew. Chem.* **2014**, *126*, 4907–4911; *Angew. Chem. Int. Ed.* **2014**, *53*, 4807–4811.
[236] D. A. Dixon, *J. Am. Chem. Soc.* **2011**, *133*, 19257.
[237] F. Bernardi, A. Bottoni, G. P. Miscione, *Organometallics* **2000**, *19*, 5529–5532.
[238] V. W.-W. Yam, E. C.-C. Cheng, *Chem. Soc. Rev.* **2008**, *37*, 1806–1813.
[239] H. Schmidbaur, A. Schier, *Chem. Soc. Rev.* **2012**, *41*, 370–412.
[240] H. Schmidbaur, *Gold Bull* **1990**, *23*, 11–21.
[241] J. E. Parks, A. L. Balch, *J. Organomet. Chem.* **1973**, *57*, C103–C106.
[242] J. E. Parks, A. L. Balch, *J. Organomet. Chem.* **1974**, *71*, 453–463.
[243] R. Aumann, E. O. Fischer, *Chem. Ber.* **1981**, *114*, 1853–1857.
[244] E. O. Fischer, M. Böck, R. Aumann, *Chem. Ber.* **1983**, *116*, 3618–3623.
[245] E. O. Fischer, M. Bock, *J. Organomet. Chem.* **1985**, *287*, 279–285.
[246] R. Usón, A. Laguna, M. D. Villacampa, *Inorg. Chim. Acta* **1984**, *81*, 25–31.
[247] G. Banditelli, F. Bonati, S. Calogero, G. Valle, F. E. Wagner, R. Wordel, *Organometallics* **1986**, *5*, 1346–1352.
[248] B. Bovio, S. Calogero, F. E. Wagner, A. Burini, B. R. Pietroni, *J. Organomet. Chem.* **1994**, *470*, 275–283.

[249] P. G. Jones, A. G. Maddock, M. J. Mays, M. M. Muir, A. F. Williams, *J. Chem. Soc., Dalton Trans.* **1977**, 1434–1439.

[250] A. S. K. Hashmi, M. Rudolph, *Chem. Soc. Rev.* **2008**, *37*, 1766–1775.

[251] C. Elschenbroich, *Organometallchemie,* 6. Aufl., Vieweg+Teubner Verlag, Wiesbaden, **2008**.

[252] R. F. Heck, J. P. Nolley, *J. Org. Chem.* **1972**, *37*, 2320–2322.

[253] N. Miyaura, A. Suzuki, *J. Chem. Soc., Chem. Commun.* **1979**, 866.

[254] H. Schmidbaur, A. Schier, *Organometallics* **2010**, *29*, 2–23.

[255] D. J. Gorin, B. D. Sherry, F. D. Toste, *Chem. Rev.* **2008**, *108*, 3351–3378.

[256] S. Doherty, J. G. Knight, A. S. K. Hashmi, C. H. Smyth, N. A. B. Ward, K. J. Robson, S. Tweedley, R. W. Harrington, W. Clegg, *Organometallics* **2010**, *29*, 4139–4147.

[257] A. S. K. Hashmi, T. Häffner, M. Rudolph, F. Rominger, *Eur. J. Org. Chem.* **2011**, *2011*, 667–671.

[258] N. Huguet, D. Lebœuf, A. M. Echavarren, *Chem. Eur. J.* **2013**, *19*, 6581–6585.

[259] G. Verniest, A. Padwa, *Org. Lett.* **2008**, *10*, 4379–4382.

[260] Y. Hu, X. Xin, B. Wan, *Tetrahedron Lett.* **2015**, *56*, 32–52.

[261] D. S. Weinberger, M. Melaimi, C. E. Moore, A. L. Rheingold, G. Frenking, P. Jerabek, G. Bertrand, *Angew. Chem.* **2013**, *125*, 9134–9137; *Angew. Chem. Int. Ed.* **2013**, *52*, 8964–8967.

[262] R. Pretorius, M. R. Fructos, H. Müller-Bunz, R. A. Gossage, P. J. Pérez, M. Albrecht, *Dalton trans.* **2016**, *45*, 14591–14602.

[263] I. M. Lorkovic, M. S. Wrighton, W. M. Davis, *J. Am. Chem. Soc.* **1994**, *116*, 6220–6228.

[264] L. Hettmanczyk, S. Manck, C. Hoyer, S. Hohloch, B. Sarkar, *Chem. Commun.* **2015**, *51*, 10949–10952.

[265] L. Hettmanczyk, L. Suntrup, S. Klenk, C. Hoyer, B. Sarkar, *Chem. Eur. J.* **2017**, *23*, 576–585.

[266] S. Klenk, S. Rupf, L. Suntrup, M. van der Meer, B. Sarkar, *Organometallics* **2017**, *36*, 2026–2035.

[267] M. Nonnenmacher, D. M. Buck, D. Kunz, *Beilstein journal of organic chemistry* **2016**, *12*, 1884–1896.

[268] D. I. Bezuidenhout, B. van der Westhuizen, A. J. Rosenthal, M. Wörle, D. C. Liles, I. Fernández, *Dalton transactions* **2014**, *43*, 398–401.

[269] P. Veit, C. Volkert, C. Förster, V. Ksenofontov, S. Schlicher, M. Bauer, K. Heinze, *Chem. Commun.* **2019**, *55*, 4615–4618.

[270] D. Huang, X. Zhang, E. J. L. McInnes, J. McMaster, A. J. Blake, E. S. Davies, J. Wolowska, C. Wilson, M. Schröder, *Inorg. Chem.* **2008**, *47*, 9919–9929.

[271] S. Preiß, J. Melomedov, A. Wünsche von Leupoldt, K. Heinze, *Chemical science* **2016**, *7*, 596–610.

[272] N. Dubouis, A. Grimaud, *Chem. Sci.* **2019**, *10*, 9165–9181.

[273] V. Smil, *World Agr.* **2011**, *2*, 9–13.

[274] T. Sakakura, J.-C. Choi, H. Yasuda, *Chem. Rev.* **2007**, *107*, 2365–2387.

[275] A. J. Esswein, D. G. Nocera, *Chem. Rev.* **2007**, *107*, 4022–4047.

[276] K. Liu, C. Song, V. Subramani, *Hydrogen and syngas production and purification technologies [Elektronische Ressource]*, Wiley, Hoboken, N.J., **2010**.

[277] J. D. Holladay, J. Hu, D. L. King, Y. Wang, *Catal. Today* **2009**, *139*, 244–260.

[278] J. L. Dempsey, A. J. Esswein, D. R. Manke, J. Rosenthal, J. D. Soper, D. G. Nocera, *Inorg. Chem.* **2005**, *44*, 6879–6892.

[279] J. Rosenthal, J. Bachman, J. L. Dempsey, A. J. Esswein, T. G. Gray, J. M. Hodgkiss, D. R. Manke, T. D. Luckett, B. J. Pistorio, A. S. Veige et al., *Coord. Chem. Rev.* **2005**, *249*, 1316–1326.

[280] D. G. Nocera, *Acc. Chem. Res.* **1995**, *28*, 209–217.

[281] J. D. Soper, S. V. Kryatov, E. V. Rybak-Akimova, D. G. Nocera, *J. Am. Chem. Soc.* **2007**, *129*, 5069–5075.

[282] J. Y. Yang, D. G. Nocera, *J. Am. Chem. Soc.* **2007**, *129*, 8192–8198.

[283] S. Y. Reece, J. M. Hodgkiss, J. Stubbe, D. G. Nocera, *Philos. Trans. R. Soc. B* **2006**, *361*, 1351–1364.

[284] J. M. Hodgkiss, J. Rosenthal, D. G. Nocera (Hrsg.) *Hydrogen-Transfer Reactions. The Relation between Hydrogen Atom Transfer and Proton-coupled Electron Transfer in Model Systems*, Wiley-VCH, Weinheim, **2007**.

[285] W. Zhang, W. Lai, R. Cao, *Chem. Rev.* **2017**, *117*, 3717–3797.

[286] Y. Han, H. Fang, H. Jing, H. Sun, H. Lei, W. Lai, R. Cao, *Angew. Chem.* **2016**, *128*, 5547–5552; *Angew. Chem. Int. Ed.* **2016**, *55*, 5457–5462.

[287] R. M. Kellett, T. G. Spiro, *Inorg. Chem.* **1985**, *24*, 2378–2382.

[288] R. M. Kellett, T. G. Spiro, *Inorg. Chem.* **1985**, *24*, 2373–2377.

[289] I. Bhugun, D. Lexa, J.-M. Savéant, *J. Am. Chem. Soc.* **1996**, *118*, 3982–3983.

[290] V. Grass, D. Lexa, J.-M. Savéant, *J. Am. Chem. Soc.* **1997**, *119*, 7526–7532.

[291] P. Kielb, M. Horch, P. Wrzolek, R. Goetz, K. H. Ly, J. Kozuch, M. Schwalbe, I. M. Weidinger, *Catal. Sci. Technol.* **2018**, *8*, 1849–1857.

[292] T. M. McCormick, B. D. Calitree, A. Orchard, N. D. Kraut, F. V. Bright, M. R. Detty, R. Eisenberg, *J. Am. Chem. Soc.* **2010**, *132*, 15480–15483.

[293] J. L. Dempsey, J. R. Winkler, H. B. Gray, *J. Am. Chem. Soc.* **2010**, *132*, 16774–16776.

[294] C. H. Lee, D. K. Dogutan, D. G. Nocera, *J. Am. Chem. Soc.* **2011**, *133*, 8775–8777.

[295] J. G. Kleingardner, B. Kandemir, K. L. Bren, *J. Am. Chem. Soc.* **2014**, *136*, 4–7.

[296] B. B. Beyene, S. B. Mane, C.-H. Hung, *Chem. Commun.* **2015**, *51*, 15067–15070.

[297] P. Du, R. Eisenberg, *Energy Environ. Sci.* **2012**, *5*, 6012.

[298] M. Wang, L. Chen, L. Sun, *Energy Environ. Sci.* **2012**, *5*, 6763.

[299] V. S. Thoi, Y. Sun, J. R. Long, C. J. Chang, *Chem. Soc. Rev.* **2013**, *42*, 2388–2400.

[300] B. B. Beyene, S. B. Mane, C.-H. Hung, *J. Electrochem. Soc.* **2018**, *165*, H481–H487.

[301] B. Mondal, K. Sengupta, A. Rana, A. Mahammed, M. Botoshansky, S. G. Dey, Z. Gross, A. Dey, *Inorg. Chem.* **2013**, *52*, 3381–3387.

[302] A. Mahammed, B. Mondal, A. Rana, A. Dey, Z. Gross, *Chem. Commun.* **2014**, *50*, 2725–2727.

[303] H. Lei, A. Han, F. Li, M. Zhang, Y. Han, P. Du, W. Lai, R. Cao, *Phys. Chem. Chem. Phys.* **2014**, *16*, 1883–1893.
[304] A. Miyake, H. Kondo, M. Aoyama, *Angew. Chem. Int. Ed.* **1969**, *8*, 520–521.
[305] M. van den Akker, F. Jellinek, *Recl. Trav. Chim. Pays-Bas* **1971**, *90*, 1101–1109.
[306] U. Koelle, P. P. Infelta, M. Graetzel, *Inorg. Chem.* **1988**, *27*, 879–883.
[307] U. Koelle, S. Paul, *Inorg. Chem.* **1986**, *25*, 2689–2694.
[308] C. V. Krishnan, B. S. Brunschwig, C. Creutz, N. Sutin, *J. Am. Chem. Soc.* **1985**, *107*, 2005–2015.
[309] U. Kölle, M. Grützel, *Angew. Chem. Int. Ed.* **1987**, *26*, 567–570.
[310] J. Derosa, P. Garrido-Barros, J. C. Peters, *Inorg. Chem.* **2022**, *61*, 6672–6678.
[311] S. Vanicek, M. Jochriem, C. Hassenrück, S. Roy, H. Kopacka, K. Wurst, T. Müller, R. F. Winter, E. Reisner, B. Bildstein, *Organometallics* **2019**, *38*, 1361–1371.
[312] H. Bönnemann, *Angew. Chem.* **1985**, *97*, 264–279; *Angew. Chem. Int. Ed. Engl.* **1985**, *24*, 248–262.
[313] A. Wiebe, T. Gieshoff, S. Möhle, E. Rodrigo, M. Zirbes, S. R. Waldvogel, *Angew. Chem.* **2018**, *130*, 5694–5721.
[314] B. A. Frontana-Uribe, R. D. Little, J. G. Ibanez, A. Palma, R. Vasquez-Medrano, *Green Chem.* **2010**, *12*, 2099.
[315] H. J. Schäfer, M. Harenbrock, E. Klocke, M. Plate, A. Weiper-Idelmann, *Pure Appl. Chem.* **2007**, *79*, 2047–2057.
[316] D. Pollok, S. R. Waldvogel, *Chem. Sci.* **2020**, *11*, 12386–12400.
[317] J. B. Sperry, D. L. Wright, *Chem. Soc. Rev.* **2006**, *35*, 605–621.
[318] K. D. Moeller, *Tetrahedron* **2000**, *56*, 9527–9554.
[319] H. Lund (Hrsg.) *Organic electrochemistry*, Marcel Dekker, New York, NY, **2001**.
[320] J. Yoshida, K. Kataoka, R. Horcajada, A. Nagaki, *Chem. Rev.* **2008**, *108*, 2265–2299.
[321] A. Meijere, K. N. Houk, J.-M. Lehn, S. V. Ley, J. Thiem, B. M. Trost, F. Vögtle, H. Yamamoto, E. Steckhan, *Electroorganic synthesis. Bond formation at anode and cathode; with 34 tables*, Springer, Berlin, **1997**.
[322] R. Francke, R. D. Little, *Chem. Soc. Rev.* **2014**, *43*, 2492–2521.
[323] E. Steckhan (Hrsg.) *Organic syntheses with electrochemically regenerable redox systems*, Springer, Berlin, **1987**.
[324] E. Steckhan, *Angew. Chem. Int. Ed.* **1986**, *25*, 683–701.
[325] C. Costentin, M. Robert, J.-M. Savéant, *Chem. Soc. Rev.* **2013**, *42*, 2423–2436.
[326] Y. Oh, X. Hu, *Chem. Soc. Rev.* **2013**, *42*, 2253–2261.
[327] C. D. Windle, R. N. Perutz, *Coord. Chem. Rev.* **2012**, *256*, 2562–2570.
[328] J. Collin, *Coord. Chem. Rev.* **1989**, *93*, 245–268.
[329] K. Xu, *Chem. Rev.* **2004**, *104*, 4303–4417.
[330] B. König, *Chemical Photocatalysis [Elektronische Ressource]*, DE GRUYTER, Berlin, **2013**.
[331] M. Liang, J. Chen, *Chem. Soc. Rev.* **2013**, *42*, 3453–3488.
[332] A. Hagfeldt, G. Boschloo, L. Sun, L. Kloo, H. Pettersson, *Chem. Rev.* **2010**, *110*, 6595–6663.

[333] J. E. Kwon, S. Park, S. Y. Park, *J. Am. Chem. Soc.* **2013**, *135*, 11239–11246.

[334] S. Park, J. E. Kwon, S. H. Kim, J. Seo, K. Chung, S.-Y. Park, D.-J. Jang, B. Milián Medina, J. Gierschner, S. Y. Park, *J. Am. Chem. Soc.* **2009**, *131*, 14043–14049.

[335] A. Shafir, M. P. Power, G. D. Whitener, J. Arnold, *Organometallics* **2000**, *19*, 3978–3982.

[336] K. N. Brown, P. T. Gulyas, P. A. Lay, N. S. McAlpine, A. F. Masters, L. Phillips, *J. Chem. Soc., Dalton Trans.* **1993**, 835.

[337] P. Zuman, *Substituent Effects in Organic Polarography*, Springer US, Boston, MA, **1967**.

[338] S. Dapperheld, E. Steckhan, K.-H. G. Brinkhaus, T. Esch, *Chem. Ber.* **1991**, *124*, 2557–2567.

[339] A. P. Davis, A. J. Fry, *J. Phys. Chem. A* **2010**, *114*, 12299–12304.

[340] L. D. Hicks, A. J. Fry, V. C. Kurzweil, *Electrochim. Acta* **2004**, *50*, 1039–1047.

[341] Y. Ding, G. Yu, *Angew. Chem.* **2017**, *129*, 8738–8740; *Angew. Chem. Int. Ed.* **2017**, *56*, 8614–8616.

[342] J. B. Raoof, R. Ojani, H. Karimi-Maleh, M. R. Hajmohamadi, P. Biparva, *Anal. Methods* **2011**, *3*, 2637.

[343] U. Jahn, *J. Org. Chem.* **1998**, *63*, 7130–7131.

[344] T. Langer, M. Illich, G. Helmchen, *Synlett* **1996**, *1996*, 1137–1139.

[345] U. Jahn, M. Müller, S. Aussieker, *J. Am. Chem. Soc.* **2000**, *122*, 5212–5213.

[346] U. Jahn, P. Hartmann, I. Dix, P. G. Jones, *Ann. Chem. Pharm.* **2001**, *2001*, 3333.

[347] F. C. Pigge, J. J. Coniglio, N. P. Rath, *J. Org. Chem.* **2004**, *69*, 1161–1168.

[348] M. P. Sibi, M. Hasegawa, *J. Am. Chem. Soc.* **2007**, *129*, 4124–4125.

[349] J.-P. Goddard, C. Gomez, F. Brebion, S. Beauvière, L. Fensterbank, M. Malacria, *Chem. Commun.* **2007**, 2929–2931.

[350] J. M. Richter, B. W. Whitefield, T. J. Maimone, D. W. Lin, M. P. Castroviejo, P. S. Baran, *J. Am. Chem. Soc.* **2007**, *129*, 12857–12869.

[351] U. Jahn, E. Dinca, *Chem. Eur. J.* **2009**, *15*, 58–62.

[352] M. Holan, R. Pohl, I. Císařová, B. Klepetářová, P. G. Jones, U. Jahn, *Chem. Eur. J.* **2015**, *21*, 9877–9888.

[353] E. S. Krygowski, K. Murphy-Benenato, M. D. Shair, *Angew. Chem.* **2008**, *120*, 1704–1708; *Angew. Chem. Int. Ed.* **2008**, *47*, 1680–1684.

[354] D. A. Khobragade, S. G. Mahamulkar, L. Pospíšil, I. Císařová, L. Rulíšek, U. Jahn, *Chem. Eur. J.* **2012**, *18*, 12267–12277.

[355] K. Foo, E. Sella, I. Thomé, M. D. Eastgate, P. S. Baran, *J. Am. Chem. Soc.* **2014**, *136*, 5279–5282.

[356] L. D. Marciasini, N. Richy, M. Vaultier, M. Pucheault, *Adv. Synth. Catal.* **2013**, *355*, 1083–1088.

[357] N. Chernyak, S. L. Buchwald, *J. Am. Chem. Soc.* **2012**, *134*, 12466–12469.

[358] L. S. Hernández-Muñoz, R. J. Fragoso-Soriano, C. Vázquez-López, E. Klimova, L. A. Ortiz-Frade, P. D. Astudillo, F. J. González, *J. Electroanal. Chem.* **2010**, *650*, 62–67.

[359] L. S. Hernández-Muñoz, A. Galano, P. D. Astudillo-Sánchez, M. M. Abu-Omar, F. J. González, *Electrochim. Acta* **2014**, *136*, 542–549.

[360] Z.-W. Hou, Z.-Y. Mao, H.-B. Zhao, Y. Y. Melcamu, X. Lu, J. Song, H.-C. Xu, *Angew. Chem.* **2016**, *128*, 9314–9318; *Angew. Chem. Int. Ed.* **2016**, *55*, 9168–9172.

[361] Z.-J. Wu, H.-C. Xu, *Angew. Chem.* **2017**, *129*, 4812–4816; *Angew. Chem. Int. Ed.* **2017**, *56*, 4734–4738.

[362] L. Zhu, P. Xiong, Z.-Y. Mao, Y.-H. Wang, X. Yan, X. Lu, H.-C. Xu, *Angew. Chem.* **2016**, *128*, 2266–2269; *Angew. Chem. Int. Ed.* **2016**, *55*, 2226–2229.

6 Appendix

6.1 Supporting Information: Polysubstituted ferrocenes as tunable redox mediators

Supporting Information

for

Polysubstituted ferrocenes as tunable redox mediators

Sven D. Waniek[1], Jan Klett*[1], Christoph Förster*[1] and Katja Heinze*[1]

Address: [1]Institute of Inorganic Chemistry and Analytical Chemistry, Johannes Gutenberg University Mainz, Duesbergweg 10–14, D-55128 Mainz, Germany

Email: Jan Klett - klettj@uni-mainz.de; Christoph Förster - cfoerster@uni-mainz.de; Katja Heinze - katja.heinze@uni-mainz.de

* Corresponding author

Measured and calculated spectra, IR data and

Cartesian coordinates

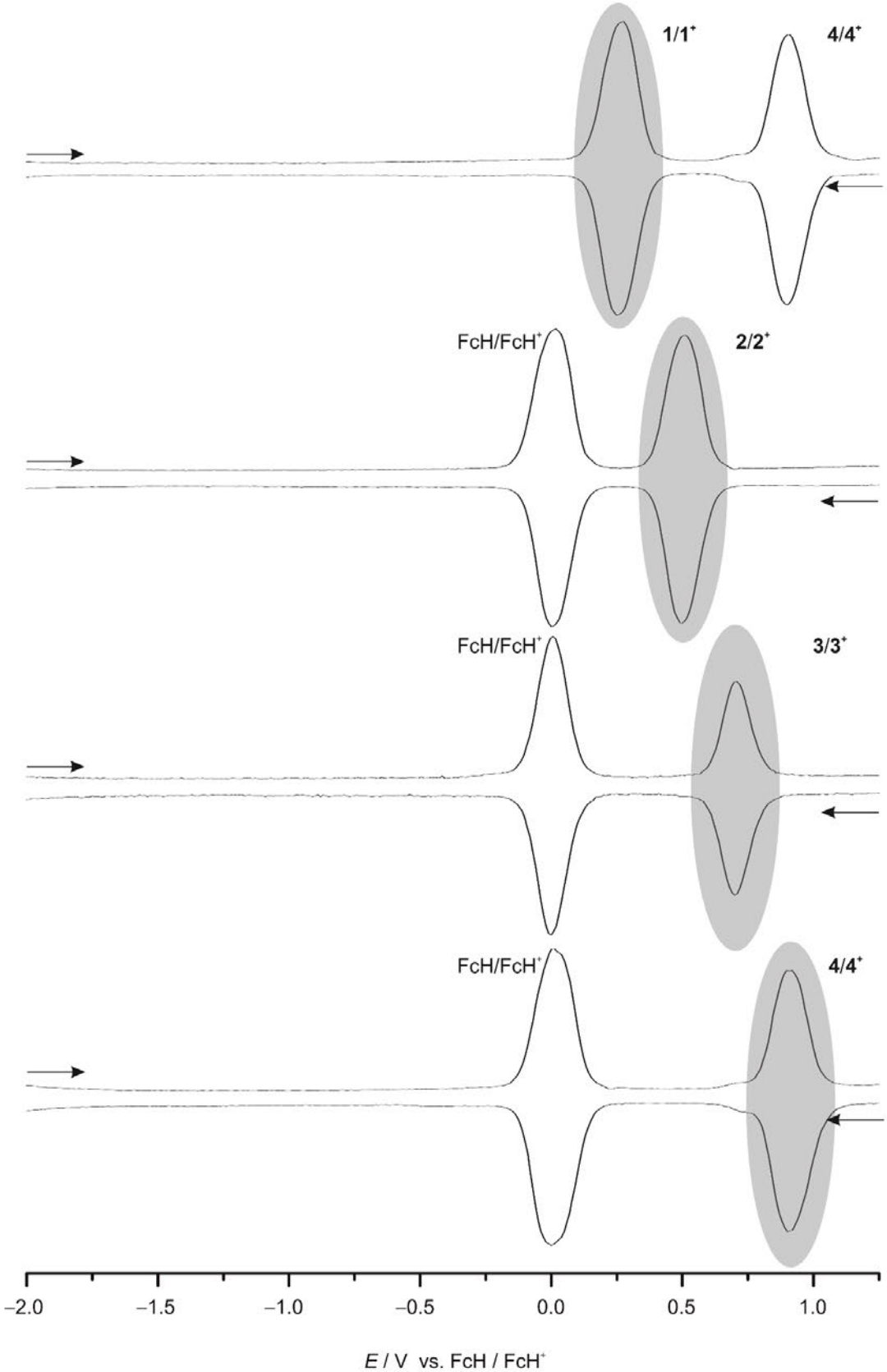

Figure S1: Square Wave voltammogram of **1–4** in dichloromethane with [*n*Bu4N][PF6], referenced against FcH/FcH+ for **2–4** and against **4/4+** for the **1/1+** couple.

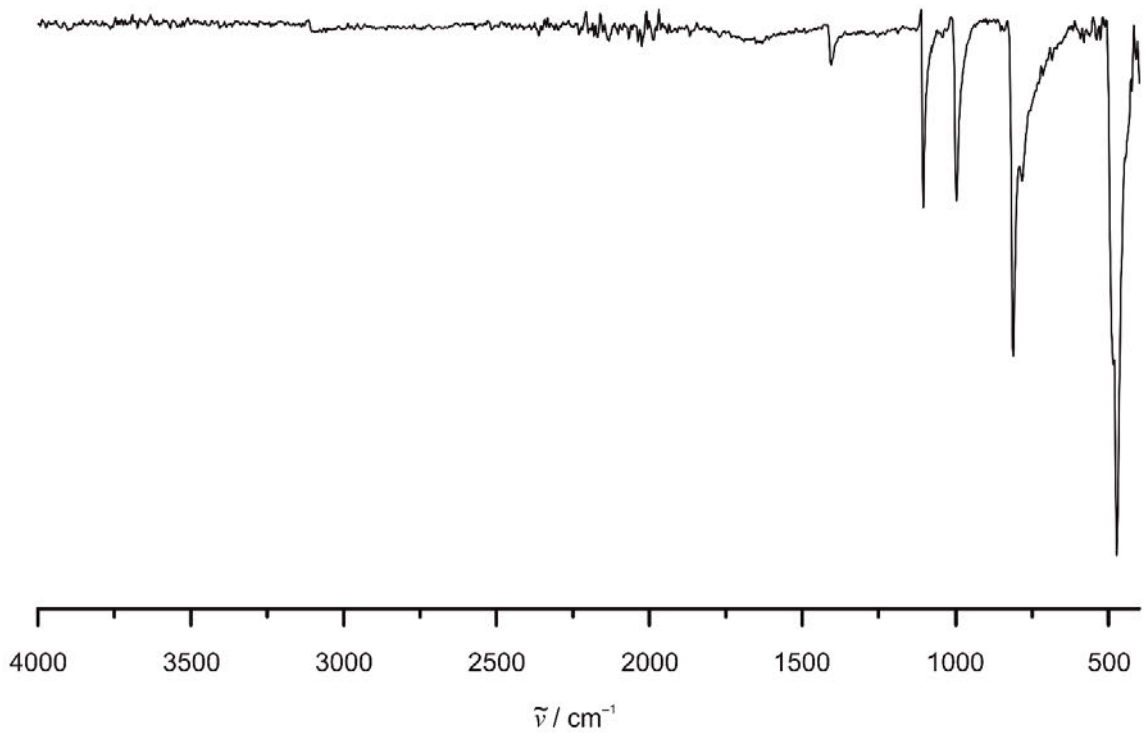

Figure S2: Solid state ATR IR spectrum of ferrocene.

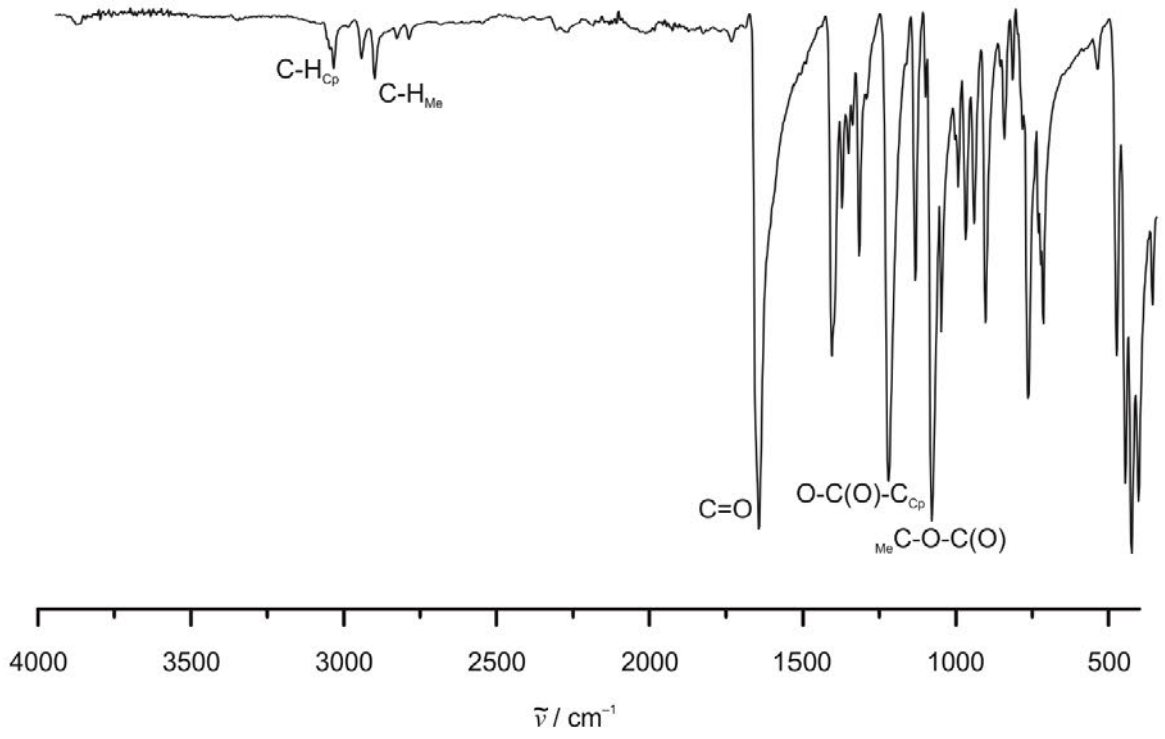

Figure S3: Solid state ATR IR spectrum of **1**.

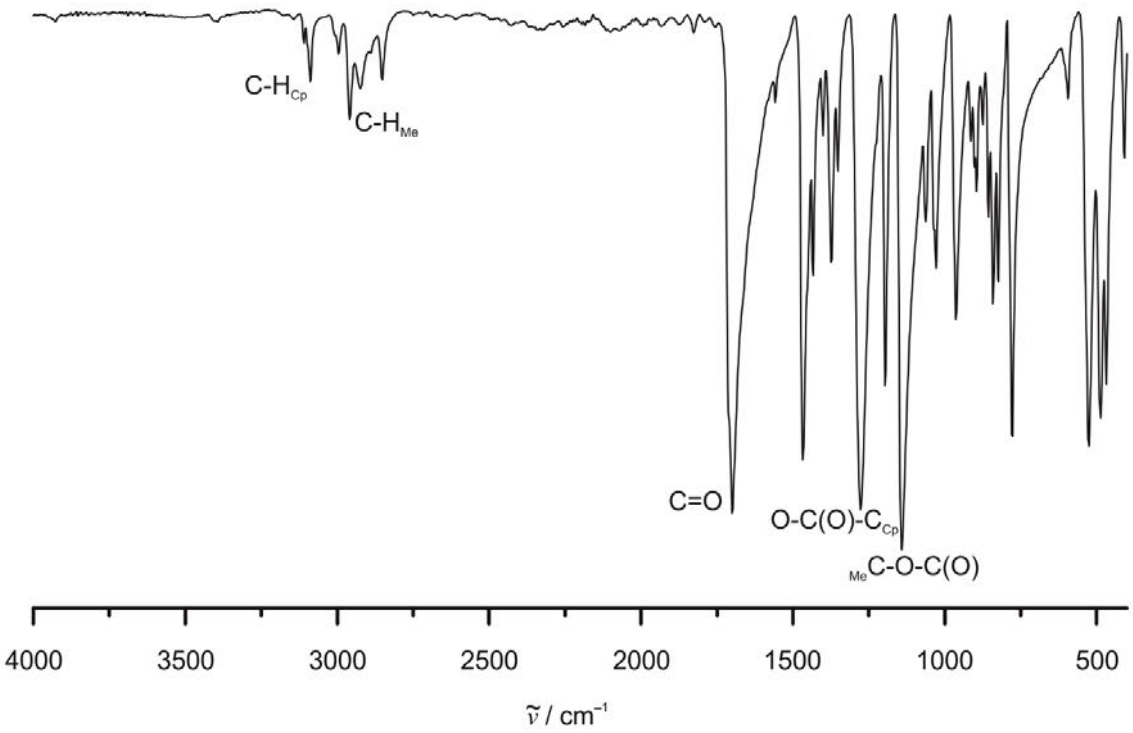

Figure S4: Solid state ATR IR spectrum of **2**.

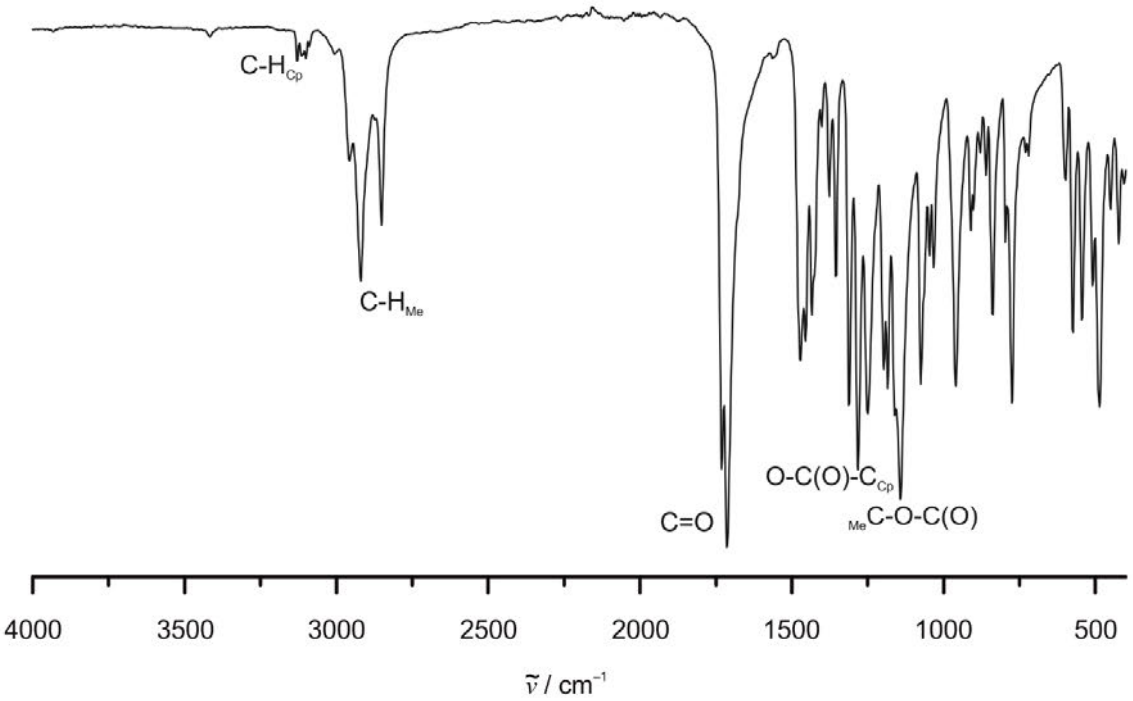

Figure S5: Solid state ATR IR spectrum of **3**.

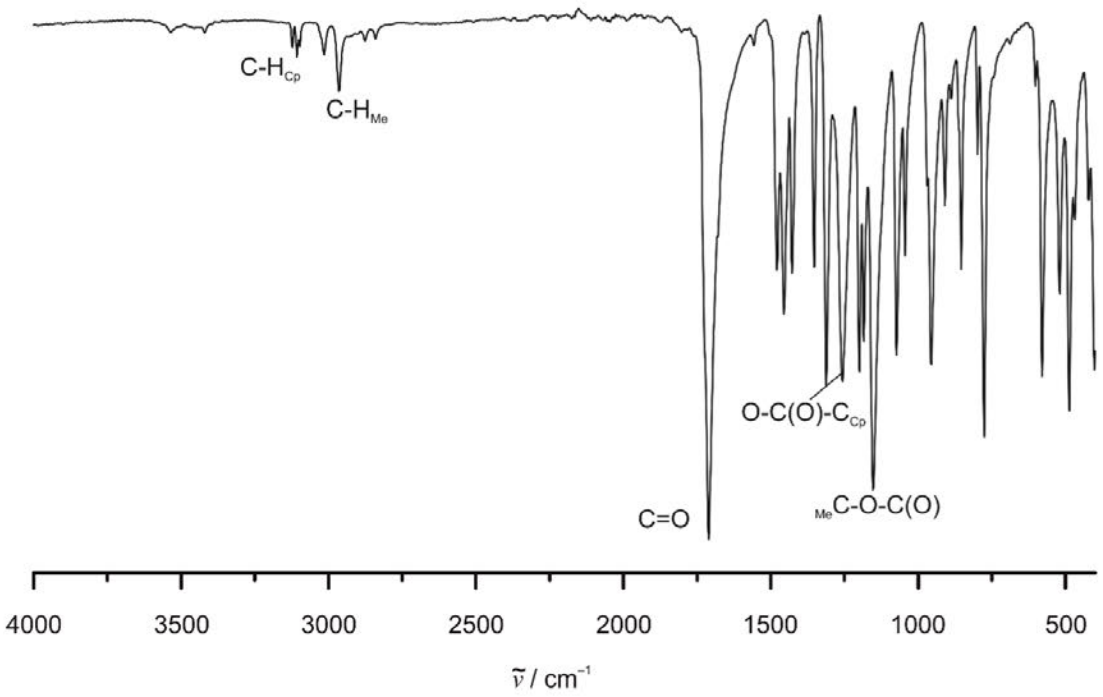

Figure S6: Solid state ATR IR-spectrum of **4**.

Table S1: IR spectroscopic data ($\tilde{\nu}_{CO}$ / cm^{-1}) of the C=O stretching vibrations of **1**–**4** and **1**$^+$–**4**$^+$, respectively and unscaled DFT[a] calculated and simulated bands ($\tilde{\nu}_{max(CO)}$ / cm^{-1}) and distinct calculated vibrations ($\tilde{\nu}_{CO}$ / cm^{-1}).

	solid	**solution**[b]	**DFT** $\tilde{\nu}_{max(CO)}$ ($\tilde{\nu}_{CO}$)
1	1709 (sh[c]), 1699	1712	1710
2	1709 (sh), 1699	1716	1712 (1715, 1711)
3	1730, 1712, 1678 (sh)	1720	1721 (1727, 1720, 1717)
4	1724 (sh), 1709, 1678 (sh)	1724	1724 (1733, 1724, 1722, 1720)
1$^+$	–	1738	1735
2$^+$	–	1740	1743 (1743, 1740)
3$^+$	–	1742	1748 (1748, 1744)
4$^+$	–	1743	1720 (1727, 1720, 1719, 1717)

[a] B3LYP, def2-TZVP, RIJCOSX, ZORA, CPCM(CH_2Cl_2),. [b] c = 68 mM (**1**) – 2 mM (**4**), CH_2Cl_2, 0.1 M [nBu$_4$N][B(C_6F_5)$_4$]. [c] sh = shoulder.

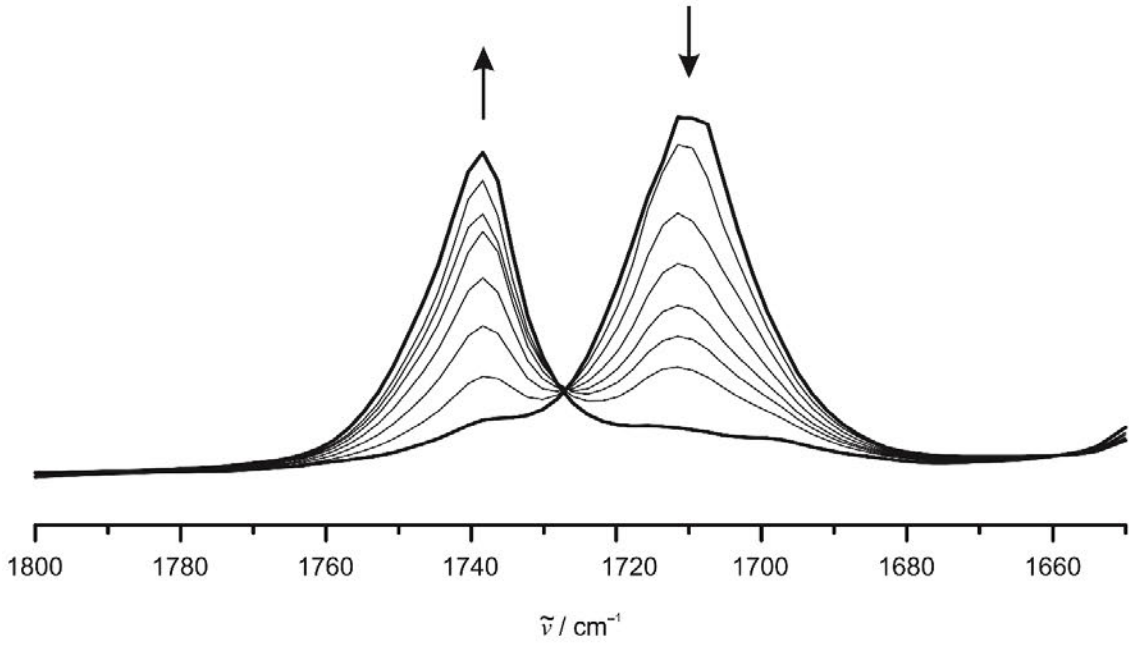

Figure S7: IR spectroelectrochemical oxidation of **1** to **1**$^+$ in CH_2Cl_2 / [*n*Bu$_4$N][B(C$_6$F$_5$)$_4$] (C=O strechting vibration region, 0.3–1.0 V vs. Ag pseudo reference electrode).

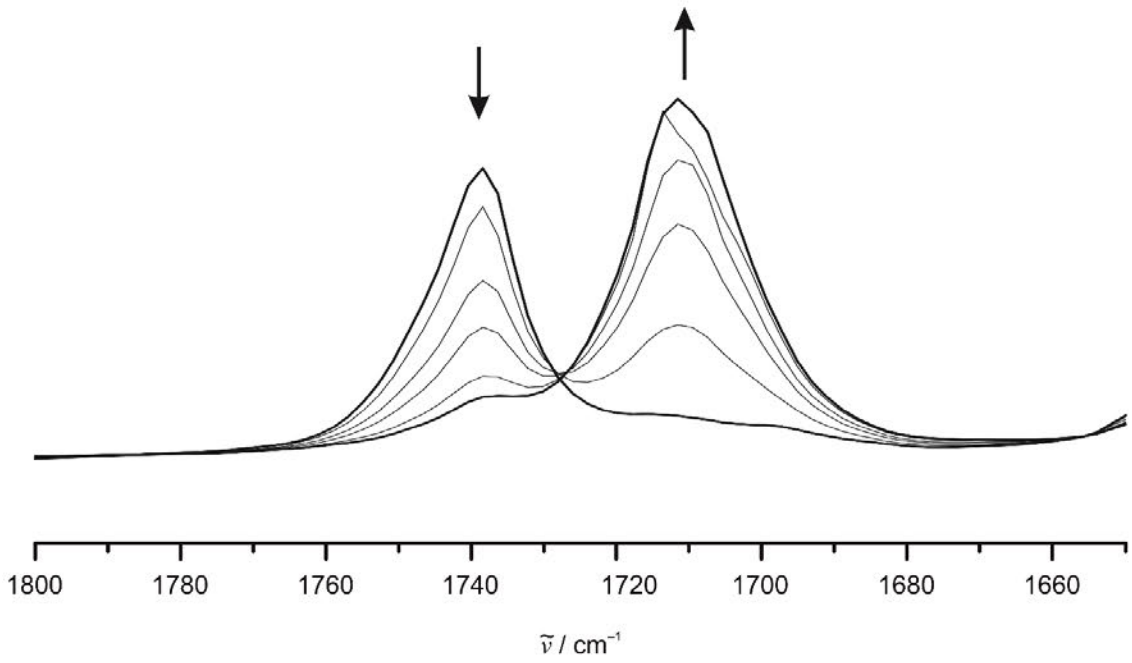

Figure S8: IR spectroelectrochemical reduction of **1**$^+$ to **1** in CH_2Cl_2 / [*n*Bu$_4$N][B(C$_6$F$_5$)$_4$] (C=O strechting vibration region, 1.0–(–0.2) V vs. Ag pseudo reference electrode).

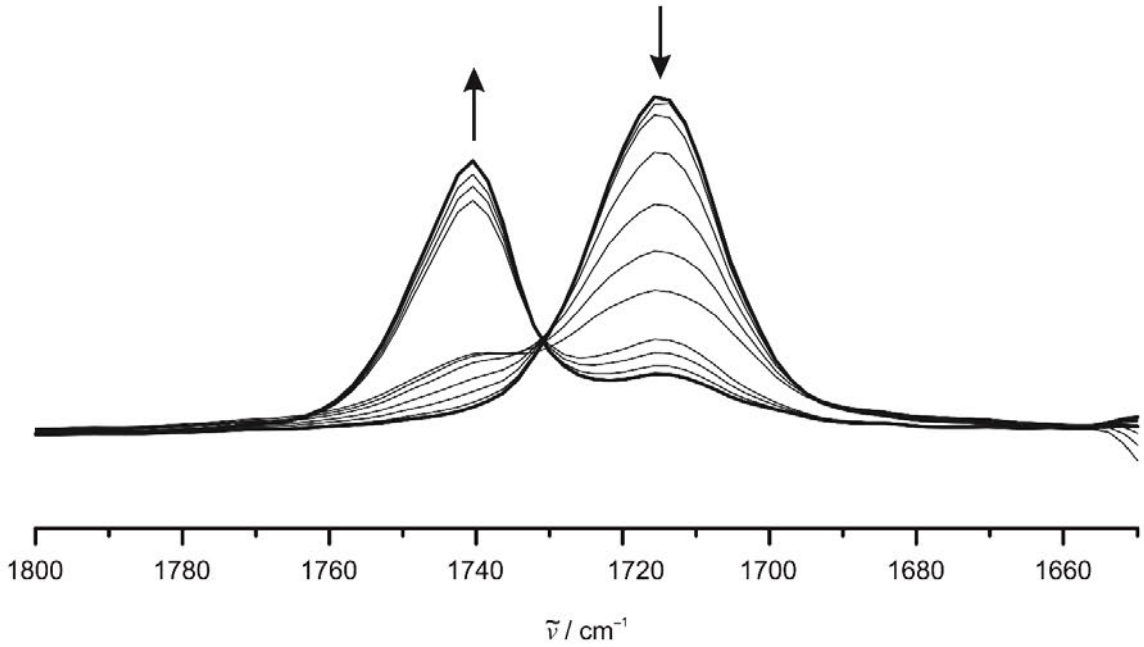

Figure S9: IR spectroelectrochemical oxidation of **2** to **2**$^{+}$ in CH_2Cl_2 / [*n*Bu$_4$N][B(C$_6$F$_5$)$_4$] (C=O strechting vibration region, 0.2–1.0 V vs. Ag pseudo reference electrode).

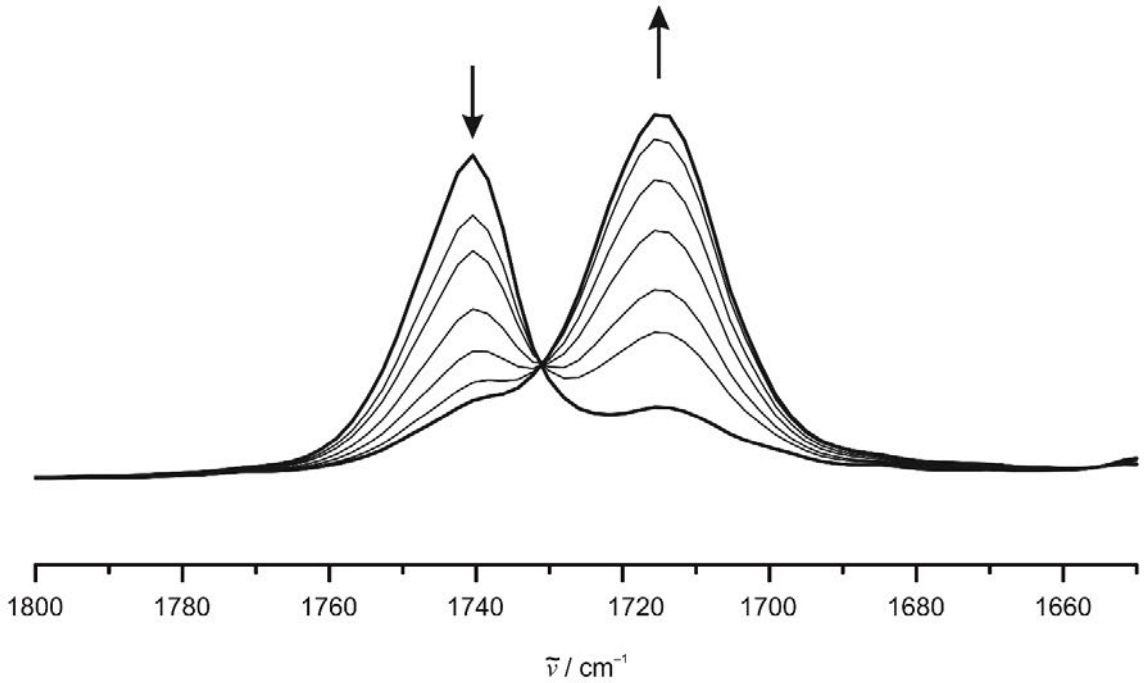

Figure S10: IR spectroelectrochemical reduction of **2**$^{+}$ to **2** in CH_2Cl_2 / [*n*Bu$_4$N][B(C$_6$F$_5$)$_4$] (C=O strechting vibration region, 1.0–0.0 V vs. Ag pseudo reference electrode).

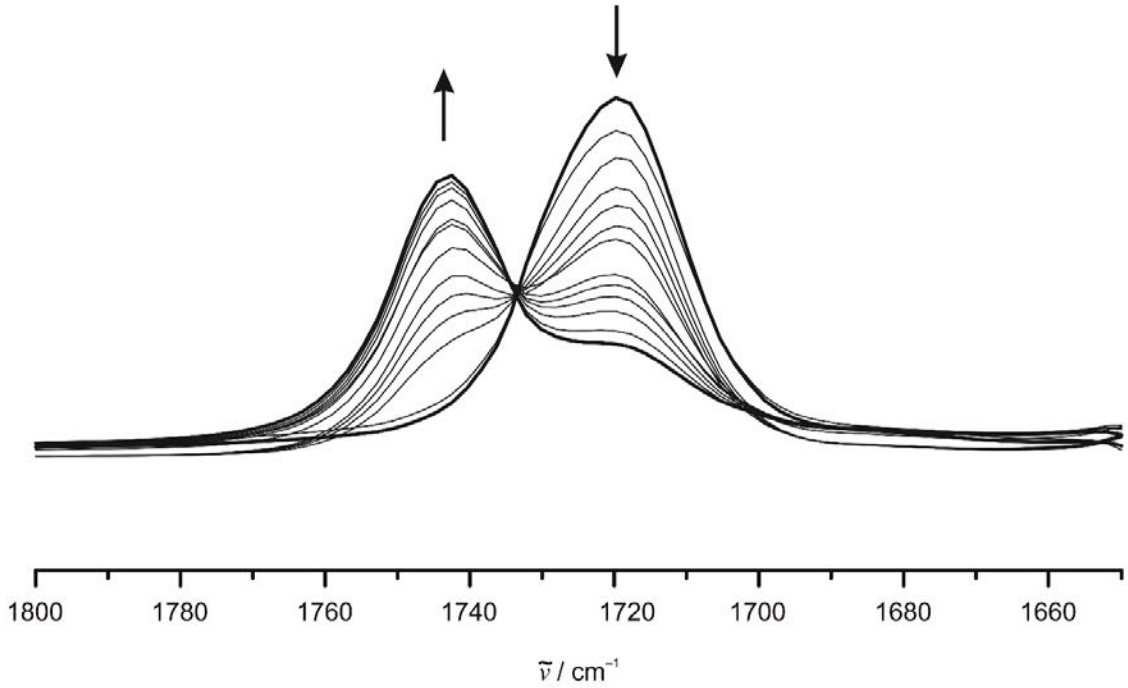

Figure S11: IR spectroelectrochemical oxidation of **3** to **3**$^{+}$ in CH_2Cl_2 / [*n*Bu$_4$N][B(C$_6$F$_5$)$_4$] (C=O strechting vibration region, 0.4–1.1 V vs. Ag pseudo reference electrode).

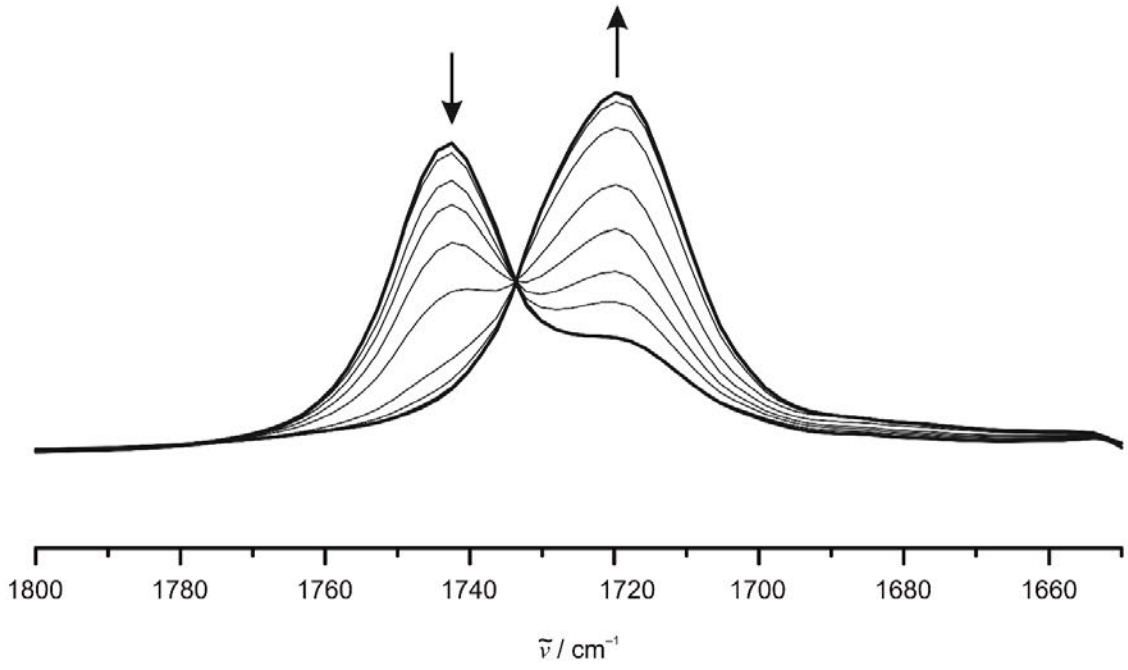

Figure S12: IR spectroelectrochemical reduction of **3**$^{+}$ to **3** in CH_2Cl_2 / [*n*Bu$_4$N][B(C$_6$F$_5$)$_4$] (C=O strechting vibration region, 1.1–(–0.2) V vs. Ag pseudo reference electrode).

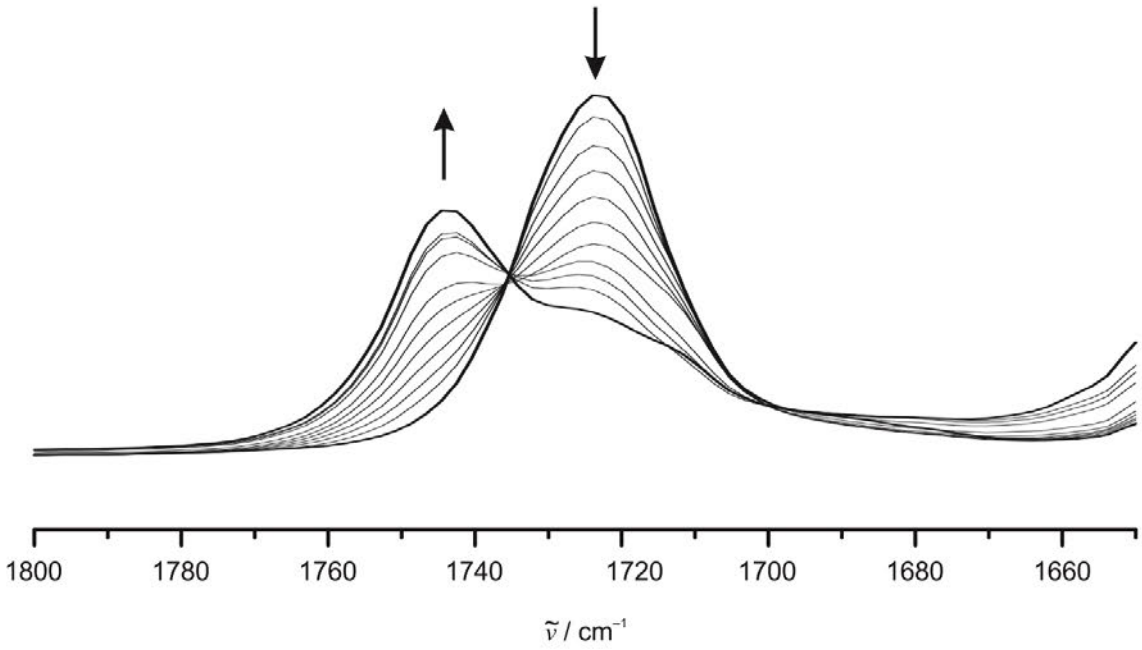

Figure S13: IR spectroelectrochemical oxidation of **4** to **4**$^{+}$ in CH_2Cl_2 / [*n*Bu$_4$N][B(C$_6$F$_5$)$_4$] (C=O strechting vibration region, 0.6–1.4 V vs. Ag pseudo reference electrode).

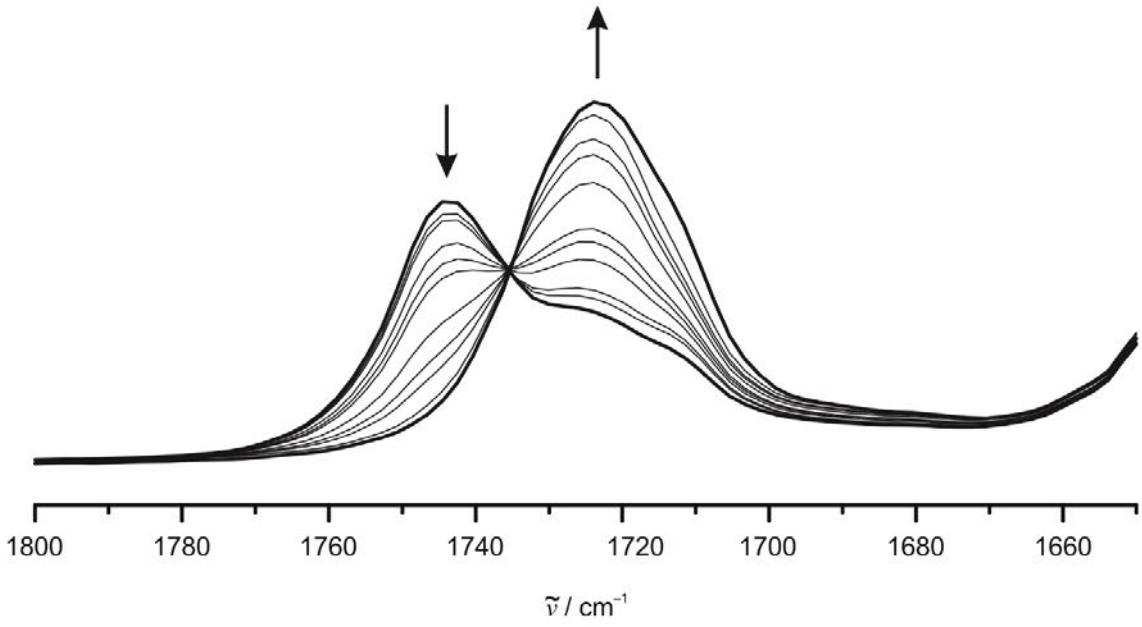

Figure S14: IR spectroelectrochemical reduction of **4**$^{+}$ to **4** in CH_2Cl_2 / [*n*Bu$_4$N][B(C$_6$F$_5$)$_4$] (C=O strechting vibration region, 1.4–(–0.3) V vs. Ag pseudo reference electrode).

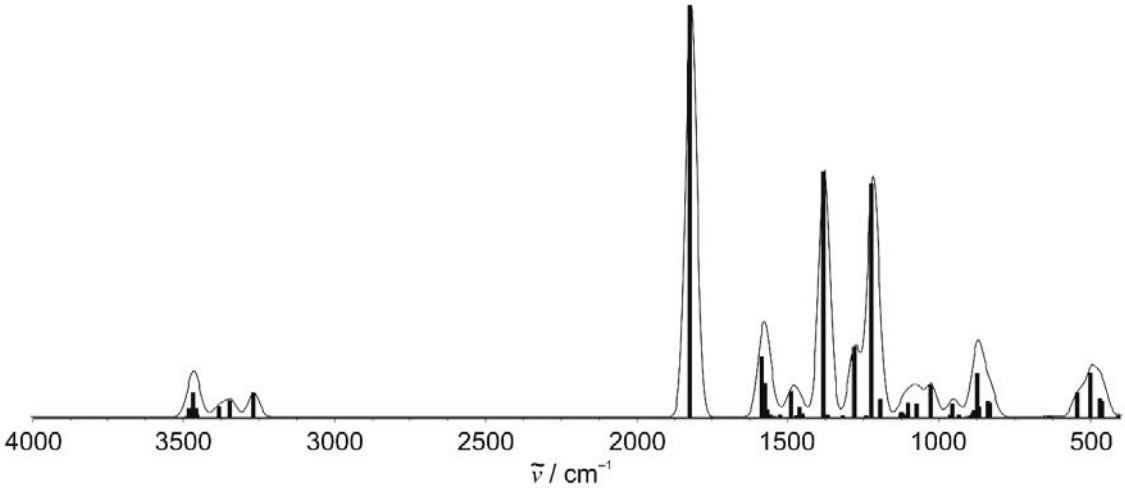

Figure S15: DFT calculated IR spectrum of **1**. [B3LYP, def2-TZVP, RIJCOSX, ZORA, CPCM(CH_2Cl_2), fwhm: 40 cm^{-1}].

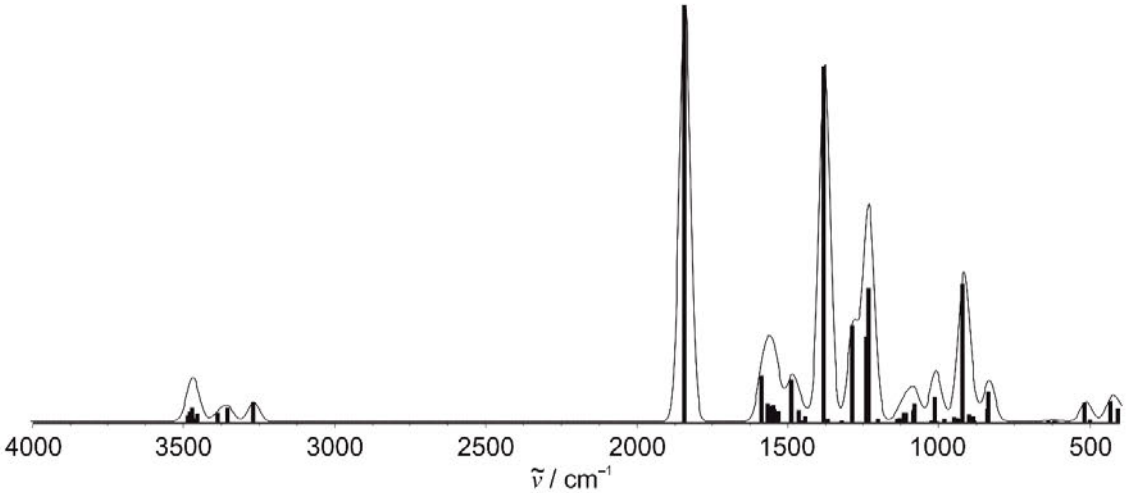

Figure S16: DFT calculated IR spectrum of **1**$^+$. [B3LYP, def2-TZVP, RIJCOSX, ZORA, CPCM(CH_2Cl_2), fwhm: 40 cm^{-1}].

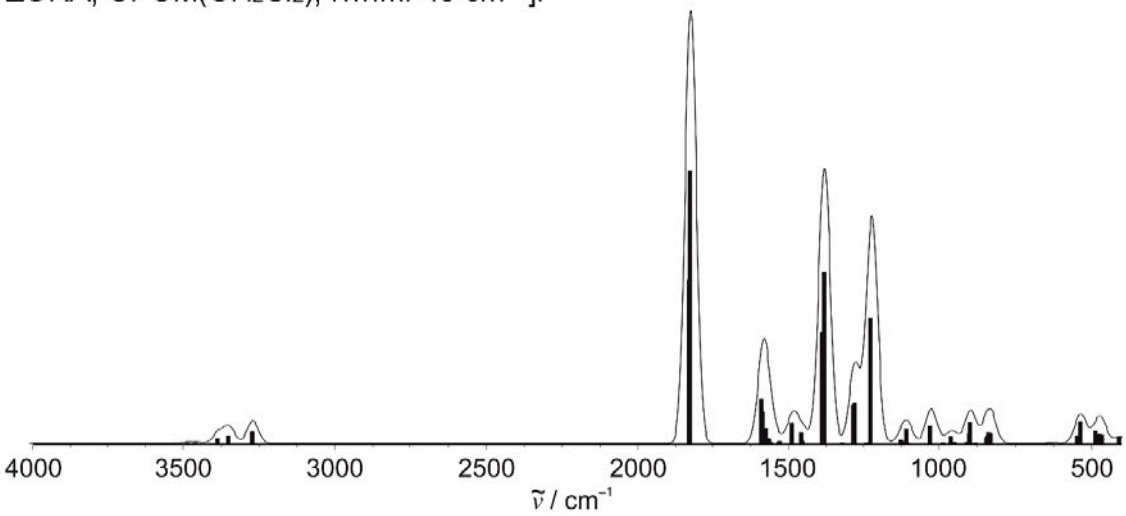

Figure S17: DFT calculated IR spectrum of **2**. [B3LYP, def2-TZVP, RIJCOSX, ZORA, CPCM(CH_2Cl_2), fwhm: 40 cm^{-1}].

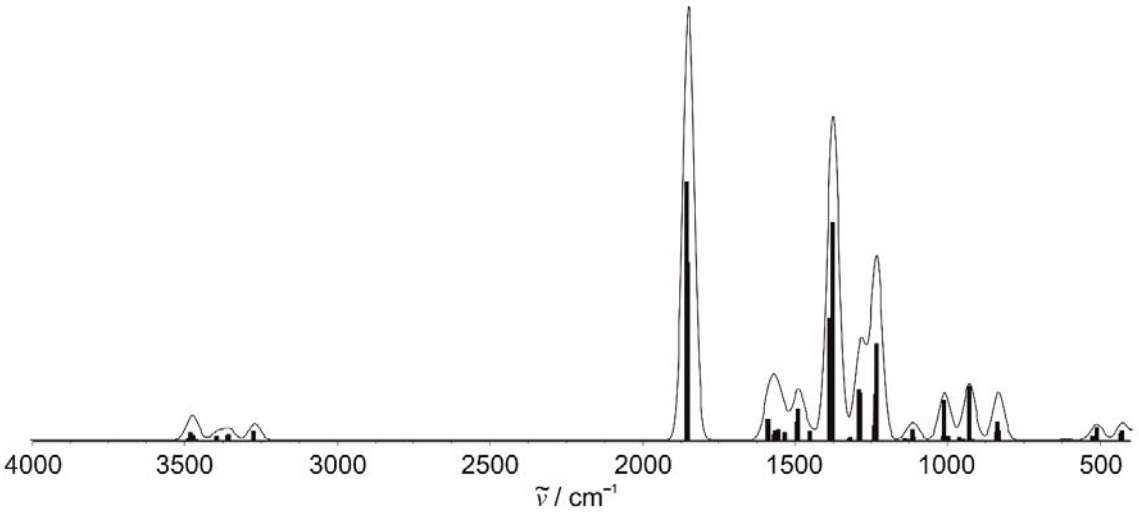

Figure S18: DFT calculated IR spectrum of **2**$^{+}$. [B3LYP, def2-TZVP, RIJCOSX, ZORA, CPCM(CH_2Cl_2), fwhm: 40 cm^{-1}].

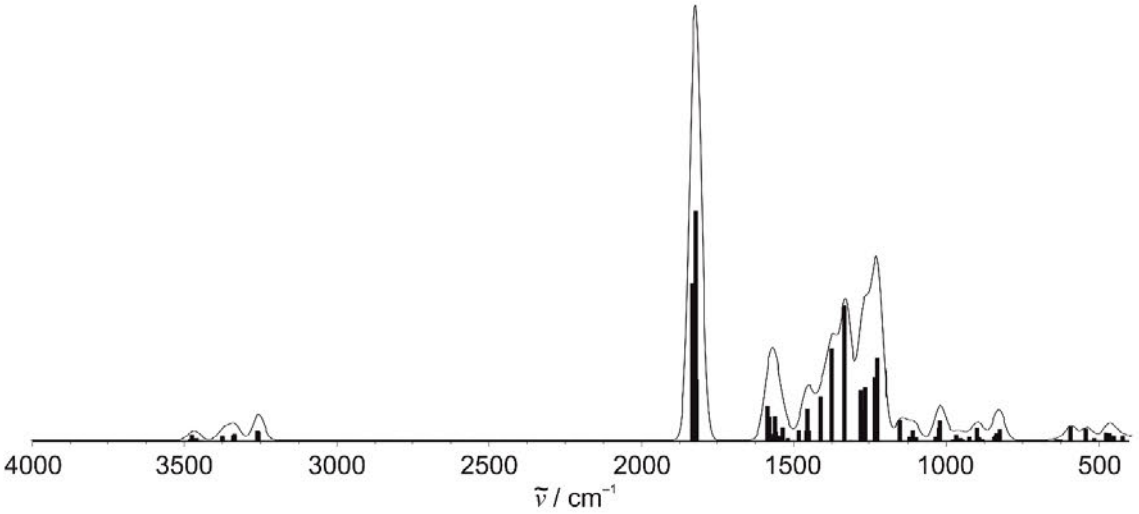

Figure S19: DFT calculated IR spectrum of **3**. [B3LYP, def2–TZVP, RIJCOSX, ZORA, CPCM(CH_2Cl_2), fwhm: 40 cm^{-1}].

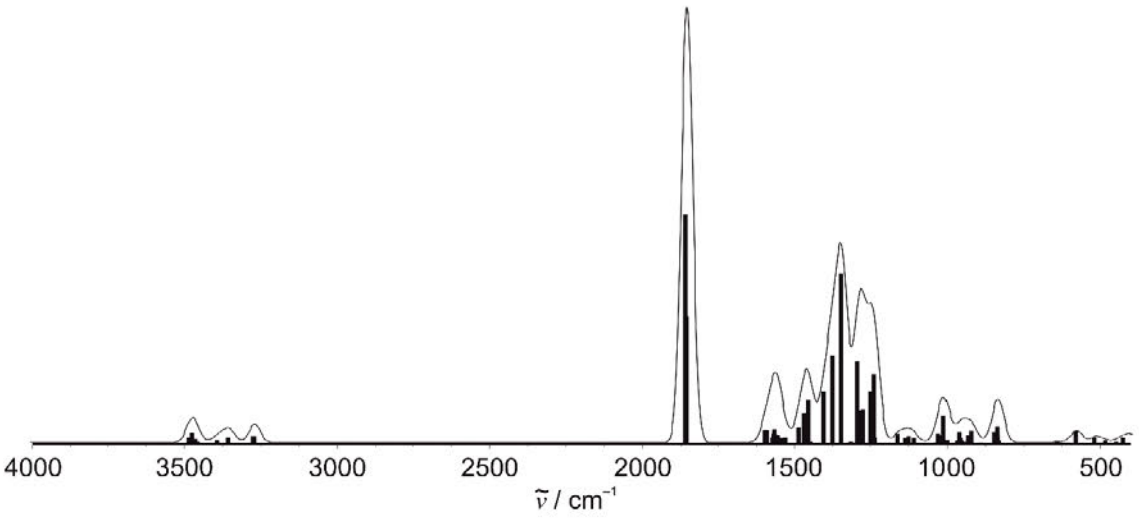

Figure S20: DFT calculated IR spectrum of **3**$^{+}$. [B3LYP, def2-TZVP, RIJCOSX, ZORA, CPCM(CH_2Cl_2), fwhm: 40 cm^{-1}].

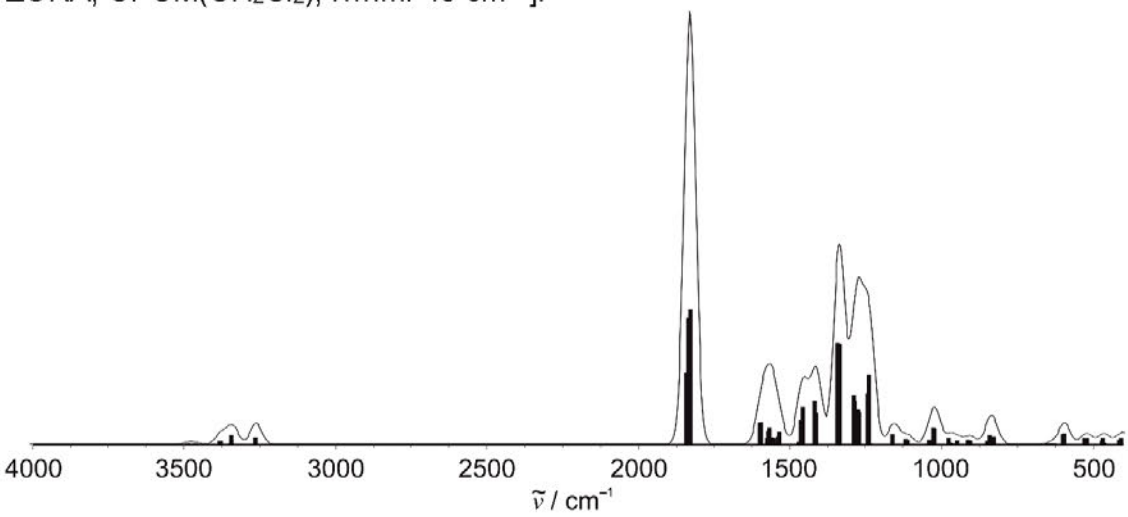

Figure S21: DFT calculated IR spectrum of **4**. [B3LYP, def2-TZVP, RIJCOSX, ZORA, CPCM(CH_2Cl_2), fwhm: 40 cm^{-1}].

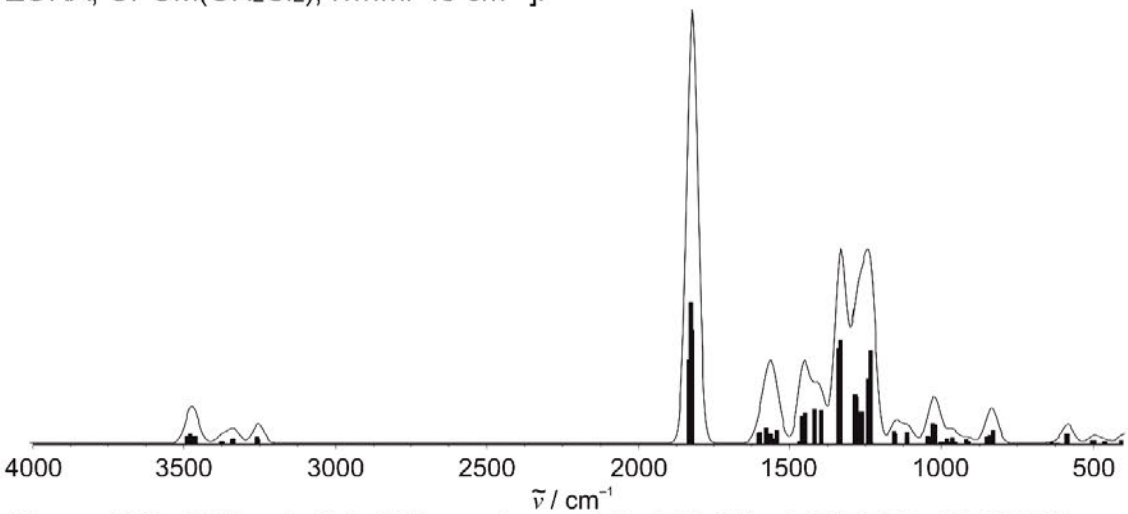

Figure S22: DFT calculated IR spectrum of **4**$^{+}$. [B3LYP, def2-TZVP, RIJCOSX, ZORA, CPCM(CH_2Cl_2), fwhm: 40 cm^{-1}].

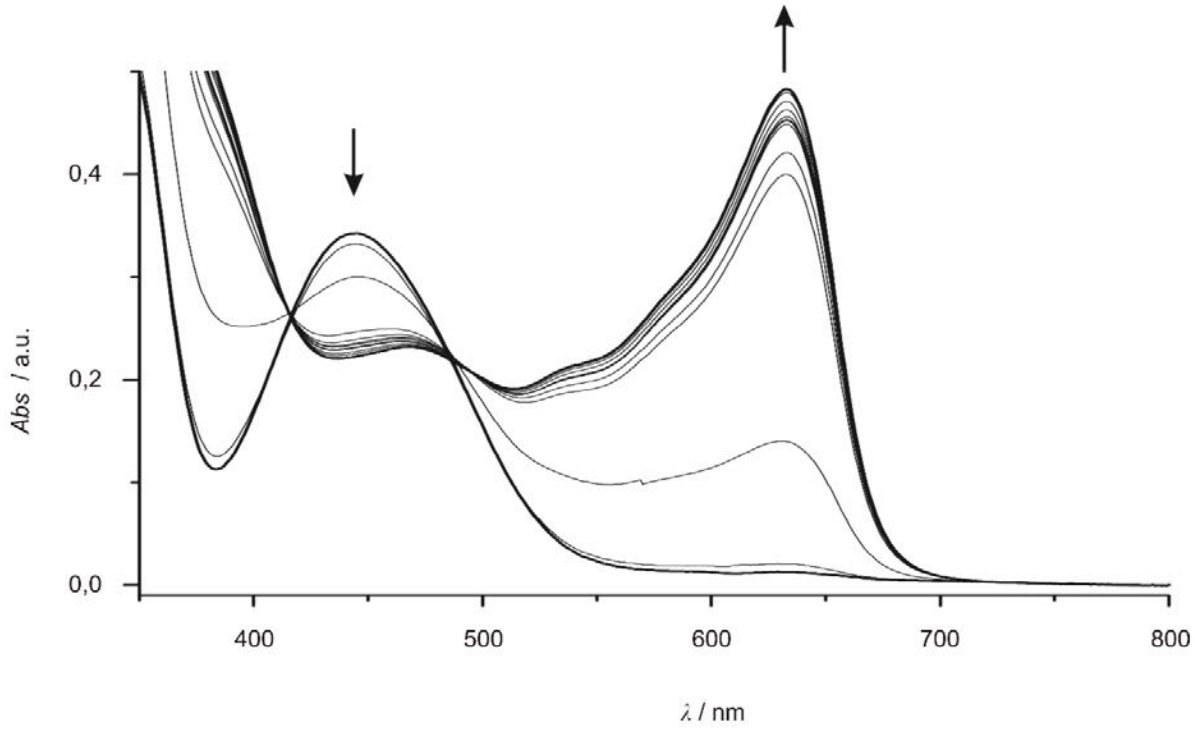

Figure S23: UV/Vis spectroelectrochemical oxidation of **1** in CH_2Cl_2 / [*n*Bu$_4$N][B(C_6F_5)$_4$] (0.3–1.0 V vs. Ag pseudo reference electrode).

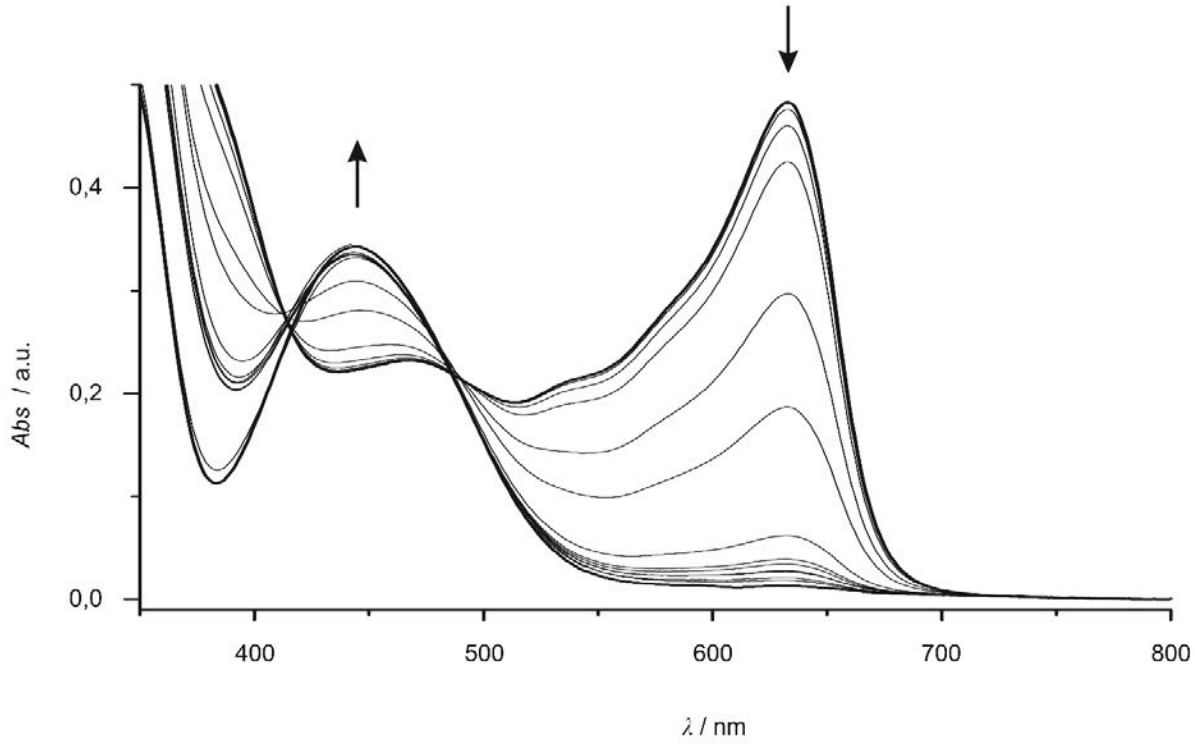

Figure S24: UV/Vis spectroelectrochemical reduction of **1**$^+$ in CH_2Cl_2 / [*n*Bu$_4$N][B(C_6F_5)$_4$] (1.0–(–0.2) V vs. Ag pseudo reference electrode).

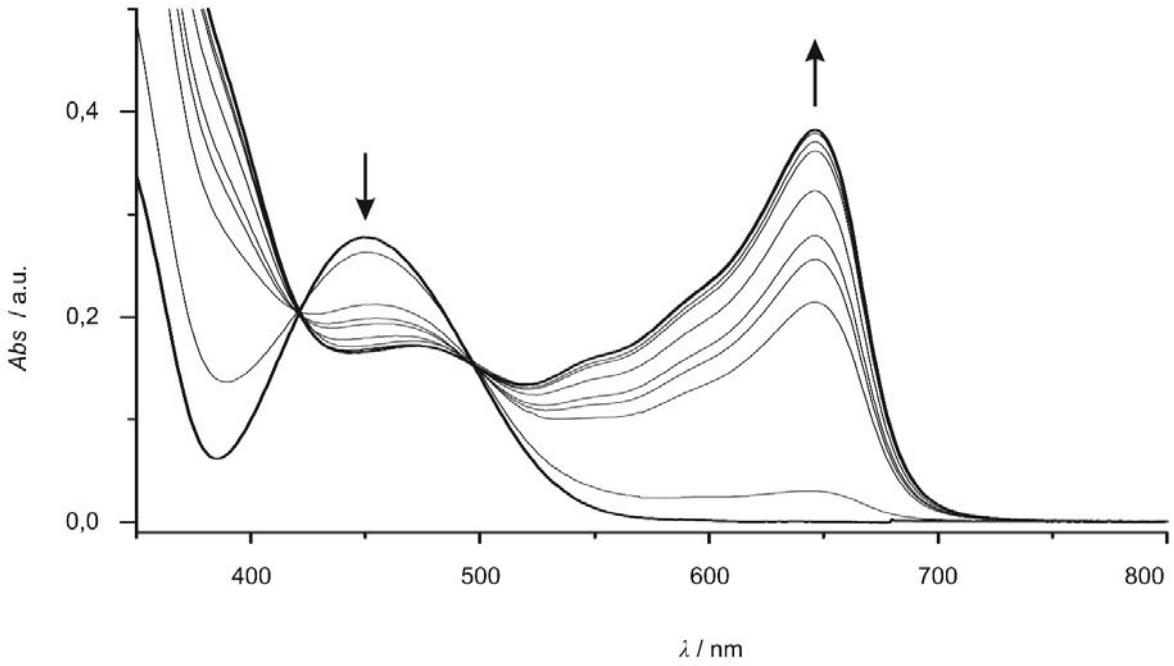

Figure S25: UV/Vis spectroelectrochemical oxidation of **2** in CH_2Cl_2 / [nBu$_4$N][B(C_6F_5)$_4$] (0.2–1.0 V vs. Ag pseudo reference electrode).

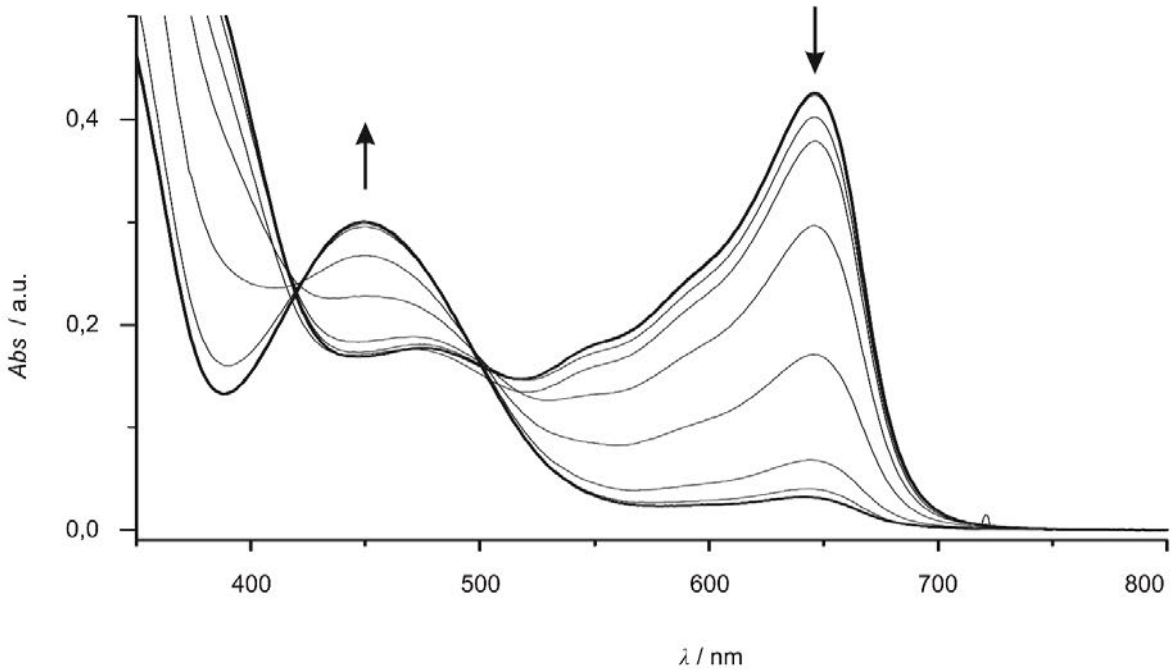

Figure S26: UV/Vis spectroelectrochemical reduction of **2**$^+$ in CH_2Cl_2 / [nBu$_4$N][B(C_6F_5)$_4$] (1.0–0.0 V vs. Ag pseudo reference electrode).

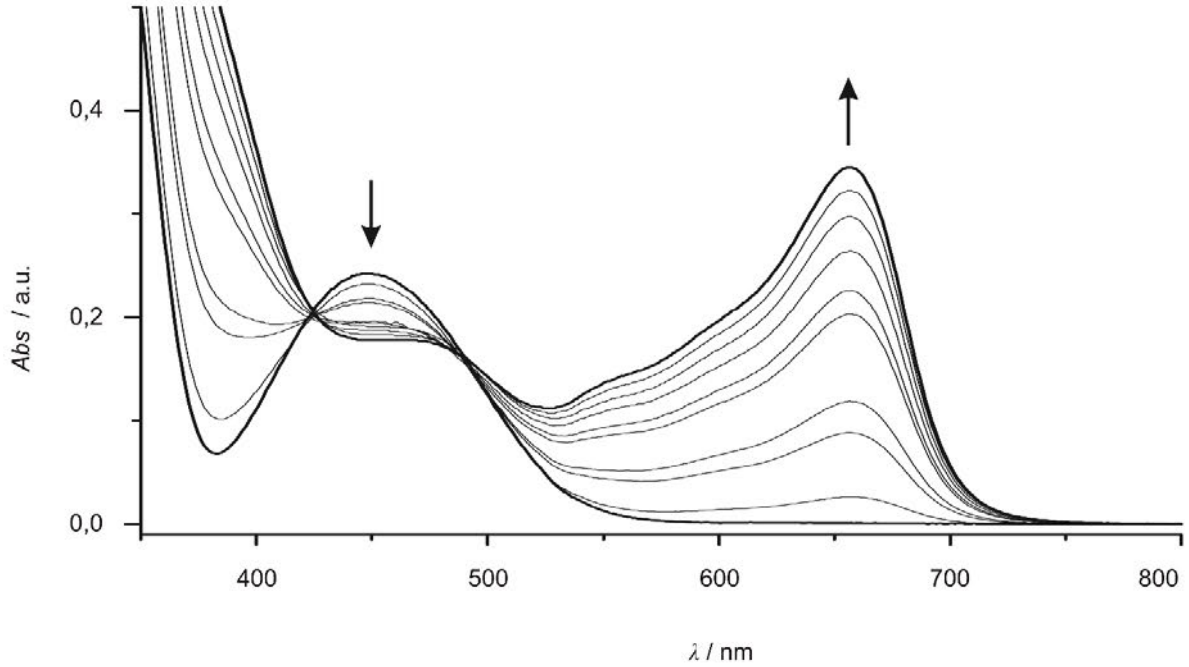

Figure S27: UV/Vis spectroelectrochemical oxidation of **3** in CH_2Cl_2 / [*n*Bu$_4$N][B(C$_6$F$_5$)$_4$] (0.4–1.1 V vs. Ag pseudo reference electrode).

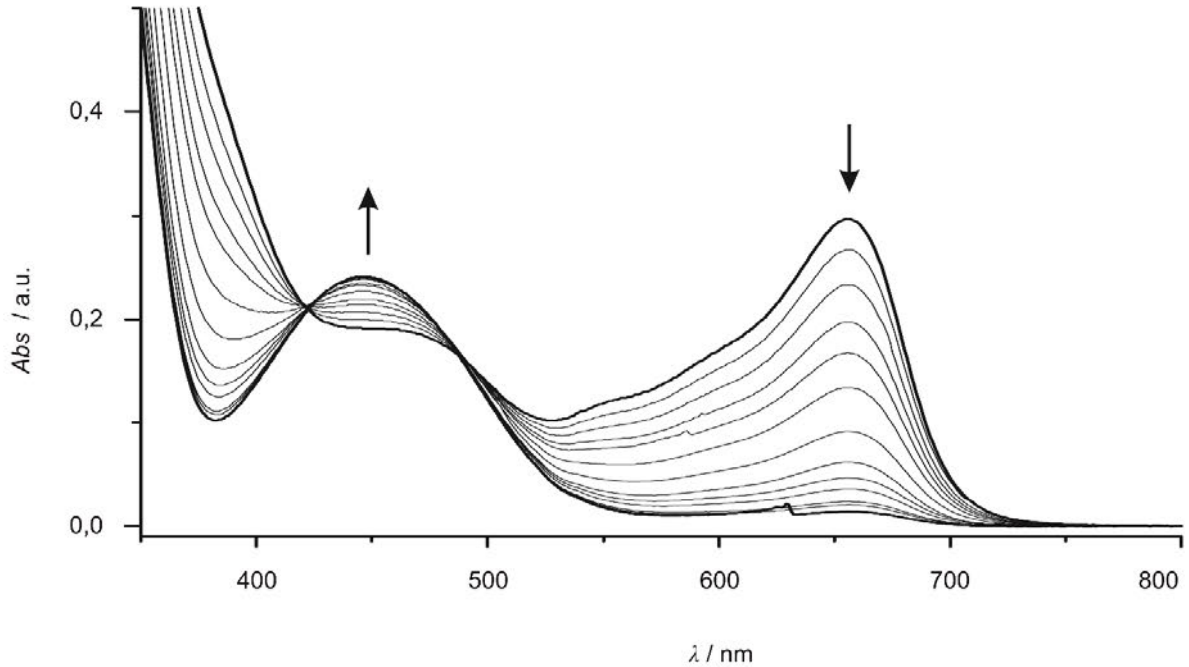

Figure S28: UV/Vis spectroelectrochemical reduction of **3**$^+$ in CH_2Cl_2 / [*n*Bu$_4$N][B(C$_6$F$_5$)$_4$] (1.1–(–0.2) V vs. Ag pseudo reference electrode).

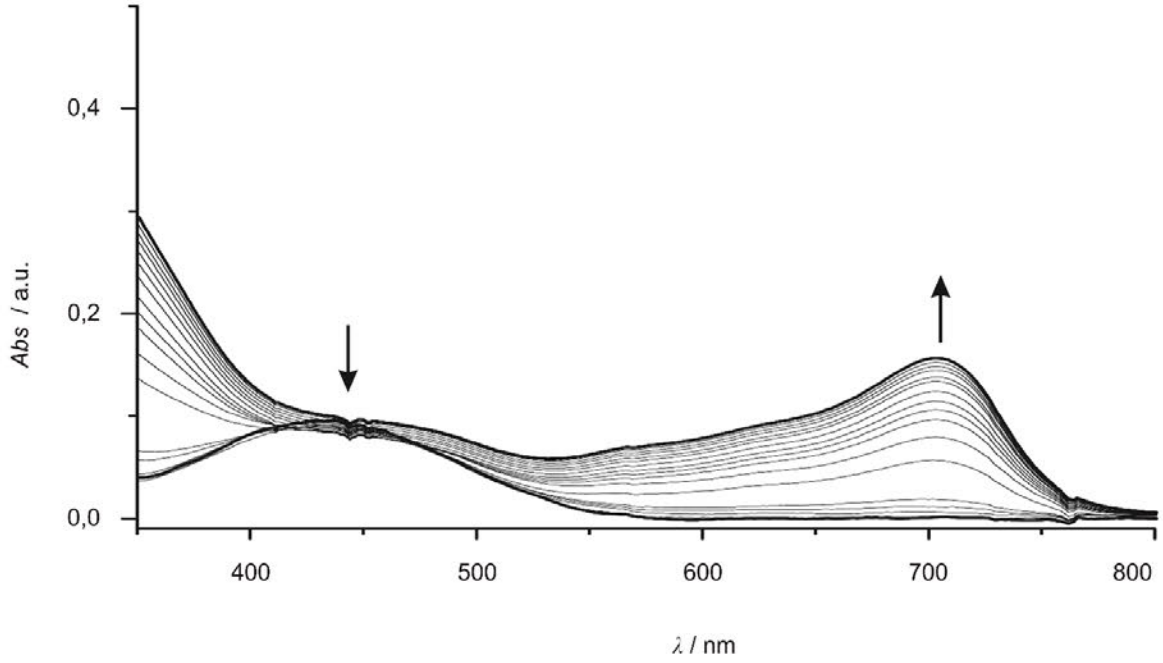

Figure S29: UV/Vis spectroelectrochemical oxidation of **4** in CH_2Cl_2 / [nBu$_4$N][B(C_6F_5)$_4$] (0.6–1.4 V vs. Ag pseudo reference electrode).

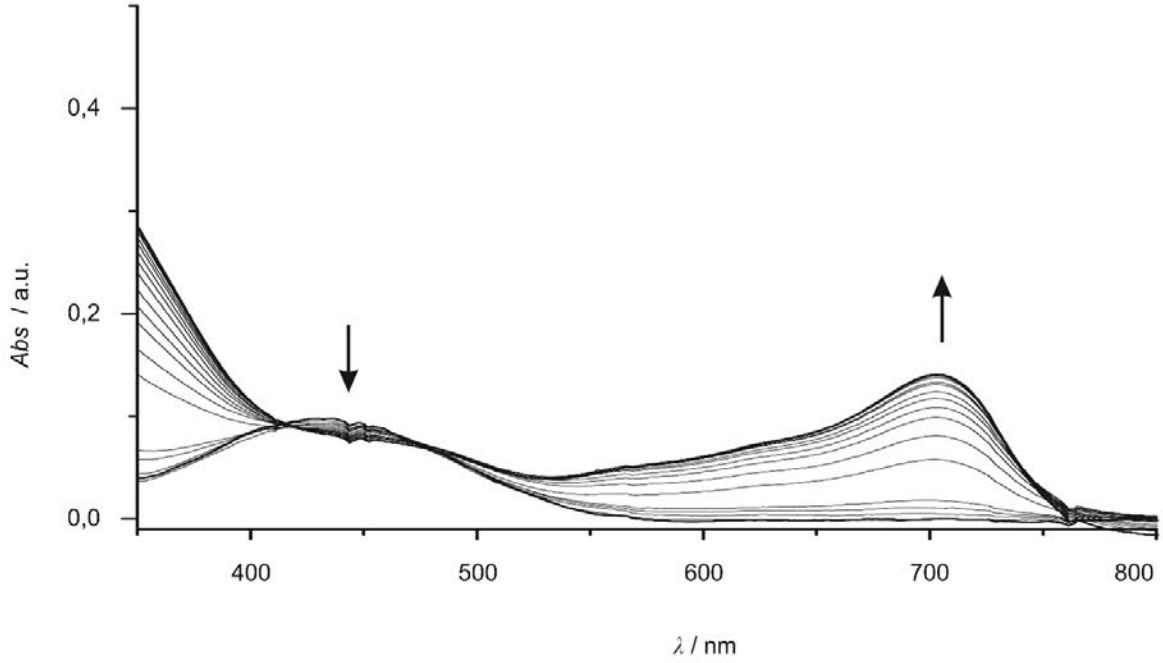

Figure S30: UV/Vis spectroelectrochemical oxidation of **4** in CH_2Cl_2 / [nBu$_4$N][B(C_6F_5)$_4$] (0.6–1.4 V vs. Ag pseudo reference electrode, with manual baseline correction).

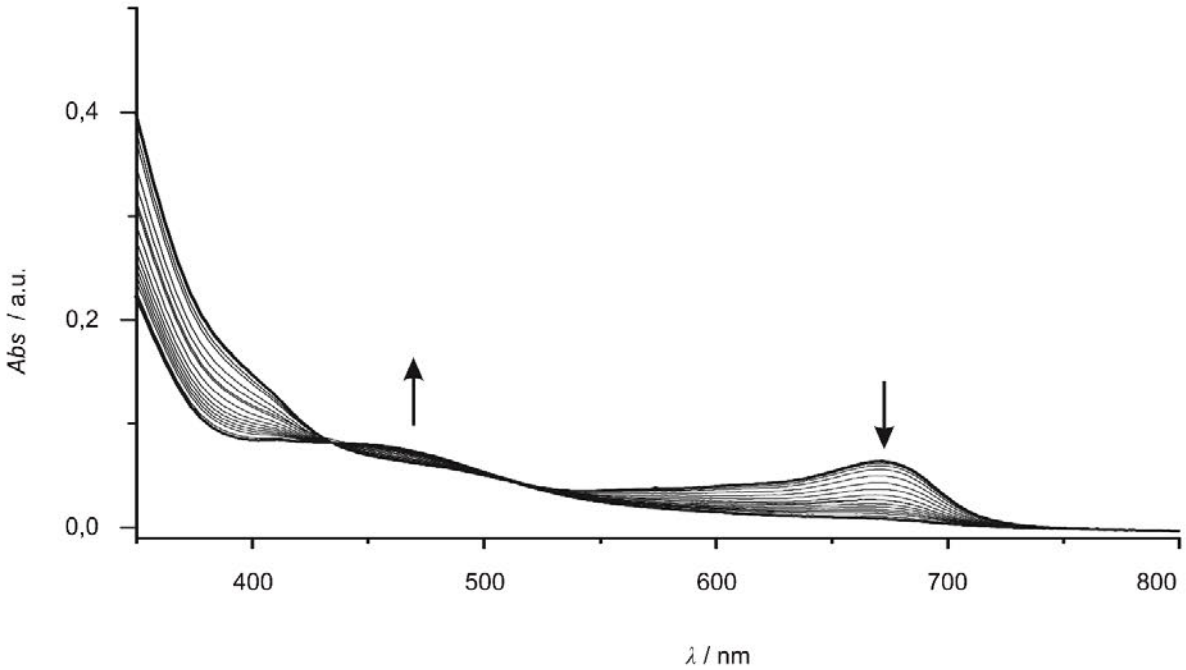

Figure S31: UV/Vis spectroelectrochemical reduction of **4**$^{+}$ in CH_2Cl_2 / [*n*Bu$_4$N][B(C$_6$F$_5$)$_4$] (1.4–(–0.3) V vs. Ag pseudo reference electrode).

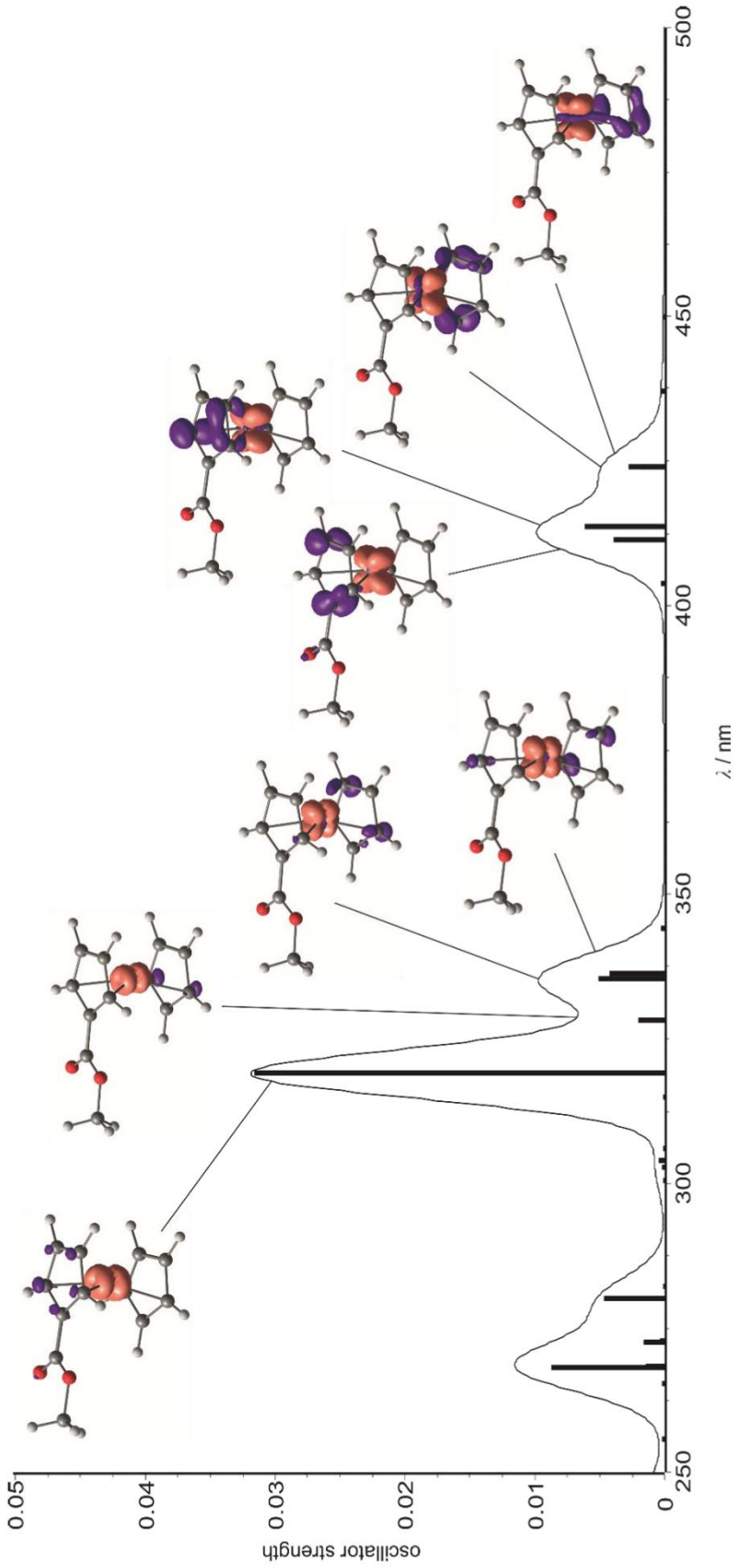

Figure S32: TD-DFT calculated UV/Vis spectrum of **1**$^{+}$ with electron difference density [B3LYP, def2-TZVP, RIJCOSX, ZORA, CPCM(CH_2Cl_2), (isosurface values 0.01 a.u.; fwhm: 10 nm)].

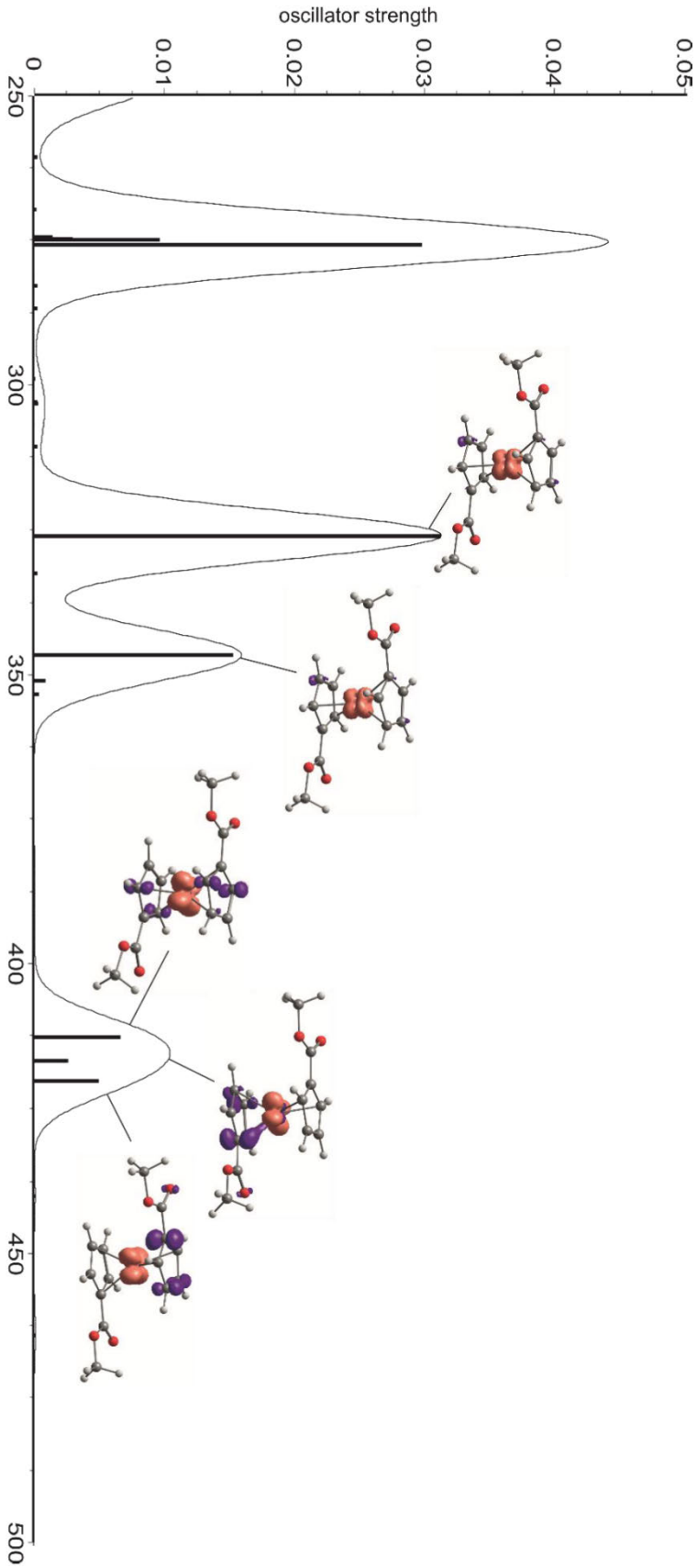

Figure S33: TD-DFT calculated UV/Vis spectrum of **2⁺** with electron difference density [B3LYP, def2-TZVP, RIJCOSX, ZORA, CPCM(CH_2Cl_2), (isosurface values 0.01 a.u.; fwhm: 10 nm)].

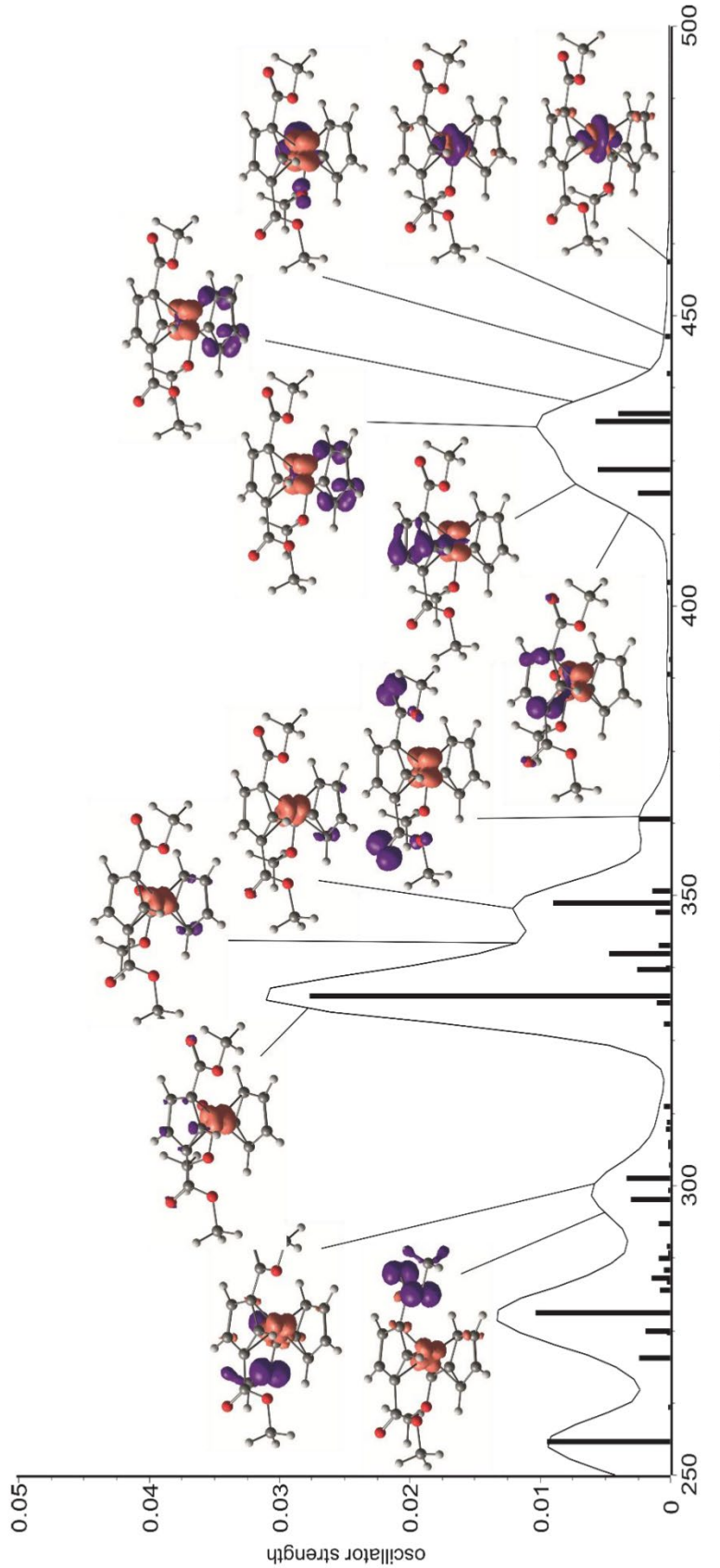

Figure S34: TD-DFT calculated UV/Vis spectrum of **3**$^{+}$ with electron difference density [B3LYP, def2-TZVP, RIJCOSX, ZORA, CPCM(CH_2Cl_2), (isosurface values 0.01 a.u.; fwhm: 10 nm)].

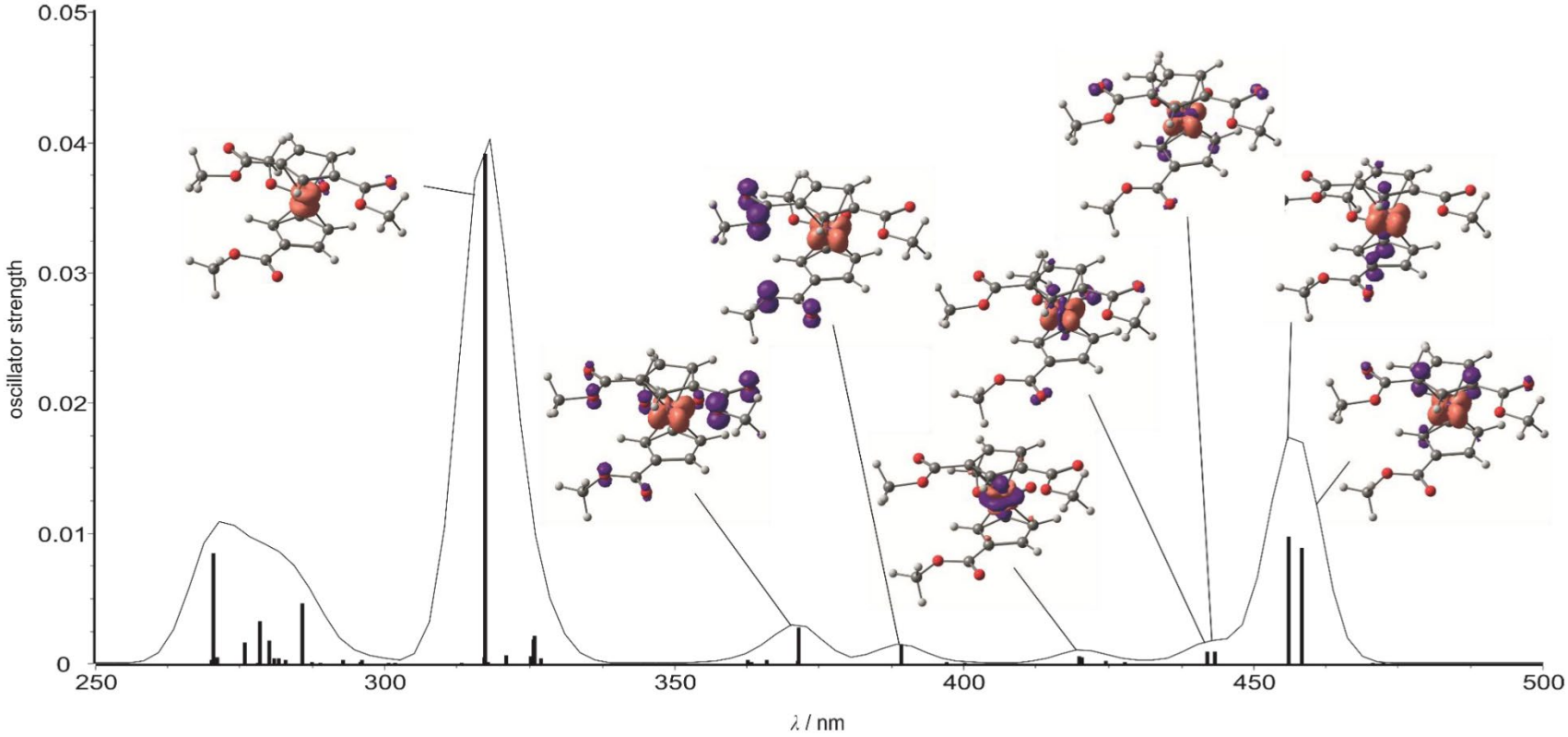

Figure S35: TD-DFT calculated UV/Vis spectrum of **4**$^{+}$ with electron difference density [B3LYP, def2-TZVP, RIJCOSX, ZORA, CPCM(CH_2Cl_2), (isosurface values 0.01 a.u.; fwhm: 10 nm)].

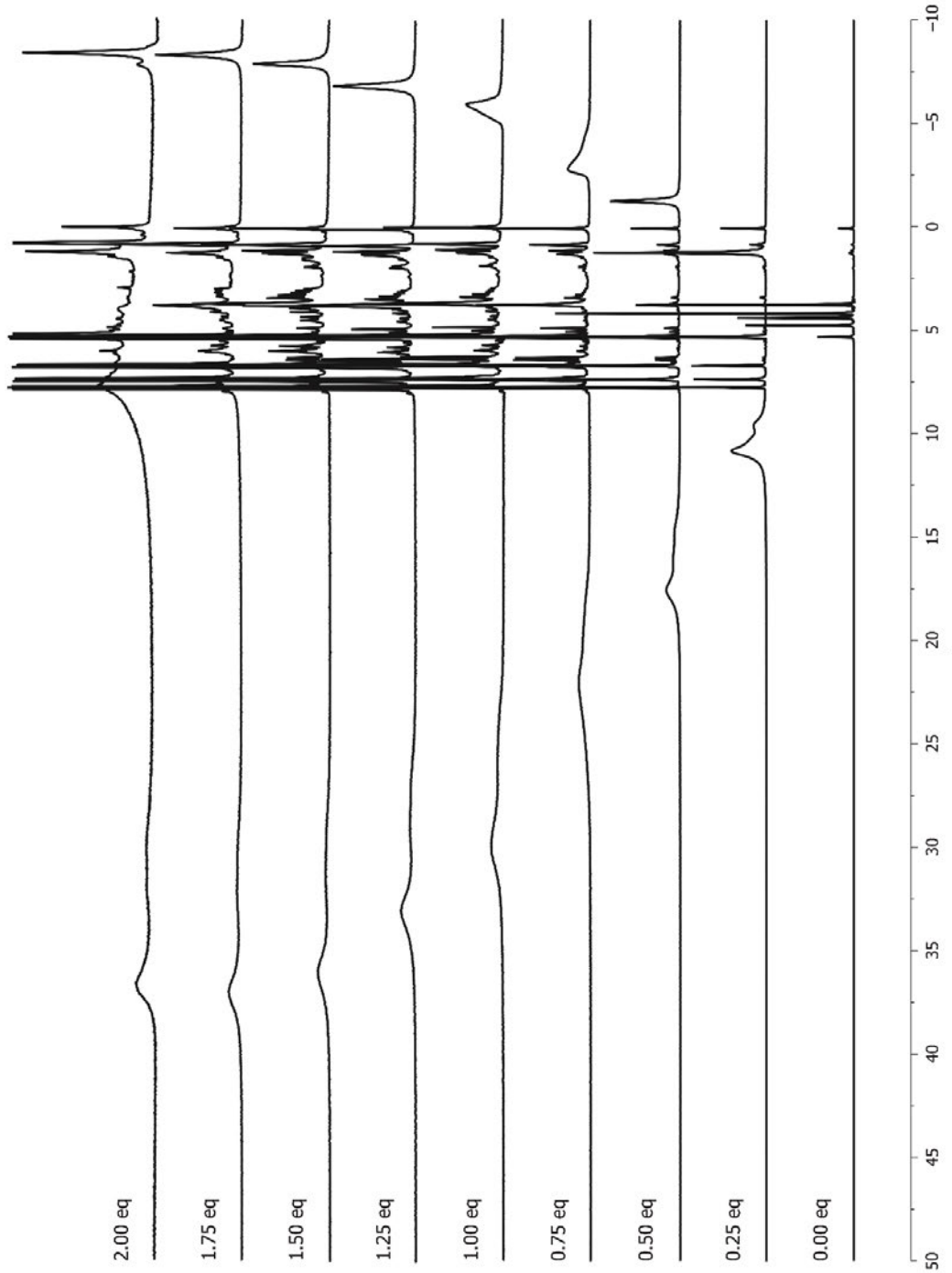

Figure S36: ^{1}H NMR oxidation titration of **1** in CD_2Cl_2 with $[N(2,4\text{-}C_6H_3Br_2)_3]^+$ as oxidant.

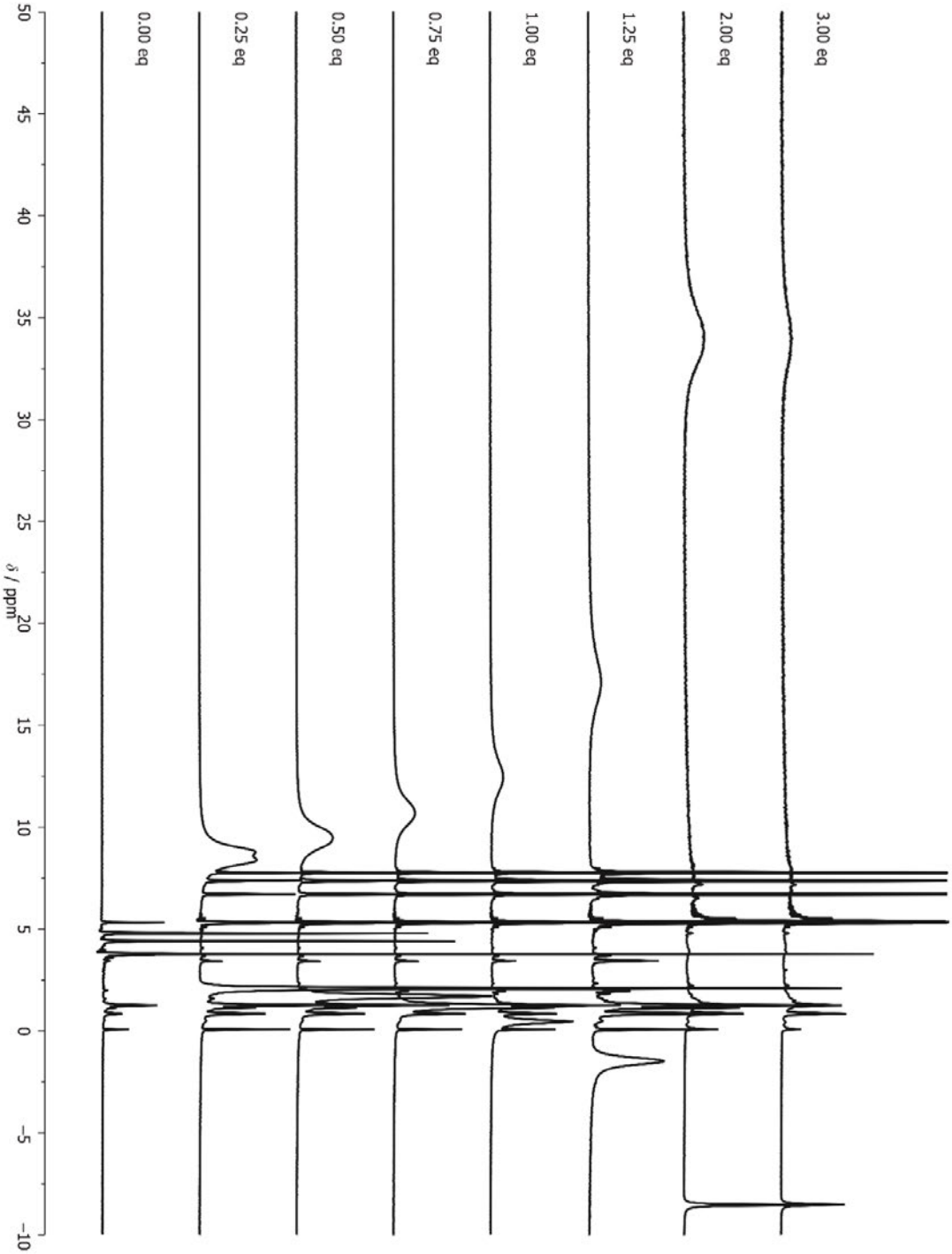

Figure S37: ^{1}H NMR oxidation titration of **2** in CD_2Cl_2 with $[N(2,4\text{-}C_6H_3Br_2)_3]^+$ as oxidant.

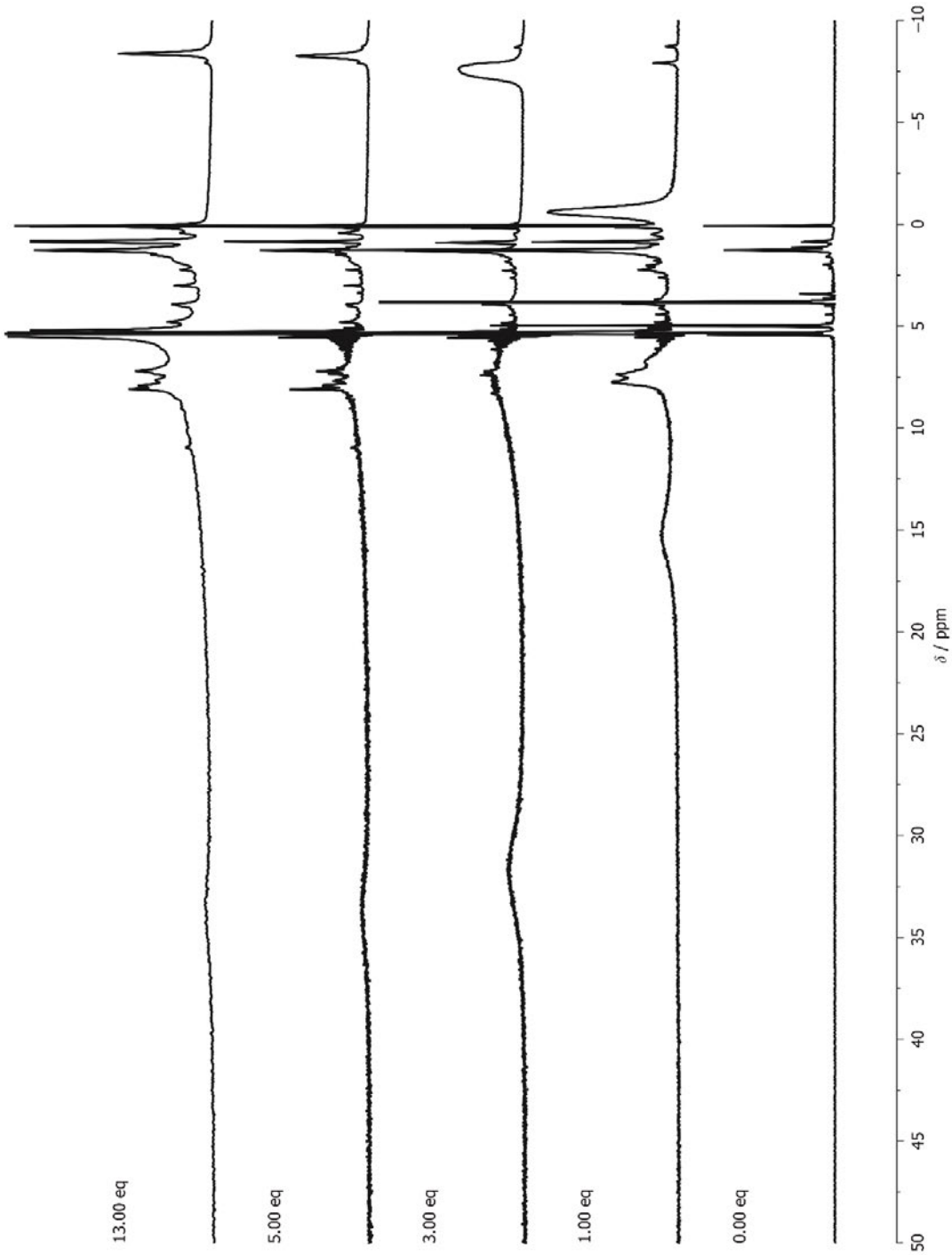

Figure S38: ^{1}H NMR oxidation titration of **4** in CD_2Cl_2 with $[N(2,4\text{-}C_6H_3Br_2)_3]^+$ as oxidant.

S24

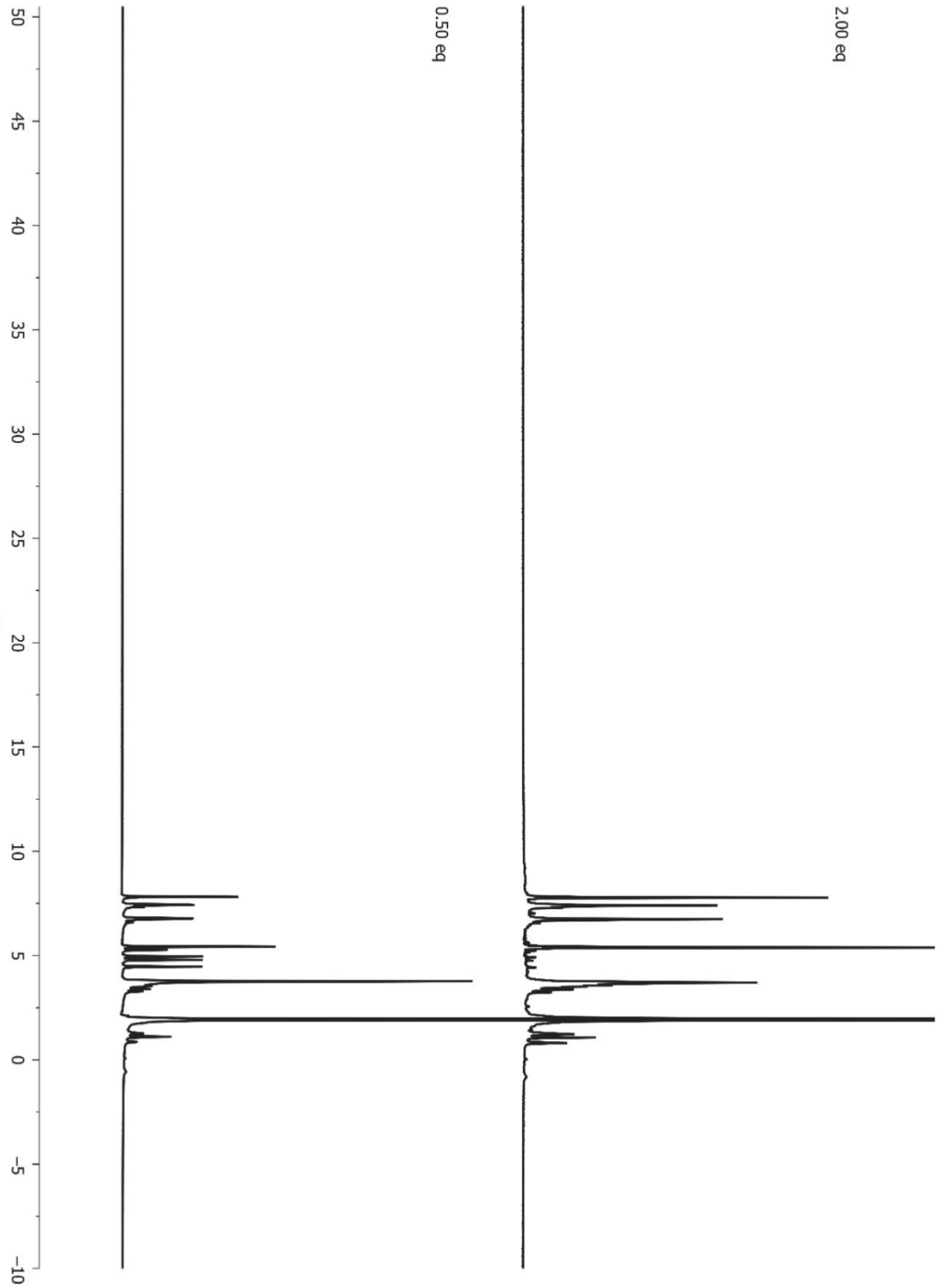

Figure S39: ^{1}H NMR oxidation titration of **3** in CD_3CN with $[N(2,4\text{-}C_6H_3Br_2)_3]^+$ as oxidant.

6.2 Supporting Information: Protic Ferrocenyl Acyclic Diamino Carbene Gold(I) Complexes

European Journal of Inorganic Chemistry

Supporting Information

Protic Ferrocenyl Acyclic Diamino Carbene Gold(I) Complexes

Sven D. Waniek, Christoph Förster,* and Katja Heinze*

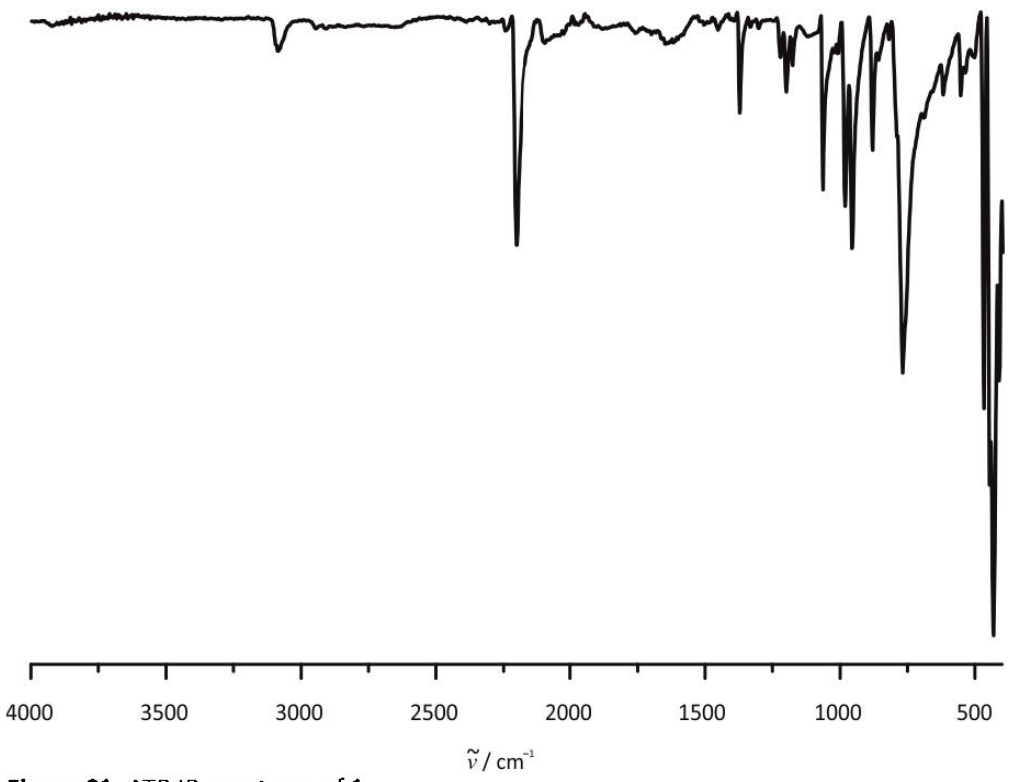

Figure S1. ATR IR spectrum of **1**.

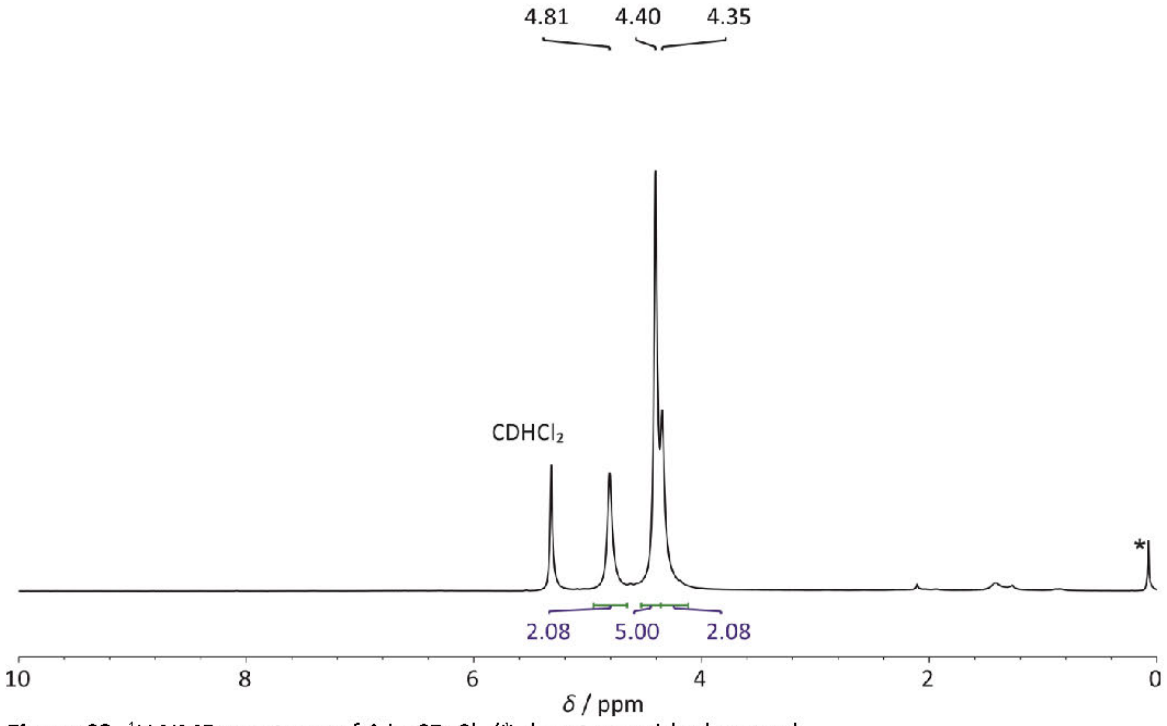

Figure S2. ^{1}H NMR spectrum of **1** in CD_2Cl_2 (* denotes residual grease).

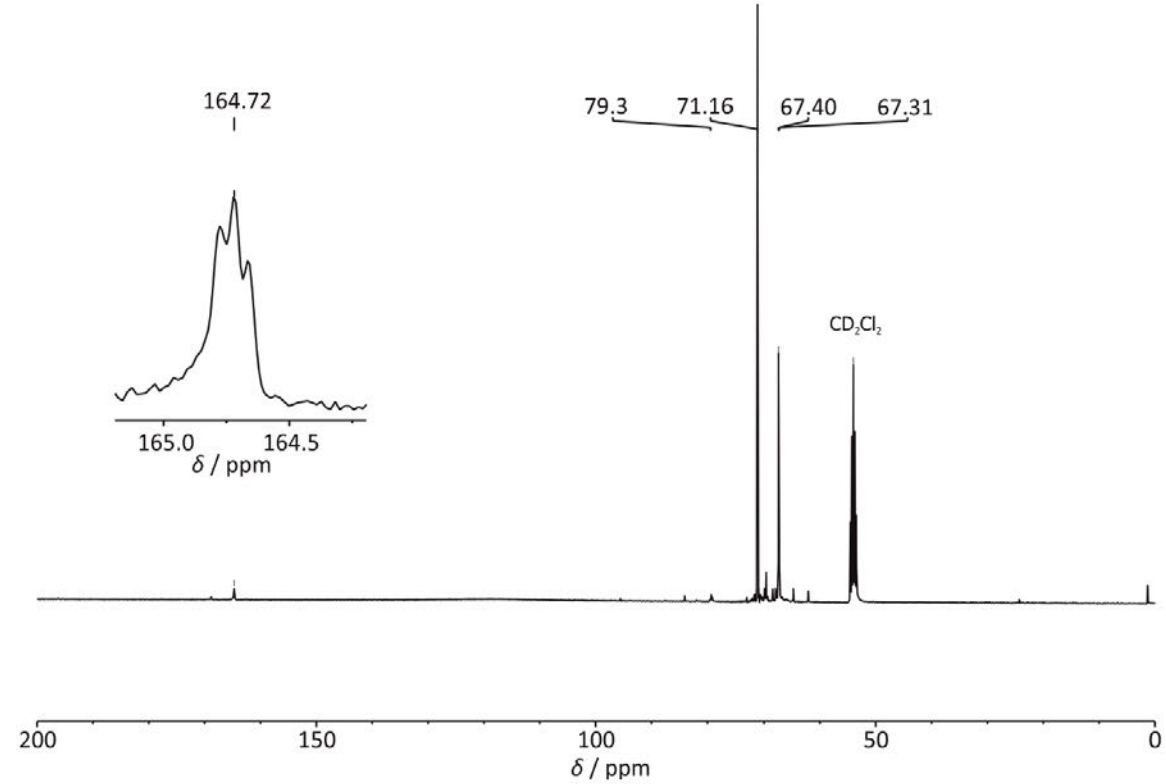

Figure S3. $^{13}C\{^{1}H\}$ NMR spectrum of **1** in CD_2Cl_2.

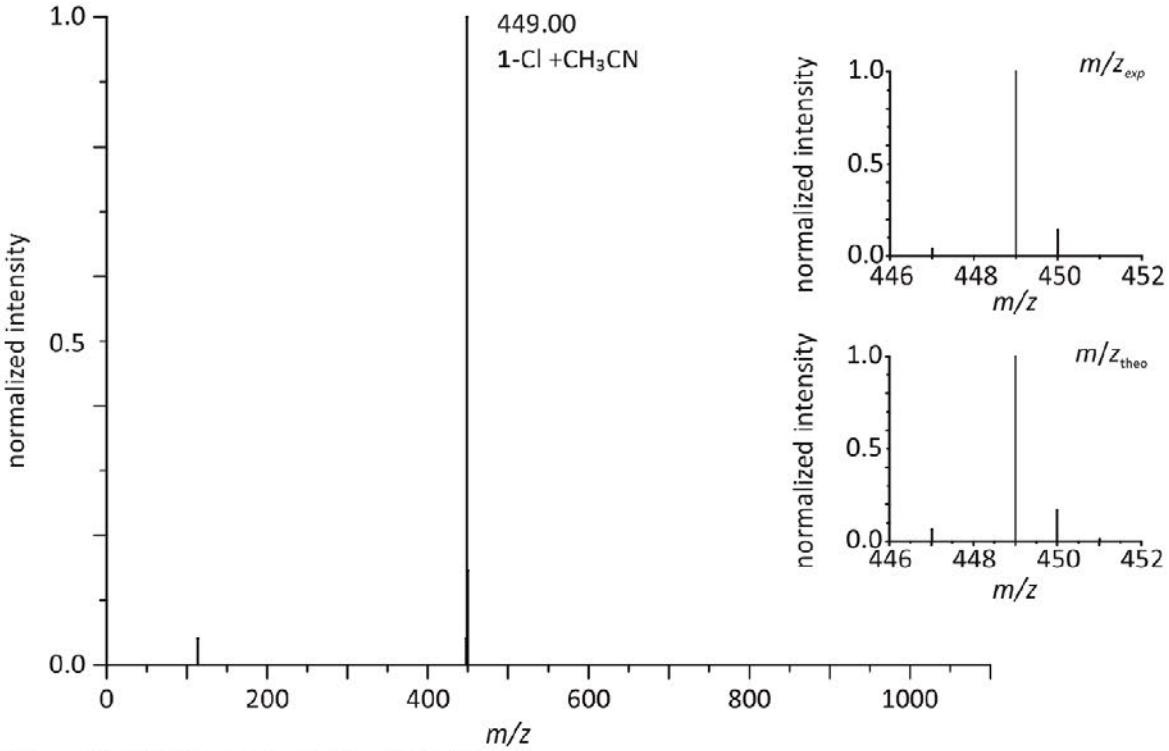

Figure S4. APCI^{+} mass spectrum of **1** in CH_3CN.

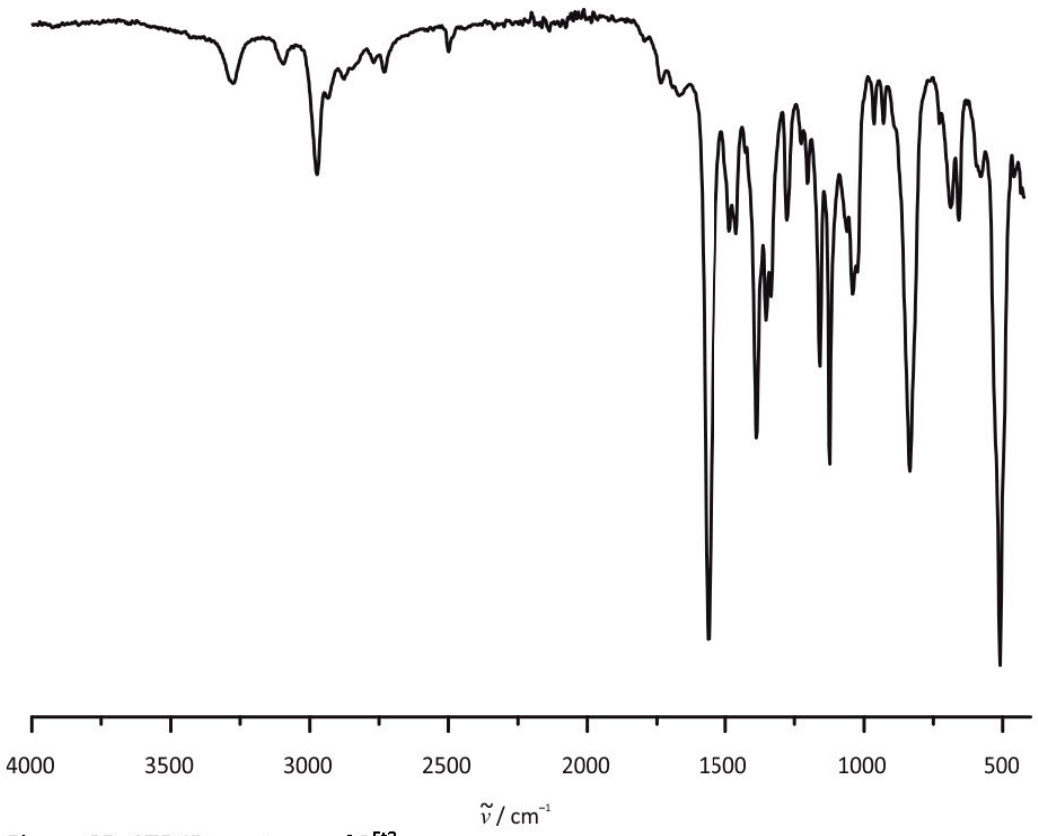

Figure S5. ATR IR spectrum of **2^{Et2}**.

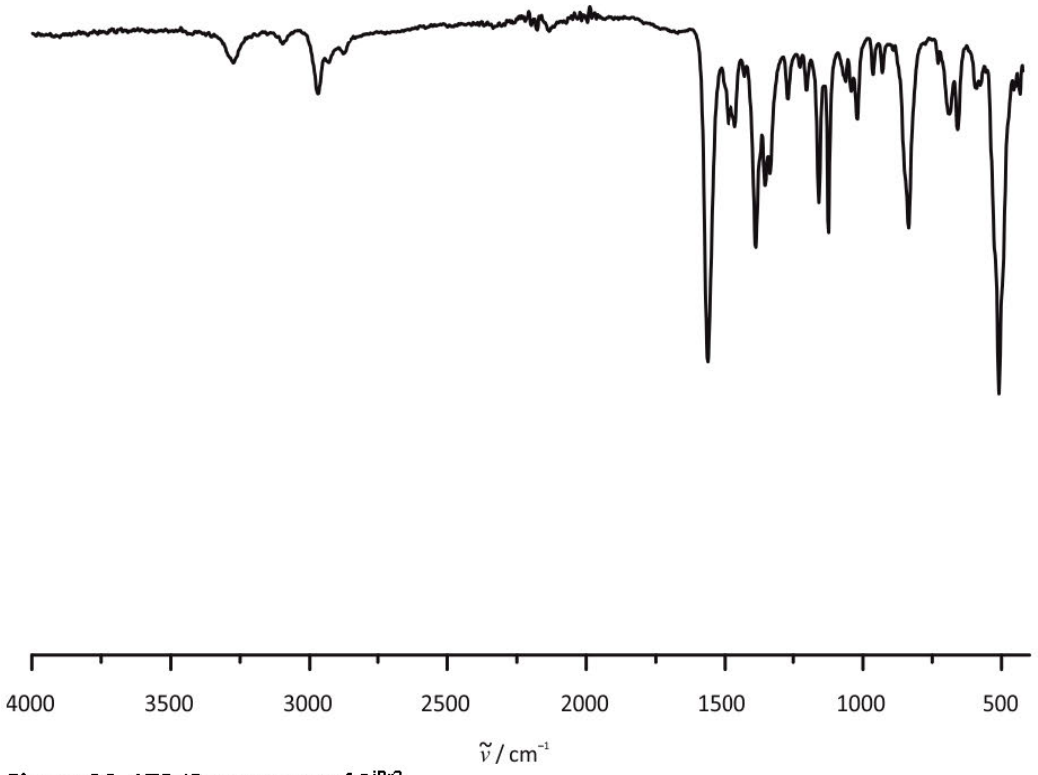

Figure S6. ATR IR spectrum of **2^{iPr2}**.

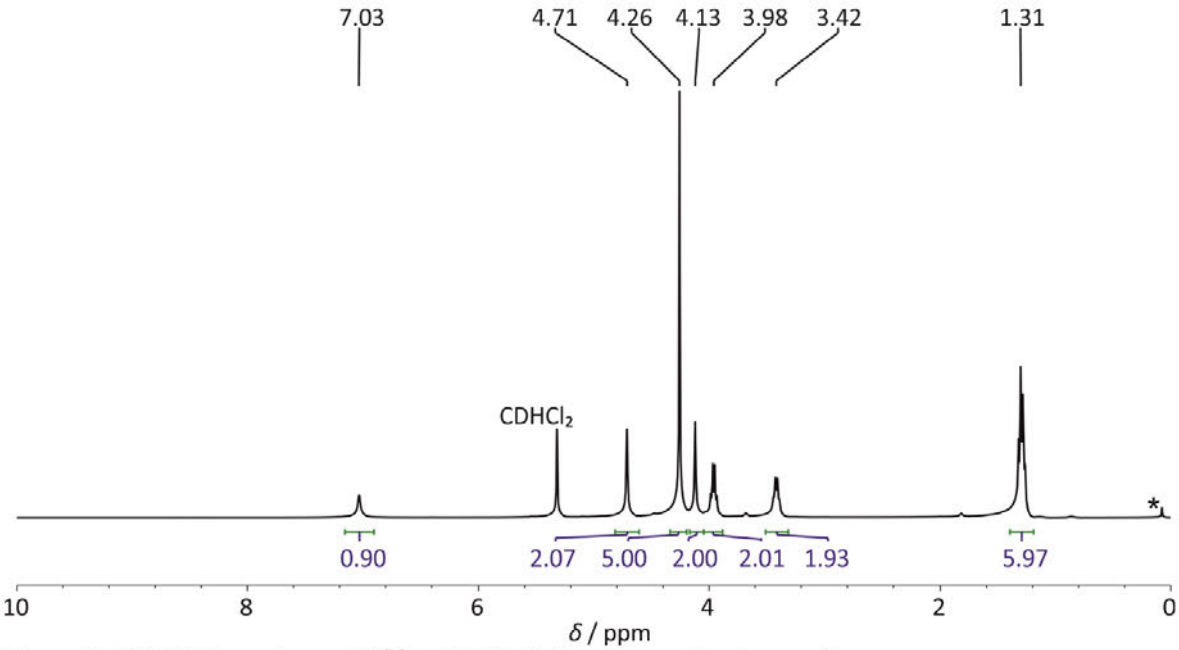

Figure S7. ^{1}H NMR spectrum of $\mathbf{2}^{Et2}$ in CD_2Cl_2 (* denotes residual grease).

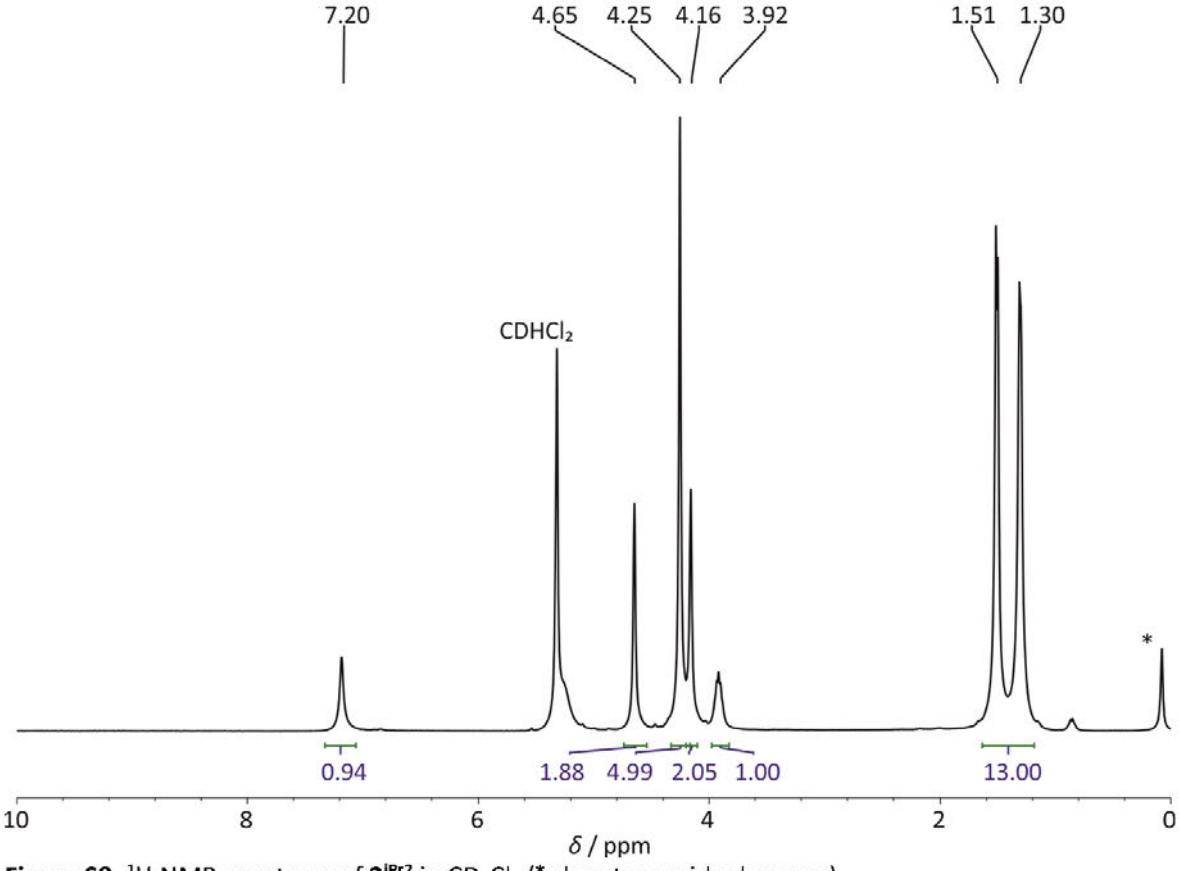

Figure S8. ^{1}H NMR spectrum of $\mathbf{2}^{IPr2}$ in CD_2Cl_2 (* denotes residual grease).

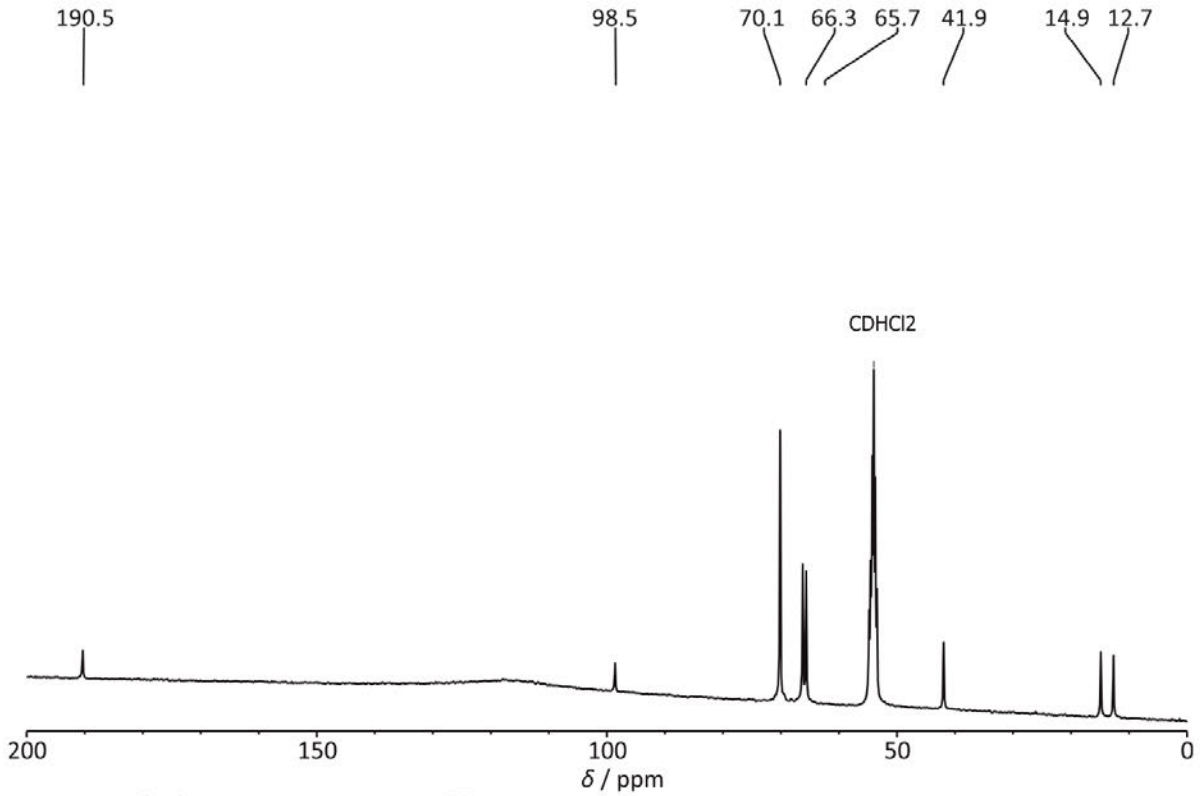

Figure S9. $^{13}C\{^{1}H\}$ NMR spectrum of $\mathbf{2}^{Et2}$ in CD_2Cl_2.

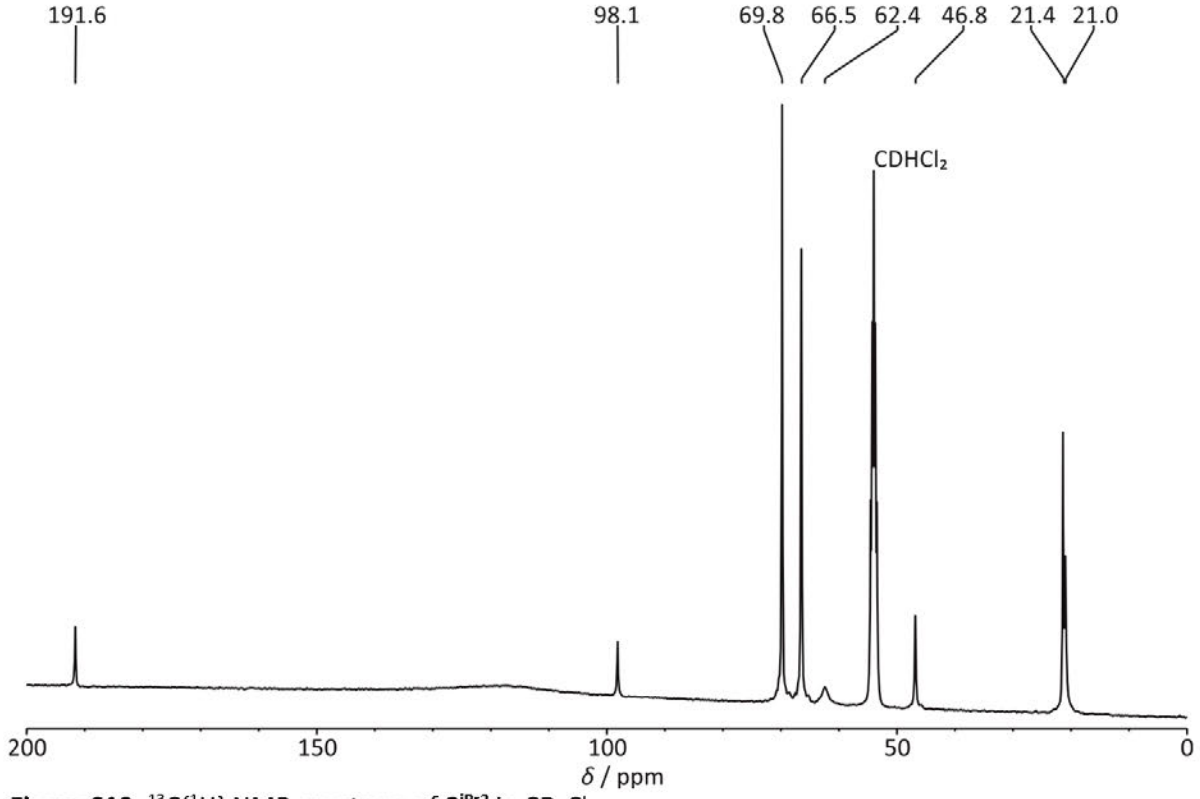

Figure S10. $^{13}C\{^{1}H\}$ NMR spectrum of $\mathbf{2}^{iPr2}$ in CD_2Cl_2.

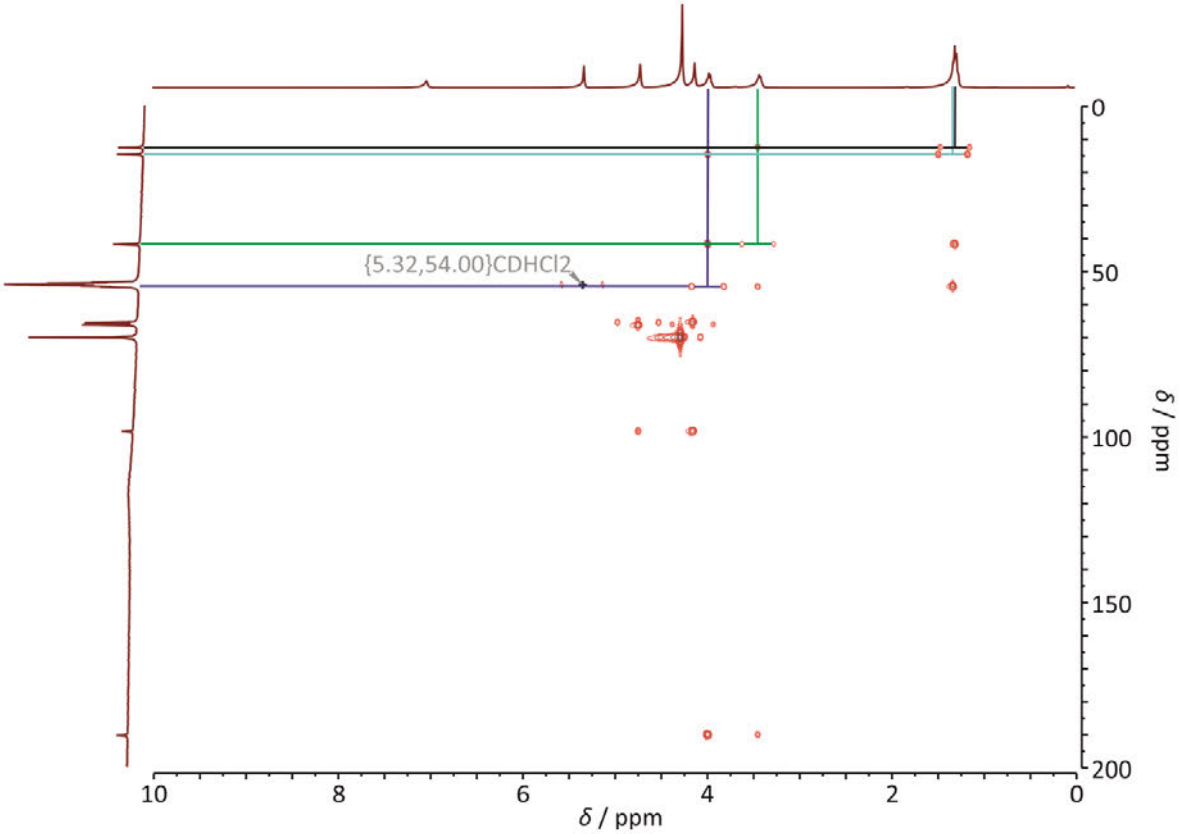

Figure S11. ^{1}H-^{13}C HMBC spectrum of **2^{iPr2}** in CD_2Cl_2. Lines indicate the assignment of the resonances of the ethyl groups as ^{13}C satellites.

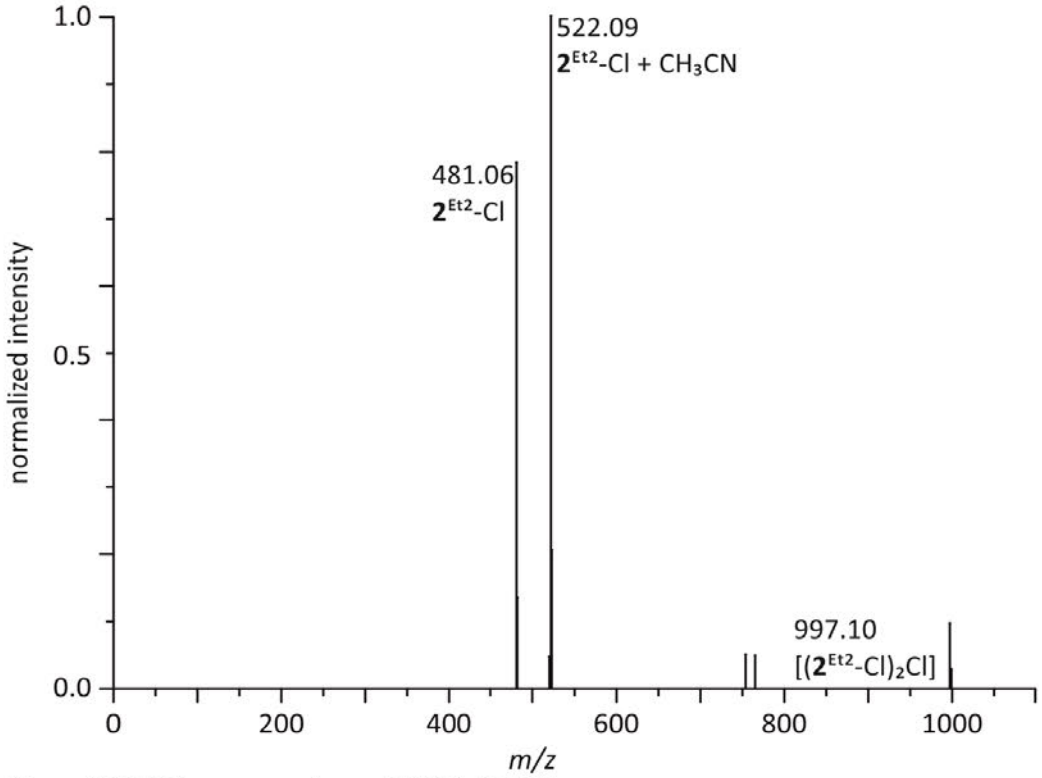

Figure S12. ESI$^+$ mass spectrum of $\mathbf{2}^{Et2}$ in CH_3CN.

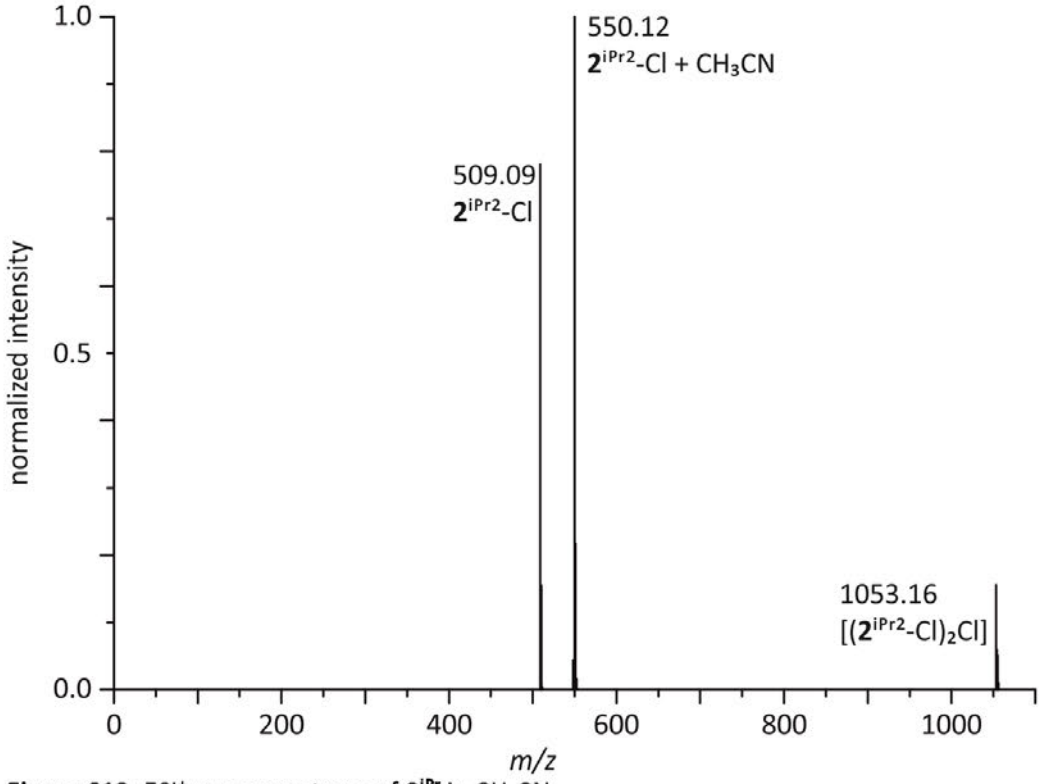

Figure S13. ESI$^+$ mass spectrum of $\mathbf{2}^{iPr}$ in CH_3CN.

Table S1. Selected bond lengths (Å) and angles (deg) of $\mathbf{2}^{Et2}$ and $\mathbf{2}^{iPr2}$ determined by XRD and DFT.

	$\mathbf{2}^{Et2}$		$\mathbf{2}^{iPr2}$	
	XRD	DFT	XRD	DFT
Au1-Cl1	2.294(12)	2.328	2.2955(8)	2.332
Au1-C11	2.008(4)	2.016	2.001(3)	2.021
Fe1-C1	2.048(5)	2.062	2.037(3)	2.067
Fe1-C2	2.023(5)	2.059	2.041(3)	2.062
Fe1-C3	2.027(5)	2.061	2.044(3)	2.062
Fe1-C4	2.045(4)	2.063	2.041(3)	2.062
Fe1-C5	2.047(4)	2.064	2.046(3)	2.067
Fe1-C6	2.040(4)	2.065	2.025(3)	2.041
Fe1-C7	2.039(4)	2.063	2.054(3)	2.062
Fe1-C8	2.041(4)	2.062	2.045(3)	2.066
Fe1-C9	2.037(4)	2.044	2.051(3)	2.069
Fe1-C10	2.042(4)	2.053	2.043(3)	2.056
C11-N1	1.345(5)	1.341	1.344(4)	1.342
C11-N2	1.332(5)	1.328	1.333(4)	1.329
Cl1-Au1-C11	179.73(13)	177.42	174.64(9)	177.42
N1-C1-N2	117.3(4)	117.6	117.7(3)	117.8
Au1···Fe1	4.9709(11)	5.083	5.1046(5)	5.031
N1···Cl1′	3.402(4)	-	-	-
Au1···Au1′	-	-	3.1897(3)	-

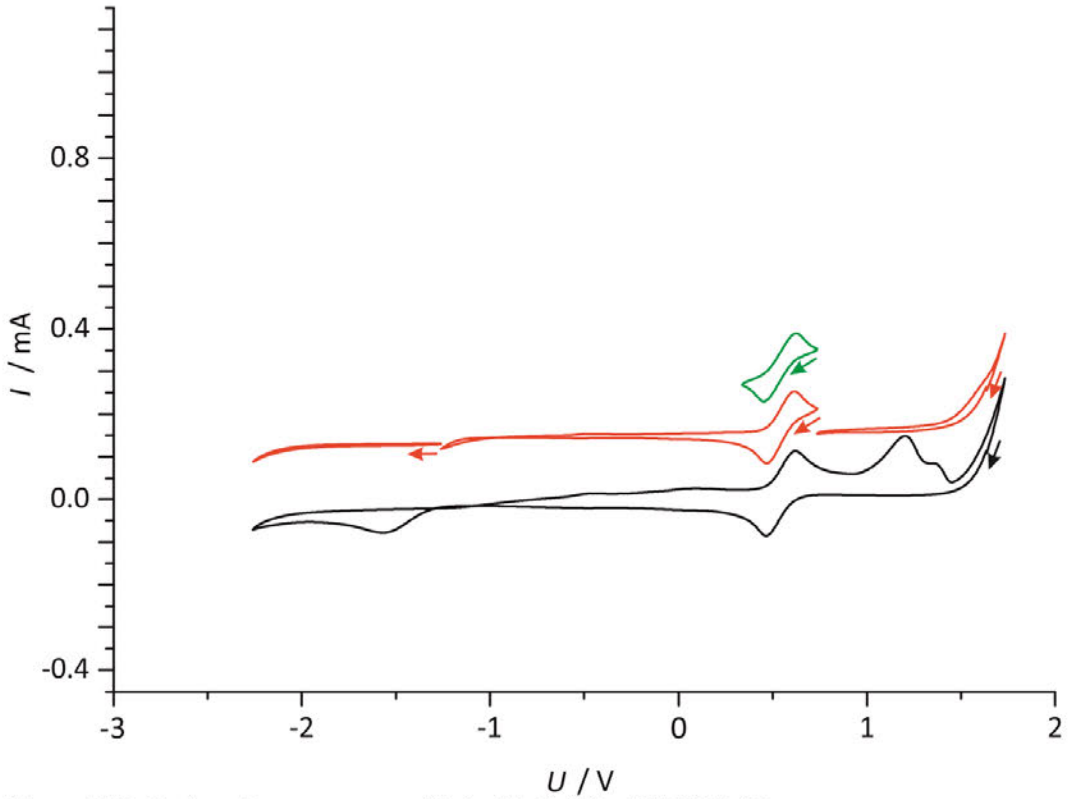

Figure S14. Cyclic voltammograms of **1** in CH_2Cl_2/[^{n}Bu$_4$N][B(C_6F_5)$_4$].

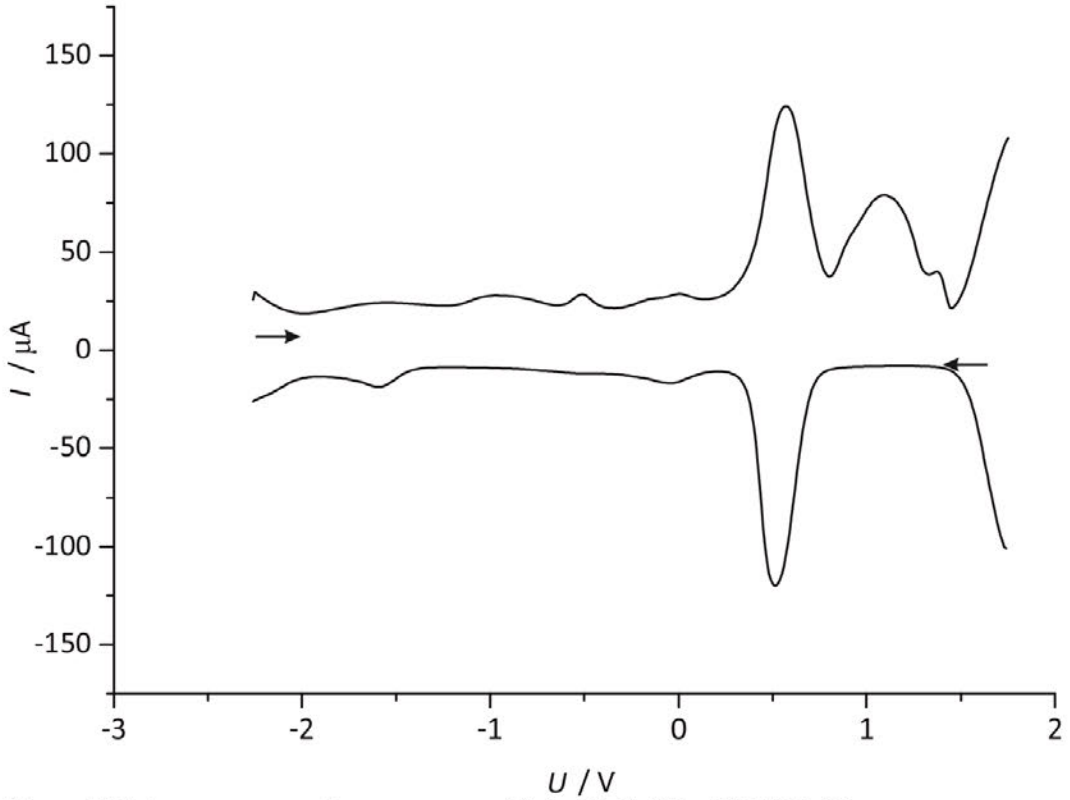

Figure S15. Square wave voltammograms of **1** in CH_2Cl_2/[^{n}Bu$_4$N][B(C_6F_5)$_4$].

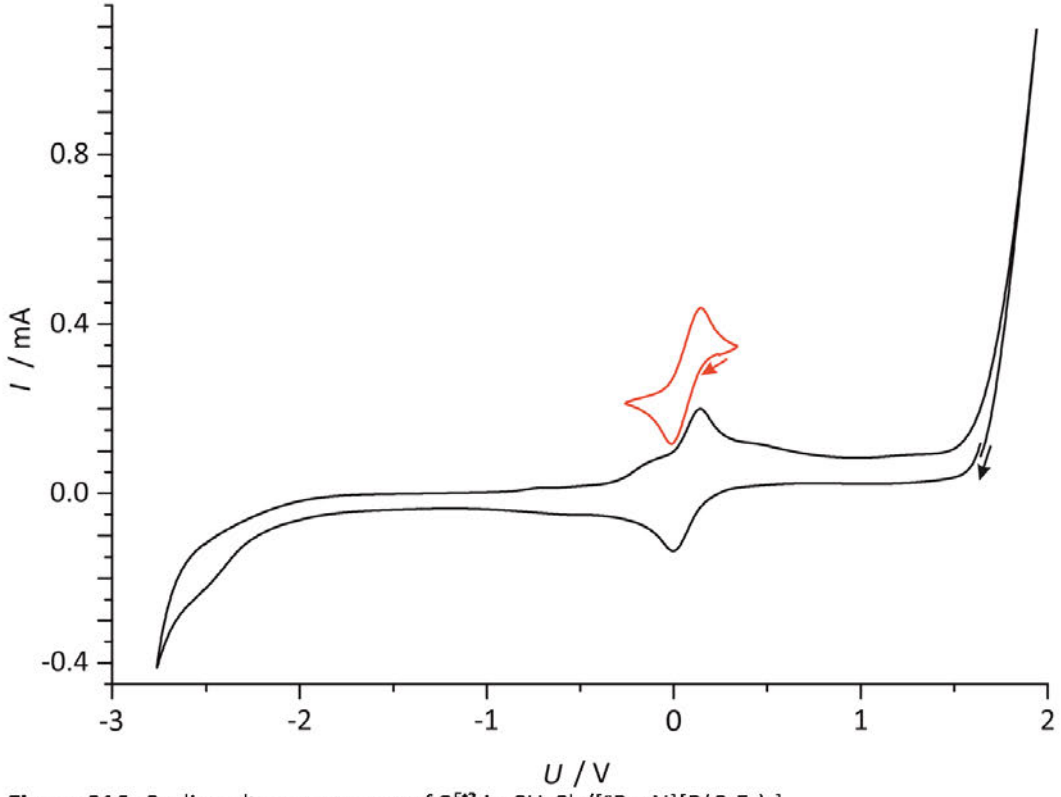

Figure S16. Cyclic voltammograms of $\mathbf{2}^{Et2}$ in $CH_2Cl_2/[^nBu_4N][B(C_6F_5)_4]$.

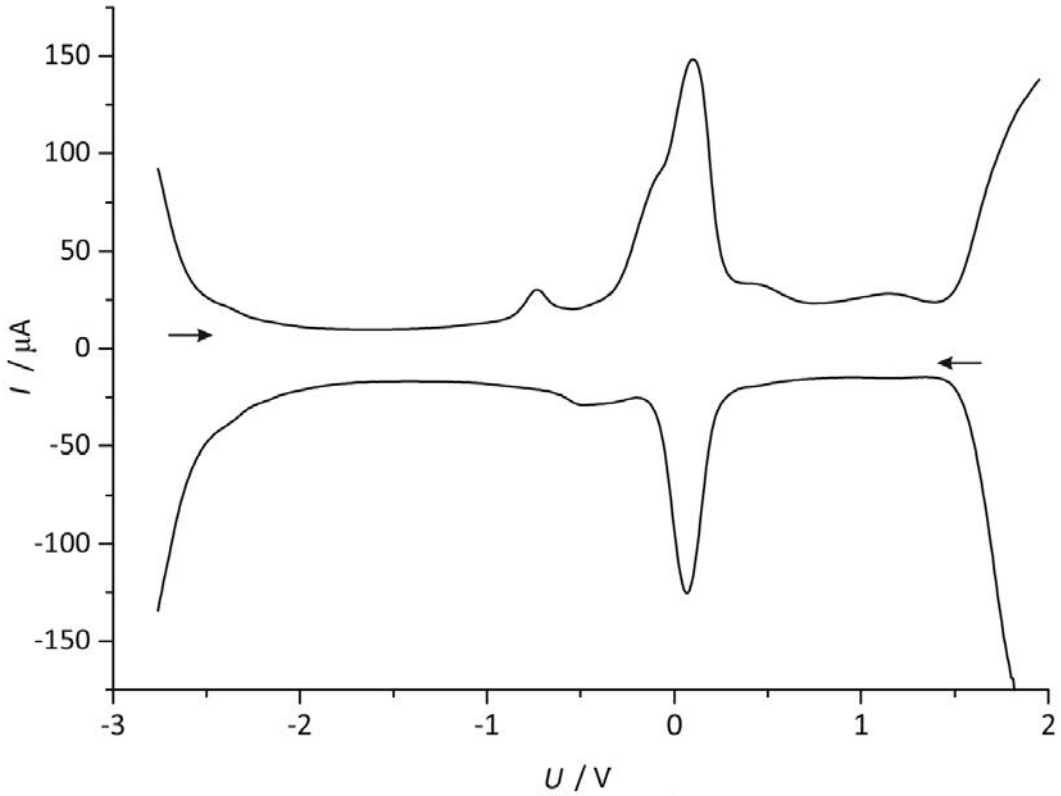

Figure S17. Square wave voltammograms of $\mathbf{2}^{Et2}$ in $CH_2Cl_2/[^nBu_4N][B(C_6F_5)_4]$.

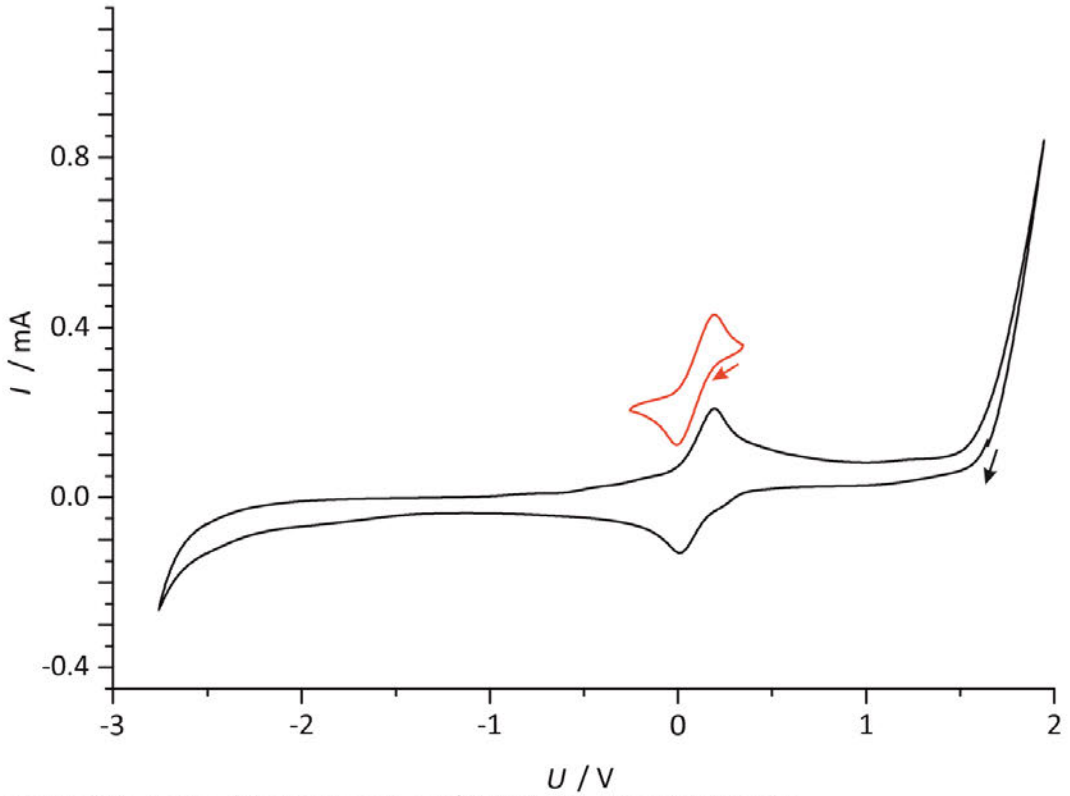

Figure S18. Cyclic voltammograms of $\mathbf{2}^{iPr2}$ in $CH_2Cl_2/[^nBu_4N][B(C_6F_5)_4]$.

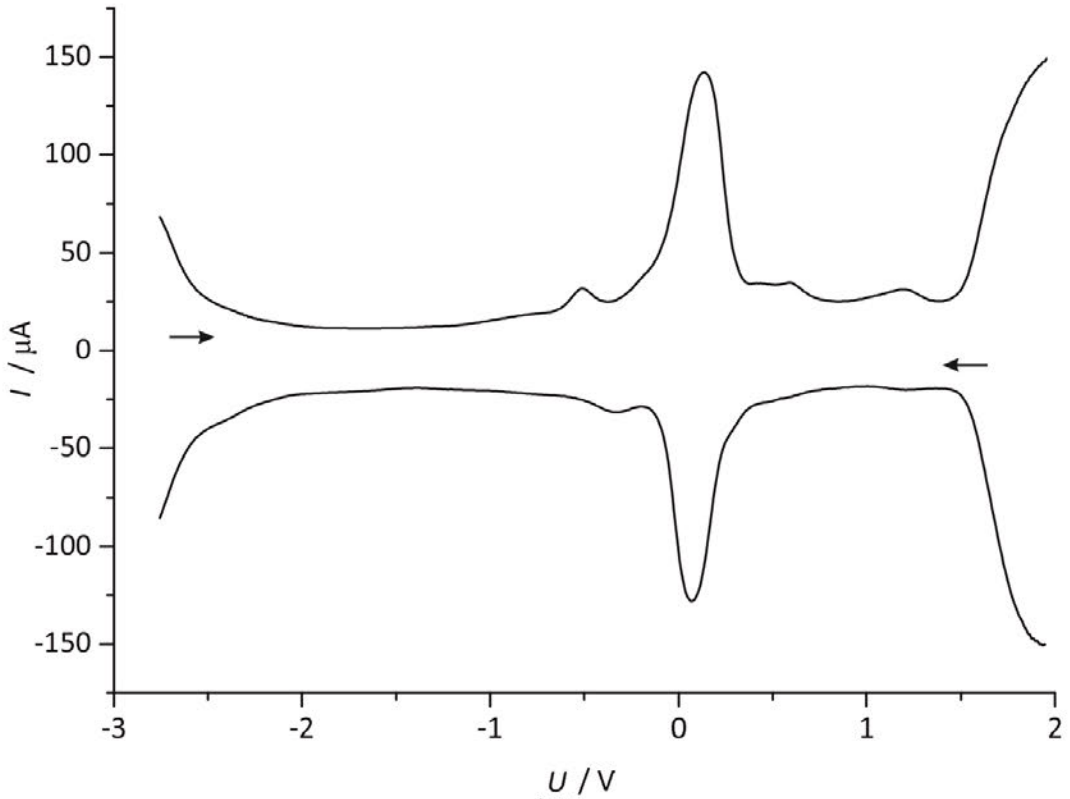

Figure S19. Square wave voltammograms of $\mathbf{2}^{iPr2}$ in CH_2Cl_2.

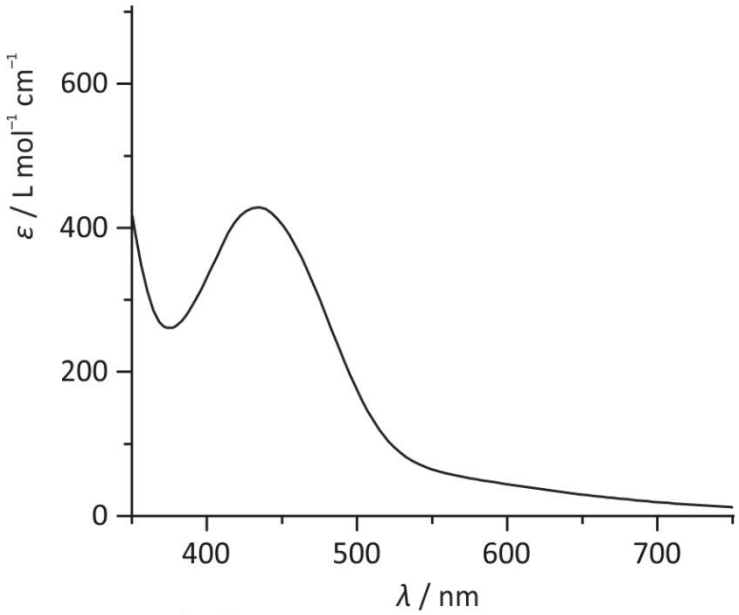

Figure S20. UV/Vis/NIR spectrum of **1** in CH_2Cl_2.

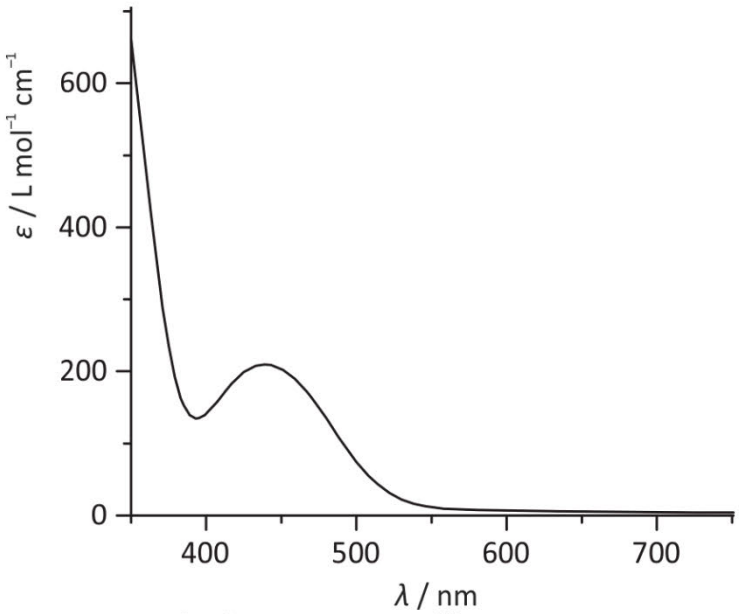

Figure S21. UV/Vis/NIR spectrum of $\mathbf{2}^{Et2}$ in CH_2Cl_2.

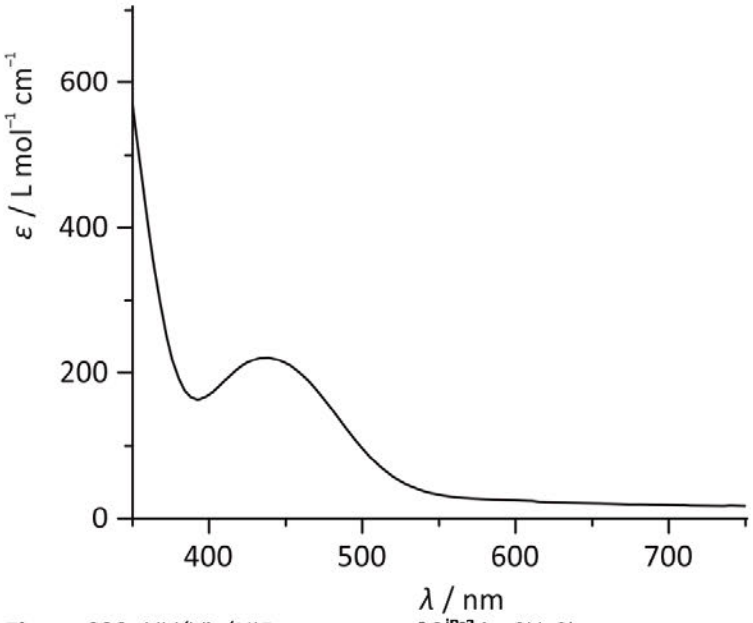

Figure S22. UV/Vis/NIR spectrum of **2**^{iPr2} in CH_2Cl_2.

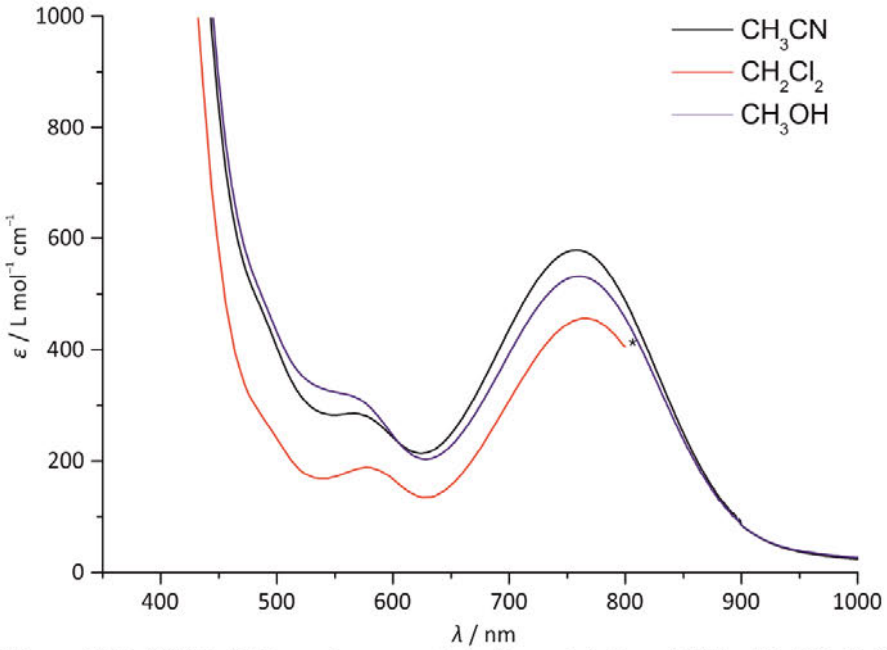

Figure S23. UV/Vis/NIR spectra recorded after oxidation of $\mathbf{2^{Et2}}$ with $[N(p\text{-}C_6H_4Br)_3][SbCl_6]$ in MeCN, CH_2Cl_2 and MeOH, respectively (* data points above 800 nm omitted due to baseline noise).

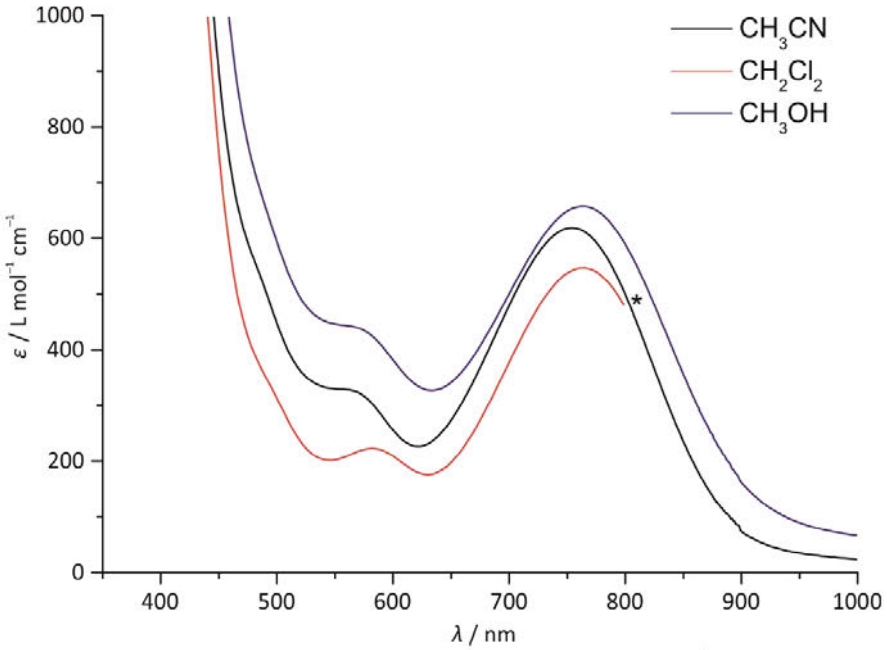

Figure S24. UV/Vis/NIR spectra recorded after oxidation of $\mathbf{2^{iPr2}}$ with $[N(p\text{-}C_6H_4Br)_3][SbCl_6]$ in MeCN, CH_2Cl_2 and MeOH, respectively (* data points above 800 nm omitted due to baseline noise).

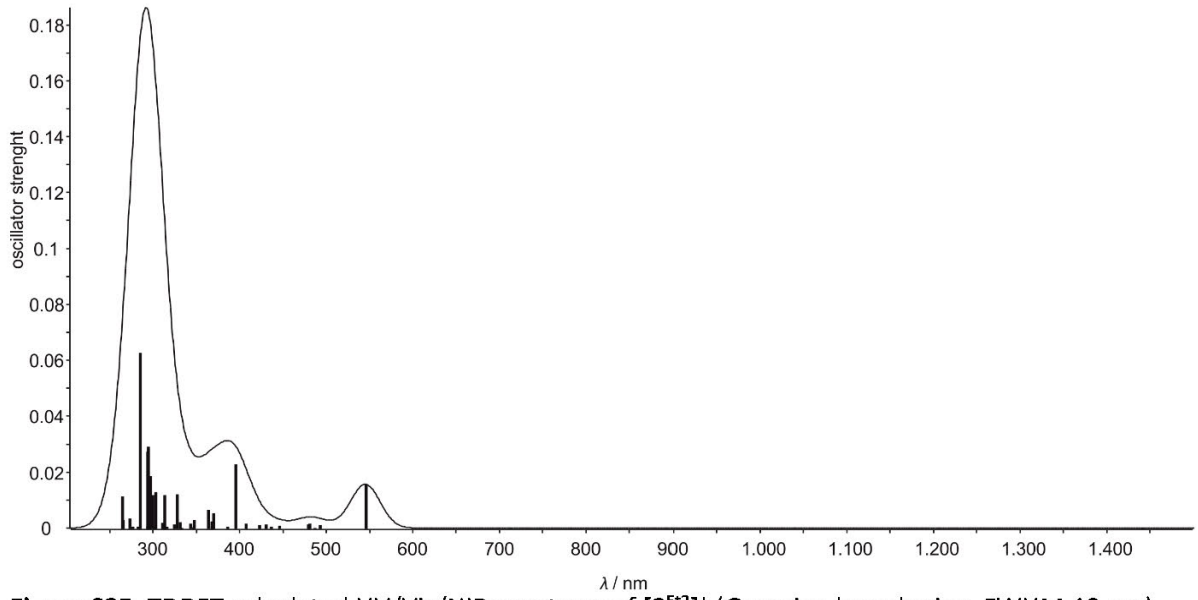

Figure S25. TDDFT calculated UV/Vis/NIR spectrum of **[2^{Et2}]$^{+}$** (Gaussian broadening, FWHM 40 nm).

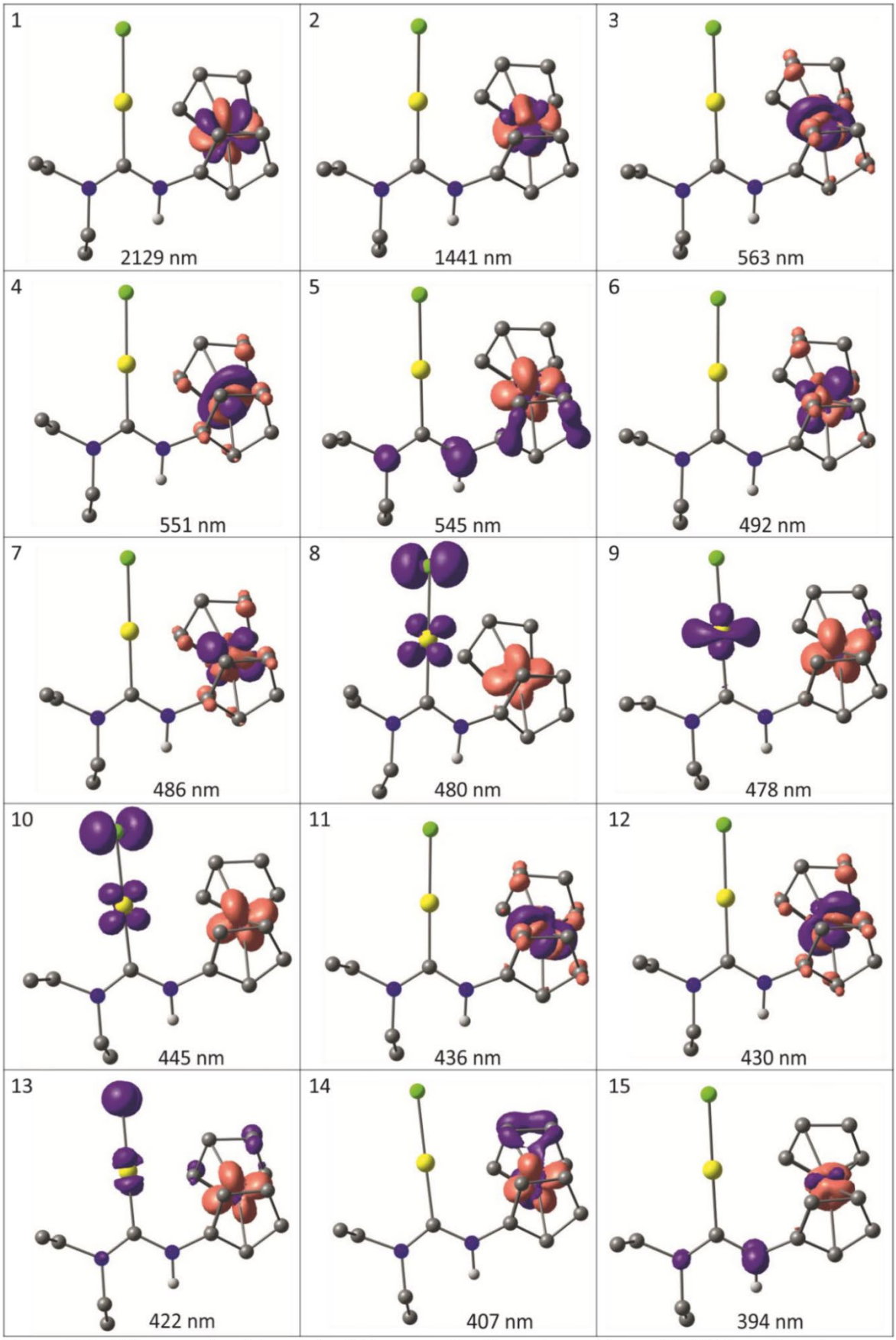

Figure S26. Difference densities of the 15 lowest spin-allowed transitions of $[\mathbf{2}^{Et2}]^+$ (purple = electron loss; orange = electron gain, ordered from low to high energy, isosurface value 0.007).

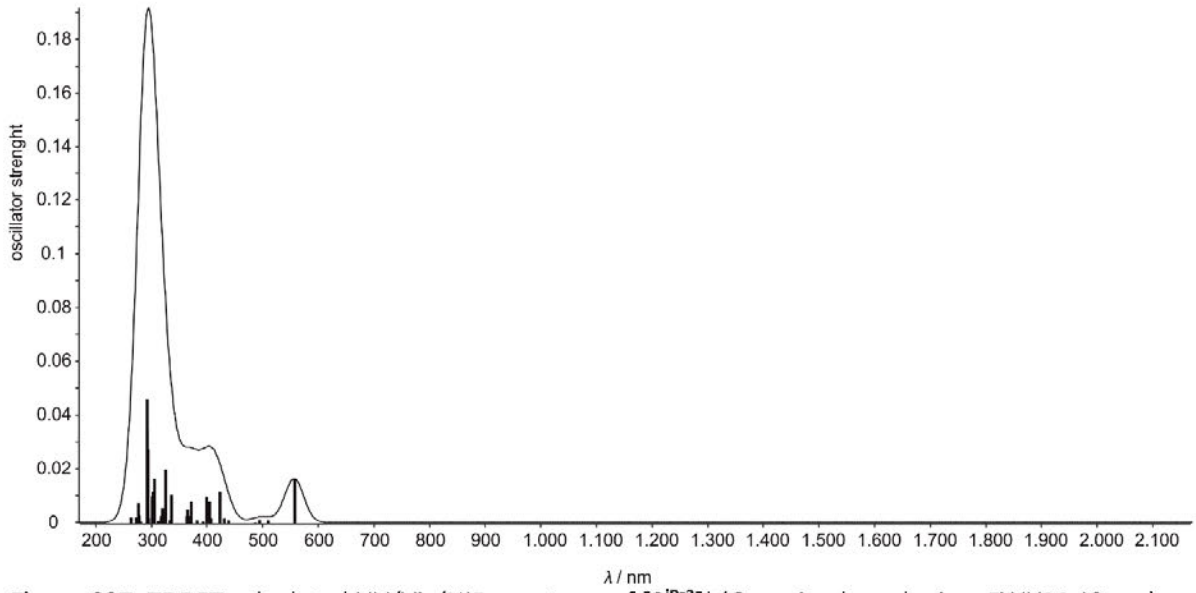

Figure S27. TDDFT calculated UV/Vis/NIR spectrum of $[\mathbf{2}^{iPr2}]^+$ (Gaussian broadening, FWHM 40 nm).

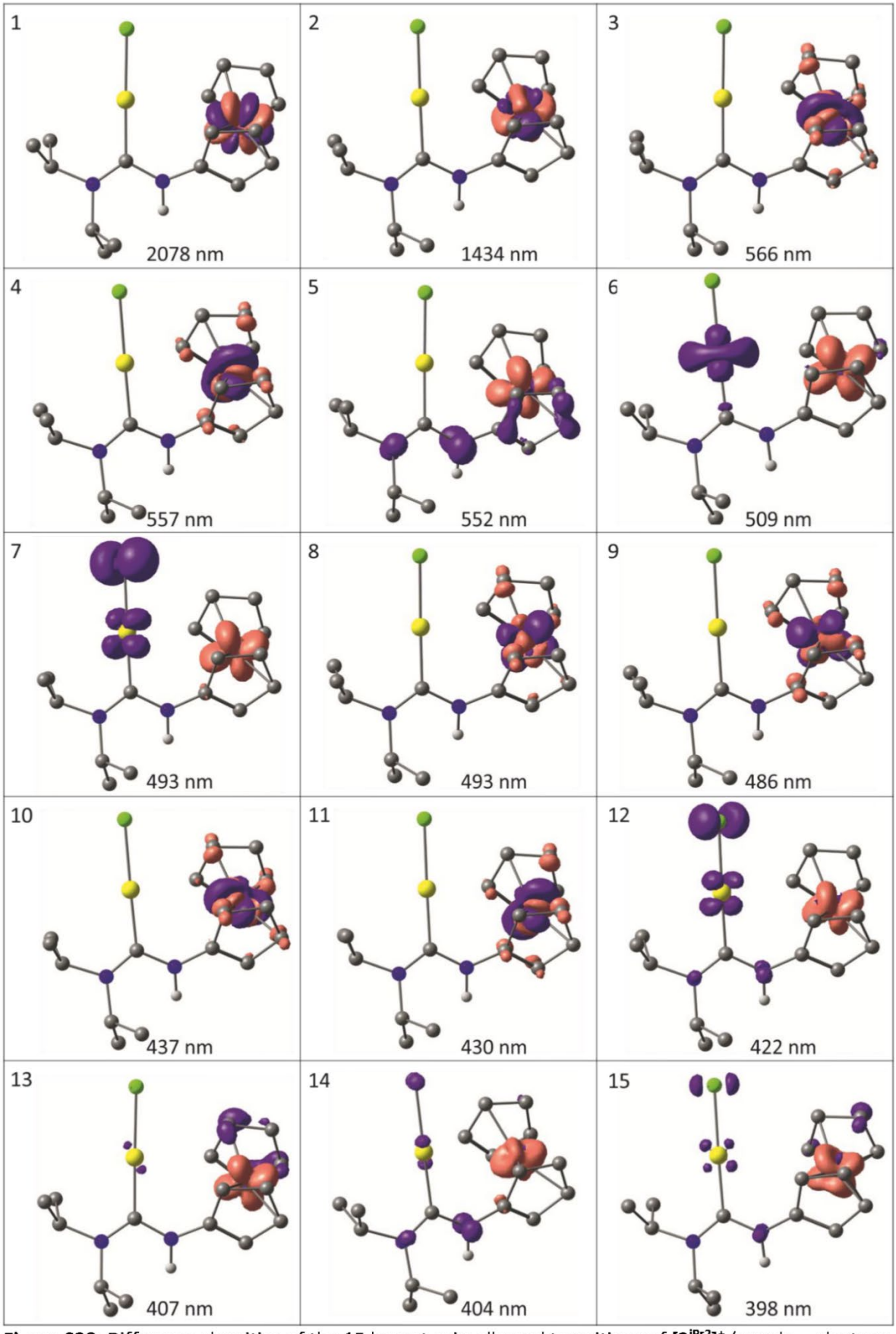

Figure S28. Difference densities of the 15 lowest spin-allowed transitions of **[2^{iPr2}]$^{+}$** (purple = electron loss; orange = electron gain, ordered from low to high energy, isosurface value 0.007).

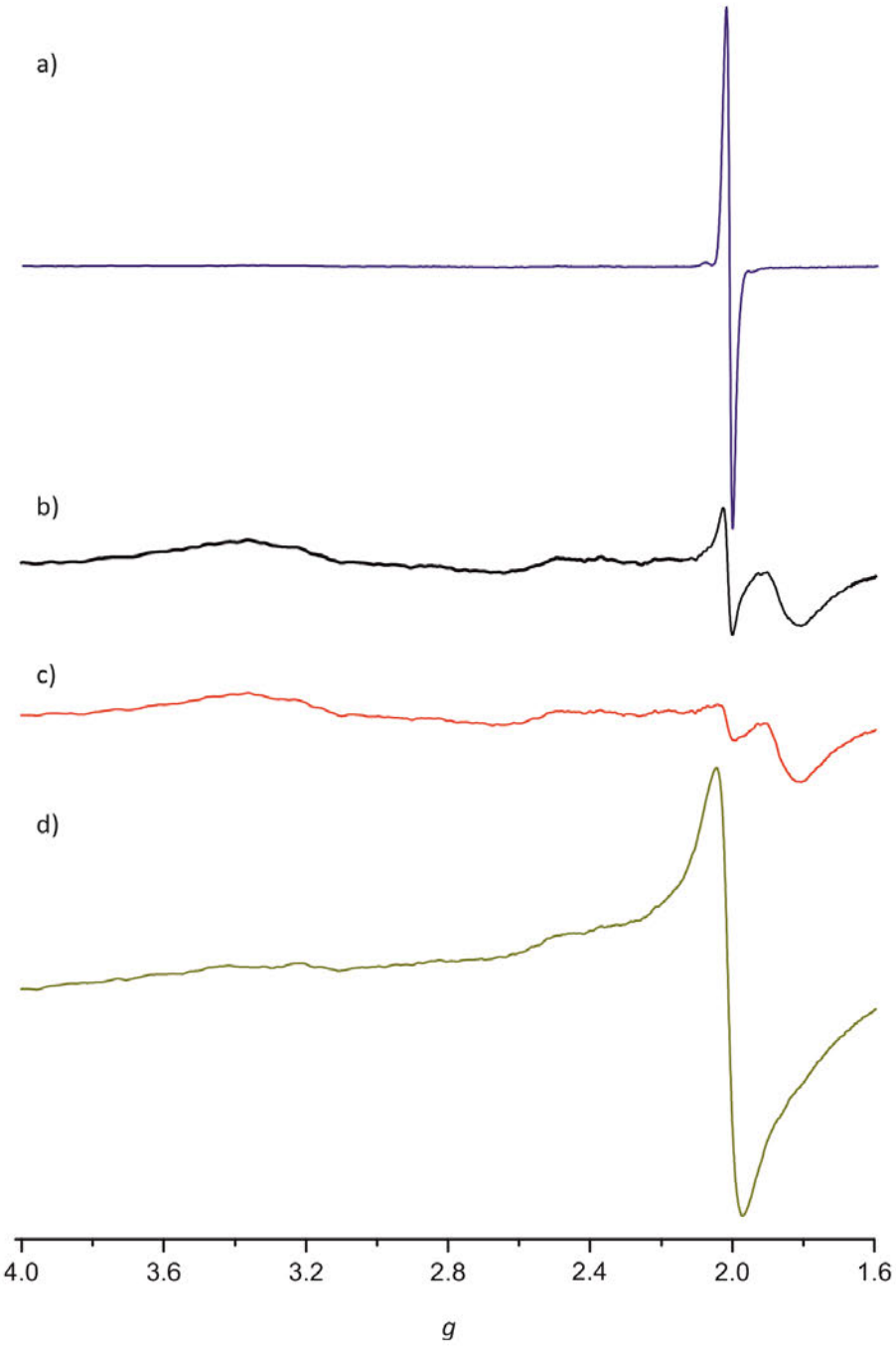

Figure S29. X-band EPR spectra of a) magic blue $[N(4\text{-}C_6H_4Br)_3][SbCl_6]$, b) a mixture of $\mathbf{2}^{Et2}$ with one equivalent of magic blue rapidly frozen, c) after storing the mixture for 30 min. at 195 K and d) followed by storing the mixture at 295 K for 3.5 h. All spectra were recorded in THF at 77 K

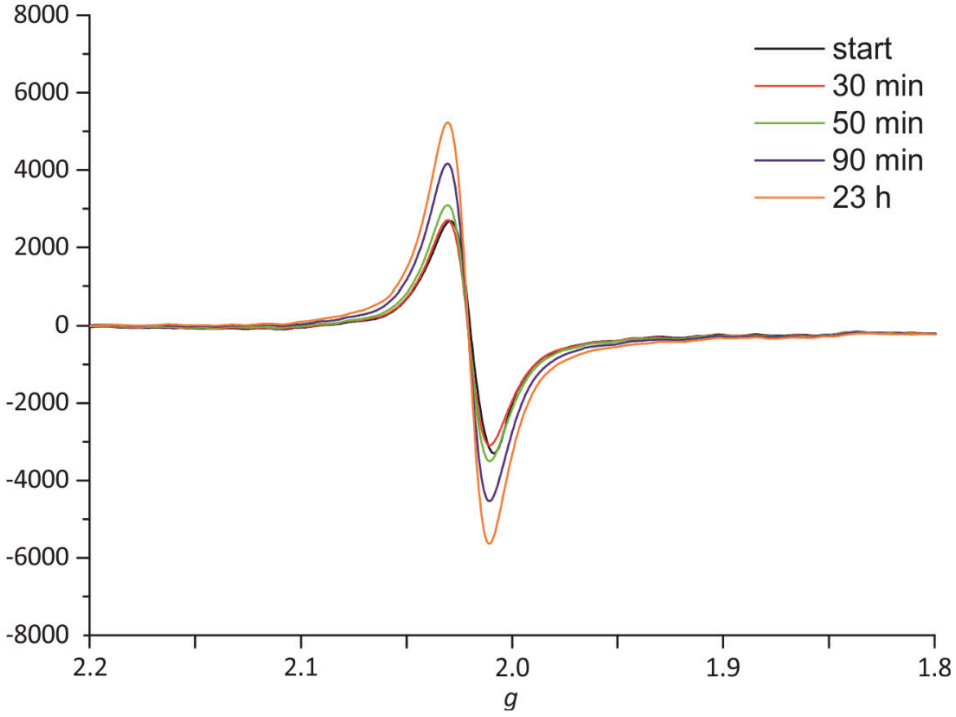

Figure S30. X-band EPR spectra of a mixture of $\mathbf{2}^{Et2}$ with one equivalent of magic blue in THF at room temperature over time.

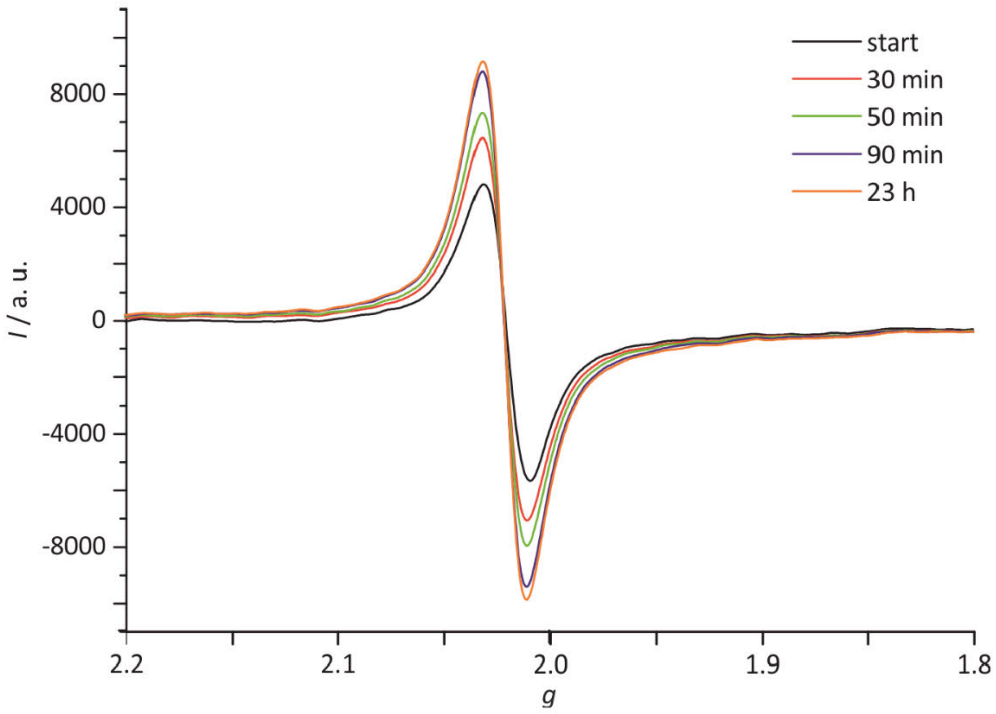

Figure S31. X-band EPR spectra of a mixture of $\mathbf{2}^{iPr2}$ with one equivalent of magic blue in THF at room temperature over time.

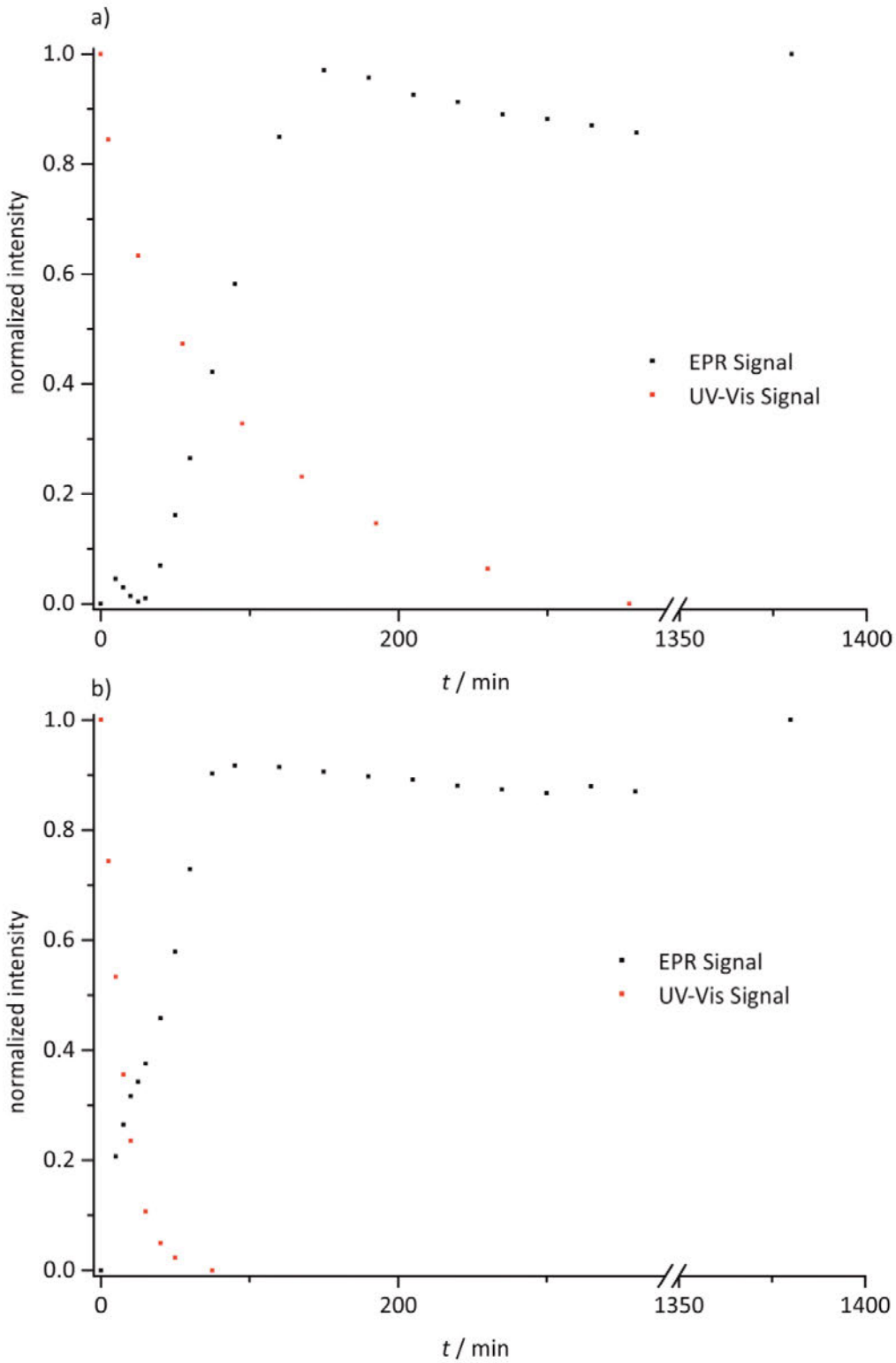

Figure S32. Intensities of EPR resonances and absorption bands (759 nm) at room temperature over time for a) $[\mathbf{2}^{Et2}]^+$ and b) $[\mathbf{2}^{iPr2}]^+$ in THF.

6.3 Supporting Information: Dicobaltocenium Amine – Proton, Electron and H Atom Transfer

Dicobaltocenium amine – proton, electron and H atom transfer

Sven D. Waniek, Christian Heine, Dimitri Zorn, Taro Lieberth, Maximilian Lauck, Christoph Förster*, and Katja Heinze*

Department of Chemistry, Johannes Gutenberg University Mainz, Duesbergweg 10–14, D-55128 Mainz, Germany

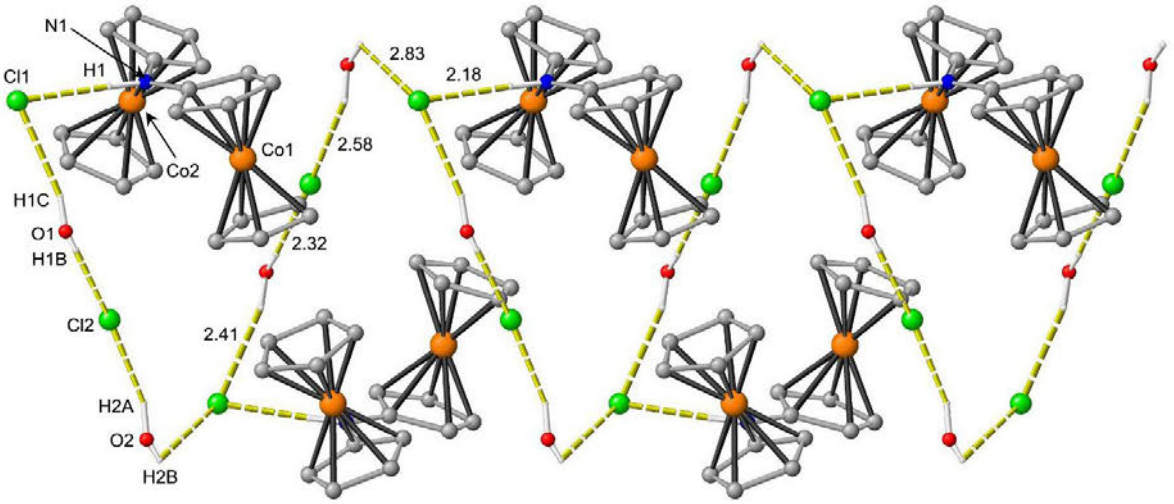

Figure S1. Hydrogen bonding in crystals of **[H–1]Cl_2** × 2 H_2O. Distances indicated in Å.

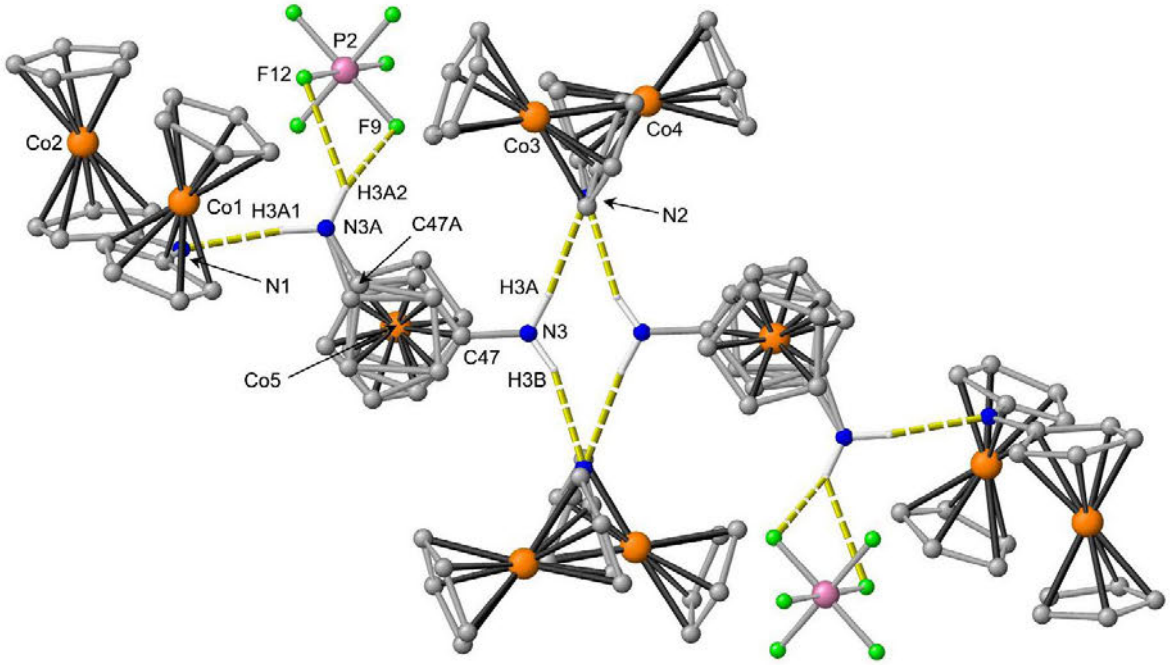

Figure S2. Hydrogen bonding in crystals of **[1]$_2$[CcNH_2][PF_6]$_3$**.

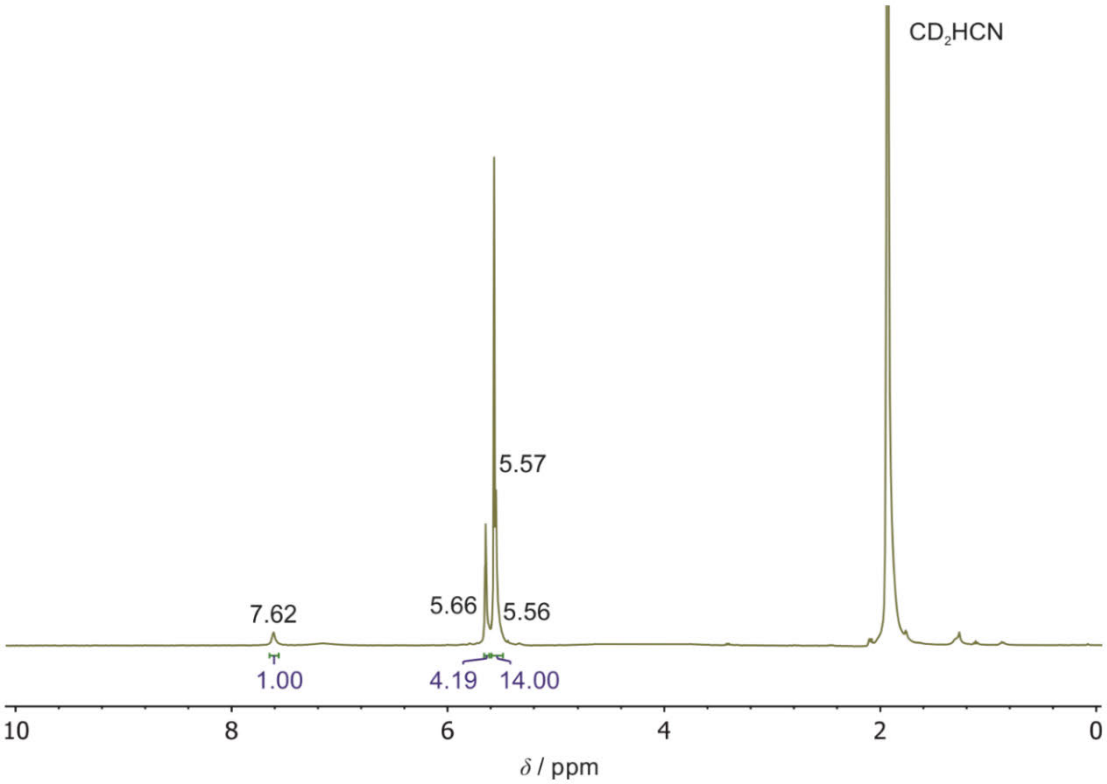

Figure S3. ^{1}H NMR spectrum of **[H–1][PF$_6$]$_2$** in CD_3CN.

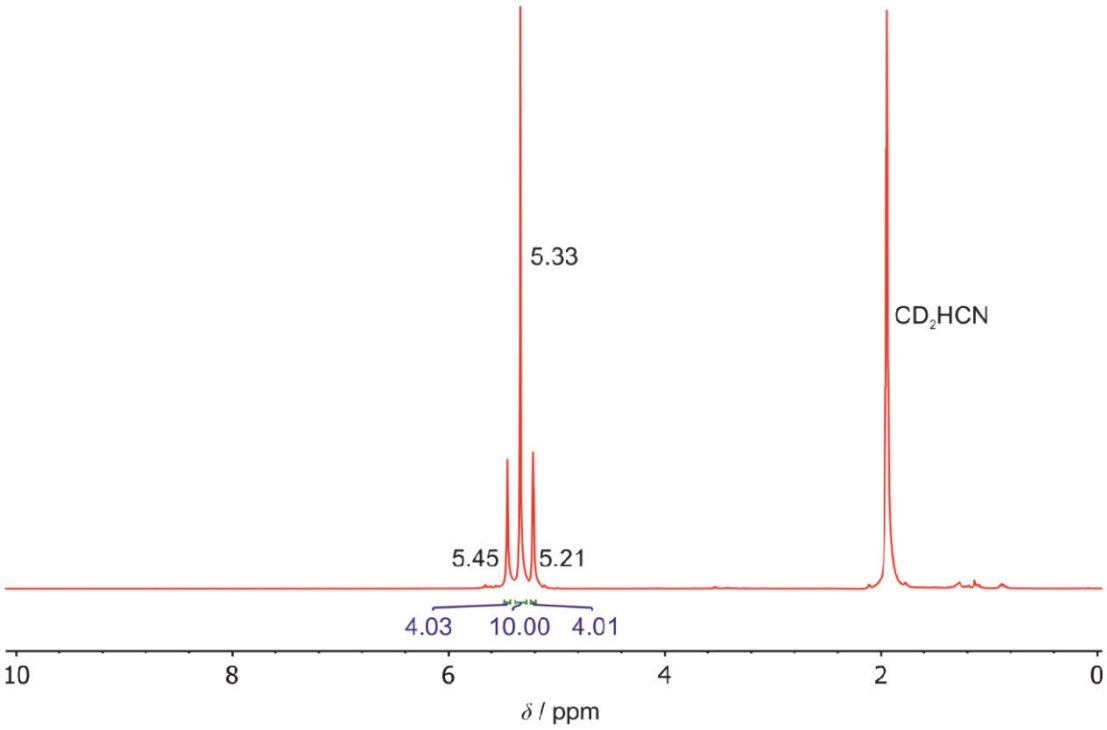

Figure S4. ^{1}H NMR spectrum of **1[PF$_6$]** in CD_3CN.

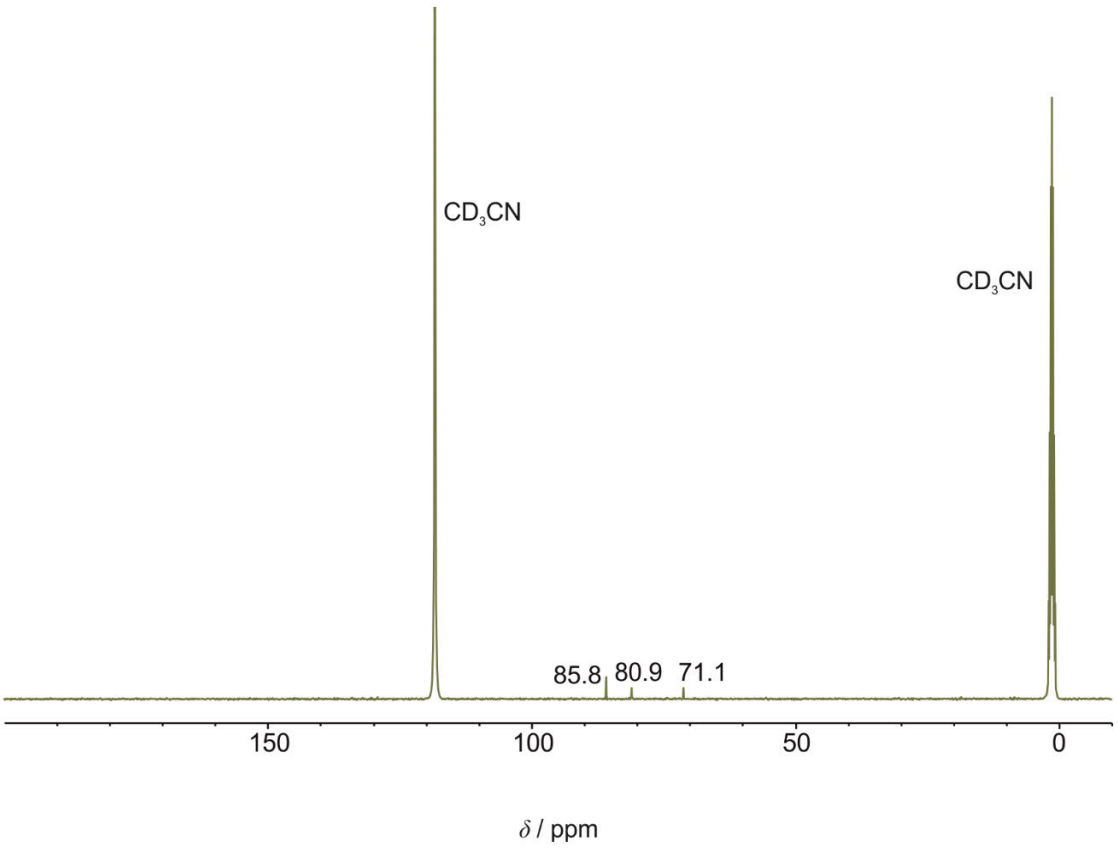

Figure S5. $^{13}C\{^{1}H\}$ NMR spectrum of **[H–1][PF$_6$]$_2$** in CD_3CN.

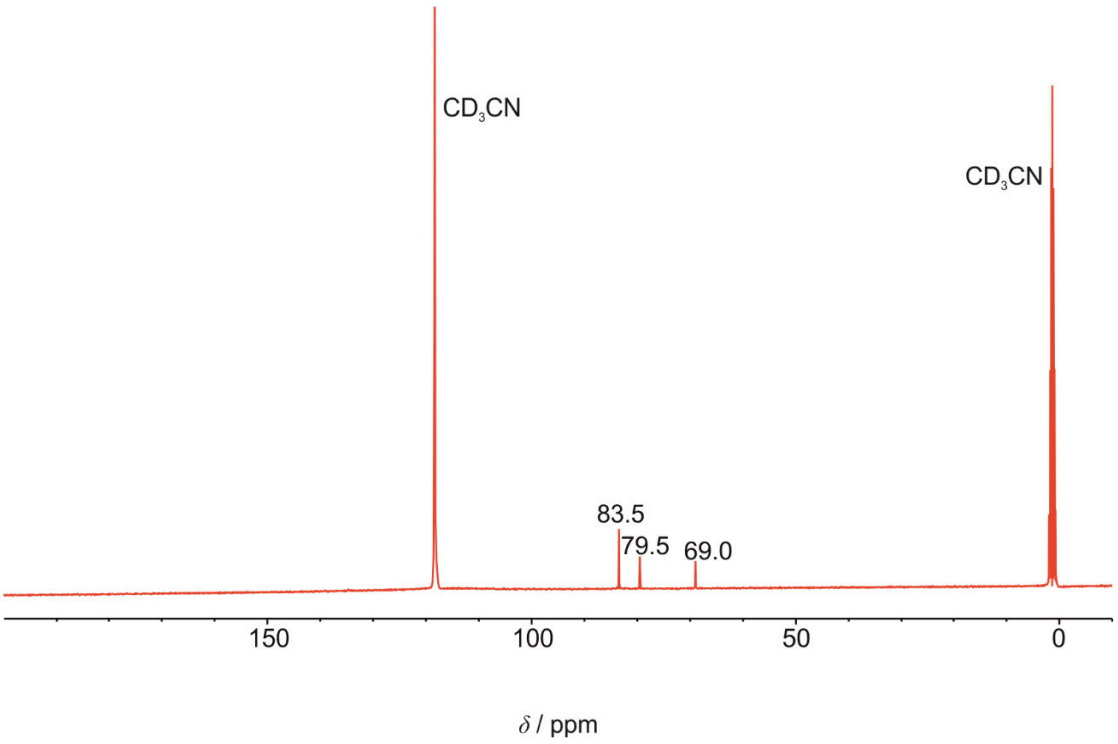

Figure S6. $^{13}C\{^{1}H\}$ NMR spectrum of **1[PF$_6$]** in CD_3CN.

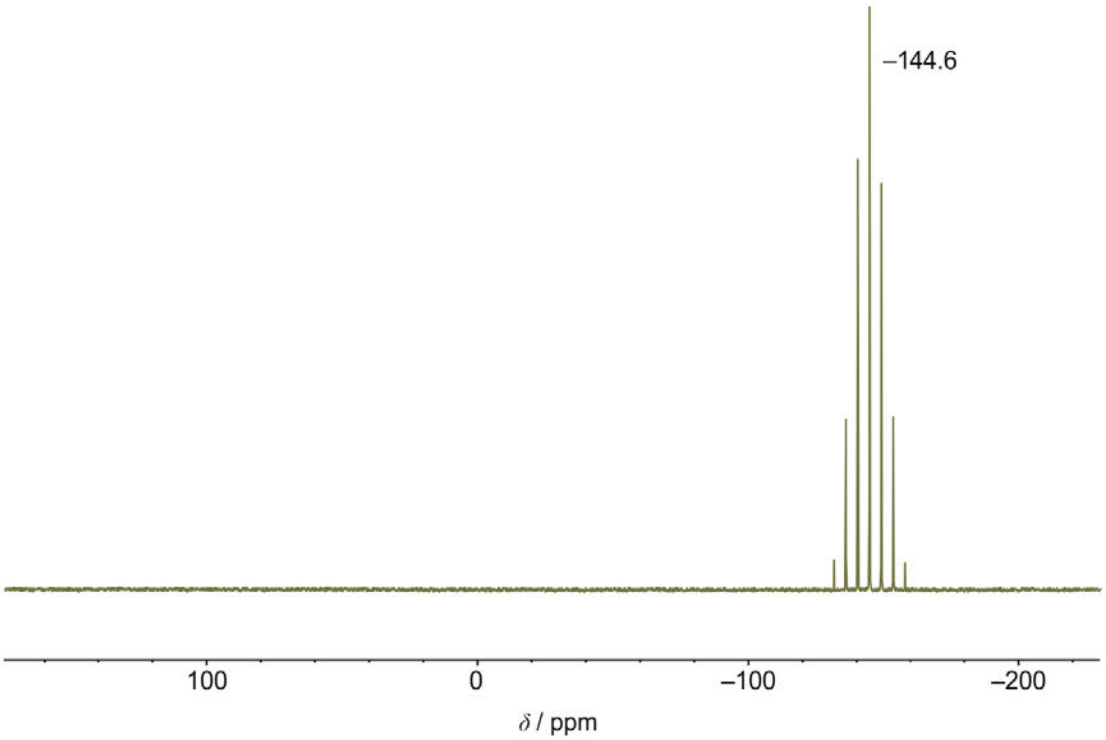

Figure S7. $^{31}P\{^{1}H\}$ NMR spectrum of **[H–1][PF$_6$]$_2$** in CD_3CN.

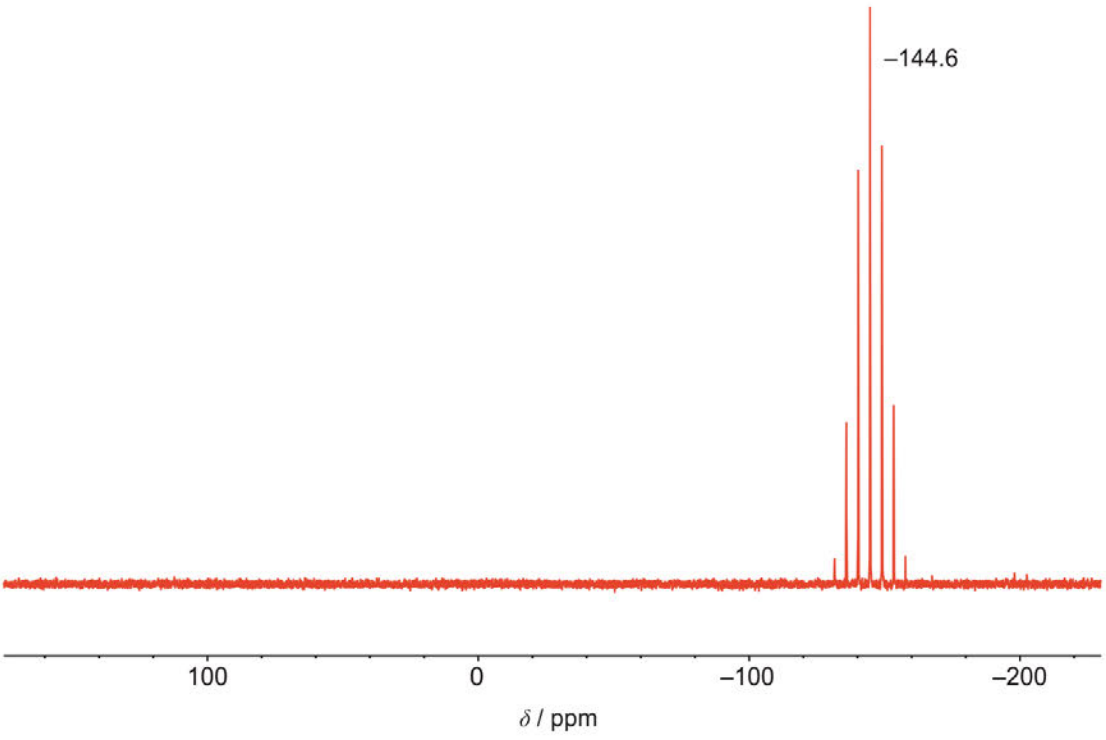

Figure S8. $^{31}P\{^{1}H\}$ NMR spectrum of **1[PF$_6$]** in CD_3CN.

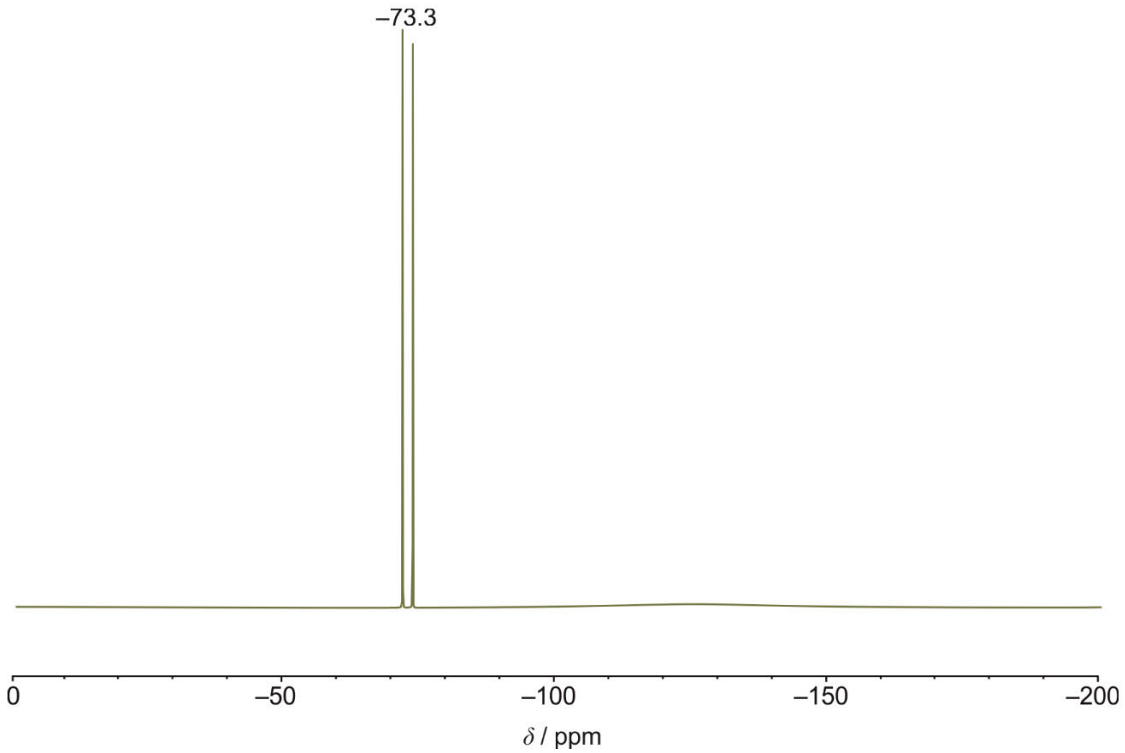

Figure S9. ^{19}F NMR spectrum of **[H–1][PF$_6$]$_2$** in CD_3CN.

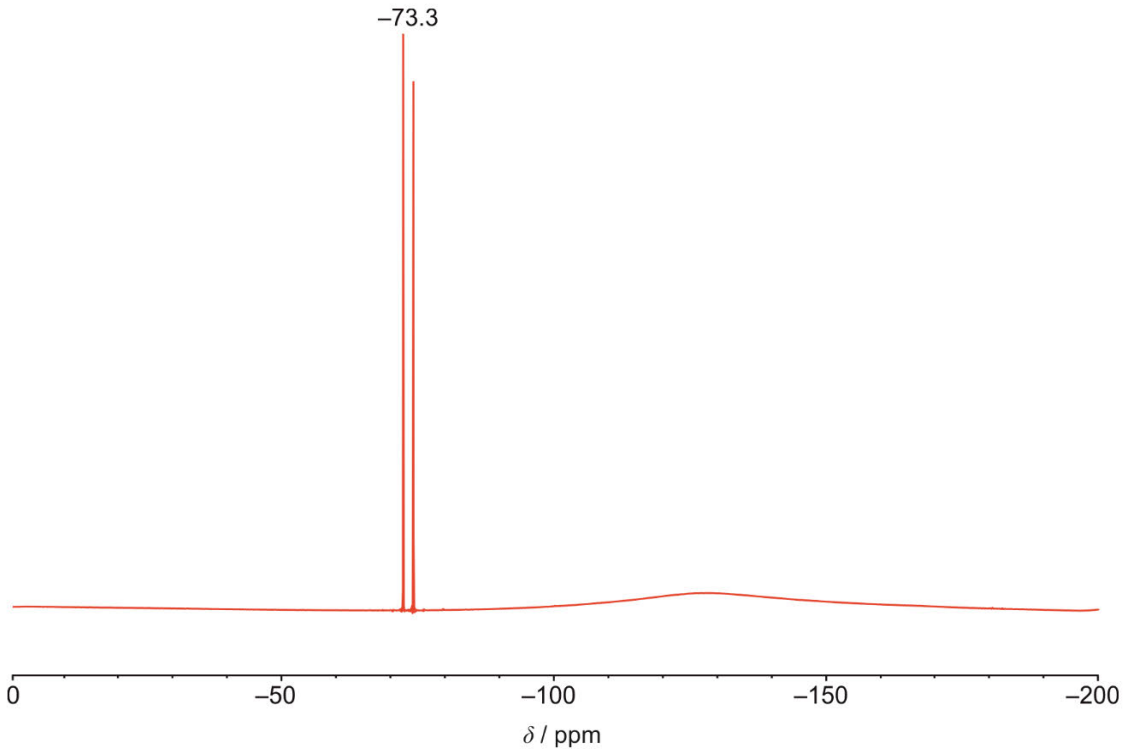

Figure S10. ^{19}F NMR spectrum of **1[PF$_6$]** in CD_3CN.

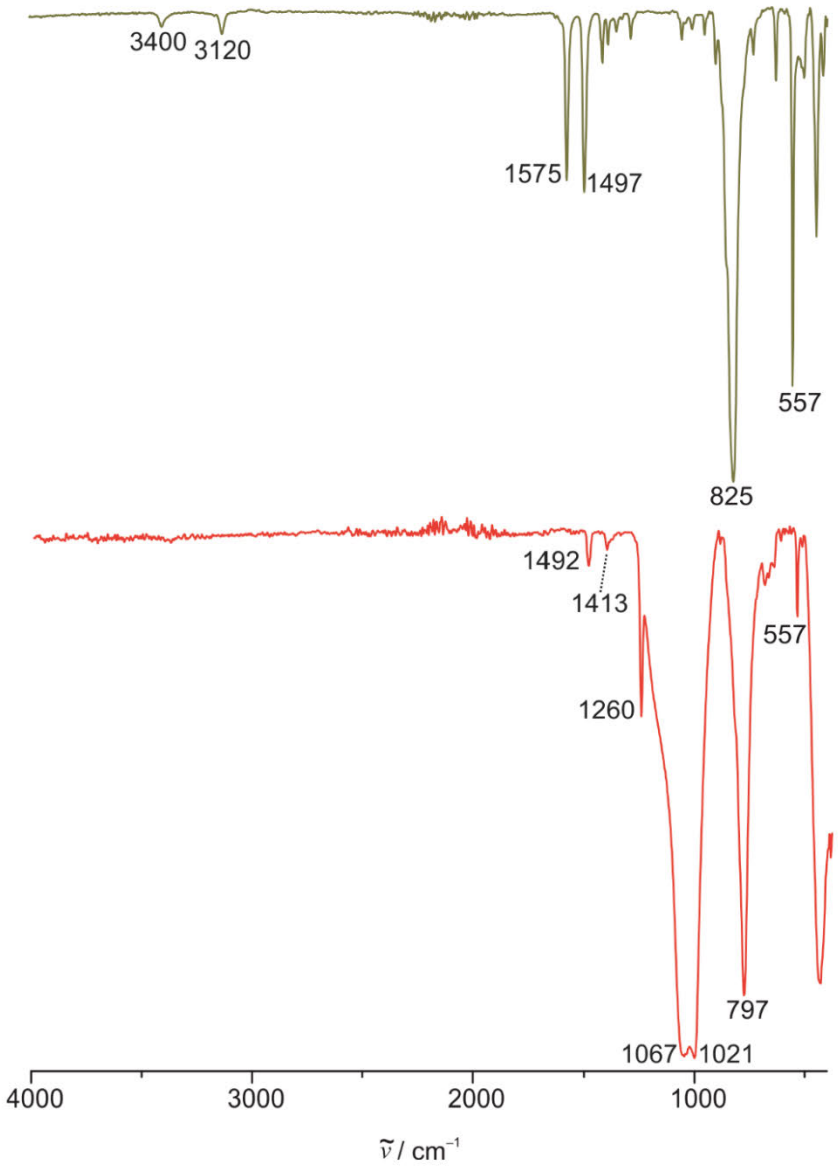

Figure S11. ATR-IR spectra of **[H–1][PF$_6$]$_2$** (beige) and **1[PF$_6$]** (red).

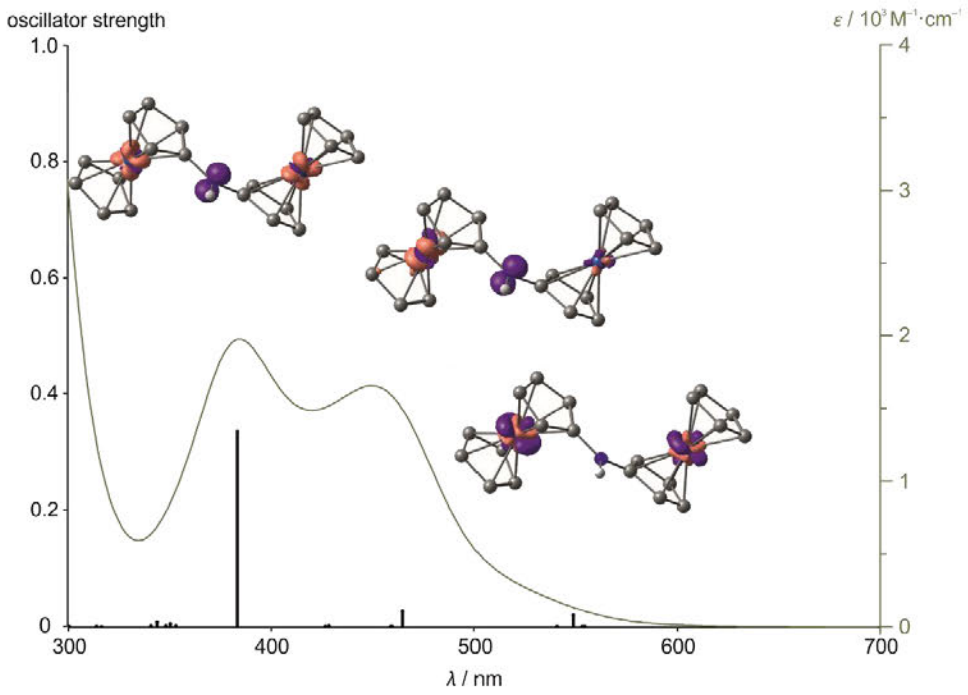

Figure S12. UV/Vis spectrum of **[H–1][PF$_6$]$_2$** in CD_3CN and TD-DFT calculated transitions of **[H–1]$^{2+}$** (transitions shifted by +0.26 eV) with difference electron densities displayed at an isosurface value of 0.01 a.u. (purple = electron loss; orange = electron gain).

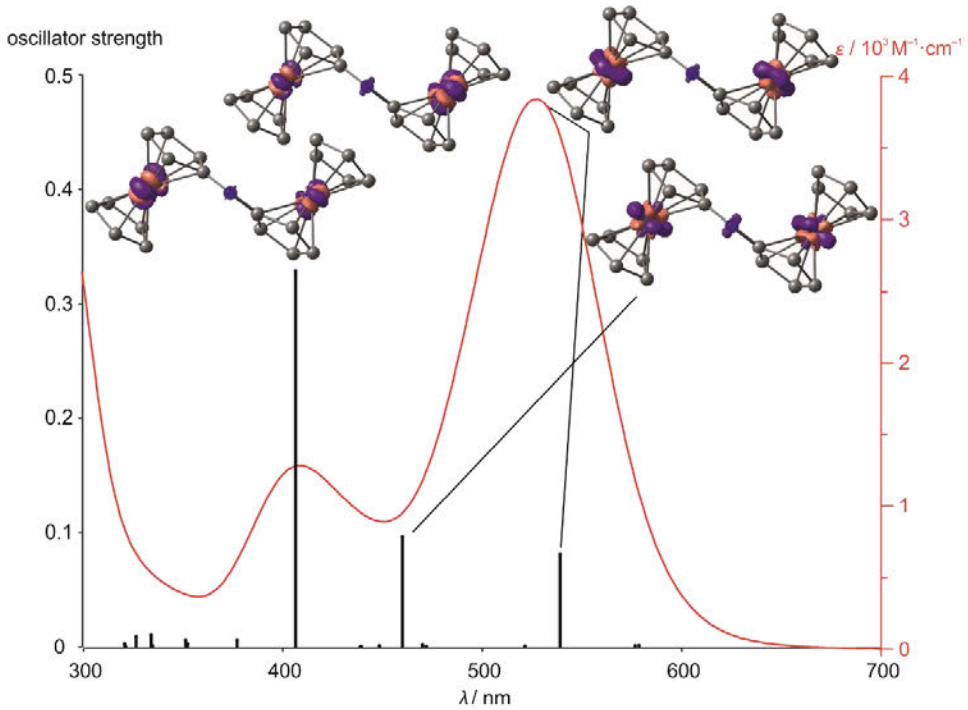

Figure S13. UV/Vis spectrum of **1[PF$_6$]** in CD_3CN and TD-DFT calculated transitions of **1$^+$** (transitions shifted by +0.14 eV) with difference electron densities displayed at an isosurface value of 0.01 a.u. (purple = electron loss; orange = electron gain).

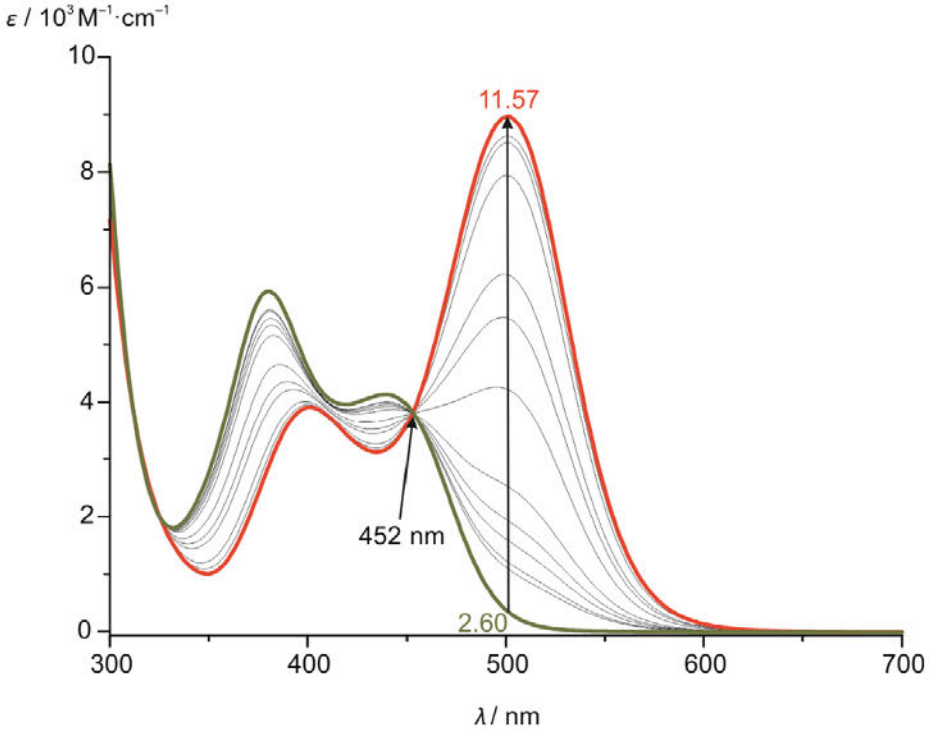

Figure S14. UV/Vis spectra during the spectrophotometric titration of **[H–1][PF$_6$]$_2$** with NaOH in H_2O showing an isosbestic point at 452 nm.

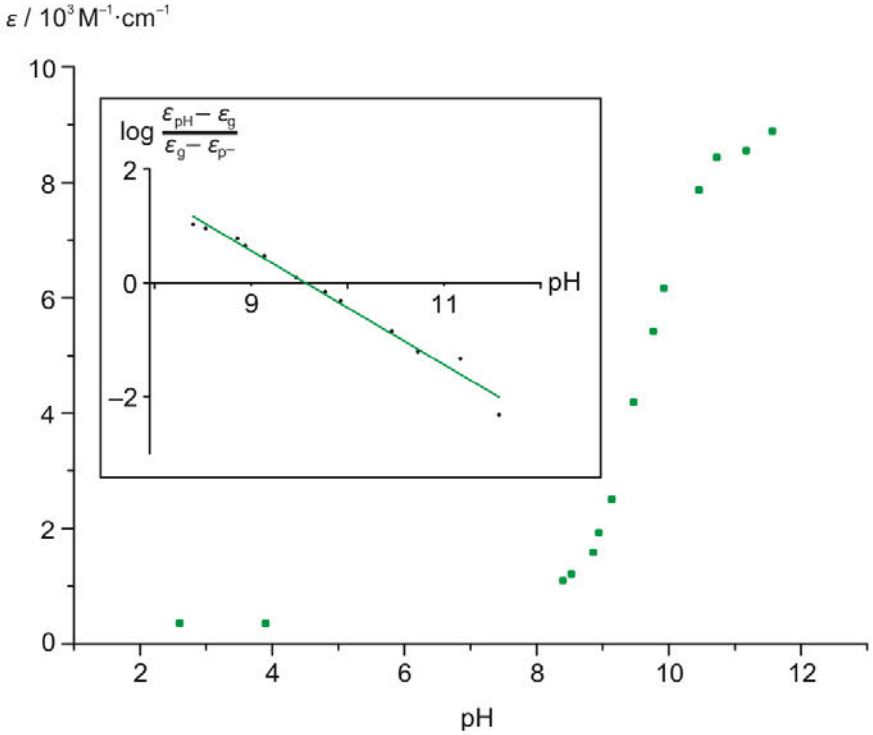

Figure S15. Spectrophotometric determination of the pK_a value of **[H–1][PF$_6$]$_2$** with NaOH in H_2O observed at λ = 501 nm. The inset shows the linear regression according to the Henderson–Hasselbalch equation with the fit line crossing the x-axis at pK_a = 9.56 (ε_{pH} = 8930 M^{-1} cm^{-1}, ε_{p^-} = 355 M^{-1} cm^{-1}, ε_g = recorded value.)

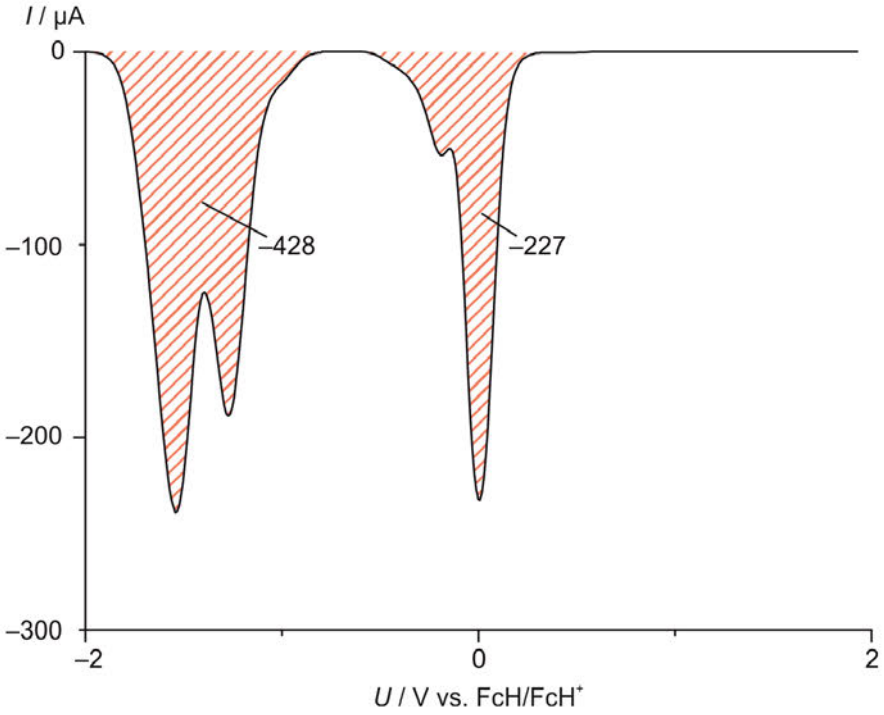

Figure S16. Reductive square-wave voltammogram of **[H–1][PF$_6$]$_2$** in CH_3CN/[^{n}Bu$_4$N][PF_6] and one equivalent ferrocene as reference. Numbers refer to the net current detected.

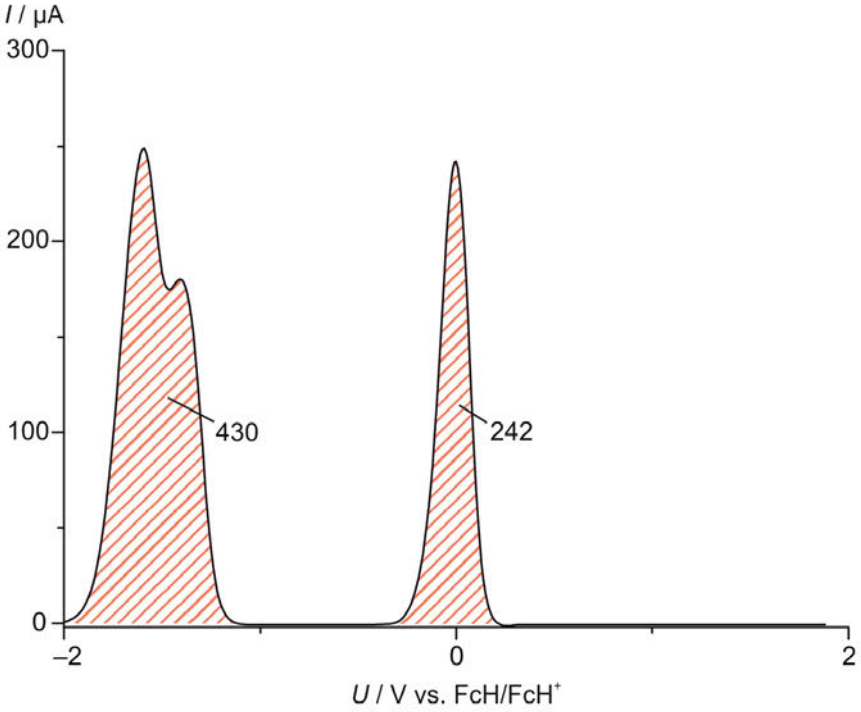

Figure S17. Oxidative square-wave voltammogram of **[H–1][PF$_6$]$_2$** in CH_3CN/[^{n}Bu$_4$N][PF_6] and one equivalent ferrocene as reference. Numbers refer to the net current detected.

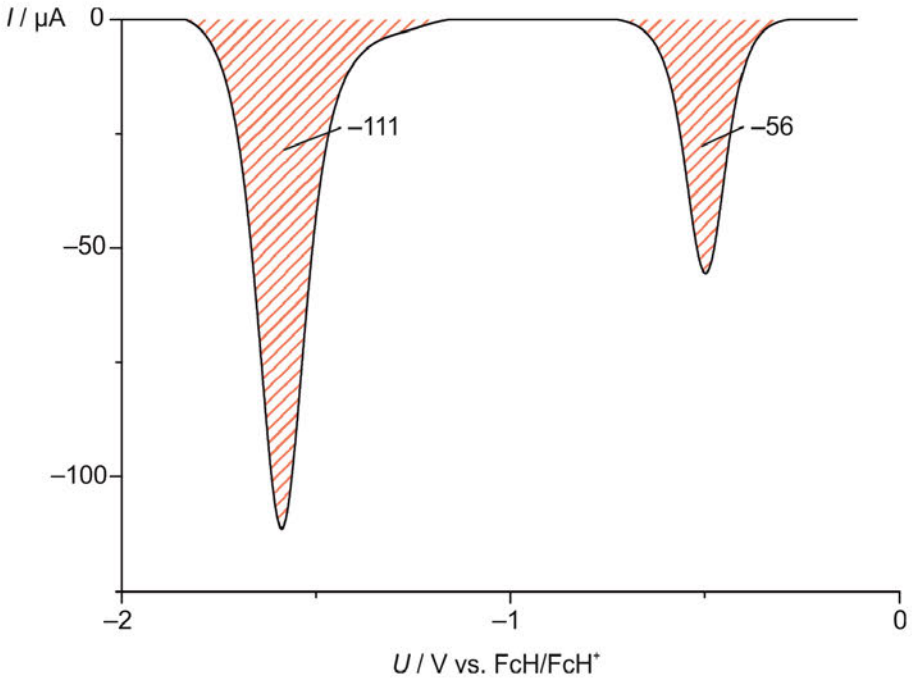

Figure S18. Reductive square-wave voltammogram of **1[PF_6]** in CH_3CN/[^{n}Bu$_4$N][PF_6] and one equivalent decamethylferrocene as reference. Numbers refer to the net current detected.

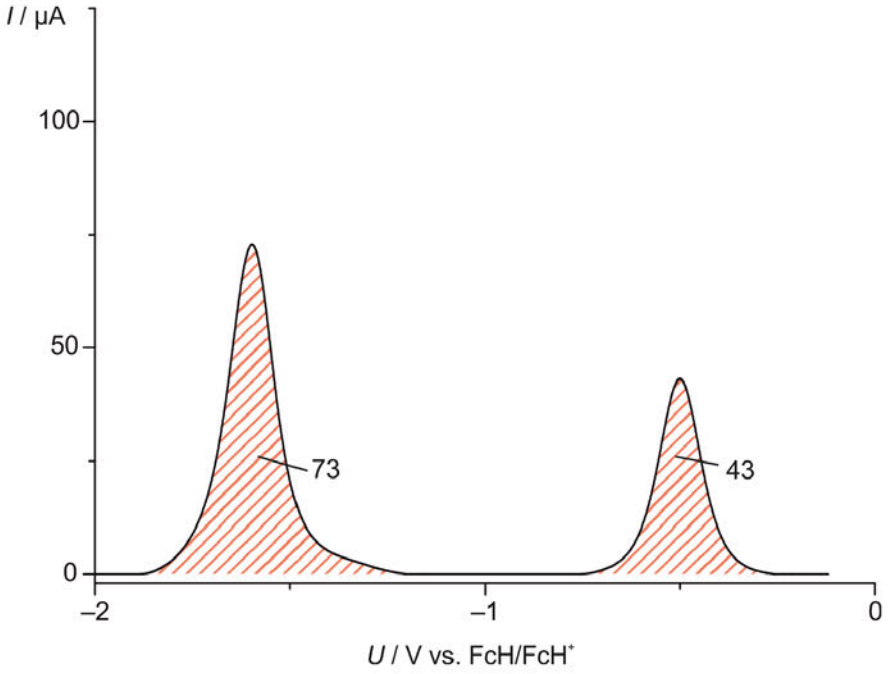

Figure S19. Oxidative square-wave voltammogram of **1[PF_6]** in CH_3CN/[^{n}Bu$_4$N][PF_6] and one equivalent decamethyl ferrocene as reference. Numbers refer to the net current detected.

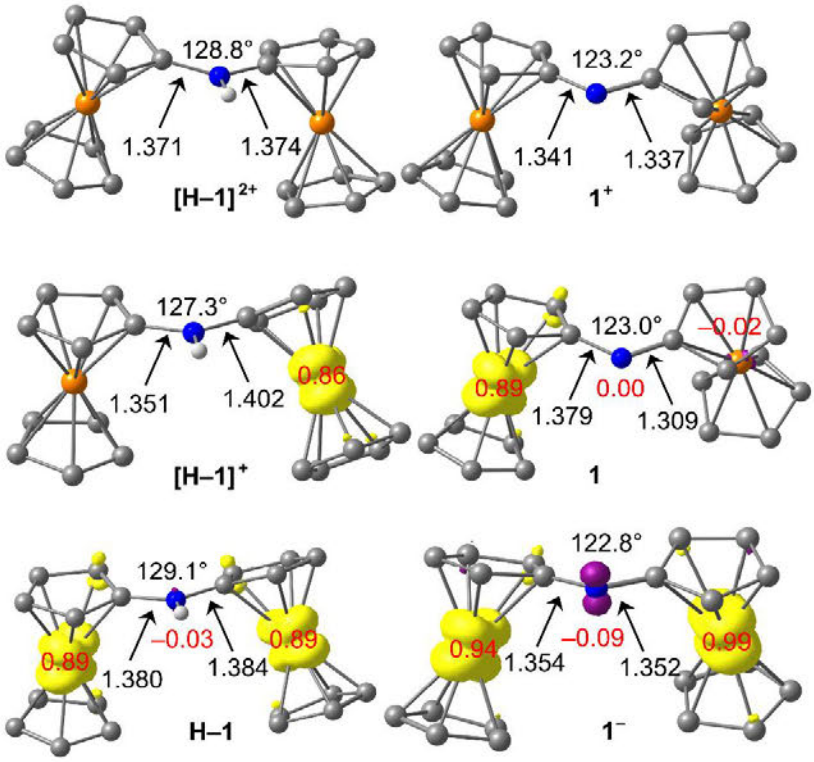

Figure S20. DFT optimized geometries of the three acid/base pairs **[H–1]**$^{2+}$**/1**$^{+}$, **[H–1]**$^{+}$**/1** and **[H–1]/1**$^{-}$ in *syn* conformations. Spin densities of open shell species are displayed in yellow/purple with isosurface values of 0.01. CH hydrogen atoms omitted. C–N distances/Å and C–N–C angles/deg indicated.

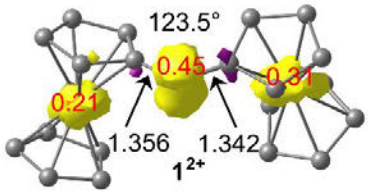

Figure S21. DFT optimized geometry of the reactive dicationic aminyl radical *syn*-**1**$^{2+}$ (S = ½). Spin densities are displayed in yellow/purple with isosurface values of 0.01. CH hydrogen atoms omitted. C–N distances/Å and C–N–C angles/deg indicated.

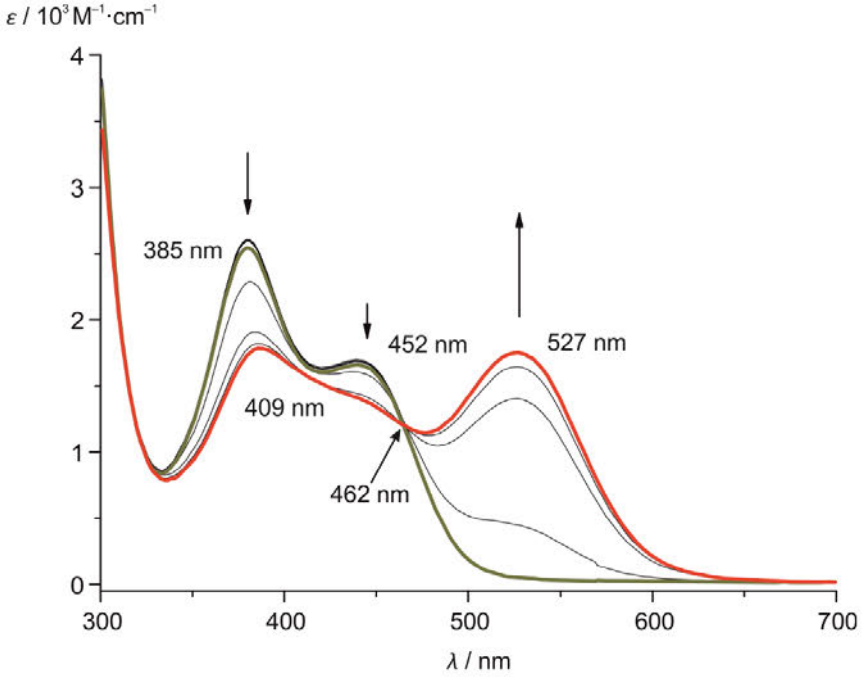

Figure S22. Spectroelectrochemical reduction of **[H–1][PF$_6$]$_2$** (beige) in CH_3CN/[^{n}Bu$_4$N][PF$_6$] yielding the UV/Vis spectrum of **1**$^+$ (red).

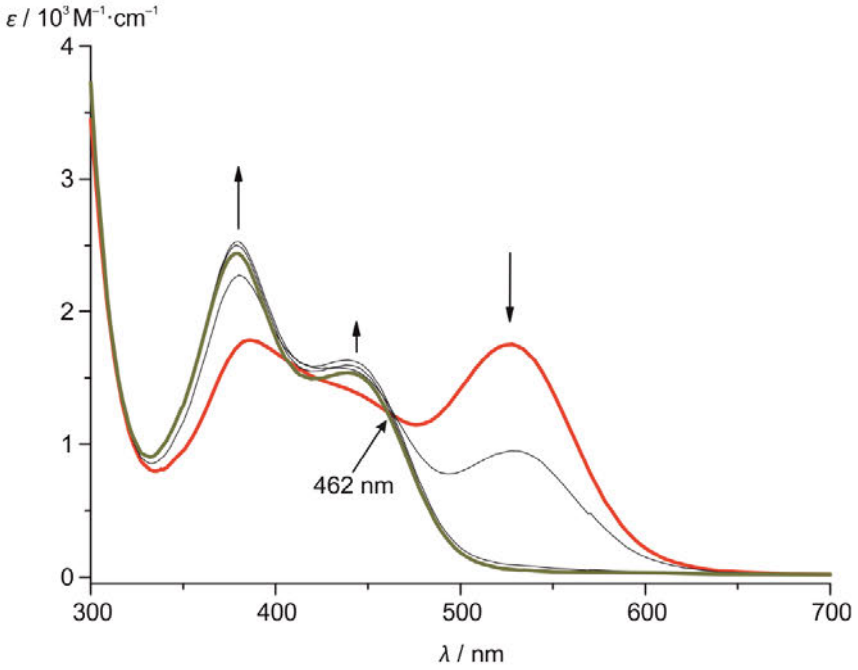

Figure S23. Spectroelectrochemical re-oxidation of the generated **1**$^+$ (red) in CH_3CN/[^{n}Bu$_4$N][PF$_6$] yielding the UV/Vis spectrum of **[H–1]**$^{2+}$ (beige).

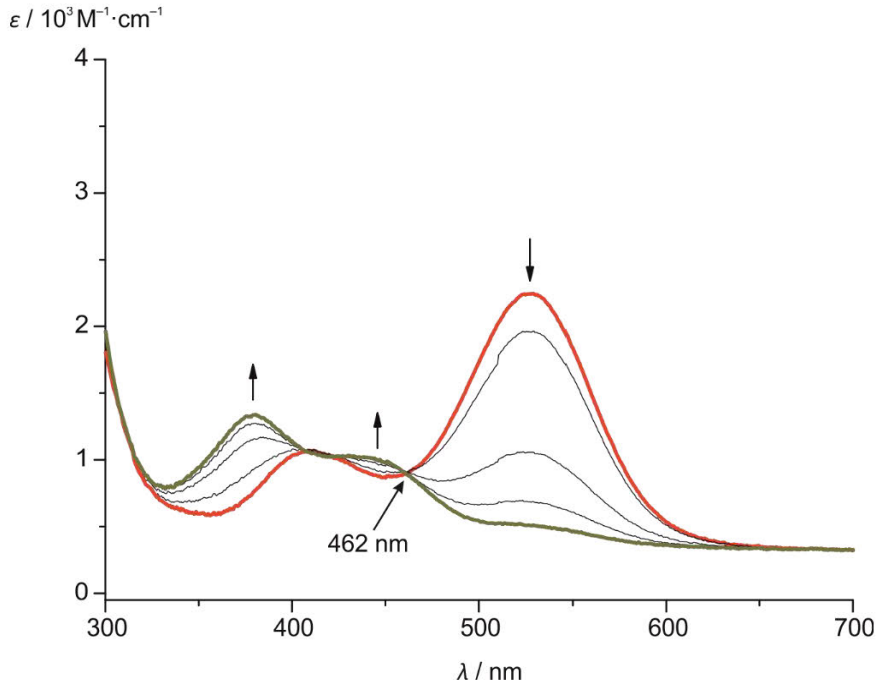

Figure S24. Spectroelectrochemical oxidation of **1[PF_6]** (red) (prepared by deprotonation of **[H–1][PF_6]$_2$** with NaH) in CH_3CN/[^{n}Bu$_4$N][PF_6] yielding the UV/Vis spectrum of **[H–1]$^{2+}$** (beige).

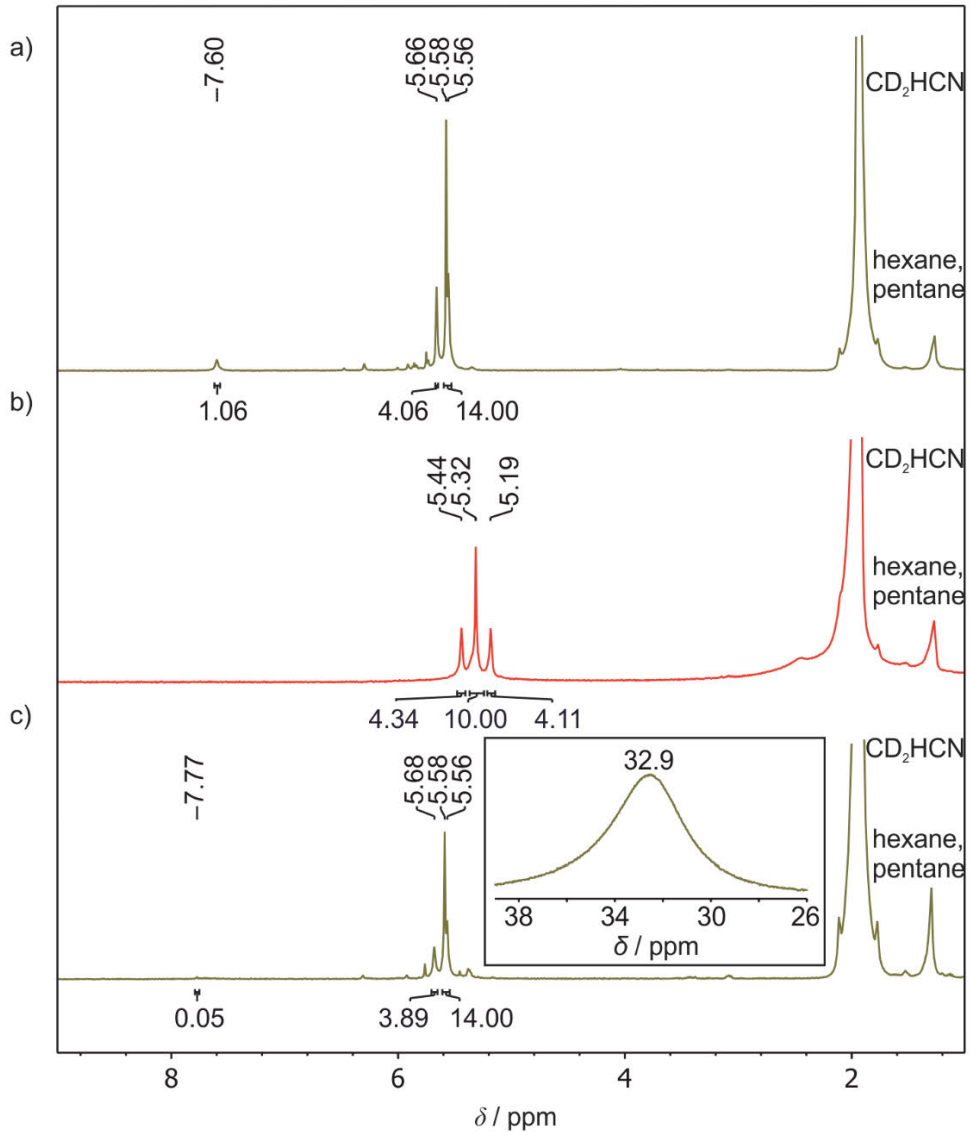

Figure S25. ^{1}H NMR spectra in CD_3CN of a) **[H–1][PF$_6$]$_2$**, b) **1[PF$_6$]** prepared by deprotonation of **[H–1][PF$_6$]$_2$** with 4 eq. NaH and subsequent syringe filtration and c) **[D–1][PF$_6$]$_2$** generated by oxidation of **1[PF$_6$]** with 1 eq. ferrocenium hexafluorophosphate, D$^{\bullet}$ abstraction from CD_3CN and subsequent syringe filtration. The inset shows the paramagnetically shifted resonance of exchanging ferrocene/residual ferrocenium ions.

Table S1. Energies of optimized complex geometries.

anti conformers	*syn* conformers
[H–1]$^{2+}$ (–3626.61141675 Eh) S = 0	**[H–1]**$^{2+}$ (–3626.60809995 Eh) S = 0
[H–1]$^{+}$ (–3626.74976778 Eh) S = ½	**[H–1]**$^{+}$ (–3626.74624707) S = ½
H–1 (–3626.87640283 Eh) S = 1	**H–1** (–3626.87533494 Eh) S = 1
1^{+} (–3626.16259152 Eh) S = 0	**1**$^{+}$ (–3626.16042197 Eh) S = 0
1 (–3626.28373446 Eh) S = ½	**1** (–3626.28229827 Eh) S = ½
1^{-} (–3626.38898249 Eh) S = 1	**1**$^{-}$ (–3626.38805533 Eh) S = 1
1^{2+} (–3625.97513433 Eh) S = ½	**1**$^{2+}$ (–3625.97120474 Eh) S = ½

Table S2. Energies of optimized CH_3CN, $^{\bullet}CH_2CN$ and $H^{\bullet}$.

CH_3CN	–132.81996137 Eh
$^{\bullet}CH_2CN$	–132.17467654 Eh
$H^{\bullet}$	–0.498930070135 Eh

7 Acknowledgements

Im Rahmen dieser Arbeit möchte ich mich bei folgenden Personen bedanken:

- [redacted], für die Möglichkeit meine Doktorarbeit im Bereich der Metallocene in ihrer Arbeitsgruppe durchzuführen. Ich bin dankbar für die Unterstützung und die konstruktiven Diskussionen, sowie für ihren Blick für das gesamte Projekt.
- [redacted], für das Einbringen seiner Erfahrung, sein offenes Ohr und das Lösen der Kristallstrukturen.
- [redacted], für die Zurverfügungstellung der Methoxycarbonylferrocene.
- [redacted], für seine entgegenkommende Art und die kompetene Unterstützung am NMR Spektrometer. Er war immer gewillt seine Erfahrung im „Matching" und „Tuning" zu nutzen um zu helfen.
- Der Zentralen Analytik Chemie um [redacted] und [redacted], für das Messen der Massenspektren und NMR Auftragsmessungen, sowie dem Bearbeiten von Sonderwünschen.
- [redacted] und [redacted], für das Messen der Kristallstrukturen
- [redacted], für die Einführung in die Arbeit mit ORCA und MOGON.
- [redacted], für ihre meisterhafte Glaskunst sowie der Bereitschaft ein zerbrochenes Röhrchen so schnell wie möglich zu reparieren.
- [redacted] und [redacted], für den regelmäßigen IT-Support, sei es das Aufsetzen der PCs, die Aktualisierung des Betriebssystems, die Installation benötigter Programme oder bei der Fehleranalyse und Hilfe bei diversen Software Problemen.
- [redacted], [redacted] und [redacted] für die Synthese von Vorstufen wie Aminoferrocen und Iodferrocen, sowie dem Nachziehen von neu synthetisierten Chemikalien wie 1,1-Diaminocobaltoceniumamin.
- den „Metallocenchemikern" [redacted], [redacted], [redacted] und [redacted], für die gemeinsame Arbeit mit den Metallocenen und ihren Input zur Handhabung dieser.
- den „Goldmenschen" [redacted], [redacted] und [redacted], für ihre Goldgeschichten und den Erfahrungsschatz, den sie mit mir geteilt haben.
- [redacted] für die Fortführung meiner Arbeit im Bereich der Aminocobaltocenium Chemie.
- [redacted] für die Fortführung der Ferrocenchemie.

- [redacted], [redacted], [redacted], [redacted], [redacted], [redacted] und [redacted], für das Korrekturlesen dieser Dissertation.
- dem gesamten [redacted], für…
  - … die Gemeinschaft
  - … das weitergeben sämtlicher Methoden
  - … die vielen lustigen Stunden mit den unterschiedlichsten Gesprächsthemen
  - … die Möglichkeit immer eine Frage stellen zu können
  - … die fachliche Unterstützung im gesamten Zeitraum meiner Zugehörigkeit
  - … die aufmunternden Worte, wenn etwas mal wieder nicht geklappt hat.
  - … alle Hinweise, die ich erhalten habe.
  - … den Ehemaligen für die regelmässige Runden, sei es von Angesicht zu Angesicht oder (gezwungenerweise) nur online.
- [redacted], für seinen Humor, dessen Zeuge ich regelmässig sein durfte, wenn du und [redacted] eine(?) Tasse Kaffee tranken.
- [redacted], für die wundervoll „mangelhaften" Torten und Kuchen mit denen du uns gemästet hast. Sie waren alle vorzüglich.
- [redacted], für seine einzigartigen Erklärungen der Welt. Von einigen Dingen hätte ich nie etwas erfahren, wenn Mauzi nicht von ihnen gesprochen hätte. Er kennt sich aus in der Finanzwelt. Und für unseren unorthodoxen Ansatz unsere Präparate zu tauschen und der daraus resultierende Erkentnis, das nicht wir Schuld sind, sondern die Chemie.
- [redacted], für seine Ordnungswut, die emotionalen Diskussionen und seine sicherheitsbewusste Art. [redacted] ist ein Original, das seinesgleichen sucht.
- [redacted], für diverse „Smash"ing Runden und seine Art unangebrachte Aussagen zu tätigen, um unser Niveau wieder auf die Erde zu bringen.
- [redacted], unserem Sorgenkind für die Unterstützung als Bayern Fan, die fussballerischen Gespräche und die Pferdelunge, die schon den halben AK kaputt gejoggt hat. Und [redacted] fing da erst mit dem Marathon an.
- [redacted], für die lustigen Spieleabende und [redacted] Glühweinparty, sowie das Antreiben, auf dass ich mir die Laufschuhe anzog und mit ihr durchs Feld joggte.
- [redacted], für seinen beispiellosen Sarkasmus gepaart mit seiner Hilfsbereitschaft. Ich wusste nie, was nun seine Antwort war. [redacted] erste Worte zu mir „Das heißt Guten Morgen!" sind ein Paradebeispiel dafür.
- [redacted], meinem Sitznachbarn für die Unterstüzung in meinen ersten Tagen im Arbeitskreis, den tiefgründigen Gesprächen und dafür, dass du die „Wahrheiten" die ich unüberlegt äußerte ausgehalten hast.

- [redacted], für seine Hilfsbereitschaft und dafür, dass er mich als seinen Sitznachbar wollte und mich dann auch noch ausgehalten hat. Sorry für das viele Fluchen.
- [redacted], der als Vorbild für uns alle dabei ist, die Welt zu retten. Und ganz speziell dafür, dass der [redacted] den Kontakt zum [redacted] hergestellt hat.
- [redacted], für die ausführlichen Gespräche zu One Piece und weiteren Manga, sowie seiner Empfehlungen für Manhuas. [redacted] war immer bereit zu helfen und seinen Input zu geben.
- meiner Modulantin [redacted], für ihre Unterstützung bei meiner Forschung und der Synthese von Mesitylaminoferrocen.
- meinen Freunden, die mir in der gemeinsamen Freizeit geduldig zugehört haben, wenn ich immer wieder nur über die Chemie und „meine" Chemie im Speziellen gesprochen habe, und mir die nötige Ablenkung verschafft haben, sei es durch gemütlich, angespannte Abende bei einem Champions League Spiel der Bayern, den gesellschaftlichen Runden mit einem gepflegten Glas Bier oder Whisky oder dem obligatorischen Silvester-Jenga.
- alle, die ich unabsichtlicherweise vergessen habe zu erwähnen, für alles, was ich erwähnt habe und das, was ich vergessen habe zu erwähnen.
- [redacted], für deine Bereitschaft, auch in deiner Freizeit mit mir über Chemie zu reden, da du als einer der wenigen überhaupt wusstest, wovon ich rede, für die Ablenkungen im Laufe der Jahre, sei es bei einem Glas Whisky, einer Runde FIFA oder einfach nur so durch gemütliches zusammensitzen. Und ganz speziell für dein Angebot im Fall der Fälle ein IR Spektrum für mich aufzunehmen, auch wenn ich dies dann doch nicht annehmen musste.
- meiner [redacted], für Ihre Unterstützung in den vergangenen Jahren, ihre aufmunternden Worte sowie den Tritten in den Hintern, damit ich endlich mal zu Potte komme. Sowie für das Korrekturlesen und Überprüfen der Formate sowohl dieser Arbeit, als auch zuvor schon bei meiner Diplomarbeit, obwohl du fast nichts verstanden hast.
- meinen [redacted], die mich seit dem Tag meiner Geburt unterstützt und gefördert haben und nur das Beste für mich wollten, dafür dass sie mir alles ermöglicht haben, was ich wollte, damit ich den Weg den ich gegangen bin auch gehen konnte, dass sie immer an meiner Seite waren und mich trotz der Dauer meines Studiums und der Promotion nie unter Druck gesetzt haben. Ohne Sie wäre ich nicht da, wo ich nun bin und hätte auch niemals versucht, diesen Weg einzuschlagen.

- meiner [redacted], für deine Unterstützung in den vergangenen Jahren, in denen sich so viel verändert hat, dafür dass du immer da warst und zugehört hast, wenn ich wieder fluchend und grummelnd heim kam weil wieder etwas nicht geklappt hat, dafür, dass du all das ausgehalten hast und dafür, dass du jeden noch so kleinen Erfolg feiern wolltest um mich aufzumuntern. Du hast immer an mich geglaubt und mich unterstützt. Und es tut mir Leid, dass ich trotz deiner Erwartungen kein neues Element „Svenium“ entdeckt habe.

Vielen Dank!

8 Curriculum Vitae

Sven Daniel Waniek

E-Mail [redacted]

Mobile Phone [redacted]

Adress [redacted]

Date of Birth 25.05.1990

Place of Birth Mainz

Education

[redacted]	Doctorate in Organometallic Chemistry "New Insights into the Metallocene Electrochemistry and their Potential use for Catalysis" [redacted], Johannes Gutenberg-Universität, Mainz
[redacted]	Diploma Studies in chemistry, grade: "Gut" "Acyclische ferrocenylsubstituierte Diaminocarbene" [redacted], Johannes Gutenberg-Universität, Mainz
[redacted]	Research Internship "Synthesis and Characterization of Silver Chromium Vanadates" [redacted], University of Houston, USA
[redacted]	A Level Martin Niemöller-Schule, Wiesbaden Grade 2.2 (good)

Community Service

07/2009–03/2010	Schulkinderhaus in the city of Hochheim

Professional Development

11/2021	GMP–Specialist, alfatraining Grade: „sehr gut" (95/100)

Language Skills

German	●●●●●
English	●●●●○
French	●●○○○

Analytical knowledge

Spectroscopy:

UV/Vis	●●●●○
IR	●●●●○
ESR	●●●○○
$^{1}H/^{13}C$-NMR	●●●●○
Electrochemistry	●●●●●

Computer Skills

MS Office	●●●●○
Chemdraw	●●●●●
Corel Draw	●●●○○
Origin	●●●●○
MestreNova	●●●●○
ORCA	●●●○○
Chemcraft	●●●●○

Miscellaneous

riding bike
playing football
fantasy and crime novels
cooking
gardening

Mainz, 21st of July 2022 Sven Waniek

8.1 List of publications

[1] S. D. Waniek, C. Heine, D. Zorn, T. Lieberth, M. Lauck, C. Förster*, K. Heinze*, *Organometallics* **2022**, 10.1021/acs.organomet.2c00211. Dicobaltocenium Amine – Proton, Electron, and H Atom Transfer

[2] S. D. Waniek, C. Förster*, K. Heinze*, *Eur. J. Inorg. Chem.* **2022**, e202100905, Protic ferrocenyl acyclic diamino carbene gold(I) complexes

[3] S. T. Hauer, A. P. W. Schneeweis, S. D. Waniek, L. P. Sorge, K. Heinze, T. J. J. Müller*, *Org. Chem. Front.* **2021**, *8*, 5744–5755. Radical cations and dications of bis[1]benzothieno[1,4]thiazine isomers

[4] S. D. Waniek, J. Klett*, C. Förster*, K. Heinze*, *Beilstein J. Org. Chem.* **2018**, *14*, 1004-1015. Polysubstituted Ferrocenes as Tunable Redox Mediators

8.2 Conference Contributions

11/2019 — 11th Central European Meeting on Molecular Electrochemistry
CEMME 2019, Chemnitz
Oral presentation:
Polysubstituted Ferrocenes as Tunable Redox Mediators

02/2018 — 16th Ferrocene Colloquium, Berlin
Oral presentation:
Polysubstituted Ferrocenes as Tunable Redox Mediators

02/2017 — Co-organizer
15th Ferrocene Colloquium 2017 in Mainz